59T

X-670-72-303

PREPRINT

NASA TM X- 66005

LINE-BLANKETED MODEL STELLAR ATMOSPHERES APPLIED TO SIRIUS

JOHN W. FOWLER

AUGUST 1972

GSFC

GODDARD SPACE FLIGHT CENTER
GREENBELT, MARYLAND

LINE-BLANKETED MODEL STELLAR ATMOSPHERES

APPLIED TO SIRIUS

by

John W. Fowler

Work performed under the auspices of the Laboratory for Optical Astronomy, Code 670, Goddard Space Flight Center and presented as a dissertation for the Ph.D. at the University of Maryland

Line-Blanketed Model Stellar Atmospheres
Applied to Sirius

ABSTRACT

The primary goal of this analysis is to determine whether the effects of atomic bound-bound transitions on stellar atmospheric structure can be represented well in models. The investigation is based on an approach which we call the method of artificial absorption edges. The method is described, developed, tested, and applied to the problem of fitting a model stellar atmosphere to Sirius. It is shown that the main features of the entire observed spectrum of Sirius can be reproduced to within the observational uncertainty by a blanketed flux-constant model with $T_{eff} = 9700°K$ and Log g = 4.26.

The profile of $H\gamma$ is reproduced completely within the standard deviations of the measurements except near line center, where non-LTE effects are expected to be significant. The equivalent width of $H\gamma$, the Paschen slope, the Balmer jump, and the absolute flux at 5550 Å all agree with the observed values. The gravity agrees with that determined from the orbital parameters of the Sirius A and B system and the observed angular diameter of Sirius. The angular diameter is also used to transform the emergent flux of the model to a corresponding value at the distance of the earth, so that comparisons to absolute flux measurements may be made. Agreement is excellent, although the observational uncertainty becomes large in the ultraviolet, reaching about fifty percent at its worst.

PREFACE

At the present stage in the development of the theory of stellar atmospheric structure, the methods available for interpretation of stellar spectra involve writing down all relevant equations, obtaining enough relations to form a determinate system, and attempting to solve for the distributions of all parameters. Because the system is composed of coupled non-linear differential equations, however, it is not possible in general to obtain analytic solutions. Therefore, approximation techniques are used to arrive at numerical solutions at selected points in the atmosphere called 'depths'. The set of physical parameters can be tabulated at all depths, and the complete simulation is called a 'model atmosphere'. In order to make the models more realistic, the set of equations must be made more realistic. The work described herein is an attempt to contribute more realism to model stellar atmospheres. This is done by providing a general tractable method for including in the calculations a physical effect which has, until very recently, either been ignored or treated in a specialized manner: the influence of the absorption associated with the tens of thousands of spectral lines due to atoms heavier than helium.

The classical calculation of a model stellar atmosphere (see, e.g., Mihalas, 1967) is based on the assumption that a unique solution set exists whose values satisfy simultaneously all of the differential equations. The numerical computation is composed of nested iterations which form a procedure for performing successive approximations, given reasonable estimates for all necessary starting parameters. The physical equations, which are themselves approximations, are used in two ways. They provide a mathematical formalism from which perturbation theory can extract algorithms for reducing the parameter inconsistencies. They also represent the final constraints which the parameter distributions must satisfy. At no time are they solved in the strict mathematical sense, which requires reducing the system to the form of algebraic equations. If the numerical procedure converges, the existence of a solution set is demonstrated. The uniqueness of this set is normally taken as physically intuitive. Except for restricted cases, rigorous proof of uniqueness has not been accomplished. Indeed, even to establish that a system has converged can be extremely difficult in some cases.

Background material upon which this work depends is covered in Chapters I and II and in the Appendices. Chapter III describes the transformation of line opacity spectra into a form which can be used in a more practical manner in atmosphere calculations. Chapter IV presents the model fit to Sirius, and the major sources of expected error are investigated in Chapter V. Finally, Chapter VI summarizes the analysis.

This work would not have been possible without the help of many friends. It is a pleasure, therefore, to acknowledge their contributions. I am extremely grateful and deeply indebted to Drs. Roger A. Bell and David Fischel, who directed this research and never failed to give advice freely upon the many occasions when it was requested. I have also benefitted in numerous ways from suggestions, criticisms, and conversations with Dr. Lawrence H. Auer, Mr. Alexander E. Barnes, Mr. Edgar M. Greville, Dr. J. Patrick Harrington, Mr. Alan H. Karp, Dr. Daniel A. Klinglesmith, Dr. David S. Leckrone, Dr. Peter Musen, Ms. Jan Owings Niebur, Mr. George Nesterczuk, Dr. Elske v. P. Smith, Dr. Anne B. Underhill, the late Dr. Uco van Wijk, and the operations crew of the Goddard IBM 360/91. Special appreciation goes to Ms. Marcia Murdock, who not only typed the manuscript, but also contributed greatly to all aspects of the final preparation.

Partial financial support for this work was provided by NASA grant NGL-21-002-033. Computer time was included under the budget of the Laboratory for Optical Astronomy, Goddard Space Flight Center, NASA.

To my parents

TABLE OF CONTENTS

LIST OF TABLES

LIST OF FIGURES

NOTATION

A_{ijk}	Einstein coefficient for spontaneous transition from level k' to level k (also $A_{ijk'k}$)
c	velocity of light (cm/sec)
E_{ijk}	energy of excitation state k in atom i, ionization state j, relative to ground state energy of the ion
f_{ijk}	oscillator strength for transition k to k' (also $f_{ijkk'}$)
F_λ	electromagnetic radiation flux at wavelength λ per unit wavelength interval (erg/cm^2/sec/sterad/Å)
F_ν	electromagnetic radiation flux at frequency ν per unit frequency interval (erg/cm^2/sec/sterad/hertz)
g	gravity at stellar surface
g_{ijk}	statistical weight of level k in atom i, ion j
K	Boltzmann's constant
ℓ_ν	mass absorption coefficient due to lines at frequency ν (cm^2/gm)
m_e	mass of the electron
m_i	mass of atom number i
n_{ijk}	number density of ions of atomic number i in ionization state j and excitation state k; population density
n_{ij}	sum of n_{ijk} over all k; ion number density
n_i	sum of n_{ij} over all j; atom number density
N	sum of n_i over all i; number density of all nuclei
N_e	number density of electrons
P_e	pressure due to electrons
P_g	pressure due to particles in the plasma

u_{ij}	partition function of atom number i, ionization state j
X_{ij}	n_{ij}/n_i , 'ionization fraction' or 'Saha fraction'
$\bar{x}$	$N_e/(N - N_e)$
Y_{ijk}	n_{ijk}/n_{ij} , 'excitation fraction' or 'Boltzmann fraction'
Z	mass abundance fraction metals
z	physical depth in an atmosphere (cm)
Γ	quantum mechanical radiation damping constant (sec^{-1})
γ	damping constant
ε	charge of the electron (e.s.u.)
κ_ν	mass absorption coefficient at frequency ν
μ	cos θ, where θ is the angle between the outward normal and the planes of stratification in a plane-parallel atmosphere; also the mean molecular weight of a plasma (a.m.u.)
ν_i	abundance fraction by number of atom number i
(ν)	the set of all ν_i
ρ	plasma density (gm/cm^3)
τ_ν	optical depth at frequency ν
τ_o	optical depth at frequency ν_o (standard frequency)

CHAPTER I

INTRODUCTION

1. The Line Opacity Problem

The interaction of electromagnetic radiation and matter is a fundamental consideration in calculating model stellar atmospheres. The physical parameter which describes how matter absorbs or scatters photons is called opacity, and the sources of opacity in a stellar atmosphere are numerous. Recent improvements in theory and computing facilities have led to the point where most known opacity sources can be reasonably well included in models. Generally available algorithms exist for most important sources of continuous opacity, i.e., opacity which influences photons whose energy lies in certain large continuous ranges. Such opacity results, for instance, when an electron absorbs electromagnetic energy in a transition whose upper state is in the continuum of free states. The effects of some selected atomic bound-bound transitions are also well known. These transitions are generally associated with photons whose energy falls in ranges several orders of magnitude smaller than those of continuous absorbers. Since absorption lines occur in great abundance in most stellar spectra, the opacity spectrum arising from them is extremely difficult to represent mathematically. For normal stars of roughly solar chemical composition, the line opacity can easily fluctuate ten times by six orders of magnitude within an interval of only one Ångstrom, for example. The structurally important spectral lines span a wavelength range on the order of 10^4Å, with effectively random positions. Since the process of computing model stellar atmospheres requires calculating the radiation field parameters at each depth at several frequencies between each opacity extremum, the number of frequency points necessary for inclusion of all known lines is about 10^5. The time required to perform one full iteration on the computer scales essentially linearly with the number of frequency points. Continuum-only models generally use ten to one hundred frequency points. The detailed handling of the atomic lines turns out to be completely precluded by present computer limitations. On the other hand, the cumulative effect of all lines can be reasonably expected to be significant for most stars. In Chapter IV it will be shown that this expectation is well-founded for dwarf A stars.

Hydrogen lines are often the most important because of the domination of that element in the general cosmic abundance distribution of chemical species. These lines have special broadening considerations also, and so they require special handling. Studies of their influence (see, e.g., Peterson, (1969)) have shown that they can contribute significantly to the determination of the atmosphere's equilibrium structure. Some other strong lines have been treated also, but the great majority of metal lines have never been explicitly included except in certain special cases.

It is the purpose of the present work to implement an idea for converting small segments of the line opacity spectrum into the form of equivalent artificial absorption edges (see, e.g., the review article by Mihalas, 1967). The complete blended line opacity spectrum can be represented as a series of such edges which spans the same wavelength range as the lines. Then the edge spectrum can be expressed in terms of a greatly reduced set of frequency points (here, 312), which brings the problem into the range of computer applicability. The only constraint on the artificial edge spectrum is that it must closely reproduce all the same effects on the model atmosphere structure as the detailed line opacity spectrum. Once the structure is correct, the emergent spectrum can be calculated in detail with ordinary methods.

Several theoretical checks can be made to test the validity of this approach. These will be described in Chapter V. In addition, the manner in which the artificial edges are constructed can be used to give strong intuitive justification for expecting the edges to conserve all the desired effects to sufficient accuracy. This justification is given as follows for the case wherein the edges interact only with an incident continuum radiation field. In reality, the line opacity interacts with radiation whose spectral distribution is determined by the line opacity at other depths, but this complication is left to Chapter V where it will be dealt with in detail. For now we consider the simpler problem.

In this case the effect of moving the central wavelength λ_0 of a line can be kept insignificant by moving it only so far that the incident continuum radiation at the line's new position varies negligibly in intensity from that at the line's natural central wavelength. In practice, consideration of the wavelength dependence of the continuous opacities and the Planck function indicates that lines may be moved by about 100 Å between continuum discontinuities. Therefore, the regions between discontinuities should be divisible into intervals of about 100 Å width, within which the lines may be re-ordered in any fashion. The manner in which the lines are re-ordered in this work is described in detail in Chapter III. A brief description of the process will suffice for present purposes.

The edges generated for this application of the method were obtained by subdividing the blended line opacity spectrum within each interval into increments several times smaller than the narrowest lines; these increments were then sorted in the interval to form a sequence ascending to the red. By choosing continuum opacity discontinuities as interval boundaries wherever possible, we insure that no line will be shifted across such discontinuities, and the total number of frequency points is kept to a minimum.

Blended line opacity spectra were calculated for a grid of electron pressures and temperatures, so that the dependence of the artificial edges on these variables could be studied and represented. Adding a velocity field, magnetic field, or radiation field dependence would have multiplied the size of the calculations beyond reason. Therefore, we neglect exotic effects, and make the assumption that the lines are formed in local thermodynamic equilibrium (LTE). Molecule formation was not included in the dissociation equilibrium, and no molecular opacity is included. Helium lines are also not included because, like molecular effects, they do not appear to be important in the temperature-pressure range where our other assumptions are expected to be valid. Hydrogen lines are included by calculating Stark-broadened profiles for Lyman α through L_{40} and H_{α} through H_{40}. An additional fourteen Paschen lines were included among the 28748 metal lines (see Appendix C).

The chemical composition of the stellar material was taken to be the set of cosmic abundances quoted by Allen (1964, see Appendix C). These abundances were used for several reasons. Firstly, since our purpose involves developing as general a blanketing method as possible, we need a basic set of abundances that is likely to be reasonable when applied to a variety of cases. Secondly, we need a fairly exhaustive list, because we wish to be able to include any known lines from any atomic species. This is because we expect the influence of thousands of weak lines to be significant. With a little interpolating for some of the heaviest elements, a list of the abundances of the first ninety atomic species can be obtained from Allen's compilation. Finally, these abundances are not drastically different from most others in current use, considering the uncertainties inherent in abundance analyses and the variation of different findings. Thus Allen's cosmic abundances appear to be the most useful at this stage. Applicability of the blanketing treatment to some other chemical compositions is discussed in section 5 below.

2. Use of the Artificial Edges

As stated in Chapter V, an arbitrary wavelength λ_0 is chosen as a standard reference at which the hydrostatic equilibrium equation is integrated. This is done because the pressure is treated as a function of optical depth in the computer program which was used to generate the models used in this investigation. This program is described briefly in Appendix B.

When the artificial absorption edges are included in the model, the standard wavelength should be one at which the line absorption may be considered negligible. The reason for this is that at the reference wavelength the stellar material should be as transparent as possible so that the truncated integration of the hydrostatic equilibrium equation proceeds to a greater physical depth than at any other wavelength. This permits the physical properties of the atmosphere to be obtained without extrapolation for all other useful optical depth scales. For most stellar atmospheres it is possible to find a wavelength where the continuum opacity is minimized and the line opacity is negligible. Here the standard wavelength is chosen as 4040 Å unless otherwise noted. The blanketing opacity is simply set to zero when the hydrostatic equilibrium equation is integrated. Otherwise the artificial edges are treated as any other opacity contributor.

3. Previous Treatments of the Blanketing Problem

Early work on the influence of absorption lines on stellar atmospheric structure showed that lines tend generally to warm the deeper layers, cool the boundary, and depress the flux spectrum which emerges from the atmosphere. Here we refer to layers as distributed in optical depth. In Chapter V a different interpretation of the line opacity influence is given. The tendency of lines to keep the heat inside the atmosphere was given the name blanketing. The warming of lower depths was called 'backwarming', and the reduction of the flux at line wavelengths was called 'blocking'. Much of this work was done by Chandrasekhar (1935), who devised the 'picket fence' method. He represented the line opacity spectrum by a series of step functions of constant amplitude whose spacing and magnitude were determined from statistical considerations. This method revealed most of the known blanketing effects.

Modifications of this approach followed, notably the work of Labs (1951), who allowed more variation of amplitude and spacing for the step functions. This provided some distinction between line cores and wings, and the step functions were adjusted to allow a temperature-pressure dependence. Labs' method has been used by Böhm (1954), and more recently by Fischel (1964), Böhm-Vitense (1969), and Carbon and Gingerich (1969), to name only a few. These works contain references to most of the older work.

The step functions used by Labs could perhaps be considered the first use of artificial edges, but the detailed re-sorting of segments of line opacity into edges was first used by Strom and Kurucz (1966). These authors developed a method which is similar in many respects to the method presented here. Some of the restrictions inherent in their work have been removed in this treatment, however. For instance, their edges must be recalculated if the sources of continuous opacity are changed. They also used different approximations in the broadening mechanisms they employed.

There is another approach to the general blanketing problem which must be mentioned, although it is too different from the edge method to be described in detail. This is the purely statistical approach, wherein the line opacity is sampled at random wavelengths for an increasing number of sample points. The line opacity is interpolated between these points, and their number is held constant after it is determined that further increase produces no further change in the model. This method has been applied to the sun by Peytremann (1971), who found the required number of frequency points to be on the order of 300. This is about the same as the number used here.

4. Generalization of the Artificial Edge Method

The blanketing method described in this paper contains a number of generalizations compared to previous treatments, but clearly no claim to complete generality can be made. The method was devised for use in a highly flexible stellar atmosphere computer program (see Appendix B), and so it was necessary to make it compatible with various combinations of continuous opacities. This meant calculating the detailed line opacity spectrum for some temperature-pressure-wavelength regions where it is usually negligible compared to the continuum. Lower cutoffs for neglecting the opacity of a given line were chosen relative to the line's central opacity. Other selection criteria are described in Chapter II.

Classical radiation damping was not used because it is independent of the atomic constants of the line, and is totally independent of the properties of the atmosphere. Instead radiation damping is represented by ten times the Einstein A coefficient for the transition multiplied by the statistical weight of the lower level. This approximation favors transitions with large A coefficients, as the quantum mechanical damping constant does (equation II-3). The statistical weight tends to increase with the square of the principal quantum number for excited states. This is used to mimic the increase in the number of terms which contribute to the sum in the quantum mechanical definition, although it is usually somewhat high for resonance lines. The factor of ten used here yields an average result of the order of the classical damping constant.

The inclusion of van der Waals damping provides the possibility of a more realistic temperature-pressure dependence in the total damping constant for lines involving a level near the ionization limit. In practice, in the range used here, the van der Waals damping constant for most lines was negligible compared to the radiation damping constant. This is because the neutral hydrogen density was too low to provide enough perturbers.

No fewer than the nearest five lines on either side of a sample point were included in the blend, and up to 250 lines on each side were made available. In the most heavily blended regions encountered, a maximum of 130 contributing lines was found.

Twenty detailed line opacity spectra were generated to fill a grid of five temperatures and four electron pressures. Details are included in Chapter II. All calculations were performed on the IBM 360/91 computer at Goddard Space Flight Center, Greenbelt, Maryland. About four and one half minutes were required to calculate the blend from 223 Å to 10533 Å. In practice, no line opacity beyond 8375 Å was used in the blanketed models. This meant keeping one wavelength interval to the red of that ending on the Paschen limit, where the line opacity was negligible. The ionization equilibrium calculation was done for elements one through ninety, with up to six ionization stages each. This approach was guided by generosity, and permitted the inclusion of line data from any such ion. It also simplified several computer arrays, and each T-P_e case required only two tenths of a second to compute. Partition functions were calculated by the method of Fischel and Sparks (1971).

The artificial edges are interesting phenomena in themselves, and some discussion of them is given later. The variation of the shapes and sizes of the edges as temperature and electron pressure are changed can be visualized easily, whereas the variation of the detailed lines is usually too complex to see. Thus the edges neatly summarize the lines in behavior, the patterns of which are described in Chapters III and V.

5. Applicability of the Present Method

All lines were assumed to be formed in pure absorption, and are corrected for stimulated emission. Non-LTE effects were neglected for several reasons. Most of the rate coefficients necessary for such a calculation are unknown. The situation is worse for collisional than radiative rates, the latter being available wherever oscillator strengths (see Chapter II) are available. However, the excitation equilibrium calculation requires radiative rate coefficients for transitions between all existing levels of a given ion. The data at hand do not permit this calculation to be made. Neglecting some levels in non-LTE calculations has been known to generate spurious effects (Auer, 1971, private communication). It is apparent in the blending of the line opacity spectrum that transfer effects in most lines are coupled to those of other lines, and a true non-LTE treatment would have to include this coupling. This would multiply an immense calculation to an incredible size. Hence a non-LTE treatment seems distant, and is probably unnecessary anyway for present accuracy in the range of spectral types considered here, since the LTE results can be expected to hold reasonably well everywhere except possibly very near the boundary of the atmosphere. This assumption is based on the behavior of the hydrogen lines, which are the best studied. There is no reason to anticipate that non-LTE effects in metal lines should be radically different from those in the hydrogen lines, and there is no better estimate available. Whereas non-LTE must be included in any fine analysis of the hydrogen lines, it appears that the atmospheric structure is essentially independent of these effects. The amount of flux affected by non-LTE mechanisms is simply too small to be significant, and an LTE description suffices. Moreover, since non-LTE deviations may increase or decrease the opacity of different lines, it is not clear that the net statistical impact of non-LTE effects will be significant even if many lines are controlled by them. The point should be checked by further investigation where possible, however.

Some work has been done along these lines by Mihalas and Luebke (1971) which tends to support these suppositions. These authors investigated the behavior of a picket fence opacity with scattering in addition to absorption. The pickets had the character of artificial two-level atomic opacities. This simplification made the problem tractable, and probably encouraged the appearance of non-LTE effects. They found that the blocking and backwarming were only weak functions of the ratio of scattering to absorption, but that the boundary temperature was sensitive to the scattering. This in itself raises no problems for us, however, and the available evidence indicates that non-LTE effects will have no structural significance for the types of atmospheres considered here.

Since molecular dissociative equilibrium and opacity were not included, the blanketing opacity derived here will not apply well to stellar atmospheres in which molecules are important. Hence stars later than early G fall outside the validity range of this particular application of the edge method. To apply this version to a later star would be an erroneous description of the opacity spectrum. Serious error could be expected, because the shape of the opacity spectrum determines the distribution of the structural parameters over optical depth.

Stars of spectral type earlier than about late B also fall outside the validity range for the following reasons. The LTE ionization and excitation theory is expected to lose its applicability because the conditions in the atmosphere do not seem to permit collisions to control the populations of the atomic states. Also, helium lines would have to be included. This could be done easily enough by treating helium lines in the same manner as the hydrogen lines, which is described in the next chapter. This is not necessary for our purpose, however, and was not done. Finally, the line opacity to the blue of about 2000 Å is not well determined because of the scarcity of line data. The opacity in that region is important for the hotter stars because their continuous spectra have maxima there. This point is discussed further in Chapters III, IV, and V.

Independence from a choice of chemical abundances cannot be obtained if the line opacity is pre-calculated, as it must be in this approach. Because of the time required to compute the blend and convert it into artificial edges, the procedure cannot yet be included as part of an atmosphere calculation. A certain amount of variation in relative metal abundances might be washed out fortuitously in the statistics, but without a definite investigation of this question, blind application of the edges to different mixes appears ill-advised. The line opacity spectrum of an element of plasma at a particular temperature and electron pressure depends upon many conditions; among these are the identities of the atoms which are responsible for the collisional broadening of all lines, and those which determine the density of the stellar material. Both of these are determined by the chemical composition.

For mixtures which have relative metal abundances equal to Allen's cosmic relative abundances (leaving the hydrogen and helium abundances free to fill out the total normalized composition fractions), the opacity calculated from the standard abundances can be suitably scaled to give a good approximation of the correct opacity. The only error that arises is in the density of neutral perturbers. As shown in Chapter II, the opacity of an absorption line depends on the number density of absorbers n_{ijk}, the density of the plasma ρ, and the broadening function for the line f_b. At fixed temperature and electron pressure, only these three quantities are influenced to first order by varying the chemical composition. Thus

$$\ell_\nu \propto \frac{n_{ijk}}{\rho} f_b \tag{I-1}$$

where ℓ_ν is the line opacity at frequency ν. Neglecting the dependence of f_b on chemical composition,

$$\ell_\nu \propto \frac{n_{ijk}}{\rho} = \frac{N\nu_i X_{ij} Y_{ijk}}{N\mu_0} = \frac{\nu_i X_{ij} Y_{ijk}}{\mu_0} \tag{I-2}$$

where $X_{ij} = n_{ij}/n_i$, $Y_{ijk} = n_{ijk}/n_{ij}$, and μ_0 is the mean molecular weight when there is no ionization. But X_{ij} and Y_{ijk} are fixed for given T and P_e through the Saha and Boltzmann equations, so that

$$\ell_\nu \propto \frac{\nu_i}{\mu_0} \tag{I-3}$$

If the metal abundance fractions are all multiplied by the same factor β, and the hydrogen and helium abundances are adjusted so that

$$\sum_i \nu_i = 1 \tag{I-4}$$

and

$$\nu_i = \beta\, \nu_i^{\text{cosmic}} \quad , \quad i > 2 \tag{I-5}$$

then

$$\frac{l_\nu}{l_\nu^{cosmic}} = \frac{\nu_i}{\mu_0}\left(\frac{\mu_0}{\nu_i}\right)_{cosmic} = \frac{\beta \nu_i^{cosmic}}{\mu_0}\left(\frac{\mu_0}{\nu_i}\right)_{cosmic} \tag{I-6}$$

or

$$l_\nu = \left[\frac{\beta \mu_0^{cosmic}}{\mu_0}\right] l_\nu^{cosmic} \tag{I-7}$$

Therefore, the opacity as calculated for cosmic abundances can be scaled by the factor $\beta\ \mu_0^{cosmic}/\mu_0$ to obtain the corresponding opacity for the new composition. As the metal abundances are scaled upwards, however, the density of neutral perturbers drops. This is because hydrogen is harder to ionize than the average metal atom, and the upward scaling makes the plasma easier to ionize. A smaller atom density can supply the electron density required by the given T and P_e, and so both the neutral and ionized atom densities drop at constant T and P_e as the plasma is made easier to ionize. Thus the scaling of the opacity as done above overestimates the van der Waals damping. This error is negligible in our case because of the relative unimportance of the van der Waals damping constant. Broadening by charged perturbers is not subject to this type of error because the opacity is treated as a function of T and P_e, and hence N_e.

Many investigations are concerned only with hydrogen-to-metals ratios, and relative metal abundances are not varied. For such cases the scaling method can be very useful. Extensive molecule formation, however, would alter the free-atom abundances in a manner unlike the scaling, and such cases must be treated specially. Other problems also arise when molecules become important, since atmospheres around type G or later are involved, and it is necessary to consider convection in the atmosphere calculation.

The work described herein makes little use of the scaling feature, because it was not needed in obtaining the basic model of Sirius. In Chapter V it is used in one instance where some evidence is presented to demonstrate that the mere inclusion of metal line blanketing produces an impact on the model atmosphere which overshadows the importance of order-of-magnitude variations of the metal abundance. This is true at least for spectral types near A0 V, and suggests in itself that minor changes in some abundances will not seriously alter the final stellar structure. These conclusions can be checked by generating the blanketing opacity spectra for different mixes, and while this approach will doubtless be pursued later, it lies beyond the present scope.

CHAPTER II

THE BLENDED LINE OPACITY SPECTRUM

1. The Opacity of a Single Absorption Line

The formulation of the mathematical description of the opacity of a single atomic transition as a function of temperature, pressure, and wavelength is presented in practically every modern textbook on astrophysics, and will not be reproduced here. Instead we shall simply employ the result, whose derivation can be found, for instance, in Aller (1963). In deriving the formula, the standard approach is to treat the electron which undergoes the transition as a classical oscillator, apply electromagnetic theory to derive the susceptibility (hence dielectric constant) of the system, and finally to use the dielectric constant to obtain the absorption coefficient as a function of frequency and the atomic constants. Then the expression is interpreted in the light of the rigorous quantum mechanical derivation, and found to be identical if two quantities are re-defined. These are the damping constant and the 'effective number of oscillators'. Here the only damping mechanism we consider is radiation damping. In the next section others are discussed.

The frequency distribution of the opacity arising from an atomic transition is

$$\ell_\nu = \frac{n_{ijk}}{\rho}\,\alpha(\nu)\,\frac{4\pi\nu}{c} \tag{II-1}$$

where

$$\alpha(\nu) = \frac{\varepsilon^2 f}{8\pi m_e \nu}\,\frac{\left(\frac{\Gamma}{2\pi}\right)}{(\nu_0-\nu)^2+\left(\frac{\Gamma}{4\pi}\right)^2} \tag{II-2}$$

and

$$\Gamma = \Gamma_{KK'} = \sum_{m<l} A_{lm}\,, \; l = K, K' \tag{II-3}$$

The Einstein A coefficients and other line parameters must be obtained from tables for each line absorption coefficient calculated with these formulae.

2. Other Contributions to the Damping

Besides the natural broadening of a line resulting from the radiation damping described in equation (II-3), other physical processes can enhance the range over which the line absorber interacts with the radiation field. For example, the effect of electric fields local to the atom's vicinity is to distort the energy levels from those which exist in an isolated environment. The statistical effect of fluctuating microscopic fields due to ions and electrons which pass near the atom in the chaos is seen in the Stark broadening of the hydrogen lines. Similarly, atomic energy levels can be distorted by van der Waals forces exerted by a neutral perturber. The motion of the absorber also influences the central line wavelength by the Doppler effect, and so an ensemble of randomly moving absorbers will interact with the radiation field over a greater range than an equal number of static absorbers. This is not a damping effect, but since it results in a broadened line, it is included here. Stark broadening is important in the hydrogen lines, but the metal lines are broadened primarily by other forms of collisional broadening. Since our main concern is the metal lines, Stark broadening will not be discussed here. In the models described in Chapter IV, the Griem (1964) theory of Stark broadening is employed for the hydrogen Lyman and Balmer lines, insofar as structural effects are concerned.

Each mechanism which produces a distortion of atomic energy levels contributes to the total broadening, which is the convolution of the different damping profiles. These profiles have a Lorentzian distribution, and so a total damping constant can be defined which is just the sum of the separate damping constants. This is a general property of the convolution integrals of Lorentzian profiles (see, for example, Woolley and Stibbs, 1953, p. 110 ff.).

Doppler Broadening is treated by assuming that the velocity distribution of the atoms is Maxwellian, so that integrals over velocity can be performed. The convolution of the damping with the Doppler broadening is the Voigt function H(a,u), where (see Hummer, 1965)

$$H(a,u) = \frac{a}{\pi}\int_{-\infty}^{\infty}\frac{e^{-y^2}\,dy}{a^2+(u-y)^2} \tag{II-4}$$

The complete opacity spectrum of one absorption line can be written

$$\ell_\nu = \frac{n_{ijk}}{\rho}\,\alpha_0\,H(a,u) \tag{II-5}$$

where

$$\alpha_0 \equiv \frac{\sqrt{\pi}\,\varepsilon^2}{m_e c}\,\frac{f}{\Delta\nu_D} \tag{II-6}$$

$$a \equiv \frac{\Gamma}{4\pi\Delta\nu_D} \tag{II-7}$$

$$u \equiv \frac{\nu-\nu_0}{\Delta\nu_D} \tag{II-8}$$

$$\Delta\nu_D \equiv \frac{\nu_0}{c}\sqrt{\frac{2KT}{m}+V_m^2} \tag{II-9}$$

and m is the mass of the absorbing atom, and v_m is the microturbulent velocity in the plasma element. Microturbulence is a controversial concept when applied to stellar atmospheres. Here its effect is only to provide a minimum Doppler width, and the value assigned throughout is $v_m^2 = 2.5 \times 10^{10}$ cm^2/sec^2. Several checks in small ultraviolet and the visible bands showed variations in the emergent flux of less than 0.1% as the microturbulence was varied from $v_m^2 = 0$ to 2.5×10^{11} .

3. Outline of the Calculation Procedure

The line opacity at a given frequency ν is the sum of all lines' contributions at that frequency, or

$$\ell_\nu = \sum_{m=1}^{n} \alpha_{o_m} \frac{N_m}{\rho} H(a_m, u_m) \tag{II-10}$$

where N_m is the n_{ijk} for the m^{th} line in the set of n lines, and the subscript 'm' has been attached to α_o, $\underline{a}$, and u to indicate those quantities defined in equations (II-6), (II-7), and (II-8) evaluated for the m^{th} line. The blended line opacity spectrum can be generated as a set of (ℓ_ν, λ) pairs by evaluating (II-10) at a sufficiently complete set of wavelengths. This set must contain all wavelengths where the line opacity spectrum has extrema, and preferably a few points in between for all but the narrowest lines.

In this investigation the densest part of the spectrum, about 2500 Å to 5000 Å, has an average wavelength separation between adjacent line centers of about 0.08 Å. Naturally the sum in equation (II-10) is not taken over all lines at each wavelength sample point in practice, because the contribution of all but the nearest lines is negligible. The limits on the sum, 1 and n, are replaced by new limits, m_1 and m_2, which are chosen so that all significant contributors are included without wasting time in computing contributions from lines whose strength does not make up for their distance from the sample point. The table of line parameters (e.g., f, λ_o, Γ, etc.; sources are given in Appendix C) is kept in wavelength order so that lines whose contributions are important will lie within one segment of the total sequence. This segment is the one bounded by lines m_1 and m_2. The rules for defining m_1 and m_2 for a given sample point are given in the next section.

The set of wavelength sample points was generated in the following way. The first point was taken at the center of the first line, λ222.791 of C IV. After summing contributions to the blend here, the sample point value was incremented according to $\lambda_{i+1} = \lambda_i + \Delta\lambda_i$, where $\Delta\lambda_i$ was chosen either to be the distance from λ_i to the center of the next line to the red or 0.1 Å, whichever was smaller. One final restriction was imposed: at least one sample point was taken between any two adjacent line centers. In covering the blend from 222.791 Å to 10533 Å, a total of 119400 sample points was generated, or one every 0.086 Å on the average. In practice, no data to the red of 8375 Å was employed in generating artificial edges.

4. Selecting the Significant Contributors

A variety of approaches is available for selecting contributors to the sum in equation (II-10) efficiently. For instance, a line may be included if its central wavelength falls within an arbitrarily specified distance from the sample point. Alternatively, its central wavelength may be required to lie within a given number of Doppler widths from the sample point. Another method is simply to include contributions from some total of nearest lines, for instance the nearest twenty-five lines. Finally, a line may be included if at the sample point it retains a certain percentage of its central opacity. These and other criteria can be used in combination, and all of them suffer drawbacks in certain uncooperative situations. As a general rule it is necessary to include many marginal cases to be certain that all the important contributions have been obtained. The selection rules used herein were:

a. if a line fell within 10 Å of the sample point, it was labelled a candidate (this permitted metal lines to have widths up to 20 Å, if so inclined; the widest noted were on the order of 5 Å to 10 Å);

b. each candidate was examined to see if its opacity at the sample point could be guaranteed to be less than a minimum acceptable fraction of its central opacity; if so, its contribution was not calculated; otherwise, it was included in the sum (the strength-dependent acceptance criterion is described below);

c. if the line was one of the five closest on either side of the sample point, it was included regardless of conditions 'a' and 'b'.

Conditions 'a' and 'c' resulted in a minimum of ten contributors and, in practice, a maximum of 130 candidates over the set of sample points. The prediction involved in 'b' is based on the behavior of the Voigt and Lorentz distribution functions, and is much faster to perform than the actual calculation of the contribution. The Lorentz distribution is

$$L(a,u) = \frac{a}{\pi} \frac{1}{a^2 + u^2} \qquad \text{(II-11)}$$

For $\underline{a} > 10^{-5}$, the Voigt and Lorentzian functions are essentially equal for $u > 5$. For such lines, the Lorentzian represents a faster method for calculating the line's wing contribution than the Voigt function, because the latter is an integral function. Therefore, we can select the cutoff point for any line's contribution to the blend by specifying a critical value for u, notated u_c, at which the Lorentzian has dropped by an arbitrary factor from L(a,0). For the types of atmospheres we are considering, all but the weakest lines have a values greater than 10^{-3}, and when their Lorentzian has dropped to 10^{-6} of its central value, the Voigt function has dropped to about 10^{-4} of its central value. For a minority of lines a is less than 10^{-3}, so that the Lorentzian has a sharp peak at u = 0, and the approximation does not apply well. The sample point selection procedure automatically includes such lines adequately, however, because lines with the smallest a values tend to be the weakest. This is due to the fact that a contains the total damping constant, which contains the Einstein A coefficient, and this is proportional to the oscillator strength.

The equation defining the critical number of Doppler widths for inclusion in the blend is therefore taken to be

$$\frac{L(a,u_c)}{L(a,0)} = 10^{-6} \qquad \text{(II-12)}$$

Since $L(a,0) = 1/\pi a$,

$$\frac{a}{\pi}\frac{1}{a^2+u_c^2} = \frac{10^{-6}}{\pi a} \qquad \text{(II-13)}$$

Solving for u_c yields

$$u_c = 10^3 a \qquad \text{(II-14)}$$

Using $u_c = \Delta\lambda_c/\Delta\lambda_D$ and $\Delta\lambda_D = \lambda_0^2\Delta\nu_D/c$,

$$\Delta\lambda_c = \frac{10^3\Gamma}{4\pi\Delta\nu_D}\frac{\lambda_0^2}{c}\Delta\nu_D = \frac{10^3\Gamma\lambda_0^2}{4\pi c} \qquad \text{(II-15)}$$

For wavelengths in Å, this becomes

$$\Delta\lambda_c = 3\times 10^{-17}\Gamma\lambda_0^2 \qquad \text{(II-16)}$$

Thus a line with central wavelength λ_0 must be included in the blend at wavelength λ if

$$|\lambda - \lambda_0| \leq \Delta\lambda_c \qquad \text{(II-17)}$$

This guarantees that any strong line will be included as long as its contribution is at least 10^{-6} of its central opacity, and intermediate lines will be included if they can contribute a larger fraction which is determined by their strength.

5. Order of the Calculation

The procedure outlined above was used to generate twenty blended line opacity spectra. In order to save computer time and to avoid duplication of calculations, the complete project was arranged in the form of a system of programs, each of which could be run separately with intermediate results stored on magnetic tape. Some of the programs dealt with calculations at a specific temperature and electron pressure, and others were involved with calculations relevant to all twenty T-P_e grid points. This approach allowed the separation of the total calculation into temperature-dependent, electron pressure-dependent, and wavelength-dependent sections. The twenty T-P_e grid points were formed by all combinations of the five temperatures, 6000°, 8000°, 11000°, 17500°, and 50000°K, and the four electron pressures 3, 30, 300, and 10000 dyne/cm^2. These values were chosen with the atmospheres of dwarf A stars in mind.

The complete system can be arranged in four phases:

A. Preparation of the line data (P_e-independent)

B. Ionization equilibrium (λ-independent)

C. Central absorption coefficients (merge of A and B)

D. Blended line opacity spectra.

These four phases will be considered separately in sections six through nine below.

The expression for ℓ_ν in equation (II-5) is written as the product of three functions:

$$\ell_\nu = \Phi_{ij}(T,P_e)\,\Theta_{ijk}(\lambda_o,T)\,H(a,u) \tag{II-18}$$

Because van der Waals damping was included, the Voigt function H(a,u) is an implicit function of pressure as well as wavelength and temperature, although in our case the dependence is negligible. The Φ and Θ functions are defined by the equations

$$\Phi_{ij}(T,P_e) \equiv \frac{N\nu_i X_{ij}}{u_{ij}\,\rho}\,\frac{\sqrt{\pi}\,\varepsilon^2}{m_e\,c}\,\frac{1}{\sqrt{\frac{2kT}{m_i}+V_m^2}} \tag{II-19}$$

$$\Theta_{ijk}(\lambda_o,T) \equiv e^{-E_{ijk}/kT}\,g_{ijk}\,f_{ijk}\,\lambda_{o_{ijk}} \tag{II-20}$$

where the oscillator strength f_{ijk} is understood to mean $f_{ijkk'}$, i.e., the oscillator strength for the transition from level k to level k', and E_{ijk} is the excitation energy of the lower level. This representation is derived as follows:

$$\ell_\nu = \frac{n_{ijk}}{\rho}\,\alpha_o\,H(a,u) \tag{II- 5}$$

$$n_{ijk} = \frac{n_{ijk}}{n_{ij}}\,\frac{n_{ij}}{n_i}\,\frac{n_i}{N}\,N \tag{II-21}$$

The Boltzmann distribution of populations over excitation states gives

$$\frac{n_{ijk}}{n_{ij}} = \frac{g_{ijk}\,e^{-E_{ijk}/kT}}{u_{ij}} \tag{II-22}$$

The Saha ionization equation (Fowler, 1970) gives

$$\frac{n_{ij}}{n_i} \equiv X_{ij} = \frac{\left(C_s \frac{T^{5/2}}{P_e}\right)^j u_{ij}\, e^{-\beta_{ij}/T}}{\sum_{m=1}^{i+1} \left(C_s \frac{T^{5/2}}{P_e}\right)^m u_{im}\, e^{-\beta_{im}/T}} \qquad \text{(II-23)}$$

The factor n_i/N is the abundance fraction ν_i, so (II-21) becomes

$$n_{ijk} = \frac{g_{ijk}}{u_{ij}}\, e^{-E_{ijk}/KT} X_{ij} \nu_i N \qquad \text{(II-24)}$$

α_0 was defined as

$$\alpha_o \equiv \frac{\sqrt{\pi}\,\varepsilon^2}{m_e c} \frac{f_{ijk}}{\Delta\nu_D} \qquad \text{(II- 6)}$$

and $\Delta\nu_D$ is

$$\Delta\nu_D = \frac{1}{\lambda_{o_{ijk}}} \sqrt{\frac{2KT}{m_i} + V_m^2} \qquad \text{(II-25)}$$

so equation (II-6) becomes

$$\alpha_o = \frac{\sqrt{\pi}\,\varepsilon^2}{m_e c} \frac{\lambda_{o_{ijk}} f_{ijk}}{\sqrt{\frac{2KT}{m_i} + V_m^2}} \qquad \text{(II-26)}$$

Therefore, equation (II-5) becomes

$$\ell_\nu = \frac{g_{ijk}}{u_{ij}\,\rho}\, e^{-E_{ijk}/KT} X_{ij} \nu_i N \frac{\sqrt{\pi}\,\varepsilon^2}{m_e c} \frac{\lambda_{o_{ijk}} f_{ijk} H(a,u)}{\sqrt{\frac{2KT}{m_i} + V_m^2}} \qquad \text{(II-27)}$$

which, with the definitions (II-19) and (II-20), becomes equation (II-18).

6. Preparation of the Line Data

Values of $\lambda_{o_{ijk}}$, g_{ijk}, f_{ijk}, $A_{ijk'k}$, (i,j), E_{ijk}, and $E_{ijk'}$ were obtained (see Appendix C) for 28748 metal absorption lines, where (i,j) denotes the atomic number and ionization state of the absorber. These sets of line parameters were ordered in increasing λ_0, and the function Θ_{ijk} was calculated for every line at all five temperatures and saved on tape. The radiation damping constant was approximated by

$$\Gamma_{rad} = 10 g_{ijk} A_{ijk'k} \tag{II-28}$$

and stored separately on tape. The van der Waals damping constant (see, e.g., Allen, 1964) is

$$\Gamma_v = 17\, C_6^{2/5} v^{3/5} N_H \tag{II-29}$$

where $N_H = n_{11}$, the number density of neutral hydrogen attoms. These were the only neutral perturbers considered. The most probable velocity of a perturber with respect to the absorber, v, is given by

$$v = \sqrt{\frac{8KT}{\pi}\left(\frac{1}{m_H} + \frac{1}{m_i}\right)} \tag{II-30}$$

for a Maxwellian velocity distribution. C_6 is a line constant approximated by the formula

$$C_6 = 1.61 \times 10^{-33} \left(\frac{13.6}{\chi_{ij} - E_{ijk}}\right)^2 \tag{II-31}$$

where χ_{ij} is the ionization potential of the ion which produces the line. With the definition

$$\Gamma_0 \equiv 17\, C_6^{2/5} v^{3/5} \tag{II-32}$$

Γ_v can be written

$$\Gamma_v = \Gamma_0 N_H \tag{II-33}$$

Γ_0 is calculated in phase A and also stored on tape. The work of Hammond (1969, private communication), Burgéss and Grindlay (1970), and Fullerton and Cowley (1970) indicates that Γ_v given in this way is probably between two and four times too small for densities appropriate to stellar atmospheres; therefore, Γ_v was arbitrarily multiplied by three throughout. Even so this damping constant was usually negligible compared to the radiation damping constant.

7. Ionization Equilibrium

The equations of ionization equilibrium are discussed in the author's review article (1970), and need not be repeated here. In this phase, the function $\Phi_{ij}(T,P_e)$ defined in equation (II-19) was calculated at all T-P_e grid points for all i and j and saved on magnetic tape. The neutral hydrogen density was also calculated and saved for use in Phase D when the van der Waals damping constant is computed.

8. Central Absorption Coefficients

The stored values of Φ_{ij} and Θ_{ijk} were multiplied in a synchronized fashion in this phase to produce twenty sets of 28748 central absorption coefficients. The output data sets were stored on magnetic tape. The total production running time up to this point was ten minutes on the 360/91.

9. Blended Line Opacity Spectra

The sets of central absorption coefficients were used with the broadening calculations in this phase to produce twenty sets of (ℓ_ν, λ) pairs, which described the line opacity spectra. The following procedure was applied to each T-P_e case. The parameters for the first 500 lines were read into the program, and the total damping constant was calculated for each. The sample wavelengths were generated as described in section 3 above. $\Delta\lambda_c$ defined in equation (II-16) was also calculated for each line. The blend was calculated at successive sample points until the wavelength passed the center of the 250^{th} line. From then on, whenever the sample wavelength passed over a line center, the bluest line in the program array was replaced with the next line in the input data set. In this way, the line parameter array underwent continuous updating at a safe distance from the sample wavelength. The nearest 250 lines on both sides of the sample point were always available for inclusion. When the sample point passed 10533 Å, the calculation ended with 119400 (ℓ_ν, λ) pairs. Each blend required about four and one half minutes computing time in this phase.

10. The Hydrogen Lyman and Balmer Lines

The wavelength quadrature points which were used to approximate integrals over frequency are listed in Appendix C. These points were chosen to coincide with continuum opacity discontinuities of hydrogen and helium whenever possible, and otherwise to coincide with the available spectral features of interest. In some cases, arbitrary points were selected to keep the size of the edges near 100 Å in width. It was not possible to select quadrature points which would provide a good implicit representation of the hydrogen lines. To remedy this, the hydrogen Lyman and Balmer lines were also cast into the form of artificial edges with the same heads as the metal edges. An alternate approach would have been to include the hydrogen lines in the blend with the metal lines. This would have eliminated the freedom to alter the metal abundance, however, by the scaling method of Chapter I, section 5. The hydrogen artificial edges were generated in a manner identical to that of the metal artificial edges, except only Lα through L_{40} and Hα through H_{40} were used in the blend, and the Stark broadening theory of Griem (1964) was employed.

CHAPTER III

THE ARTIFICIAL ABSORPTION EDGES

1. Calculation of the Artificial Absorption Edges

The twenty sets of (ℓ_ν, λ) pairs which represent the line opacity spectra were converted into twenty similar sets describing the artificial edge spectrum by application of the approach discussed in Chapter I. Each T-P_e case was treated identically, so the description here will be limited to one case. In the subsequent sections the variation of typical edges with T and P_e is described, and special handling of the ultraviolet region, where line data are particularly scarce. The inclusion of the edge opacity in a stellar atmosphere calculation is discussed in the last section.

For a given T and P_e, the line opacity spectrum was obtained from the results in the previous chapter. The blend is then divided into 75 regions, each ending on one of the wavelength limits (i.e., artificial heads) listed in Appendix C. To the red of 8375 Å, the edge opacity is neglected because the line opacity is negligible compared to the continuum for all T and P_e used here. The line opacity of each such region is converted into one artificial edge, which results in a total of 75 edges. Each edge replaces a section of the blend, and is designed to produce the same transfer effects. In particular we desire the atmosphere to have the same flux, mean intensity, and flux derivative independent of whether the detailed blend or artificial edges are used in solving the transfer equation. A test on this is described in Chapter V.

In order to form the edge from its segment of the blended line opacity spectrum, the blend must be subdivided into small slices and sorted into a sequence which ascends toward the red within the interval. Each blend sample was assigned a width in trapezoidal fashion, i.e.,

$$\Delta\lambda_i = \frac{1}{2}\left(\lambda_{i+1} - \lambda_{i-1}\right) \tag{III-1}$$

This width definition guarantees appropriate influence to each sample, and also that the integrated area under the blend will be the same as that under the edge. Thus the (ℓ_ν, λ) pairs which iescribe the blend are in one-to-one correspondence with the (ℓ_ν, λ) pairs which describe the edges.

2. Regions of Scant Data

In Figure III.2-1 a well-established edge is plotted along with its corresponding blend. The shape and behavior of such edges is statistically well-behaved and intuitively plausible. In the far ultraviolet, on the other hand, the line data are extremely scarce. This lack of data, depicted in Figure III.2-2, results in very crudely-shaped and ill-behaved edges which do not appear to be a sufficiently good representation to elicit confidence. The systematic resemblance among the visible edges disappears abruptly at 2000 Å, where the line data thin out rather sudenly toward the blue. This suggests that if all the missing lines could have been included, the UV edges probably would have shared in the resemblance pattern. This supposition is the basis for the arbitrary re-shaping of the UV edges which is described in the following paragraphs. The situation in the red is acceptable, because although the lines are less crowded, the edges there retain the same basic shape and behavior of the visible edges.

There are three methods for employing the data in the UV. Firstly, the line opacity there could be neglected. This would be unwise,

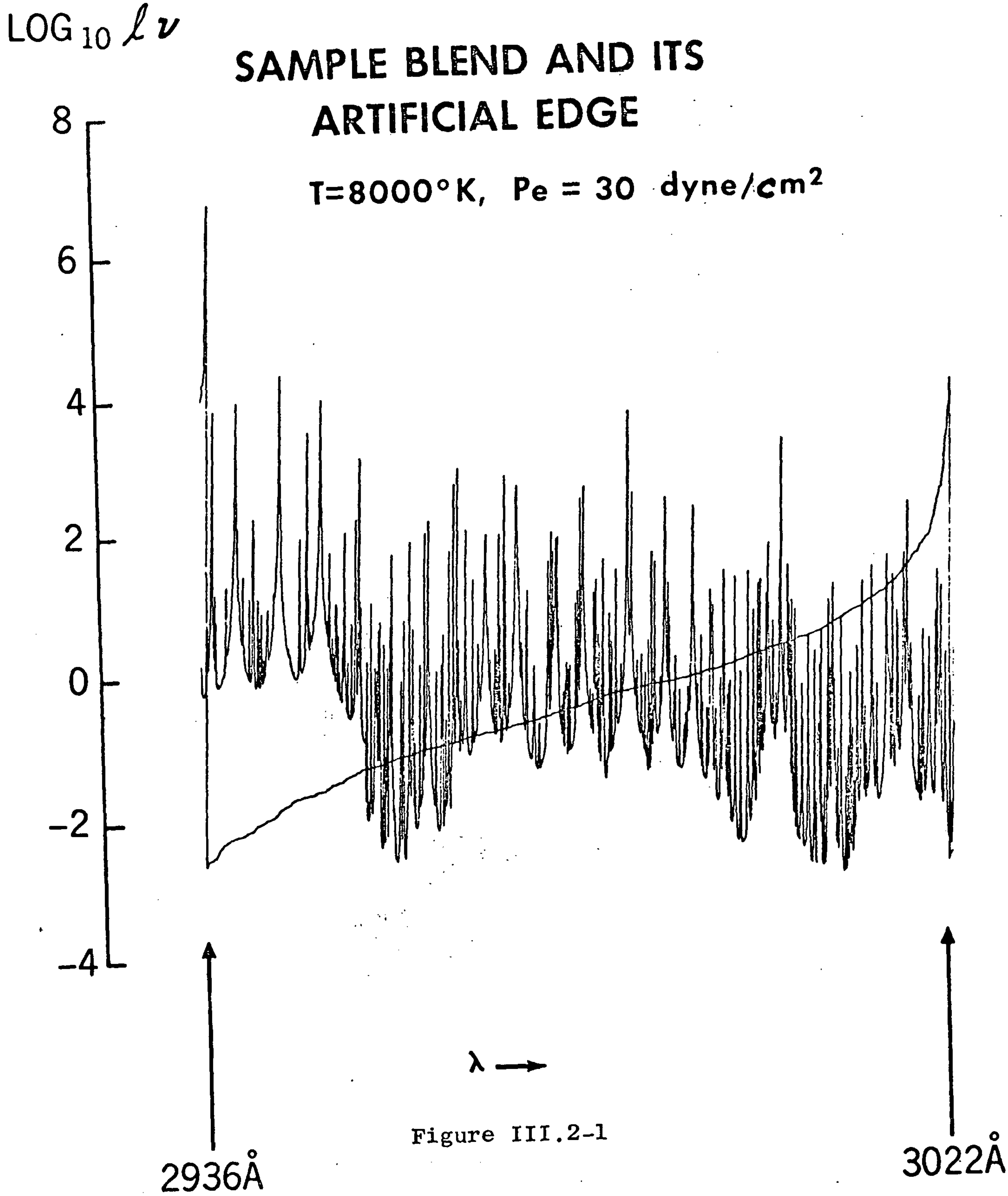

Figure III.2-1

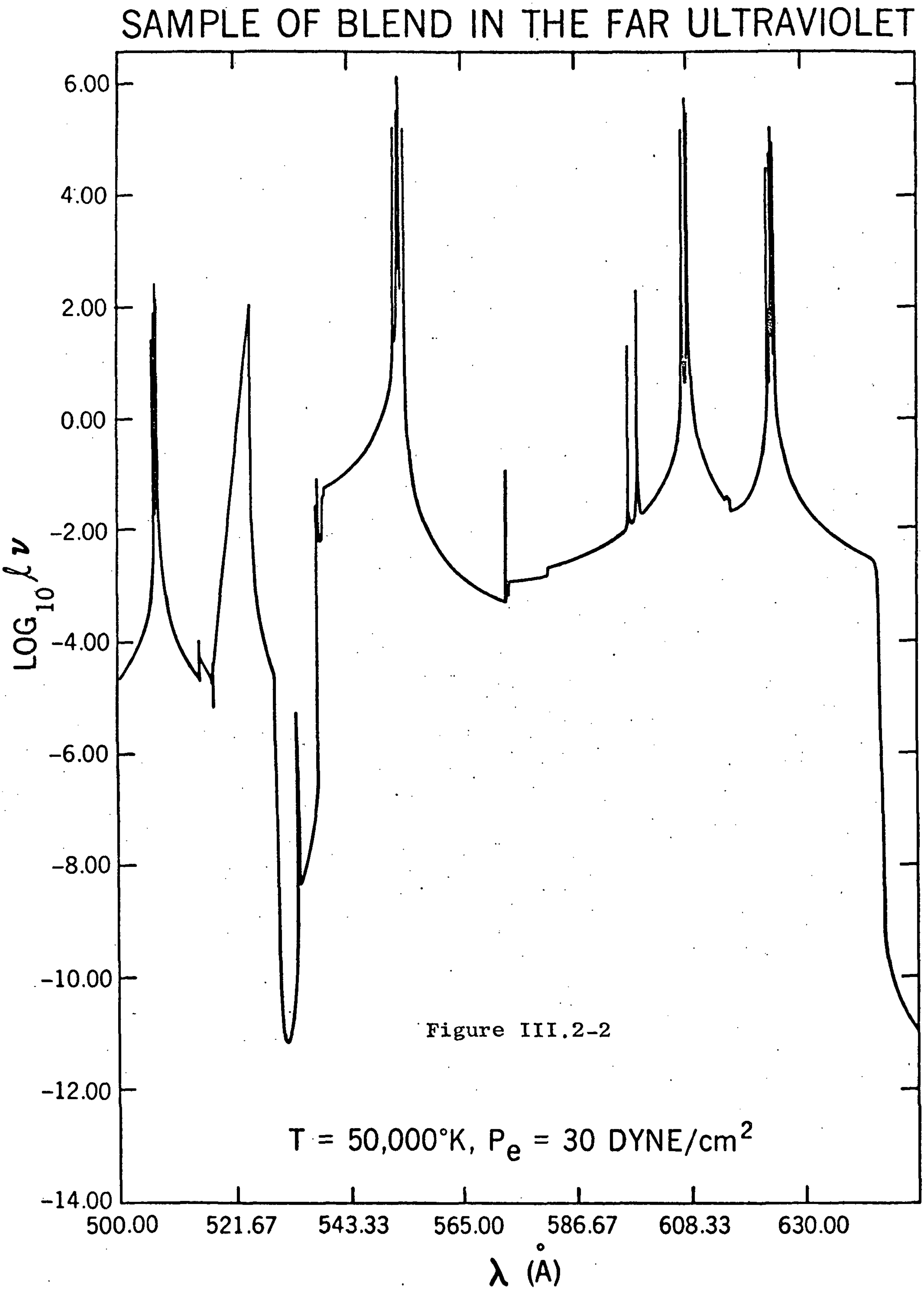

Figure III.2-2

however, because it would leave an opacity hole through which flux could escape when in reality it should have been radiated at different wavelengths. Secondly, the UV edges could be used as they stand. This also is rejected, because there is no similarity from one edge to the next, which is intuitively unacceptable. Furthermore, the UV edge deficiencies obviously stem from the paucity of data, and any reasonable arbitrary guess for the edge shapes and sizes would seem superior as a representation of the UV line opacity. Therefore, the third method must be chosen, namely to attempt to estimate the UV edges from the data which are available in the UV and from the properties of the well-determined edges. The danger in doing this is that the end result will be an overestimate. It is essential to see that this does not happen, even at the risk of underestimating the UV edges. Because we are forced to apply this fix-up, we must accept that the detailed structure of the UV emergent flux will not carry reliable information, and we look to the grosser flux distribution in the UV as the only meaningful quantity. If the amount of blanketing is approximately correct, then the visible spectral features should be about right. An investigation covering these points is described in Chapter V.

The following guidelines were observed in the UV re-shaping:

a. if the interval contained any strong lines, these defined the red end of the edge;

b. if there were no strong lines, then an average maximum opacity of the nearest well-determined edges defined the red end;

c. once the red end of the new edge was fixed, an average shape of unit width and unit maximum opacity was applied to fill out the rest of the edge; this average shape was also determined from the nearest well-established edges;

d. if the new edge fell below the old one at any point, then the red end of the new edge was moved up until this was no longer the case, keeping the same average shape;

e. if the effect of 'd' was to raise the red end to conspicuous prominence, it was set back again, and the edge shape similarity was sacrificed in order to avoid overestimation.

In practice, the entire edge was not treated in this manner; only the edge opacity at the quadrature points was actually adjusted.

3. Behavioral Properties of the Artificial Absorption Edges

Figure III.3-1 illustrates the variation in shape and size of a typical visible edge as T is varied. Figure III.3-2 shows the P_e dependence. The qualitative behavior is essentially what one would expect. In the visible, most of the lines arise from neutral or singly ionized atoms, and so as ionization is enhanced by increasing T or decreasing P_e, these edges diminish in magnitude. The red edges behave in a generally similar fashion. The UV edges tend to increase as ionization progresses because of the domination of ion lines. This edge behavior is a summary of the line behavior. At 50000°K the net variation as P_e increases is upward in magnitude at all wavelengths. At lower temperatures, there is a crossover point where an increase in P_e produces a density increase which just cancels an ionization decrease, leaving the opacity unchanged. Alternatively, an increase in T produces a greater Doppler broadening which offsets an ionization increase. This crossover point usually falls between 1800 and 3000 Å for the T-P_e values employed here. The edges at different T (P_e constant) or different P_e (T constant) tend not to intersect each other except at the

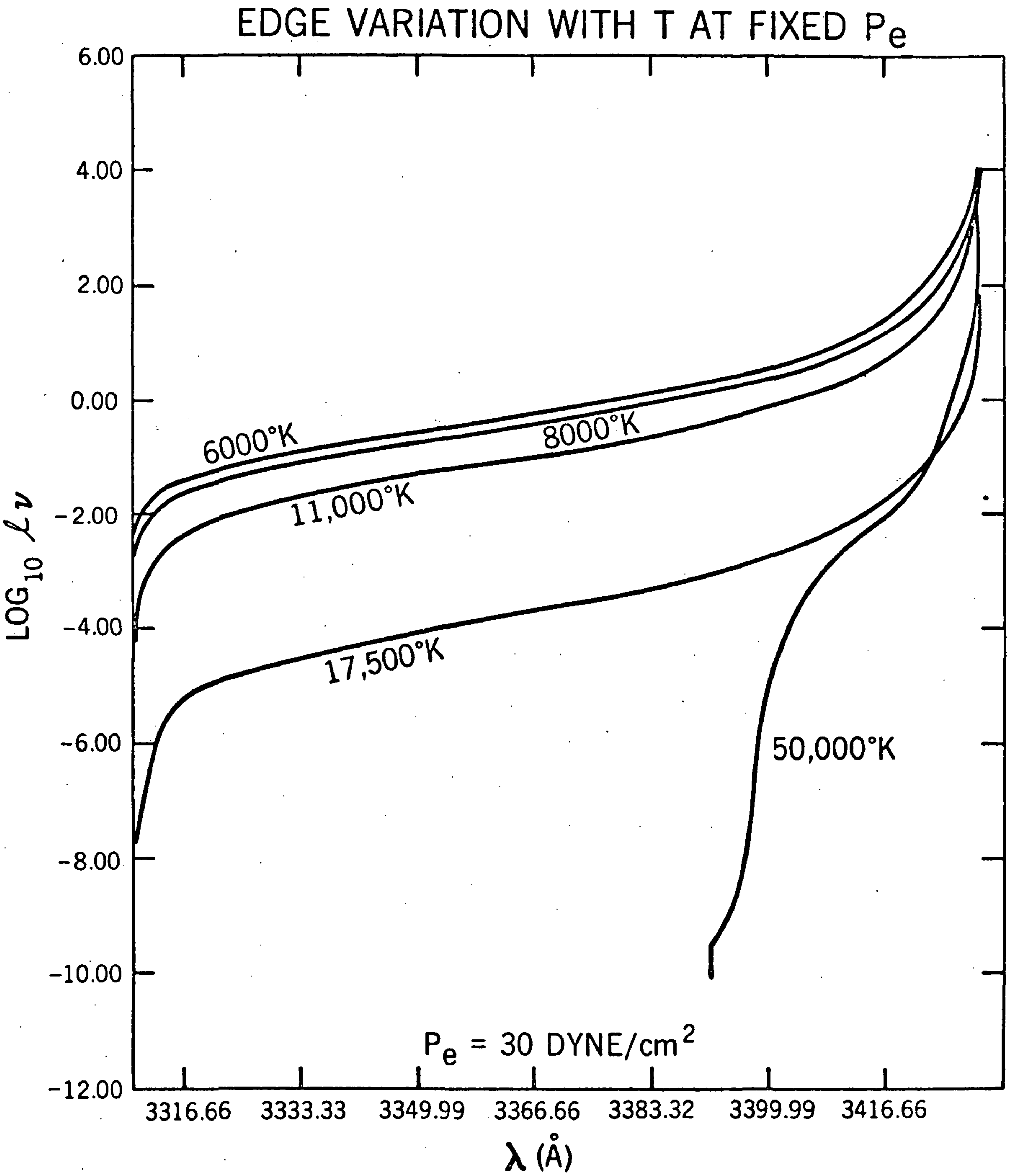

Figure III.3-1

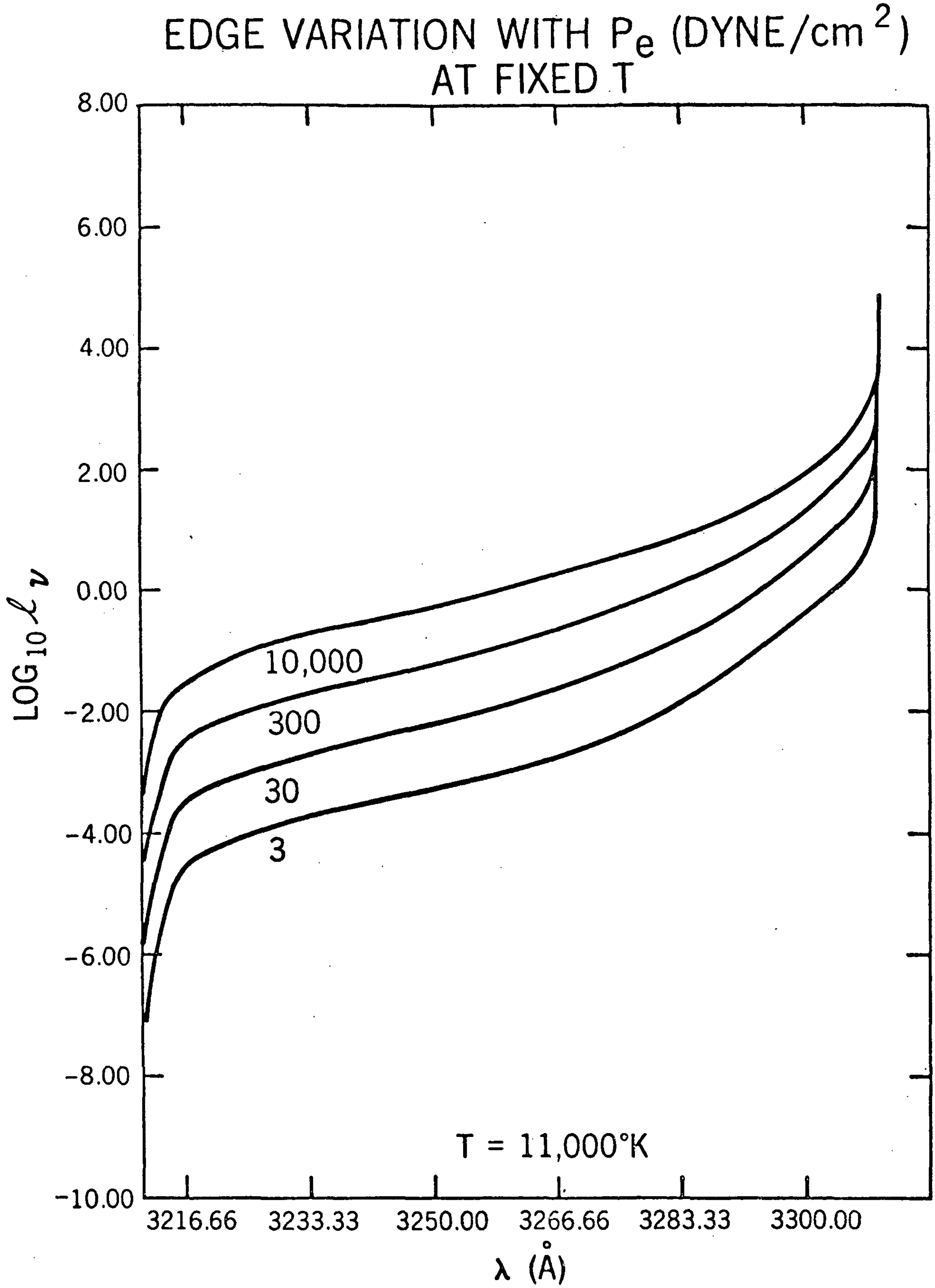

Figure III.3-2

crossover point and at the extremes of the spectrum. In Chapter V a different application of the statistical behavior of the edges is described.

4. Application of the Edge Spectrum

In Chapter I it was stated that the process of calculating a model stellar atmosphere includes integrating certain variables over frequency. When this is done, some sort of quadrature method must be used, because the variables usually cannot be represented in analytically integrable form. The atmosphere computer program which produced the models employed later in this investigation (see Appendix B) uses a Lobatto-Gauss quadrature to perform frequency integrations (third order in the blanketed models). Once the heads of the real and artificial edges are specified, the regions between are assigned four quadrature points. In addition to the 75 edges of the metal opacity, three more infrared hydrogen heads are included, resulting in 78 heads, and hence 312 quadrature points altogether.

At a given quadrature frequency, the edge opacity is a function of T and P_e. The program deals with only one frequency at a time, and so the twenty values of the edge opacity at all T-P_e grid points are read into memory as needed. The program performs double linear interpolations in T and log P_e for the log of the opacity at each depth. The blanketing opacity thus obtained is added to the other opacities for the same frequency.

CHAPTER IV

A BLANKETED MODEL OF SIRIUS

1. Fitting Parameters for Sirius

As an example of an application of the method of artificial edges, a basic blanketed model of Sirius was calculated. The cosmic abundances were employed, and it was not necessary to adjust any abundance in fitting the model to the star. The following spectral features and gravity were used to obtain the best-fit model:

a. the profile and equivalent width of Hγ

b. the absolute flux at 5550 Å

c. the Balmer jump

d. the dynamically determined gravity

e. the slope of the Paschen continuum

f. the relative amount of flux escaping in the Balmer continuum and its general wavelength distribution.

2. The Profile and Equivalent Width of Hγ

The Hγ profile of Sirius has been extensively examined over the years, with the result that it must be considered well-determined. The values of residual intensity as a function of wavelength separation from line center are taken from Peterson (1969). These are listed in Table IV.7-1 with the corresponding values from the model. The Griem theory of Stark broadening was used in calculating the blanketed models, but the ESW profiles (Edmonds, Schlüter, and Wells, 1967) are so similar that the atmospheric structure is independent of which theory was used. The Hγ profile, however, is very sensitive to the detailed frequency dependence of the Hγ opacity, and so both Griem and ESW profiles were used in the fitting process.

The equivalent width employed here was measured from some unpublished observations by R. C. Bless (1969, private communication). The data were obtained with the Pine Bluff 36 inch telescope. Photometric scans in both directions were taken with 10 Å resolution. I measured two forward and two backward scans, and took the residual intensity to be unity at 43 Å from line center. The equivalent widths predicted by the models were calculated accordingly, although the models have residual intensities near 0.96 at $\Delta\lambda$ = 43 Å. This is entirely reasonable, since noise and blended lines make it nearly impossible to follow Hγ with precision much farther in the observations. The result of my measurement is 16.15 ± 0.15 Å, which is in agreement with past determinations.

Twenty-four models were calculated to cover a range in effective temperature, T_{eff}, and in gravity, expressed as Log g. All the fitting parameters were evaluated for each model, and their behavior in the T_{eff} - Log g plane near (10000, 4) was established. Contours in this plane were then located which enclosed the models that gave results within the observational uncertainties. Figure IV.2-1 shows these contours for the equivalent width and detailed profile of Hγ. To fit the profile, the standard deviation of the fit was required to be less than the standard deviation of the uncertainty distribution of the observations, namely σ = 0.015. The behavior of the equivalent width is discussed in section 10 below.

FITTING CONTOURS FOR Hγ

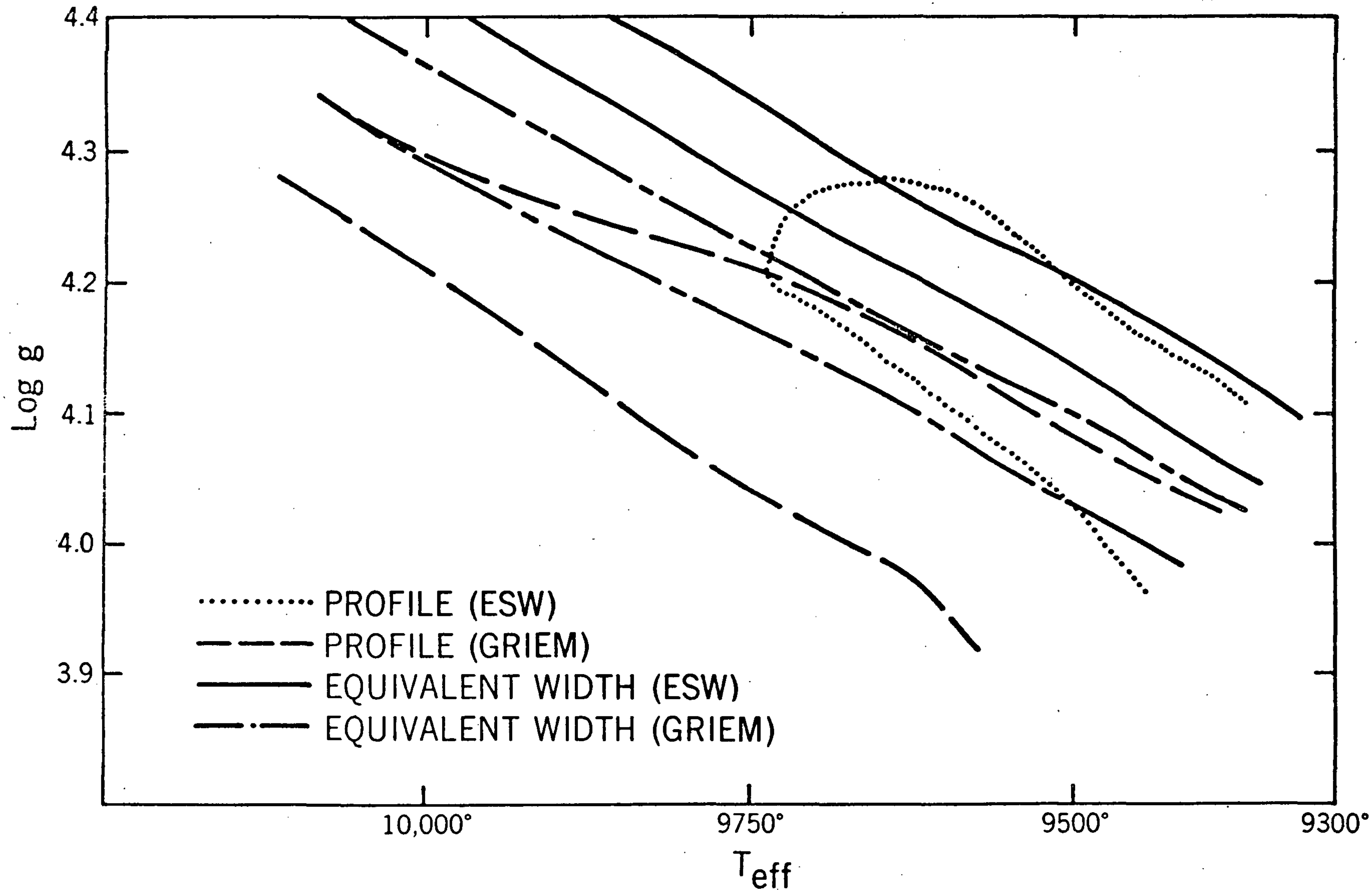

Figure IV.2-1

3. The Absolute Flux at 5550 Å

A number of observers have made absolute measurements of the flux from A stars incident at the top of the earth's atmosphere. These results are reduced to a common basis, and are presented as a flux from a star with V = 0 and B - V = 0. This work is reviewed by Latham (1970), who also gives references for the various sources of data employed. The result for the absolute flux at 5550 Å is $\pi F = (3.58 \pm 0.14) \times 10^{-9}$ erg/sec/cm^2/Å. Applying this to Sirius, with V = -1.46, and using the angular diameter of Sirius to convert to flux emergent from the stellar surface, gives $\pi F = 6.25 \times 10^7$ erg/sec/cm^2/Å. The angular diameter is also used in obtaining the gravity, and will be mentioned again in section 5. The models show negligible gravity dependence in πF_{5550}, and the 5% uncertainty places the model between 9550°K and 9935°K in T_{eff}.

4. The Balmer Jump

The data of Schild, Peterson, and Oke (1971) were plotted, and the Balmer Jump of Sirius was obtained graphically. The exact same procedure was used to calculate the Balmer jumps in the models. The observed value for Sirius is 0.516 ± 0.010, where the standard definition is used, i.e., BJ = log (F_{3700^+}/F_{3700^-}). This quantity is the least regularly behaved of the fitting parameters, lacking monotonicity in T_{eff} and log g in the range of consideration here. The models predict a local maximum at about (9600, 4.2), where the Balmer jump is 0.56.

5. Log g

The gravity of Sirius can be determined from the orbital parameters of the Sirius A and B system. Latham (1970) gives results and references for this work. The result is influenced by stellar atmosphere theory only in correcting the observed angular diameter for limb darkening.

The gravity was actually the last parameter considered in the fitting process. Separate fitting was done for Griem and ESW profiles of $H\gamma$, and except for Log g, both broadening theories had an area of the T_{eff} - Log g plane where all the fitting areas intersected. The Griem area, however, lay significantly outside the gravity contour. The orbital determination requires Log g to lie between 4.255 and 4.310. The best Griem model had Log g = 4.18. The determination of Log g makes use of the angular diameter obtained by Hanbury Brown _et al_ (1967), which incorporates a limb darkening correction based on a linear limb darkening law. Thus it was necessary to calculate the limb darkening in the models to decide whether the linear law was applicable to sufficient accuracy to warrant forsaking the Griem model. A discussion of the limb darkening is given separately below. Here we need only mention that the linear law is generally quite good for the models, i.e., it describes the non-linear limb darkening quite well. The limits on the gravity were thus maintained, and the attempt to fit Sirius with Griem $H\gamma$ profiles ended in failure.

The angular diameter employed is $(6.12 \pm 0.10) \times 10^{-3}$ arc seconds. In order to salvage the Griem model, the limb darkening would have had to be so severe as to produce a corrected angular diameter of 6.81×10^{-3} arc seconds. But in fact, this would not have saved any models; such an angular diameter would have made agreement with the πF_{5550} parameter impossible for all the models. Instead, it was necessary to fit Sirius with ESW profiles alone for $H\gamma$.

6. The Paschen Slope and Balmer Flux Distribution

The Paschen slope and Balmer flux fitting parameters are the least useful in arriving at the best-fit model of Sirius. This is because the Paschen slope is more sensitive to the selection of wavelengths employed in its definition than to T_{eff} and Log g, and the Balmer flux distribution is not well-established by the observations. Yet both of these parameters represent final constraints on the best-fit model. Here we simply require the final model to satisfy these constraints after the other fitting parameters are optimized. As luck would have it, we shall see that this can be done, so that we escape without further complications. In the absence of a universal definition of the Paschen slope, I have used the expression

$$S_p = -(m_{4245} - m_{7900})/(7900 - 4245)$$

where $m_\lambda = -2.5 \log F_\lambda$. Applying this to the data reported by Latham yields $S_p = (5.63 \pm 0.11) \times 10^{-4}$ mag/Å. The Paschen slopes of the models were calculated with the same definition.

The spectral distribution of the Balmer flux is very sensitive to the shape of the UV blanketing opacity, which is as significant as the continuous opacities. The T-P_e dependence of the blanketing opacity appears to be equally important. Unfortunately, the T-P_e-λ dependence cannot be deduced from the flux spectrum, since the problem is underdetermined. This handicap could be alleviated if at some future time the limb darkening could be measured in Sirius. Admittedly, this would require a substantial advance in observational techniques. A complete set of line data would suffice for calculating the theoretical T-P_e-λ distribution of the UV blanketing uniquely. In the meantime, we must proceed by making reasonable estimates, while attempting to ascertain the consequences of estimating wrongly. This last topic is deferred until Chapter V. For now, we simply aim at obtaining the best-looking total amount of flux in the Balmer continuum, which for Sirius appears to be quite close to 30% of the total flux. Since we have been forced to re-shape the UV edges in a fashion based on intuition and designed not to overestimate the opacity, we must be careful in interpreting the detailed shape of the UV emergent spectra of the models. Most of the spuriously generated features appear to be removed effectively by combining each three edge intervals into one larger band in the UV. This minimal smoothing leaves the gross flux distribution in a condition which can still be compared to the observations. The spectra of the blanketed models which are to be given later (see Appendix A) employ this form of representation.

Observations of the UV spectrum of Sirius are extremely difficult to make because of all the usual technical problems which arise in this part of the spectrum. To date the best results differ by up to 50% in magnitude and spectral distribution. Nevertheless they indicate convincingly that there is substantially less flux in the Balmer continuum than in the Paschen. Attempts to fit Sirius with hydrogen line-blanketed models have tended to require effective temperatures greater than 10000°K, in which case the Balmer continuum carries about half the total flux (Latham, 1970; also corroborated by my own hydrogen line-blanketed models). Furthermore the $T(\tau_0)$ distribution is always too high near the surface to reproduce the hydrogen lines well. The inclusion of metal line blanketing cures this affliction, because a large amount of flux becomes redistributed from the Balmer continuum to the Paschen. This boosts the flux at 5550 Å, and lower effective temperatures can be used in the fitting. The lowered effective temperatures result in even less Balmer flux, and the blanketed $T(\tau_0)$ distributions reproduce the hydrogen lines quite well. This is because the cores are formed at lower temperatures, while the wings are formed at equally high temperatures.

The overall spectrum of Sirius to which the models are compared is put together from the rocket data of Evans (1971) and Stecher (1970), and the ground-based visible data of Schild, Peterson, and Oke (1971). The best-fit model is determined independently of the UV flux, but is judged on the basis of whether significant agreement or discrepancy develops.

The data of Evans and Stecher are employed here because they are the most recent, they are in fair agreement over much of the Balmer continuum, and they tend to fall into the middle of the scatter of past observations. The Wisconsin Experiment Package on the OAO-II satellite also observed Sirius (Bless, Fairchild, and Code, 1971), and the data it obtained agree well with those of Evans and Stecher between 2000 and 2800 Å. Below 2000 Å the OAO-II data lie thirty to fifty percent above Evans' data. The OAO-II instrument was designed primarily for observing stars much fainter than Sirius, but whether this is significant is still part of a continuing investigation.

This observational discrepancy is of more concern to the observers than to this stage of model fitting, however, because of the following reason. As shown in Chapters V and VI, various approximations for the UV blanketing opacity may drastically alter the shape of the emergent flux in the Balmer continuum, while the atmospheric structure and spectral features of the Paschen continuum may be negligibly changed. In view of the uncertainties in both the UV observations and the blanketing opacity, we look for qualitative agreement only between theory and measurement in the UV.

7. The Best-fit Model of Sirius

The contours of all the fitting parameters intersect in a small area of the T_{eff} - Log g plane if ESW profiles of Hγ are used. This area lies at $9610° \leqslant T_{eff} \leqslant 9725°K$ and $4.255 \leqslant \text{Log } g \leqslant 4.265$. The point whose fit I prefer for subjective reasons is (9700, 4.26), but there is scarcely any latitude for preferences in any case. The quality of the Hγ fit is shown in Table IV.7-1, and the observed and synthesized profiles are plotted in Figure IV.7-1. In order to judge the Hγ fit, it is necessary also to interpret the observed profile from the point of view of the model. In other words, taking the model as gospel temporarily, would the observed profile follow? At $\Delta\lambda = 40$ Å the residual intensity is 2.2% greater in the observed profile, which seems reasonable by the same argument we used in discussing the equivalent width. If the model were correct, however, then a re-normalization of the observed profile to a 2.2% greater continuous flux should not destroy the fit. This correction is made, and the results are also listed in Table IV.7-1. In fact, the fit is improved. The significance of this is not a proof that the model is 'correct', but only that the model is not proved to be incorrect. Nevertheless it is encouraging, because the standard deviations of the observed residual intensity are about equal to the discrepancy in the fit. The synthesized profile is acceptable without the correction, however, and it seems clear that only the inclusion of non-LTE effects could improve the fit by bringing the core down slightly.

C.2

Table IV.7-1

Hγ Profile

$\Delta\lambda$	$I(\Delta\lambda)/I(0)$ Model	Observed	Error(%)	$I(\Delta\lambda)/I(0)$ Observed(Corrected)
1	0.306	0.281	8.9	0.275
1.5	0.332	0.313	6.2	0.306
2	0.357	0.340	4.9	0.333
3	0.402	0.389	3.3	0.381
4	0.443	0.435	1.8	0.426
5	0.482	0.475	1.4	0.465
6	0.519	0.515	0.7	0.504
7	0.554	0.552	0.3	0.540
8	0.588	0.589	-0.2	0.576
9	0.620	0.622	-0.3	0.609
10	0.650	0.655	-0.7	0.641
12	0.706	0.708	-0.3	0.693
14	0.753	0.760	-0.9	0.744
16	0.793	0.805	-1.5	0.788
18	0.826	0.840	-1.7	0.822
20	0.853	0.869	-1.8	0.850
22	0.875	0.895	-2.2	0.876
24	0.893	0.911	-2.0	0.891
26	0.907	0.929	-2.4	0.909
28	0.919	0.940	-2.2	0.920
32	0.937	0.959	-2.3	0.938
38	0.953	0.975	-2.2	0.954

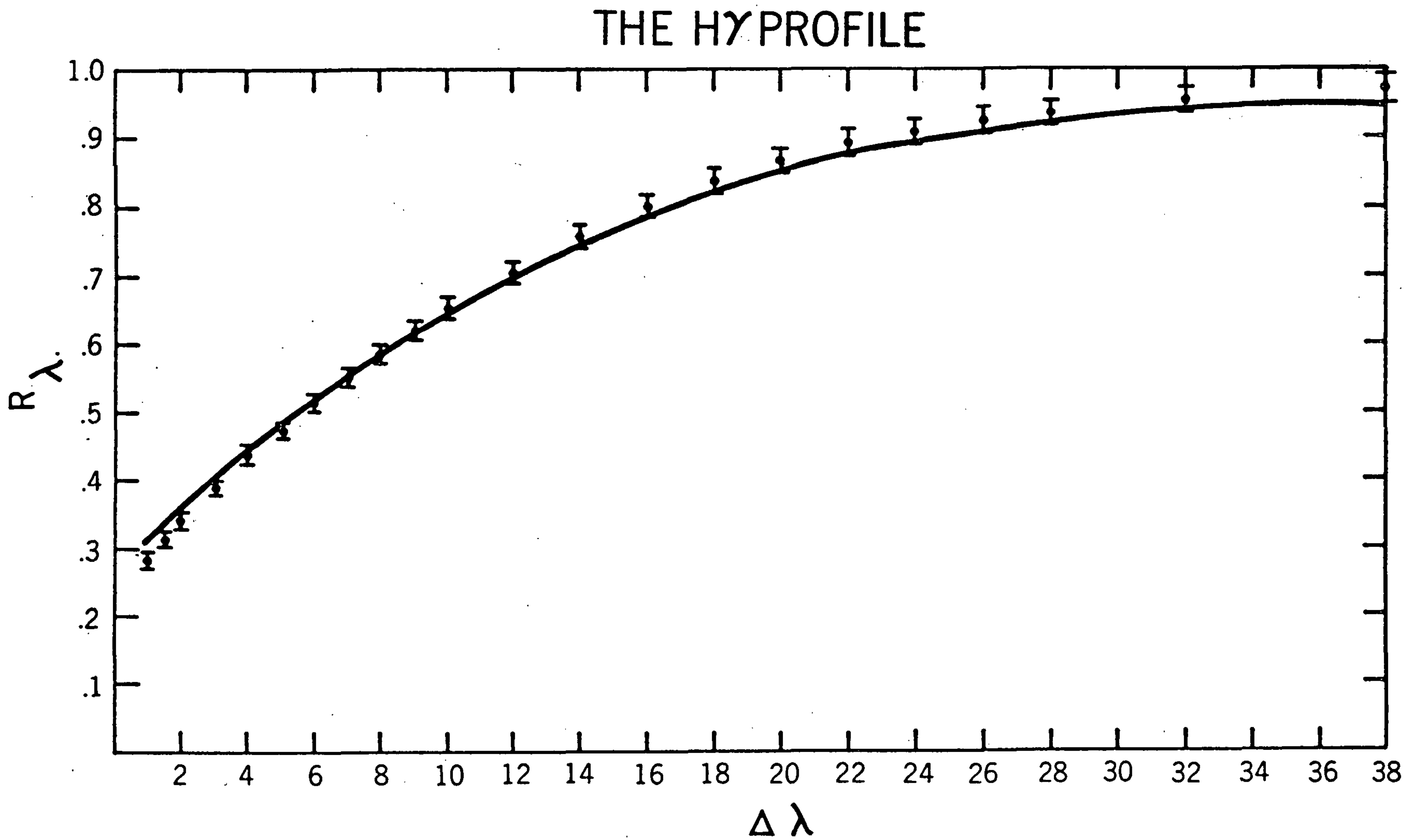
THE Hγ PROFILE
1.0
.9
.8
.7
.6
.5
.4
.3
.2
.1
R_λ
2 4 6 8 10 12 14 16 18 20 22 24 26 28 30 32 34 36 38
Δλ

Figure IV.7-1

The equivalent width of Hγ also appears to be reproduced optimally by the model, where it has the value 16.06 Å. The missing non-LTE core is about all that is necessary to explain the difference between this and the observed 16.15 ± 0.15 Å.

As we had hoped, the Paschen slope of the model agrees closely with the observed value, with an insignificant discrepancy of 0.35%. The flux πF_{5550} is also well-reproduced by the model, since 9700°K lies almost at the middle of the fitting area for that parameter. The Balmer jump is 0.499 in the model, which lies within the intersection of uncertainties on the low side. It has the greatest discrepancy of all the fitting parameters, being 3.4% off the central value of the observation. In Chapter V it is shown that this is probably due to the UV blanketing opacity being slightly underestimated. The model's gravity lies within the uncertainty of the orbital determination on the low side. These results are summarized in Table IV.7-2.

In Figure IV.7-2 the overall spectrum of the model is plotted along with the observed data. The model spectrum has not been normalized to the observations. The model flux is obtained by applying the angular diameter of Sirius to convert from emergent flux at the stellar surface to flux incident at the earth, ignoring the apparently remote possibility of reddening. Below 3400 Å the model is represented as if observed with a 300 Å filter. Above 3400 Å a 100 Å filter applies. The UV model spectrum at 100 Å resolution suffers too much from the effects of spurious opacity windows, which were generated in the re-shaping when enough lines existed in an interval so that a higher estimate was not used, but the same lines did not represent the strongest lines that probably should have been included if the line data were effectively

Table IV.7-2

Sirius Fitting Parameters

Parameter	Observed	Model	-- Error -- Absolute	Relative
Hγ Profile (σ)	0.0150	0.0149		
Hγ Equivalent Width (Å)	16.15 ± 0.15	16.06	0.09	0.56%
Paschen Slope (mag/Å)	5.63×10^{-4} ± 2%	5.65×10^{-4}	2×10^{-6}	0.35%
πF_{5550} (erg/sec/cm^2/Å)	6.252×10^7	6.242×10^7	10^5	0.16%
Balmer Jump	0.516 ± 0.010	0.499 ± 0.010	0.017	3.4 %
Log g	4.282 ± 0.03	4.26	0.022	0.51%

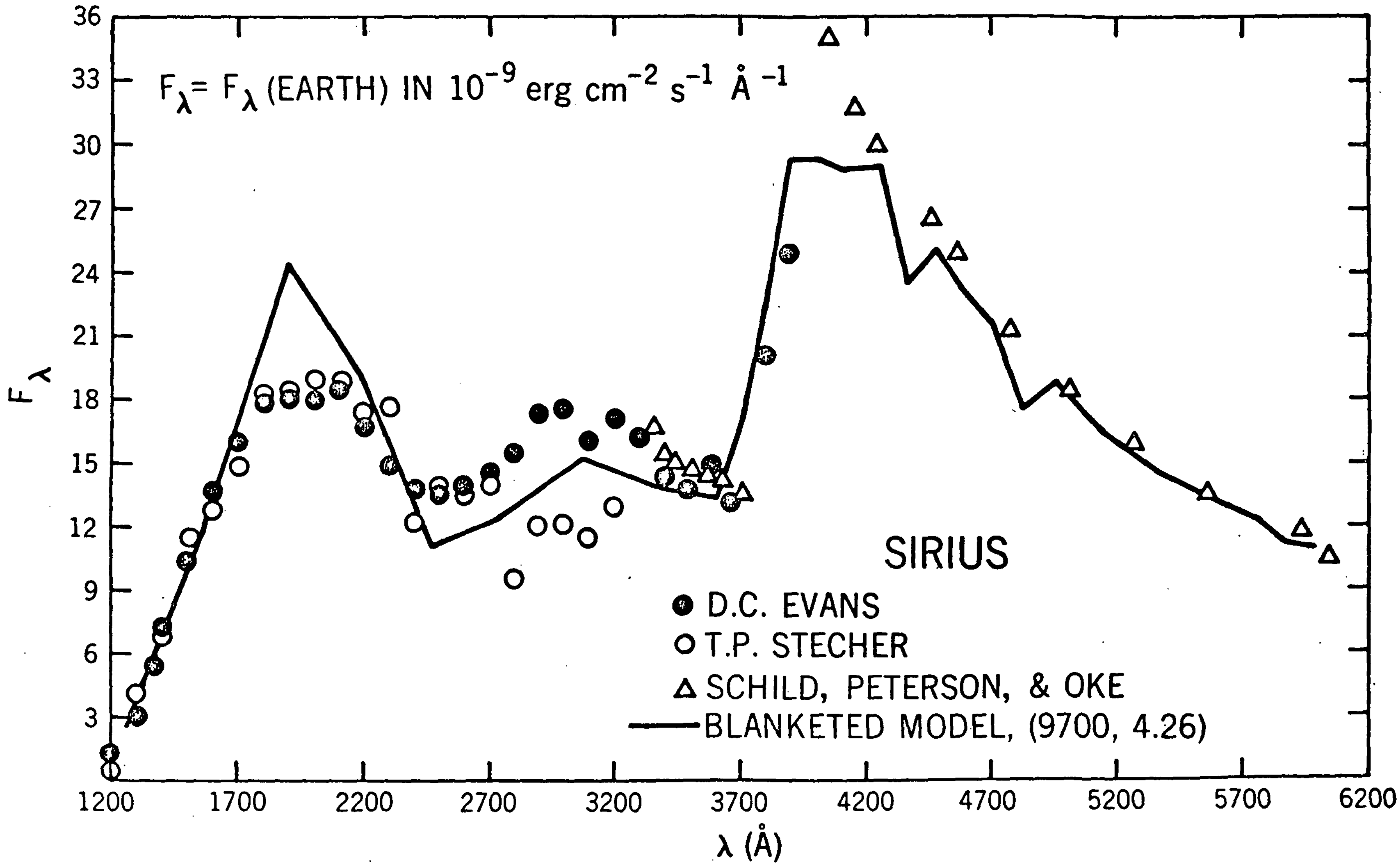

$F_\lambda = F_\lambda$ (EARTH) IN 10^{-9} erg cm^{-2} s^{-1} Å^{-1}
SIRIUS
D.C. EVANS
T.P. STECHER
SCHILD, PETERSON, & OKE
BLANKETED MODEL, (9700, 4.26)
F_λ
36
33
30
27
24
21
18
15
12
9
6
3
1200
1700
2200
2700
3200
3700
4200
4700
5200
5700
6200
λ (Å)

Figure IV.7-2

complete. This interpretation is compatible with the idea that the UV edges are slightly underestimated, as is the slightly low Balmer jump. Further discussion may be found in Chapter V.

The temperature range of the fit is determined by Hγ, whose profile and equivalent width are both unacceptable beyond the endpoints. To the hot side the Balmer jump also drops too low. The gravity parameter places the lower limit on Log g at 4.255, and the upper limit is also set by Hγ.

Figure IV.7-2 shows that a remarkable agreement exists between theory and observation over the entire spectrum. The fit in the Balmer continuum is very gratifying for several reasons. Firstly, the model predictions lie well within the observational scatter everywhere except near 1800 Å, and there the discrepancy is equal to the Evans--OAO-II discrepancy. Also the total amount of flux in the Balmer continuum is in good apparent agreement. The model has 31% of its total flux in this region, and Sirius has very nearly the same, depending upon which sets of data one weights the most heavily. The total flux matches to the same accuracy. Thus the Balmer-to-Paschen flux redistribution is as close to being correct as can now be determined, and this effect is the most easily identified of the metal blanketing influences. The structure of the atmosphere appears to be quite realistic in spite of the approximations that were made along the way. The blanketed structure does very well in the Paschen continuum also, strengthening the claim of realism, which must be preceded by self-consistency. Between Hδ and the ionization limit, the data of Schild, Peterson, and Oke do not show the large fluctuations produced by the Balmer lines. Instead they followed the continuum between lines as far as possible. The model flux as plotted follows the smoothed fluctuating spectrum, and it fits Bless's data very well. The actual amount of discrepancy is negligible. The models' Balmer jumps are corrected for this effect, which is the source of the uncertainty quoted in the theoretical values.

Finally it must be recalled that the goal of this analysis involved attempting to describe the blanketing opacity as correctly as possible without overestimating it. In Chapter V it is argued that we have come sufficiently close to this goal for present purposes, and have indeed slightly underestimated the blanketing. Furthermore, compared to Evans' data, the additional blanketing required to achieve agreement to unwarranted precision would be too small to produce significant changes in the structure or the Paschen spectral features. This point is discovered in calculating an over-blanketed model in the next chapter. Detailed tables of the rest of the models' parameters are given in Appendix A.

8. Blocking Factors

In the evolution of stellar atmosphere theory, continuum models logically preceded line-blanketed models. Not so long ago the primary concern in fundamental theory was the correct specification of the continuous opacities, after which came the problem of non-grey methods. Stellar spectra were interpreted in terms of these continuum models, and the flux blocked by lines was treated as a separate problem. It is interesting at this time to compare a blanketed model to the same kind of continuum models that have been used in the past. It is also of interest to compare the flux of a continuum model to a corresponding 'continuous' flux from the blanketed model. It must not be forgotten, however, that the 'continuous' flux of an atmosphere whose structure incorporates line blanketing cannot be given a rigorous physical interpretation. Instead we make the mathematical definition of this continuous flux to be the transfer solution for zero blanketing opacity based on the blanketed structure. Since the structure is coupled to the flux through the constraint of radiative equilibrium, to neglect the blanketing in the transfer is to neglect this coupling. This inconsistency is the reason why the 'continuous' flux must be treated as an academic concept except at such wavelengths where the line opacity at all depths may be considered negligible. The numerical approach, however, precludes mathematically perfect radiative equilibrium. At best, most models retain some flux error at all depths, usually of the order of one half of one percent. To this extent the coupling may be neglected, since it is the limit on the model's physical meaning.

The concept of a blocking factor was designed to relate observed spectra to theoretical continuum models. Blocking factors should not be considered a representation of the interaction between line opacity and continuous flux. They are simply the best way to make spectrum corrections for an effect whose calculation is time-consuming. The flux in the continuum model is generally very different from the flux with which the line opacity interacts in a blanketed model. Furthermore, the structure of the continuum model may be a poor representation of the 'correct' structure, even though a set of reasonable blocking factors may be able to transform one spectrum into the other.

A set of blocking factors is presented below which relates the blanketed flux of the Sirius model to the mathematically defined 'continuous' flux of the same model. This is the best estimate of the blocking factors that would apply to Sirius. But if one were forced to work without blanketed models, as in the past, one would not have the blanketed structure to work with. Therefore, another set of blocking factors would be of interest, one which relates the blanketed flux to the flux of a continuum model which might have been chosen as a theoretical basis for an analysis of Sirius. But a given investigator would apply his own set of fitting parameters to select an appropriate continuum model, so no unique set of blocking factors can be derived here. In order to make any comparison, we note that since the integrated flux of the Sirius model corresponds to an effective temperature of 9700°K, and since the present absolute measurements imply that this is indeed about right for Sirius, then a 9700° continuum model seems to be an excellent choice. Unfortunately this choice leads to blocking factors over most of the spectrum which describe negative flux blockage. Actually this is perfectly all right, except that it clearly does not mimic past blocking factor analyses. If only hydrogen lines are included with the continuous opacities in the transfer solution, then the integrated flux of the Sirius structure corresponds to 10390°. Without any lines, the effective temperature is 11160°. Blocking factors based on a 11160° continuum model come out generally close in the ultraviolet to those based on the hypothetical zero-blanketing continuum of the Sirius model. The utility of these blocking factors might be challenged on the basis that there would have been no way to know that 11160° was a good effective temperature. In fact, absolute flux measurements in the Paschen continuum would indicate a substantially lower value. Since there is really no need to resolve these issues, we include two sets of blocking factors, one based on a 9700° continuum model and one based on an 11160° continuum model. The three sets are listed in Table IV.8, along with the midpoints and widths of the bands within which the fluxes are calculated. We take the blocking factor to be the ratio of the blanketed flux to the corresponding continuous flux, and use the following notation:

F_B = blanketed flux from the Sirius model

F_C = 'continuous' flux from the Sirius model

F_{C1} = continuous flux from the 9700° continuum model

F_{C2} = continuous flux from the 11160° continuum model.

9. Limb Darkening

The monochromatic linear limb darkening coefficient was calculated as in the paper by Klinglesmith and Sobieski (1970), where the limb darkening is fit with a non-linear law and transformed to an equivalent linear representation. This results in a coefficient for the linear law which can be compared to that used by Hanbury Brown et al (1967) in obtaining the angular diameter of Sirius. The linear law is

$$\frac{I_\lambda(\mu)}{I_\lambda(1)} = 1 - u_\lambda(1-\mu)$$

Hanbury Brown used $u_\lambda(4425\ \text{Å}) = .6$, and showed that variation from zero to one produced a variation of only about 2% in the angular diameter. The limb darkening coefficients here are slightly smaller, but are in good agreement with those of Klinglesmith and Sobieski. They are wavelength dependent because the depth variation of the total opacity is wavelength dependent. The limb darkening depends mostly on the distribution of the opacity over τ_0. If the opacity is nearly constant over depth, the limb darkening is small. As the opacity becomes stronger only the surface can be seen at disk center and limb, and so

TABLE IV.8 BLOCKING FACTORS

BAND	MID LAMBDA	WIDTH	FB/FC	FB/FC1	FB/FC2
1	252.	504.	1.0079	1.1815	0.7992
2	658.	307.	1.0001	1.1070	0.8623
3	970.	319.	0.0084	0.0247	0.0094
4	1282.	304.	0.0318	0.0850	0.0331
5	1592.	316.	0.2541	0.6075	0.2423
6	1901.	301.	0.7212	1.5478	0.6461
7	2199.	295.	0.7193	1.4114	0.6242
8	2473.	254.	0.5017	0.9168	0.4300
9	2768.	336.	0.6326	1.0869	0.5420
10	3073.	275.	0.8844	1.4316	0.7619
11	3378.	334.	0.9053	1.3972	0.7862
12	3596.	102.	0.9460	1.4134	0.8268
13	3702.	110.	0.3648	0.5238	0.3527
14	3797.	80.	0.5101	0.7276	0.4919
15	3894.	113.	0.7245	1.0279	0.6975
16	3995.	90.	0.7809	1.1004	0.7504
17	4111.	142.	0.8359	1.1706	0.8015
18	4245.	126.	0.9266	1.2863	0.8865
19	4365.	114.	0.8195	1.1302	0.7828
20	4475.	106.	0.9363	1.2835	0.8934
21	4589.	122.	0.9375	1.2778	0.8936
22	4705.	109.	0.9474	1.2828	0.9014
23	4822.	127.	0.8358	1.1251	0.7945
24	4945.	118.	0.9531	1.2753	0.9051
25	5053.	98.	0.9718	1.2934	0.9220
26	5147.	90.	0.9437	1.2503	0.8948
27	5248.	112.	0.9458	1.2474	0.8963
28	5361.	113.	0.9470	1.2428	0.8970
29	5486.	138.	0.9631	1.2569	0.9116
30	5627.	144.	0.9788	1.2702	0.9260
31	5753.	108.	0.9937	1.2829	0.9398
32	5858.	101.	0.9605	1.2351	0.9081
33	5959.	102.	0.9992	1.2801	0.9446
34	6056.	92.	0.9927	1.2673	0.9383
35	6154.	103.	0.9678	1.2312	0.9145
36	6258.	107.	0.9763	1.2379	0.9227
37	6376.	129.	0.9832	1.2416	0.9292
38	6482.	82.	0.9712	1.2223	0.9175
39	6593.	140.	0.8712	1.0928	0.8230
40	6713.	100.	0.9954	1.2439	0.9405
41	6813.	100.	0.9976	1.2431	0.9428
42	6913.	101.	0.9984	1.2409	0.9437
43	7018.	108.	0.9877	1.2237	0.9334
44	7141.	138.	0.9873	1.2192	0.9327
45	7270.	119.	0.9929	1.2225	0.9389
46	7383.	108.	0.9929	1.2187	0.9388
47	7513.	151.	0.9822	1.2015	0.9286
48	7669.	162.	0.9965	1.2151	0.9426
49	7820.	140.	0.9641	1.1721	0.9125
50	7968.	155.	0.9734	1.1798	0.9213
51	8125.	160.	0.9813	1.1852	0.9292
52	8290.	170.	0.9665	1.1768	0.9268
53	11482.	6213.	1.0000	1.1745	0.9599
54	18691.	8206.	1.0000	1.1157	0.9666
55	27809.	10029.	1.0000	1.1016	0.9691
56	32823.	32823.	1.0000	1.0851	0.9703

the darkening coefficient goes to zero. When the opacity is strong at depth but weak at the surface, the limb darkening is of intermediate proportion, and it is at such wavelengths that most observational studies are done. When the opacity is strong at the surface but weak at depth, the darkening is maximized, and u_λ occasionally becomes greater than unity, indicating that the linear law cannot describe the limb darkening at that wavelength. This occurs only inside strong absorption lines. Table IV.9 lists the coefficients at all quadrature wavelengths for the Sirius model. The values tend to vary in wavelength with a period of four quadrature points. This results from the fact that each artificial edge covers four points, each of which has successively greater opacity.

10. The Behavior of the Hγ Equivalent Width in the T_{eff} - Log g Plane

In the course of matching a model to an observed star, the behavior of all fitting parameters in the T_{eff} - Log g plane must be investigated. This behavior is deduced by generating a grid of models over a section of the plane. Some parameters behave in a complicated fashion and are difficult to describe with simple relations, such as the Balmer jump. Others are trivial, such as πF_{5550}. Some are multi-dimensional, such as the detailed profile of Hγ. One important parameter is the equivalent width of Hγ, whose theoretical calculation was discussed in section 2 above. It is also well-behaved, and its relationship to T_{eff} and Log g can be described well by an empirical equation.

The lines of constant Hγ equivalent width in the region of interest here are graphed in Figure IV.10-1. These lines show the behavior predicted by the models, and are represented to an accuracy of 0.1% by the formula

$$W(H\gamma) = \frac{\log g - 4.9 \times 10^{-5}(T_{eff} - 10^{4}) - 1.848}{3.41 \times 10^{-5}(T_{eff} - 10^{4}) + .1616}$$

It must be noted that the equivalent width given by this formula corresponds to a measurement wherein $H\gamma$ is followed out to 43 Å from line center. Far from (10000, 4) in the plane, this ceases to mimic the observational process.

TABLE IV.9 U(LAMBDA)

THE MONOCHROMATIC LINEAR LIMB DARKENING COEFFICIENT

LAMBDA	U	LAMBDA	U	LAMBDA	U
130.68	0.0	1521.08	1.254	2791.32	0.660
151.63	0.0	1548.18	1.612	2829.86	0.648
204.75	0.0	1594.13	0.278	2894.53	0.631
261.34	0.0	1623.92	0.013	2935.99	0.0
261.36	0.0	1623.94	1.248	2936.01	0.602
289.34	0.0	1656.92	1.602	2959.28	0.594
349.97	0.0	1713.23	0.056	2997.73	0.602
402.03	0.0	1749.98	0.0	3021.99	0.198
402.05	0.0	1750.00	1.140	3022.01	0.570
425.91	0.0	1776.54	1.132	3048.73	0.561
471.15	0.0	1821.23	1.179	3092.99	0.559
504.26	0.0	1849.99	0.073	3120.99	0.453
504.28	0.0	1850.01	1.103	3121.01	0.536
529.82	0.0	1874.85	1.147	3145.32	0.529
577.11	0.0	1916.49	0.937	3185.46	0.531
610.81	0.0	1943.16	0.247	3210.78	0.450
610.83	0.0	1943.18	1.059	3210.80	0.507
634.69	0.0	1971.95	1.049	3237.62	0.499
677.51	0.0	2020.34	1.104	3281.97	0.501
706.99	0.0	2051.46	0.449	3309.99	0.079
707.01	0.0	2051.48	1.009	3310.01	0.477
732.99	0.0	2073.76	1.007	3342.32	0.468
779.33	0.0	2110.85	1.110	3395.97	0.461
811.02	0.0	2134.45	0.289	3429.99	0.453
811.04	0.0	2134.47	0.969	3430.01	0.444
836.58	0.0	2165.20	0.955	3461.04	0.436
881.50	0.0	2216.83	0.943	3512.45	0.426
911.75	0.0	2249.99	0.185	3544.99	0.452
911.77	1.026	2250.01	0.915	3545.01	0.415
939.12	0.762	2275.74	0.941	3572.64	0.408
987.01	0.178	2318.65	0.606	3618.26	0.398
1019.13	0.0	2345.99	0.030	3647.04	0.219
1019.15	1.659	2346.01	0.868	3647.06	0.499
1047.52	1.713	2365.74	0.947	3676.77	0.536
1096.93	0.094	2398.37	0.368	3725.87	0.513
1129.87	0.0	2418.99	0.0	3756.88	0.164
1129.89	1.620	2419.01	0.830	3756.90	0.466
1152.36	1.777	2443.85	0.836	3778.78	0.437
1190.68	0.097	2485.14	0.825	3814.74	0.384
1215.66	0.0	2511.37	0.203	3837.30	0.209
1215.68	1.486	2511.39	0.807	3837.32	0.499
1239.60	1.810	2535.39	0.792	3867.81	0.478
1280.37	0.087	2575.21	0.049	3918.19	0.433
1306.94	0.0	2600.45	0.0	3949.99	0.336
1306.96	1.600	2600.47	0.744	3950.01	0.502
1339.76	0.535	2625.93	0.751	3974.53	0.497
1396.48	0.401	2668.19	0.364	4014.86	0.415
1433.99	0.0	2694.99	0.0	4040.19	0.424
1434.01	1.255	2695.01	0.703	4040.21	0.497
1457.06	1.361	2720.95	0.722	4078.43	0.486
1495.96	0.877	2764.00	0.228	4141.82	0.427
1521.06	0.067	2791.30	0.009	4181.99	0.264

TABLE IV.9 U(LAMBDA)

THE MONOCHROMATIC LINEAR LIMB DARKENING COEFFICIENT

LAMBDA	U	LAMBDA	U	LAMBDA	U
4182.01	0.486	5698.53	0.368	7072.01	0.287
4216.15	0.483	5728.10	0.366	7109.62	0.285
4272.59	0.476	5775.60	0.363	7171.32	0.282
4308.23	0.061	5805.99	0.386	7209.99	0.239
4308.25	0.473	5807.01	0.361	7210.01	0.280
4339.10	0.460	5834.57	0.359	7242.51	0.279
4389.96	0.380	5879.73	0.356	7295.71	0.276
4421.99	0.417	5907.99	0.182	7328.99	0.267
4422.01	0.466	5908.01	0.354	7329.01	0.275
4450.80	0.464	5935.85	0.352	7358.59	0.273
4498.19	0.460	5981.45	0.350	7406.96	0.271
4527.99	0.120	6009.99	0.352	7437.18	0.273
4528.01	0.457	6010.01	0.348	7437.20	0.270
4561.08	0.455	6035.15	0.346	7478.27	0.268
4615.62	0.450	6076.29	0.343	7545.70	0.265
4649.99	0.040	6101.99	0.356	7587.99	0.232
4650.01	0.447	6102.01	0.342	7588.01	0.263
4679.63	0.445	6130.13	0.340	7632.10	0.261
4728.36	0.440	6176.18	0.337	7704.53	0.258
4758.99	0.298	6204.99	0.242	7749.99	0.267
4759.01	0.432	6205.01	0.335	7750.01	0.256
4793.43	0.426	6234.12	0.333	7788.20	0.254
4850.19	0.337	6281.80	0.330	7850.80	0.252
4885.95	0.454	6311.64	0.283	7889.99	0.040
4885.97	0.427	6311.66	0.328	7890.01	0.250
4918.03	0.422	6346.88	0.326	7932.25	0.248
4970.80	0.409	6404.72	0.322	8001.55	0.246
5003.99	0.483	6440.99	0.400	8044.99	0.121
5004.01	0.419	6441.01	0.318	8045.01	0.244
5030.71	0.417	6463.58	0.316	8088.83	0.242
5074.53	0.413	6500.44	0.307	8160.76	0.239
5101.99	0.553	6523.43	0.267	8205.86	0.166
5102.01	0.412	6523.45	0.312	8205.88	0.274
5126.68	0.410	6561.43	0.304	8251.94	0.273
5167.11	0.407	6623.83	0.246	8327.56	0.270
5192.41	0.015	6662.99	0.076	8374.99	0.125
5192.43	0.405	6663.01	0.308	8375.01	0.269
5222.79	0.402	6690.35	0.306	9492.43	0.238
5272.68	0.399	6735.06	0.303	12105.90	0.184
5303.99	0.076	6762.99	0.313	14588.20	0.150
5304.01	0.396	6763.01	0.303	14588.22	0.166
5334.89	0.394	6790.35	0.301	16200.16	0.150
5385.62	0.390	6835.06	0.299	19727.09	0.123
5417.46	0.084	6862.99	0.304	22794.08	0.106
5417.48	0.388	6863.01	0.298	22794.09	0.114
5454.80	0.385	6890.53	0.296	24896.70	0.104
5516.29	0.381	6935.54	0.294	29264.53	0.090
5554.99	0.306	6963.65	0.293	32823.47	0.080
5555.01	0.378	6963.67	0.293	32823.49	0.080
5593.94	0.376	6993.28	0.291	38086.98	0.070
5658.11	0.371	7041.72	0.289	51431.62	0.052
5698.51	0.473	7071.99	0.273	65646.96	0.041

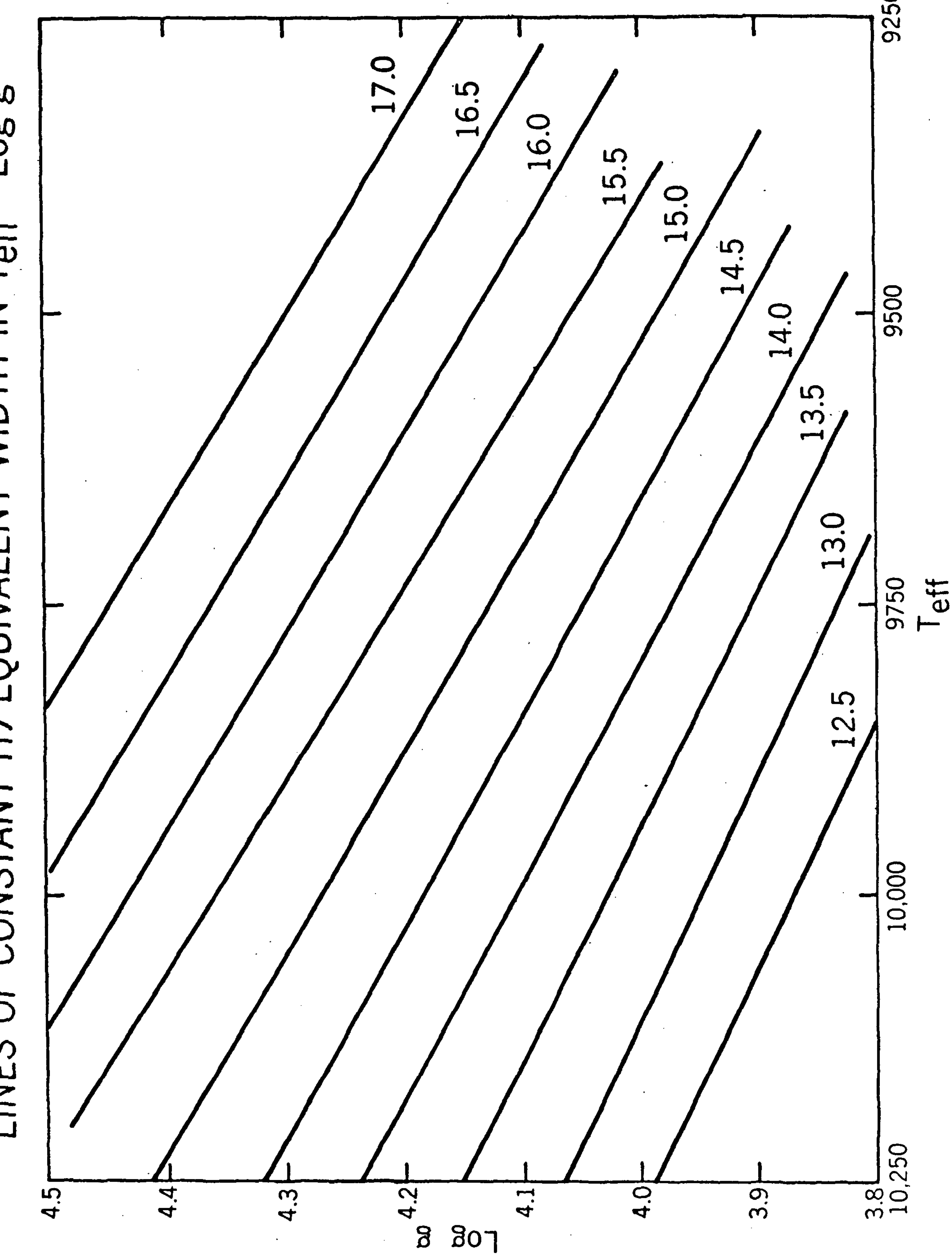

Figure IV.10-1

CHAPTER V

BLANKETING EFFECTS AND THE SENSITIVITY OF THE METHOD TO THE ASSUMPTIONS

1. A Theoretical Test of the Artificial Edge Method

There are several potential sources of trouble in this analysis which must now be investigated. We have argued the plausibility of re-ordering the line opacity into the form of artificial edges. Below a direct comparison of the transfer solutions for both forms of the opacity is made. The problem of the re-shaping of the UV edges and of uncertainties in the corresponding oscillator strengths is treated later in the chapter. The influence of variations in the metal abundance is also examined.

So far the justification for the edge approach to blanketing has been confined to remarks about flux transfer through one layer, with the assumption that the incident flux is continuous. The suggestion has been made (Auer, 1971, private communication) that it is not obvious that saturation effects can be neglected in the transformation from the detailed line opacity to the edge. In arguing that the edge will pass the correct total flux through any given layer, we have not faced the problem of guaranteeing the correct transfer throughout the atmosphere. The flux incident at any layer has a spectral shape which is determined by transfer through other layers. This is true for both the edge case and the detailed line case. The question now is whether the modification of the flux spectrum by transfer through other layers vitiates our previous argument which assumed incident continuous flux only. This is not the only possible source of error. The opacity re-ordering in effect exposes a given line to a different incident flux even if this flux is continuous. The quadrature methods are also different in the two approaches. There is a possibility of table interpolation error too, but these last three sources of potential discrepancy can be kept small.

The artificial edges always have their maxima at the red end. Clearly, this is not the case in the segment of the blend to which the edge corresponds. An unknown error arises from the fact that different lines generally dominate in different layers. These lines occur at effectively random wavelengths, but the edge approach treats them as though they were all at about the same wavelength within the band. Thus these strong lines interact to some extent with each other, and spurious saturation seems possible. We now address ourselves directly to the flux, mean intensity, and flux derivative solutions from the transfer equation, evaluated in both the detailed case and the edge case for a given band.

The test was performed in three bands. No re-shaped edges could be used. The first band extended from 2346 Å to 2419 Å, where the blanketing opacity is very important. Another covered the spectrum from 7750 Å to 7890 Å, where the mixture of neutral and high ion lines produces a variety of lines to dominate different depths. In this particular region, however, the blanketing is dominated by the continuous opacity, and was too weak to be significant. The third band extended from 3837.32 Å to 3950 Å, where the line opacity is strong and the continuous opacity is weak. This band provided a check on the results obtained in the first band.

The detailed transfer problem was performed by modifying the author's emergent line profile program to integrate the flux (H), the mean intensity (J) and the flux derivative ($\partial H/\partial \tau$) over the band at all depths. Frequency positions were chosen as in generating the blended line opacity spectrum. A trapezoidal integration over these points was employed. Various orders of interpolation were used to obtain the edge opacity from its T-P_e tables. The most reliable scheme employed linear interpolations in T and Log P_e for the log of the opacity. The maximum discrepancy in the flux between cases is 4%, and it is usually much less. The mean intensity shows only half as much discrepancy. This is illustrated in Figure V.1-1, where the detailed solutions are taken as 'correct'. Subscripts 'd' and 'e' denote the detailed and edge cases, respectively. Figure V.1-1 shows the run over depth of $(H_d - H_e)/H_d$ and $(J_d - J_e)/J_d$. It must be noted that the test employed an atmospheric structure which is flux constant for the edge opacity. If the atmosphere could be re-converged for the detailed opacity, the structure would adjust very slightly, and the effects of small systematic opacity discrepancies would disappear.

The flux derivatives had much greater discrepancies, however, but for good reason: the actual value of $\partial H/\partial \tau$ is about equal to the discrepancy in H, i.e., several percent of H. Thus the correlation between cases is lost for the flux derivative. The importance of the integrated flux derivative is its use in temperature corrections, however, and its value is correct in each case. The blanketed models converge in normal fashion, and so this last discrepancy causes no harm.

In order to obtain an estimate of the accuracy of the trapezoidal integration, the detailed case was re-calculated at double resolution in wavelength. The result was that more flux was passed in the middle and surface of the atmosphere, and less at depth. This drew the H_e and

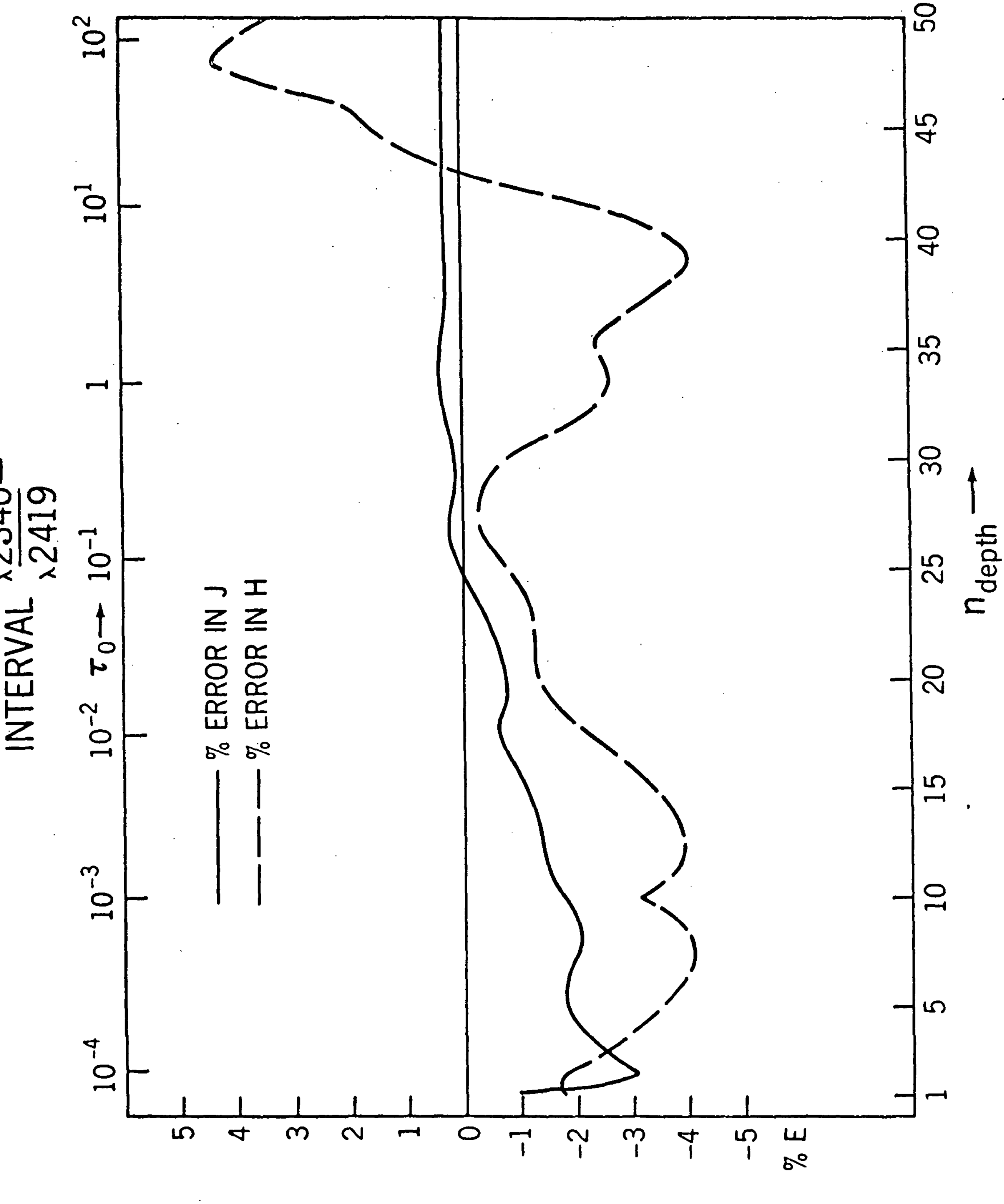

INTERVAL λ2346—λ2419
τ0 ⟶
10^-4
10^-3
10^-2
10^-1
1
10^1
10^2
— % ERROR IN J
— — % ERROR IN H
5
4
3
2
1
0
-1
-2
-3
-4
-5
% E
1
5
10
15
20
25
30
35
40
45
50
n_depth ⟶

Figure V.1-1

H_d values closer at all depths by about 0.5%, indicating that the curves of Figure V.1-1 are slightly pessimistic.

The complete discrepancy cannot be removed by going to sufficiently high resolution, however, because another test established that the bulk of the disagreement stems from the table interpolations for the edge opacity. This was found by converting the detailed opacity in the band to the form of an edge before solving the transfer equation. The integration was done with a Lobatto-Gauss quadrature, and so edges were used without table interpolation or trapezoidal integration. About 80% of the previous discrepancy was removed, and so the edge method itself appears to have introduced no significant error.

The same calculations were applied to the third band to reduce the probability that peculiarities had prejudiced the analysis. All conclusions were the same as before. This indicates that each interval suffers discrepancies of the same sign and approximate magnitude, which is reasonable since each interval is treated the same in the interpolation procedure. Thus the interpolation error produces a small grey-like error, to which it is well-known that atmosphere models are relatively insensitive. Therefore, we may expect the edges to duplicate the effects of the detailed blend quite closely.

2. Metal Abundances

Since the number of ways to vary the chemical composition is infinite, we must limit our considerations in some manner. This will leave many cases uncovered, but we can argue that at least if one species should have had N times its cosmic abundance, the error is less than if all species should have had N times their cosmic abundances.

Therefore, we shall consider only variations in the total metal abundance, Z. Extreme cases may certainly be imagined wherein our conclusions may not hold, but we can learn a great deal from simply scaling Z, and the ease and importance of the calculation make it the obvious way to investigate the influence of composition.

Regarding the value of Z in Sirius, two remarks need to be made. The literature concerning abundance analyses of Sirius is quite voluminous, but recent studies (e.g., Latham, 1970) indicate that cosmic abundances are not unreasonable. As we shall see in this section, no great precision in Z is necessary for the task of fitting Sirius, and it is not clear that present theory can provide a value of Z for Sirius which is precise beyond one significant digit.

Two model atmospheres were calculated identically except that one had cosmic metal abundance, $Z_c = 0.014$, and the other had ten times this value, $Z_m = 0.14$, where we use 'c' and 'm' to denote 'cosmic' and 'metal-rich', respectively. The extra metals were inserted at the expense of hydrogen. Since helium is basically only a filler in this T_{eff} - Log g region, this should encourage discrepancies. Both models had helium mass fractions of 0.36, $T_{eff} = 10000°K$, Log g = 4, and were fully blanketed. The following conclusions resulted from a comparison of the two models:

a. the Hγ profile of Sirius would have required a slightly higher effective temperature if the metal-rich mix were used, about 9800°K;

b. the equivalent width of Hγ was about 4% greater in the metal-rich model;

c. the Balmer jump was 6% greater in the cosmic model, which also had 5% more hydrogen by number;

d. $T(\tau_0)$ was essentially unchanged near the surface, and at depth $T_m(\tau_0)$ was several percent larger than $T_c(\tau_0)$;

e. $P_{g(m)}(T)$ was generally about 15% greater than $P_{g(c)}(T)$;

f. an additional 4% of the total flux was shifted from the Balmer to the Paschen continuum in the metal-rich model.

The 4% variation of the Hγ equivalent width corresponds to about ±0.1 in Log g and ± 150°K in T_{eff} for $Z = Z_c$. If we had used a slightly smaller Z in fitting Sirius, we would have arrived at a gravity more toward the quoted observational best value. Higher Z would have led to some combination of higher T_{eff} and lower gravity, assuming it would have been possible to satisfy all fitting parameters simultaneously. Nevertheless, the drastic increase in Z produced only marginal alterations of the fitting contours, and the major differences between the blanketed and unblanketed models remained fairly intact.

3. Magnitude and Temperature Dependence of the UV Blanketing

The temperature dependence of the UV blanketing opacity is difficult to estimate. This opacity arises primarily from ion lines, and ion densities increase with depth in the model. One might expect, therefore, that the UV blanketing opacity should increase with depth, too. Broadening mechanisms also grow in importance with depth, however, and the issue becomes clouded by questions involving the depression of central absorption coefficients, obliteration of energy levels, and line scattering. Furthermore, it is well-established that as ionization increases, there is a blue-ward motion of the boundary between the spectral region where line opacity is important and that where it is negligible. Here we refer to the region in which the continuum dominates and the wavelengths to the red where there is no significant flux. At the surface of the Sirius model, the line opacity red of Hα falls into the region of negligibility. At some point as ionization progresses, this region must move into the UV. Therefore, the safest guess for the behavior of the UV blanketing opacity is that it increases with depth for a distance, after which it drops off until it is negligible. The edges used for Sirius had this general behavior, but the re-shaping process casts doubt on whether too much depth dependence was borrowed from the visible edges.

In order to estimate the importance of these effects, a different blanketing opacity was generated. To the red of 2900 Å it was identical to the regular blanketing, but to the blue its form was constructed without the constraint that overestimation must be carefully avoided. In fact the approach that was used was designed to estimate as closely as possible the real blanketing opacity, but to err on the high side. This was done by basing the entire opacity below 2900 Å on the statistical behavior of the edges above 2900 Å. At a given temperature and electron pressure, the magnitude of the red ends of these edges can be represented by a linear least squares fit with a standard deviation of typically 10%. This linear approximation was calculated for all twenty (T, P_e) points, and the red ends of the ultraviolet edges were obtained by extrapolating the lines toward zero wavelength. Then the average shape was calculated at all intervals between 2900 Å and 6000 Å, and the average wavelength dependence of the edge shape was applied to the shape at 2900 Å to extrapolate the shapes of the ultraviolet edges for all (T, P_e) values. The resulting ultraviolet edge spectra appear to be the best estimate obtainable from the linear approximations. These new edges have a very smooth dependence on T, P_e, and λ, without any of the windows which appeared in the regular ultraviolet edges where approximation was necessary. The magnitudes of these edges were typically several times the more conservative estimate used for Sirius, although the available UV line data contained enough strong lines so that the purely statistical edges fell slightly below the others at several wavelengths. The statistical edges constitute a substantially greater opacity than those used in the models, however. These edges are listed in Appendix C.

As compared to increasing the blanketing by adding more metals to the composition, this use of greater UV opacity does not alter the ionization equilibrium at fixed T and P_e. Consequently, the model which results can be viewed as the product of greater UV oscillator strengths, with the increase being of the order of a factor of five, roughly (depending on λ). Current work on UV oscillator strengths suggests that corrections should be applied for some lines which are of this order, notably iron (see, e.g., Bell and Upson, 1971). Since I have effectively applied this correction to all UV lines and minimized opacity windows, I expect the statistical edges to produce over-blanketing.

$T(\tau_0)$ is plotted for the Sirius model, the statistical UV model, and an unblanketed model in Figure V.3-1. The difference between the two blanketed models is clearly insignificant compared to the difference between them and the unblanketed model. The same remark applies to $P_g(T)$, shown in Figure V.3-2. The structural parameters of the two blanketed models are all within a few percent agreement. But the question remains: are the statistical edges really an overestimate of the

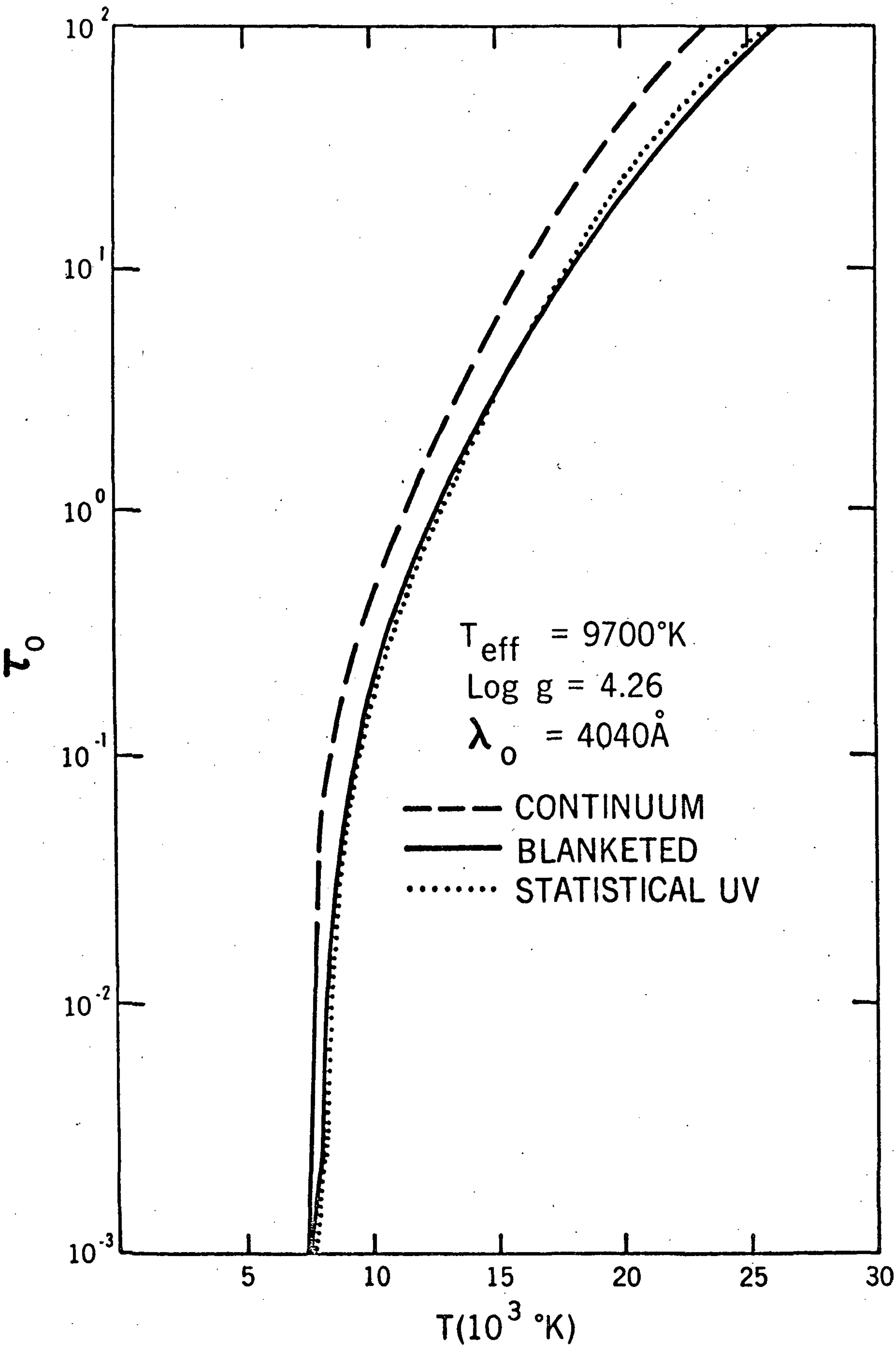
10^2
10^1
10^0
10^{-1}
10^{-2}
10^{-3}
τ_0
T_{eff} = 9700°K
Log g = 4.26
λ_o = 4040Å
CONTINUUM
BLANKETED
STATISTICAL UV
5
10
15
20
25
30
T(10^3 °K)

Figure V.3-1

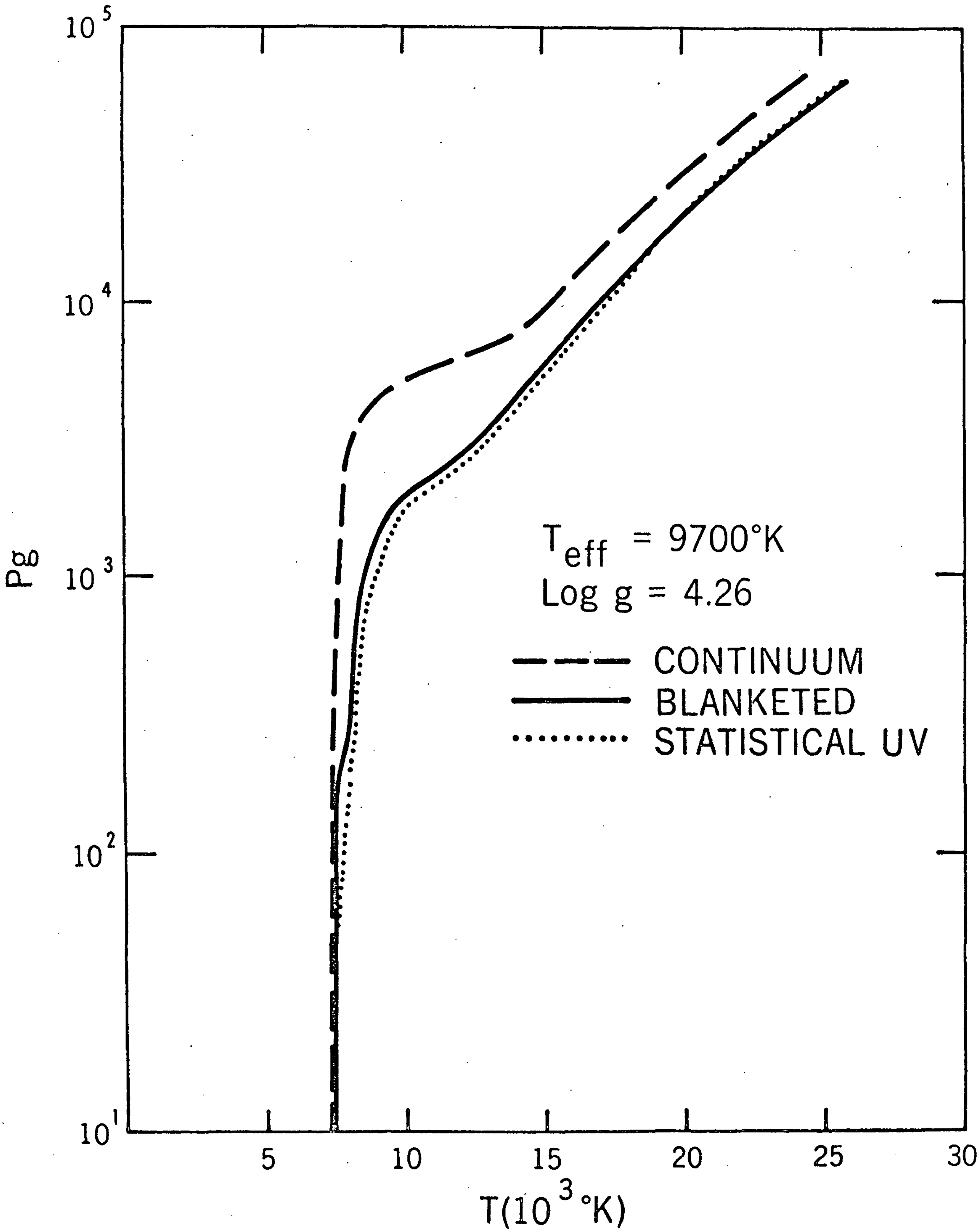

10^5
10^4
10^3
10^2
10^1
P_g
5
10
15
20
25
30
$T(10^3\,°K)$
T_{eff} = 9700°K
Log g = 4.26
CONTINUUM
BLANKETED
STATISTICAL UV

Figure V.3-2

blanketing opacity? If we assume that we are at least in the vicinity of the ballpark, we can obtain evidence by examining the main features which we associate with blanketing. Thus we are interested in the spectral distribution of the Balmer flux, and the Balmer-to-Paschen flux redistribution.

In Figure V.3-3 the spectra of the two blanketed models are plotted. The most obvious feature of the graph is the similarity of the two Paschen continua. In fact, most of the fitting parameters are still acceptable for Sirius. The Balmer jump fits better than before, indicating that more flux has been shifted from the Balmer to the Paschen continuum. In fact, the statistical model has 1.6% less of its total flux in the Balmer continuum, with a corresponding increase in the Paschen continuum. This indicates stronger blanketing effects in the statistical model, whose Balmer flux distribution also shows greater blanketing effects. This flux is clearly being controlled by the blanketing opacity over a much greater range in wavelength than that of the regular Sirius model. This flux distribution shows too much blanketing compared to the observed spectrum of Sirius, and therefore, we make the connection between the statistical blanketing and a significantly overestimated blanketing opacity.

Of the well-observed Sirius spectral features, the Balmer jump is the most sensitive to the UV blanketing. This is because the line opacity just short of 3647 Å, though large, is nevertheless dwarfed by the hydrogen continuous opacity, and large variations of the line opacity there have no effect. The red side of the Balmer discontinuity, on the other hand, is controlled by the well-known local opacities and the Balmer-to-Paschen flux redistribution. I interpret the fact that

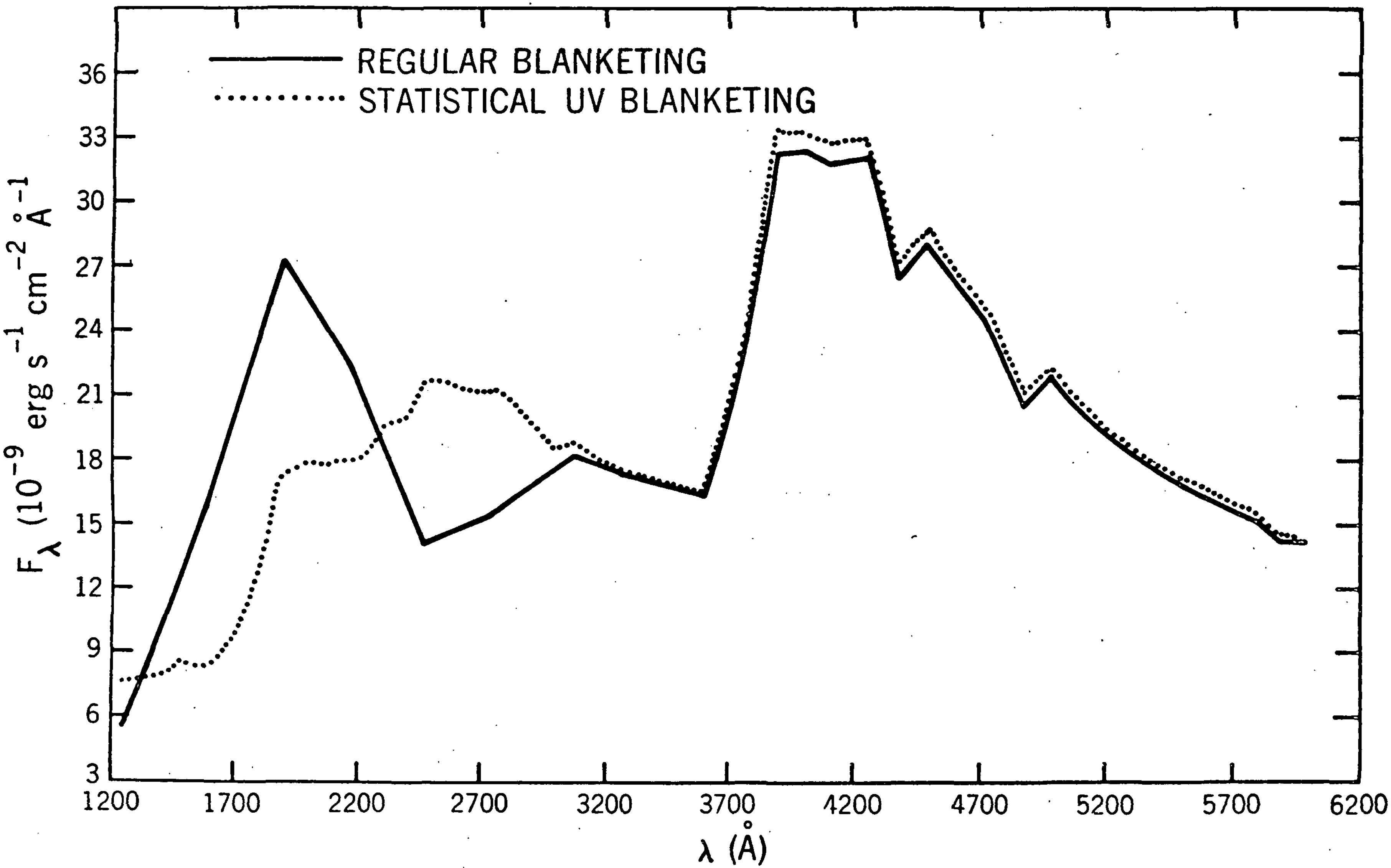
REGULAR BLANKETING
STATISTICAL UV BLANKETING
36
33
30
27
24
21
18
15
12
9
6
3
F_λ (10^{-9} erg s^{-1} cm^{-2} $Å^{-1}$)
1200
1700
2200
2700
3200
3700
4200
4700
5200
5700
6200
λ (Å)

Figure V.3-3

the Sirius model's Balmer jump is on the small side to be further evidence that the UV blanketing in that model is slightly underestimated.

The two Balmer continua in Figure V.3-3 practically form an envelope for the most recent observational data. It is clear that some intermediate blanketing opacity could essentially reproduce Evans' data, which is the most appealing from a theoretical viewpoint. It is also clear that if the regular UV blanketing opacity were made weaker, the fit would degrade, and if the statistical edges were made stronger, that fit would get worse in the other direction. Therefore, these two blanketing opacities are identified as extremes which form a qualitative bracket on the correct blanketing. With this interpretation, we must conclude that the 'correct' structure for Sirius must be well represented by either model, since they are almost identical. The only significant differences are the spectral features, primarily the Balmer flux distribution and the slightly higher Paschen continuum.

From these arguments, it seems safe to conclude that possible errors in the regular UV blanketing opacity have no significant structural repercussions. The opacity as applied in the model does quite well in reproducing the observed spectrum if the overt effects of the opacity windows in the UV are suppressed by going to lower resolution. It appears that revisions of the UV oscillator strengths will not seriously alter our results.

These conclusions and those of the previous sections indicate that none of the potential sources of trouble have enough influence to cast doubts on the quality of the final Sirius model. Until more demanding observational data becomes available, greater precision of fit is unwarranted. Slight optimization of the fit might be possible by using a smaller value for the metal abundance and slightly stronger UV blanketing opacity, but these changes are not required for a self-consistent fit at this time.

4. Some Effects of Blanketing

A very large number of comparisons can be made between blanketed and unblanketed or partially blanketed models. Figures V.3-1 and V.3-2 represent two such comparisons. Much has been said about the impact of blanketing on the emergent spectrum, and more is contained in Chapter VI. Here we re-examine $T(\tau_0)$ and $P_g(T)$ for a nearby point in the T_{eff} - Log g plane. Five models were calculated with T_{eff} = 10000°K and Log g = 4:

A pure hydrogen, H and H^- continuous opacity

A' cosmic abundance, H, H^-, He, He^+, He^-, Rayleigh H scattering, electron scattering continuous opacities

B cosmic abundances, H line-blanketing, and above continuous opacities

C cosmic abundances, metal line-blanketing, above continuous opacities

D cosmic abundances, H and metal line-blanketing, and above continuous opacities.

The A' model was virtually indistinguishable from the A model, and so it was not of interest. The A model is the standard archetype, and case D is one of the models used to fit Sirius. The temperature distributions of these four model atmospheres are displayed in Figure V.4-1. All have fifty depth points and are flux constant to at least 0.5% over at least 90% of these depths. The archetype is the coolest, and the two partially blanketed models are very similar over most of the depths. The fully blanketed model is by far the hottest and has the greatest

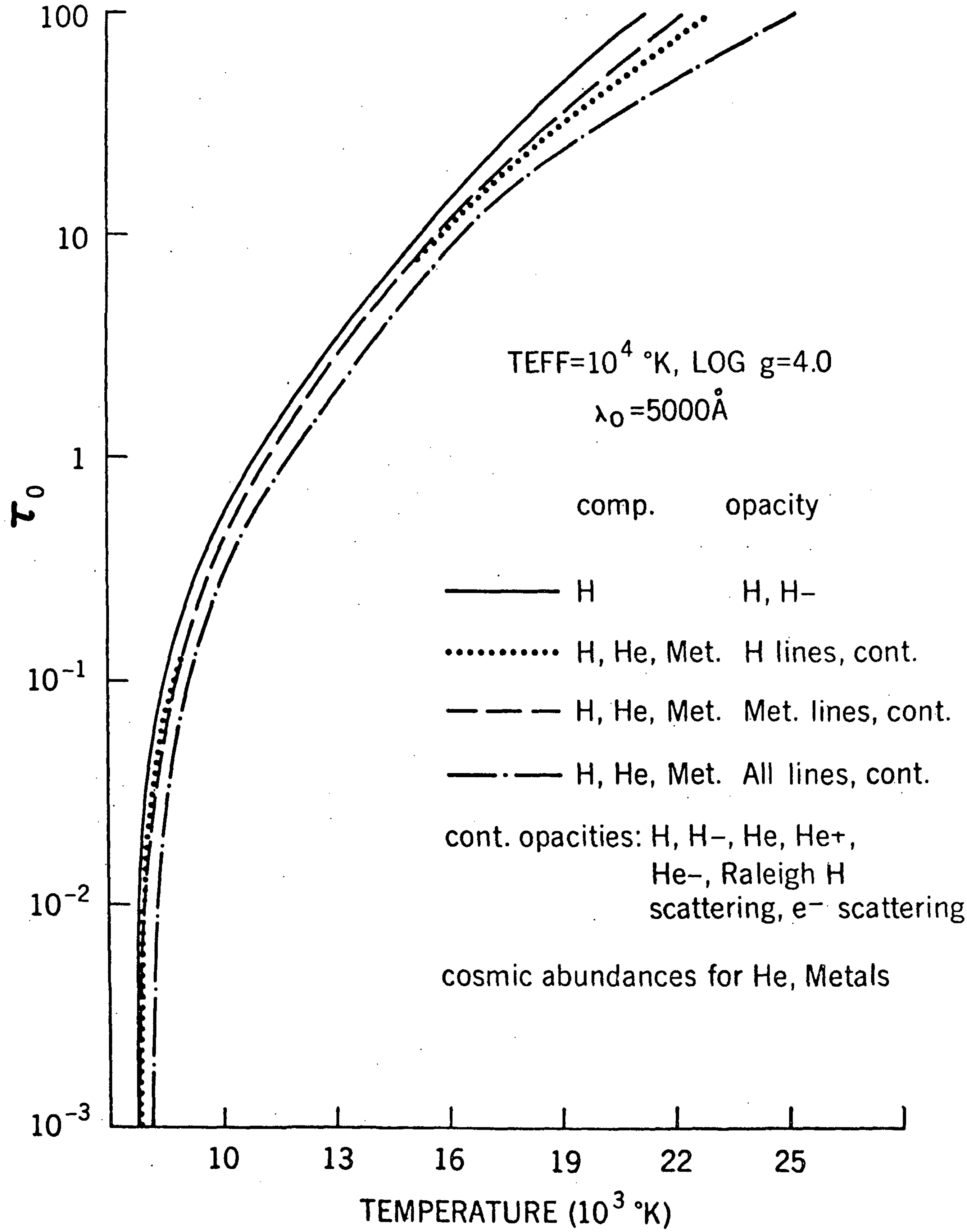

100
10
1
10^{-1}
10^{-2}
10^{-3}
τ_0
TEFF=10^4 °K, LOG g=4.0
λ_0=5000Å
comp. opacity
H H, H−
H, He, Met. H lines, cont.
H, He, Met. Met. lines, cont.
H, He, Met. All lines, cont.
cont. opacities: H, H−, He, He+, He−, Raleigh H scattering, e− scattering
cosmic abundances for He, Metals
10
13
16
19
22
25
TEMPERATURE (10^3 °K)

Figure V.4-1

temperature gradient, as would be expected. From $\tau_0 = 10^{-4}$ to the boundary at $\tau_0 = 10^{-9}$ the fully blanketed model is the coolest, although there is no room to show it on the graph. It has a boundary temperature of 7690°K, whereas the others are all within 15° of 7795°K.

The relationship between T and P_g is shown in Figure V.4-2. The differences stem from the importance of radiation pressure and the structural coupling to the blanketing opacity, which produces different temperatures, ionization equilibrium, and opacity. The differences between the fully blanketed model and the archetype are quite similar to the same differences between the blanketed models and continuum model shown in Figures V.3-1 and V.3-2.

5. A Final Look at Blanketing

Because of the form of the equations which define the stellar atmosphere problem, the physical depth z is not a convenient parameter with which to work. Currently two depth coordinate transformations are in general use, namely

$$d\tau_0 = (\chi_0 + \sigma_0)\rho\, dz$$

and

$$dm = \rho\, dz$$

Nevertheless, the physical depth is an interesting parameter to use in representing the final model because it can be visualized most easily, and it does not depend on the selection of a standard wavelength. The only problem is that of establishing a zero point, and this can be done arbitrarily. Here we define z to be zero at $\tau_0 = 10^{-4}$, where $\lambda_0 = 4040$ Å. The three models whose $T(\tau_0)$ distributions are plotted in Figure V.3-1 have their T(z) distributions plotted in Figure V.5-1.

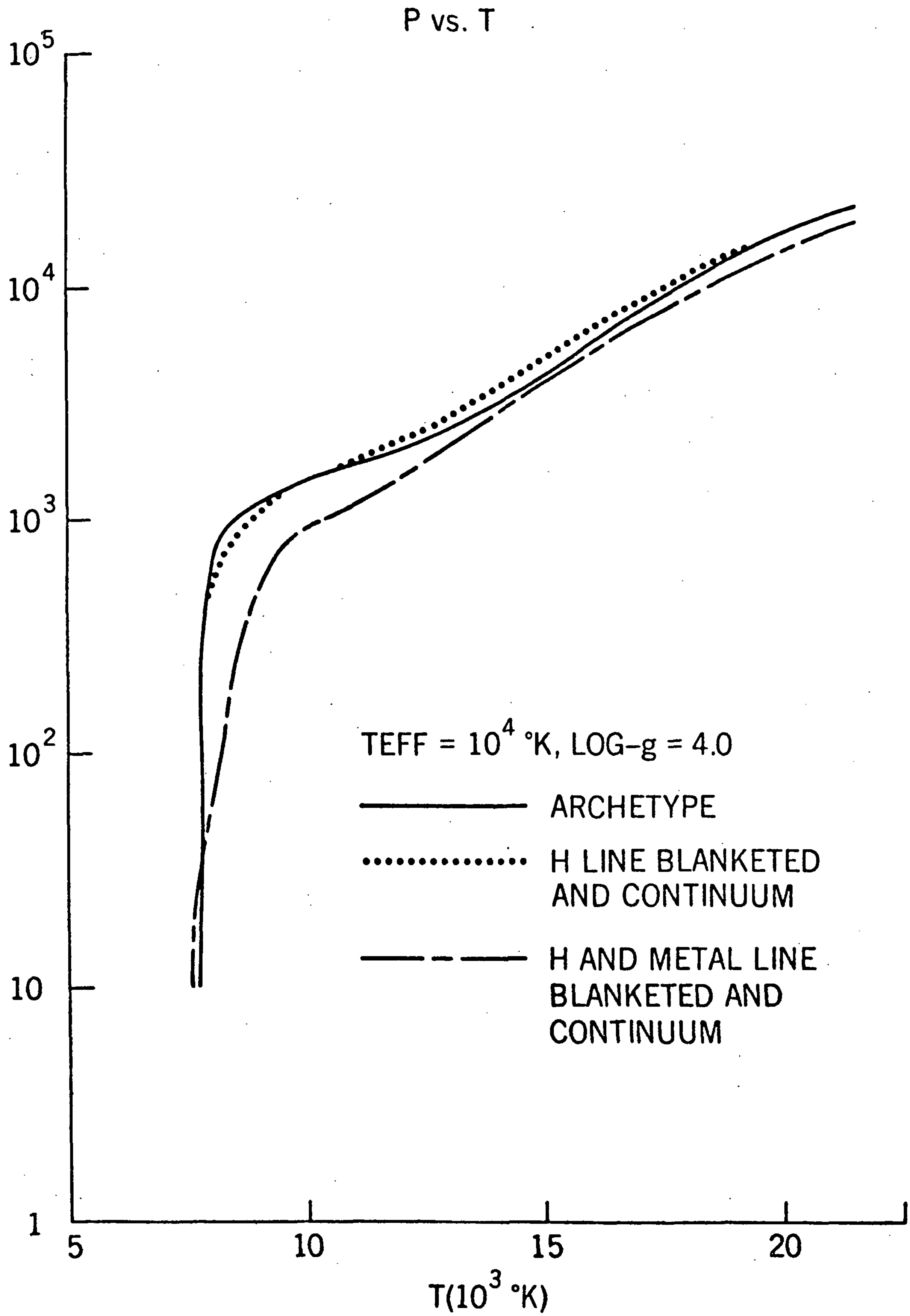
P vs. T
10^5
10^4
10^3
10^2
10
1
5
10
15
20
T(10^3 °K)
TEFF = 10^4 °K, LOG-g = 4.0
ARCHETYPE
H LINE BLANKETED AND CONTINUUM
H AND METAL LINE BLANKETED AND CONTINUUM

Figure V.4-2

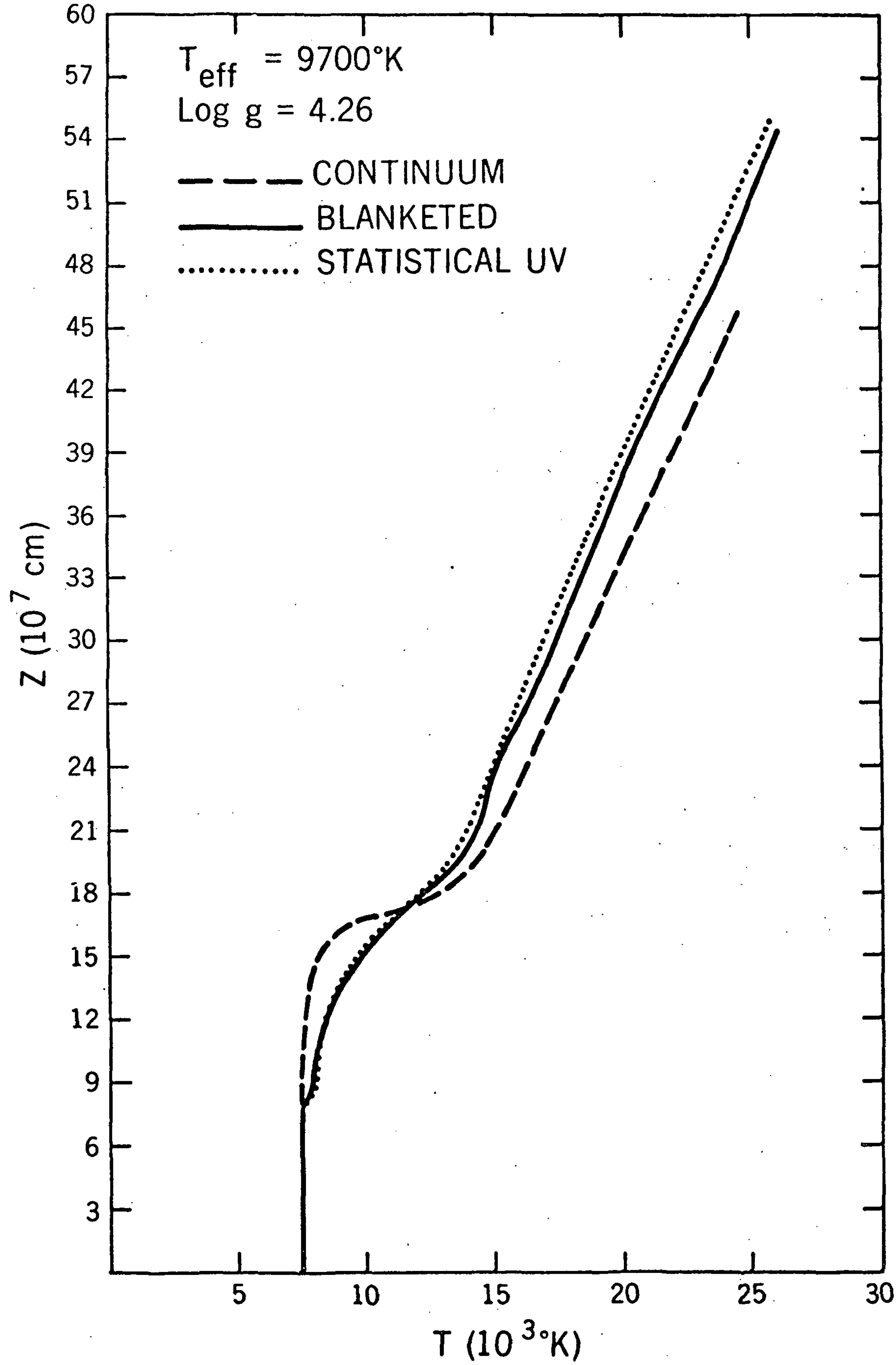

T_{eff} = 9700°K
Log g = 4.26
CONTINUUM
BLANKETED
STATISTICAL UV
Z (10^7 cm)
T (10^3°K)
60
57
54
51
48
45
42
39
36
33
30
27
24
21
18
15
12
9
6
3
5
10
15
20
25
30

Figure V.5-1

A comparison of the two graphs shows that the two representations are quite different. Between 8×10^7 cm and 17×10^7 cm, the blanketed models are hotter than the unblanketed model. Below this depth, which occurs near $\tau_0 = 1$, the unblanketed model is actually the hottest. Thus in the continuum we can 'see' deeper in the blanketed models. This is because the continuous opacity above $\tau_0 = 1$ has been decreased by the higher temperature and more rarefied plasma. For $\tau_0 > 1$ the temperature is slightly lower in the blanketed models than in the unblanketed model at the same z, but in the τ_0 representation the temperature appears to be higher in the blanketed models because we see to hotter depths.

Thus if we take a flux-constant continuum model, add blanketing, and re-converge to flux constancy, a process takes place which we can visualize in either of two ways. From the τ_0 viewpoint, the atmosphere can no longer get all of the required flux through the upper layers, and therefore begins backwarming. This scarcely influences the surface layers, but at depth the temperature rises about five or six thousand degrees. This generates a much stronger continuous flux at all wavelengths, enough of which escapes at redder frequencies so that the correct total flux emerges. The steeper temperature gradient produces a small amount of cooling at the boundary.

In the z-representation, the flux blockage occurs mostly in the layers near 15×10^7 cm deep. The atmosphere responds by heating its upper layers, which are absorbing too much flux. The heating tends to reduce the obstacle to the flux, but also reduces the hydrogen continuous opacity near the surface, allowing more of the deep flux to reach the surface, especially to the red of the Balmer discontinuity. The increased surface opacity enhances the contribution of radiation pressure to the total pressure, and the higher temperature adds to the forces causing the gas to expand, becoming more rarefied. If we fix our distance scale to $\tau_0 = 100$, we interpret the process as a slight expansion of the atmosphere, with a heating of the upper layers and little change in the lower layers. The emergent spectrum has changed in that much of the flux which had been emerging in the Balmer continuum now finds its way out of the atmosphere in the Paschen continuum, because the continuous opacity there has been diminished by the heating. Except for a slight increase in slope, the primary effect on the Paschen continuum is that it is generally raised several percent outside of the strong absorption lines which have now appeared. The blocking in these lines does not, in itself, seriously affect the gross shape of the flux distribution.

CHAPTER VI

SUMMARY AND CONCLUSIONS

We have applied conventional LTE line absorption theory to produce blended line opacity spectra for a grid of (T, P_e) points. These have been converted into artificial absorption edge spectra, and were included as another opacity source in calculating a grid of model atmospheres. In order to do this we have had to make a few assumptions based on the statistical behavior of the visual data. These were used to make up for the lack of sufficient line data in the ultraviolet. In the process, some opacity windows were generated in the ultraviolet where the danger of overestimation precluded using higher estimates.

Tests on the relationship of the detailed line transfer with the edge transfer in the same bands have indicated that the major source of error is the table interpolation for the blanketing opacity. This error is small enough to neglect, although a larger set of (T, P_e) grid points would be preferable in the future. The artificial edge method itself produced no measurable errors.

The grid of blanketed models was used to predict the variation of certain spectral features in the T_{eff} - Log g plane in the range $9250° \leqslant T_{eff} \leqslant 10250°$ and $3.8 \leqslant \text{Log } g \leqslant 4.5$. This range was chosen because it offers the most hope of being free of several contaminating problems such as non-LTE effects, molecular absorption, and convection. Then Sirius was taken as a test case because it appeared to lie in this range, has strong metal lines, is bright enough to offer good observing possibilities, shows no noticeable magnetic, rotational, or reddening effects, and is part of a binary system whose orbital parameters are well determined.

The blanketed model of Sirius which best reproduces the observed spectral features has an effective temperature of 9700°K and Log g = 4.26. This model satisfactorily reproduces the observed Hγ profile, the Paschen slope, Balmer jump, absolute flux at 5550 Å, the dynamically determined gravity, and the flux distribution in the Balmer continuum. Only ESW profiles for Hγ produce this level of self-consistency; the gravity cannot be fit if Griem profiles are used.

We have obtained measures of the influence of the errors of approximation, with the result that removal of all error would be expected to alter the final results only marginally, especially when compared to the large differences which separate continuum models from fully-blanketed models. This applies to errors in re-shaping the UV edges, in abundances, in oscillator strengths, and in table interpolations. Therefore it appears that Sirius should be quite well-represented by the model, which is free of several problems which have plagued past attempts to fit Sirius with unblanketed or partially-blanketed models. These problems stem from being unable to resolve the following discrepancies simultaneously:

a. Hγ too bright at line center;

b. too much flux in the Balmer continuum;

c. too little flux at 5550 Å.

The blanketed model boosts its flux at 5550 Å at the expense of its Balmer flux, removing 'b' and 'c'. Its temperature structure causes the core of Hγ to be formed at cooler temperatures while the wings are formed at the same temperatures, eliminating 'a'.

There are two reasons why the core of Hγ is formed at lower temperatures if we fit Sirius with a blanketed model instead of a continuum model. The steeper gradient of $T(\tau_0)$ results in a slightly cooler boundary temperature, but this effect is unimportant. The primary reason is that when blanketing is included a substantially lower effective temperature can be used. For instance, Latham (1970) used hydrogen-line blanketed models to fit Sirius, and found that the best model, on the basis of essentially the same fitting parameters used here, had T_{eff} = 10290°K and Log g = 4.3. I have calculated such a model, i.e., with hydrogen lines as the only blanketing opacity, and my results are in close agreement with Latham's. But comparing my hydrogen line-blanketed (10290, 4.3) model with my fully-blanketed (9700, 4.26) model shows that the 9700° model is 70° cooler at the boundary, 400° cooler at $\tau_0 = 10^{-3}$, and remains about 400° cooler down to $\tau_0 = 100$.

Figure IV.7-2 shows that an effective temperature of 9700°K produces about the correct total flux from Sirius, as well as can be judged. Even though the Balmer flux may be uncertain by, say, 30%, the Balmer flux constitutes only at most a third of the total flux, so that the total flux is uncertain by about 10%. Taking 9700° as the best estimate, the uncertainty would require the effective temperature to be between about 9450°K and 9950°K. Thus only blanketed models can be used for Sirius, because the others require much higher effective temperatures to reproduce the absolute flux at 5550 Å.

It must be recognized that this analysis has been centered on the most hospitable part of the T_{eff} - Log g plane. The reason why the blanketing could be so uncertain in the Balmer continuum without dire consequences is that the hydrogen continuous opacity dominates the Paschen continuum and stays even in the Balmer continuum. To the blue of the Balmer discontinuity the continuous opacity dominates so strongly that even our overestimated version of the blanketing opacity could not make a significant contribution. The atmospheric structure parameters $T(\tau_0)$, $P_g(T)$, $P_e(T)$, etc., depend almost completely on the shape of the total opacity spectrum over the range containing the major part of the flux as given by the Planck function. The degree to which the addition of blanketing alters the structure is proportional to the amount of re-shaping of the total opacity spectrum which takes place. Normally the radiation pressure dominates the total pressure only in the layers which are extremely close to the boundary; as long as this is true, the actual magnitude of the total opacity spectrum is unimportant. Scale factors operating on the entire spectrum do not influence the emergent spectrum or the structural parameters when they are treated as functions of τ_0. Only changes in the shape of the opacity spectrum produce changes in structure or spectra. Of course the structural parameters expressed as functions of physical depth z depend on the absolute magnitude of the opacity spectrum, but this does not change the fact that the emergent spectrum depends on the distribution of the structural parameters in τ_0. Also it is clear that if the opacity spectrum were scaled so high that radiation pressure dominates the pressure balance over too much of the atmosphere, the above statements would no longer be valid.

Just to the red of Lyman α the blanketing opacity dominates completely, independent of variations of an order of magnitude. If this opacity is scaled slightly upwards, a little more flux is absorbed near the surface, the upper layers heat up slightly, and a little more hydrogen is ionized. This causes the neutral hydrogen continuous opacity to diminish slightly over the entire spectrum. In the Paschen continuum this drop just scales the dominating hydrogen opacity down a bit, but the detailed spectral features are not significantly altered. The flux distribution scales slightly upwards with a small increase in slope which is caused by the flux from deeper and hotter layers which can now escape and which has a steeper slope in the Paschen region.

In the Balmer continuum, the blanketing increase causes changes of greater complexity. The drop in neutral hydrogen density also scales the continuous opacity down here, and this extends the range over which the blanketing opacity dominates. This results in a redward redistribution of flux within the Balmer continuum, but the continuous opacity near 3400 Å and on over to the Balmer discontinuity, though reduced, still keeps the atmosphere effectively opaque. Thus the deep flux still cannot reach the surface at these wavelengths, and the emergent flux near 3400 Å does not change. Even though a substantial amount of flux shifting may take place in the Balmer continuum, only a small amount manages to emerge in the Paschen continuum.

This combination of circumstances results from the relative behavior of the hydrogen continuous opacity and the blanketing opacity, the fact that to the red of Lyman α even a relatively weak blanketing opacity can dominate and cause severe flux blocking, and the presence of the peak of the deep flux spectrum in the Balmer continuum. For some other values of T_{eff}, Log g, and chemical composition, a more thorough knowledge of the ultraviolet blanketing opacity might well have been crucial.

It appears in retrospect that several phases of the project could have been accomplished somewhat differently. The primary areas where immediate improvement is possible are the expansion of the (T, P_e) grid size and point density, application of the blend and edge computer programs to the latest body of line data, and preparation of blanketing opacity spectra for different chemical compositions. Afterwards some of the finer points can be applied to enlarge the range of applicability. If further work meets with comparable success, then another revision of the effective temperature scale can be performed, and abundance analyses can be carried out on a firmer foundation. This, together with the continued growth of the observational art, should constitute a significant step toward expanding our understanding to encompass the stars.

APPENDIX A

THE MODELS

Final parameters for seventeen model atmospheres are presented. The tables are limited by space requirements, and distributions over τ_0 are interpolated into a smaller set of standard points in depth. This optical depth scale is derived from the continuous opacities at $\lambda = 4040$ Å. The spectral parameters are presented with the lowered UV resolution. All models are flux-constant to better than 0.5% over at least 90% of the 50 depths, and the flux errors never reach 1%. All used 312 frequency quadrature points. Each model covers four pages of tables. The last thirteen are taken from the grid employed in fitting Sirius. The first model is the final Sirius model. Next is the corresponding model which employed the statistical UV blanketing opacity (see section 3, Chapter V). The following two models are the continuum models used to calculate some of the blocking factors for section 8 of Chapter V. In the order presented, the models are:

1. (9700, 4.26) Final Sirius Model
2. (9700, 4.26) Statistical UV Model
3. (9700, 4.26) Continuum Model
4. (11160, 4.26) Continuum Model
5. (10250, 4.2) Sirius Grid Model
6. (10000, 3.8) Sirius Grid Model
7. (10000, 4.0) Sirius Grid Model
8. (10000, 4.2) Sirius Grid Model
9. (10000, 4.4) Sirius Grid Model
10. (9750, 3.8) Sirius Grid Model

11. (9750, 4.0) Sirius Grid Model
12. (9750, 4.2) Sirius Grid Model
13. (9750, 4.4) Sirius Grid Model
14. (9500, 4.0) Sirius Grid Model
15. (9500, 4.2) Sirius Grid Model
16. (9500, 4.4) Sirius Grid Model
17. (9375, 4.0) Sirius Grid Model

Continuum opacities include H, H^-, He, He^-, He^+, electron scattering, and Rayleigh scattering from neutral hydrogen.

FINAL SIRIUS MODEL

TEFF = 9700.   LOG G = 4.26   PI F = 5.019D 11

BALMER JUMP = .499   PASCHEN SLOPE = 5.651D-04 MAG/A

PERCENT OF THE FLUX IN THE DIFFERENT HYDROGEN CONTINUA:

LYMAN	BALMER	PASCHEN	THE OTHERS
0.00	31.36	54.41	14.22

TAU	TEMP DEG.K	H ERG/CM**2/SEC/STERADIAN	J ERG/CM**2/SEC/STERADIAN	P TOTAL --- DYNE/CM**2 ----	P GAS --- DYNE/CM**2 ----
1.0D-08	7497.	4.017D 10	7.006D 10	7.968D 00	1.019D-03
1.0D-07	7497.	4.017D 10	7.006D 10	7.977D 00	1.045D-02
1.0D-06	7497.	4.017D 10	7.008D 10	8.071D 00	1.047D-01
1.0D-05	7497.	4.016D 10	7.021D 10	9.014D 00	1.047D 00
1.0D-04	7498.	4.015D 10	7.155D 10	1.844D 01	1.047D 01
2.5D-04	7500.	3.992D 10	7.210D 10	3.727D 01	2.929D 01
5.0D-04	7502.	3.984D 10	7.265D 10	6.926D 01	6.127D 01
7.5D-04	7504.	3.981D 10	7.311D 10	1.006D 02	9.259D 01
1.0D-03	7505.	3.981D 10	7.355D 10	1.310D 02	1.230D 02
2.5D-03	7985.	3.990D 10	7.687D 10	2.492D 02	2.389D 02
5.0D-03	8065.	3.981D 10	7.985D 10	3.590D 02	3.483D 02
7.5D-03	8139.	3.980D 10	8.248D 10	4.513D 02	4.403D 02
1.0D-02	8209.	3.981D 10	8.493D 10	5.307D 02	5.193D 02
2.5D-02	8539.	3.993D 10	9.759D 10	8.601D 02	8.467D 02
5.0D-02	8925.	4.000D 10	1.151D 11	1.168D 03	1.152D 03
7.5D-02	9200.	3.999D 10	1.303D 11	1.358D 03	1.340D 03
1.0D-01	9431.	4.000D 10	1.444D 11	1.498D 03	1.478D 03
2.5D-01	10455.	4.015D 10	2.178D 11	1.955D 03	1.925D 03
5.0D-01	11506.	3.987D 10	3.195D 11	2.386D 03	2.342D 03
7.5D-01	12209.	4.000D 10	4.052D 11	2.749D 03	2.693D 03
1.0D 00	12750.	3.996D 10	4.813D 11	3.100D 03	3.033D 03
2.5D 00	14653.	3.992D 10	8.368D 11	5.080D 03	4.964D 03
5.0D 00	16293.	3.994D 10	1.276D 12	7.962D 03	7.784D 03
7.5D 00	17344.	3.995D 10	1.637D 12	1.046D 04	1.023D 04
1.0D 01	18135.	3.993D 10	1.955D 12	1.271D 04	1.244D 04
2.5D 01	20804.	3.994D 10	3.388D 12	2.374D 04	2.327D 04
5.0D 01	23139.	3.996D 10	5.188D 12	3.844D 04	3.771D 04
7.5D 01	24761.	3.997D 10	6.784D 12	5.128D 04	5.034D 04
1.0D 02	26041.	3.989D 10	8.297D 12	6.302D 04	6.186D 04

TAU	PE DYNE/CM**2	DENSITY GM/CM**3	MU A.M.U.	K ZERO CM**2/GM	DEPTH CM
1.0D-08	2.483D-04	1.737D-15	0.74957	2.475D-01	-5.48D 07
1.0D-07	2.373D-03	1.818D-14	0.74987	2.474D-01	-5.47D 07
1.0D-06	2.362D-02	1.827D-13	0.75292	2.466D-01	-5.43D 07
1.0D-05	2.361D-01	1.827D-12	0.78338	2.380D-01	-4.93D 07
1.0D-04	2.361D 00	1.827D-11	1.08800	1.519D-01	0.0
2.5D-04	4.510D 00	5.582D-11	1.18774	1.420D-01	3.04D 07
5.0D-04	6.944D 00	1.223D-10	1.24413	1.433D-01	5.08D 07
7.5D-04	8.794D 00	1.886D-10	1.27081	1.473D-01	6.21D 07
1.0D-03	1.031D 01	2.536D-10	1.28647	1.518D-01	6.97D 07
2.5D-03	2.797D 01	4.462D-10	1.24044	3.765D-01	8.75D 07
5.0D-03	3.811D 01	6.496D-10	1.25107	4.552D-01	9.84D 07
7.5D-03	4.750D 01	8.150D-10	1.25334	5.334D-01	1.05D 08
1.0D-02	5.663D 01	9.516D-10	1.25179	6.140D-01	1.10D 08
2.5D-02	1.074D 02	1.462D-09	1.22699	1.101D 00	1.25D 08
5.0D-02	1.868D 02	1.826D-09	1.17744	1.972D 00	1.35D 08
7.5D-02	2.588D 02	1.984D-09	1.13451	2.854D 00	1.41D 08
1.0D-01	3.275D 02	2.060D-09	1.09467	3.769D 00	1.44D 08
2.5D-01	6.678D 02	2.032D-09	0.91868	8.849D 00	1.56D 08
5.0D-01	9.912D 02	1.982D-09	0.81026	1.242D 01	1.68D 08
7.5D-01	1.197D 03	2.068D-09	0.78069	1.316D 01	1.77D 08
1.0D 00	1.375D 03	2.196D-09	0.76845	1.343D 01	1.86D 08
2.5D 00	2.308D 03	3.057D-09	0.75187	1.477D 01	2.27D 08
5.0D 00	3.685D 03	4.246D-09	0.74008	1.729D 01	2.70D 08
7.5D 00	4.917D 03	5.169D-09	0.72980	1.947D 01	2.99D 08
1.0D 01	6.044D 03	5.948D-09	0.72227	2.124D 01	3.21D 08
2.5D 01	1.154D 04	9.508D-09	0.70809	2.766D 01	4.00D 08
5.0D 01	1.880D 04	1.378D-08	0.70457	3.313D 01	4.70D 08
7.5D 01	2.513D 04	1.720D-08	0.70360	3.655D 01	5.17D 08
1.0D 02	3.090D 04	2.009D-08	0.70319	3.892D 01	5.53D 08

EMERGENT SPECTRUM (LAMBDA IN ANGSTROMS, FLUX IN ERG/CM**2/S/A)

BAND	MID LAMBDA	BAND WIDTH'	AVG.F LAMBDA	AVG.M LAMBDA
1	196.	131.	1.306D-09	22.210
2	332.	141.	1.306D-09	22.210
3	453.	102.	3.859D-05	11.034
4	558.	107.	5.408D-02	3.167
5	659.	96.	1.490D 01	-2.933
6	759.	104.	3.550D 02	-6.376
7	861.	101.	6.112D 03	-9.465
8	965.	107.	7.303D 04	-12.159
9	1075.	111.	6.112D 05	-14.465
10	1173.	86.	2.891D 06	-16.153
11	1261.	91.	8.750D 06	-17.355
12	1370.	127.	1.754D 07	-18.110
13	1478.	87.	3.118D 07	-18.735
14	1573.	103.	4.754D 07	-19.193
15	1687.	126.	7.200D 07	-19.643
16	1800.	100.	9.457D 07	-19.939
17	1897.	93.	1.071D 08	-20.075
18	1997.	108.	1.029D 08	-20.031
19	2093.	83.	9.531D 07	-19.948
20	2192.	116.	8.455D 07	-19.818
21	2298.	96.	6.345D 07	-19.506
22	2383.	73.	5.416D 07	-19.334
23	2465.	92.	4.931D 07	-19.232
24	2556.	89.	5.118D 07	-19.273
25	2648.	95.	5.340D 07	-19.319
26	2743.	96.	5.609D 07	-19.372
27	2864.	145.	6.289D 07	-19.496
28	2979.	86.	6.736D 07	-19.571
29	3072.	99.	6.916D 07	-19.600
30	3166.	90.	6.689D 07	-19.563
31	3260.	99.	6.499D 07	-19.532
32	3370.	120.	6.319D 07	-19.502
33	3488.	115.	6.173D 07	-19.476
34	3596.	102.	6.079D 07	-19.460
35	3702.	110.	7.763D 07	-19.725
36	3797.	80.	1.007D 08	-20.008
37	3894.	113.	1.328D 08	-20.308
38	3995.	90.	1.326D 08	-20.306
39	4111.	142.	1.304D 08	-20.288

EMERGENT SPECTRUM (LAMBDA IN ANGSTROMS, FLUX IN ERG/CM**2/S/A)

BAND	MID LAMBDA	BAND WIDTH'	AVG.F LAMBDA	AVG.M LAMBDA
40	4245.	126.	1.312D 08	-20.295
41	4365.	114.	1.067D 08	-20.070
42	4475.	106.	1.131D 08	-20.134
43	4589.	122.	1.050D 08	-20.053
44	4705.	109.	9.834D 07	-19.982
45	4822.	127.	8.049D 07	-19.764
46	4945.	118.	8.501D 07	-19.824
47	5053.	98.	8.112D 07	-19.773
48	5147.	90.	7.443D 07	-19.679
49	5248.	112.	7.028D 07	-19.617
50	5361.	113.	6.592D 07	-19.548
51	5486.	138.	6.242D 07	-19.488
52	5627.	144.	5.866D 07	-19.421
53	5753.	108.	5.559D 07	-19.362
54	5858.	101.	5.080D 07	-19.265
55	5959.	102.	5.009D 07	-19.249
56	6056.	92.	4.732D 07	-19.188
57	6154.	103.	4.388D 07	-19.106
58	6258.	107.	4.199D 07	-19.058
59	6376.	129.	3.988D 07	-19.002
60	6482.	82.	3.739D 07	-18.932
61	6593.	140.	3.180D 07	-18.756
62	6713.	100.	3.432D 07	-18.839
63	6813.	100.	3.283D C7	-18.791
64	6913.	101.	3.137D 07	-18.741
65	7018.	108.	2.959D 07	-18.678
66	7141.	138.	2.798D 07	-18.617
67	7270.	119.	2.659D 07	-18.562
68	7383.	108.	2.530D 07	-18.508
69	7513.	151.	2.367D 07	-18.435
70	7669.	162.	2.248D 07	-18.380
71	7820.	140.	2.043D 07	-18.276
72	7968.	155.	1.943D 07	-18.221
73	8125.	161.	1.837D 07	-18.160
74	8290.	169.	2.077D 07	-18.294
75	11482.	6213.	8.386D 06	-17.309
76	18691.	8206.	1.418D 06	-15.380
77	27809.	10029.	3.078D 05	-13.721
78	49235.	32823.	4.411D 04	-11.611

STATISTICAL UV MODEL

TEFF = 9700.　　LOG G = 4.26　　PI F = 5.019D 11

BALMER JUMP = .511　　PASCHEN SLOPE = 5.729D-04 MAG/Å

PERCENT OF THE FLUX IN THE DIFFERENT HYDROGEN CONTINUA:

LYMAN	BALMER	PASCHEN	THE OTHERS
0.00	29.81	55.84	14.34

TAU	TEMP DEG.K	H ERG/CM**2/SEC/STERADIAN		P TOTAL --- DYNE/CM**2	P GAS ----
1.0D-08	7491.	4.014D 10	7.028D 10	7.939D 00	1.028D-03
1.0D-07	7491.	4.014D 10	7.029D 10	7.948D 00	1.054D-02
1.0D-06	7491.	4.014D 10	7.030D 10	8.044D 00	1.056D-01
1.0D-05	7491.	4.014D 10	7.044D 10	8.995D 00	1.057D 00
1.0D-04	7491.	4.014D 10	7.185D 10	1.851D 01	1.057D 01
2.5D-04	7496.	3.995D 10	7.234D 10	3.752D 01	2.956D 01
5.0D-04	7499.	3.993D 10	7.286D 10	6.970D 01	6.173D 01
7.5D-04	7512.	3.995D 10	7.336D 10	1.010D 02	9.296D 01
1.0D-03	7704.	4.001D 10	7.417D 10	1.280D 02	1.191D 02
2.5D-03	8010.	3.998D 10	7.692D 10	2.133D 02	2.029D 02
5.0D-03	8101.	3.999D 10	7.996D 10	3.203D 02	3.095D 02
7.5D-03	8193.	4.001D 10	8.269D 10	4.080D 02	3.967D 02
1.0D-02	8270.	4.002D 10	8.518D 10	4.821D 02	4.703D 02
2.5D-02	8582.	3.996D 10	9.760D 10	7.908D 02	7.771D 02
5.0D-02	8913.	3.979D 10	1.144D 11	1.096D 03	1.080D 03
7.5D-02	9174.	3.975D 10	1.293D 11	1.294D 03	1.276D 03
1.0D-01	9415.	3.980D 10	1.435D 11	1.439D 03	1.419D 03
2.5D-01	10535.	4.012D 10	2.229D 11	1.898D 03	1.866D 03
5.0D-01	11707.	3.996D 10	3.385D 11	2.330D 03	2.283D 03
7.5D-01	12404.	3.962D 10	4.292D 11	2.708D 03	2.648D 03
1.0D 00	12942.	3.971D 10	5.090D 11	3.075D 03	3.004D 03
2.5D 00	14759.	4.001D 10	8.601D 11	5.112D 03	4.992D 03
5.0D 00	16229.	3.995D 10	1.255D 12	7.985D 03	7.809D 03
7.5D 00	17155.	3.996D 10	1.566D 12	1.043D 04	1.021D 04
1.0D 01	17853.	3.994D 10	1.836D 12	1.262D 04	1.236D 04
2.5D 01	20354.	3.994D 10	3.104D 12	2.326D 04	2.282D 04
5.0D 01	22707.	3.994D 10	4.813D 12	3.748D 04	3.681D 04
7.5D 01	24390.	3.995D 10	6.388D 12	5.006D 04	4.916D 04
1.0D 02	25726.	3.987D 10	7.903D 12	6.164D 04	6.054D 04

TAU	PE	DENSITY	MU	K ZERO	DEPTH
	DYNE/CM**2	GM/CM**3	A.M.U.	CM**2/GM	CM
1.0D-08	2.480D-04	1.758D-15	0.74958	2.475D-01	-5.43D 07
1.0D-07	2.370D-03	1.842D-14	0.74989	2.474D-01	-5.43D 07
1.0D-06	2.359D-02	1.850D-13	0.75296	2.465D-01	-5.38D 07
1.0D-05	2.358D-01	1.851D-12	0.78371	2.378D-01	-4.89D 07
1.0D-04	2.358D 00	1.851D-11	1.09123	1.502D-01	0.0
2.5D-04	4.510D 00	5.645D-11	1.18970	1.409D-01	3.03D 07
5.0D-04	6.949D 00	1.234D-10	1.24523	1.427D-01	5.06D 07
7.5D-04	8.920D 00	1.890D-10	1.26954	1.496D-01	6.19D 07
1.0D-03	1.339D 01	2.316D-10	1.24799	2.170D-01	6.84D 07
2.5D-03	2.620D 01	3.726D-10	1.22343	3.820D-01	8.43D 07
5.0D-03	3.717D 01	5.677D-10	1.23611	4.722D-01	9.68D 07
7.5D-03	4.764D 01	7.195D-10	1.23624	5.691D-01	1.04D 08
1.0D-02	5.732D 01	8.433D-10	1.23382	6.610D-01	1.09D 08
2.5D-02	1.067D 02	1.319D-09	1.21234	1.147D 00	1.25D 08
5.0D-02	1.777D 02	1.711D-09	1.17417	1.914D 00	1.36D 08
7.5D-02	2.460D 02	1.896D-09	1.13509	2.739D 00	1.42D 08
1.0D-01	3.154D 02	1.981D-09	1.09402	3.666D 00	1.46D 08
2.5D-01	6.680D 02	1.922D-09	0.90324	8.987D 00	1.58D 08
5.0D-01	9.887D 02	1.868D-09	0.79658	1.210D 01	1.71D 08
7.5D-01	1.190D 03	1.985D-09	0.77407	1.260D 01	1.81D 08
1.0D 00	1.369D 03	2.132D-09	0.76468	1.285D 01	1.91D 08
2.5D 00	2.324D 03	3.050D-09	0.75110	1.456D 01	2.33D 08
5.0D 00	3.692D 03	4.282D-09	0.74090	1.750D 01	2.76D 08
7.5D 00	4.891D 03	5.236D-09	0.73227	1.990D 01	3.04D 08
1.0D 01	5.980D 03	6.035D-09	0.72559	2.186D 01	3.25D 08
2.5D 01	1.129D 04	9.556D-09	0.70993	2.874D 01	4.01D 08
5.0D 01	1.834D 04	1.372D-08	0.70512	3.409D 01	4.68D 08
7.5D 01	2.453D 04	1.705D-08	0.70381	3.725D 01	5.15D 08
1.0D 02	3.023D 04	1.990D-08	0.70330	3.942D 01	5.50D 08

EMERGENT SPECTRUM (LAMBDA IN ANGSTROMS, FLUX IN ERG/CM**2/S/A)

BAND	MID LAMBDA	BAND WIDTH	AVG.F LAMBDA	AVG.M LAMBDA
1	196.	131.	1.256D-09	22.252
2	332.	141.	1.256D-09	22.252
3	453.	102.	3.843D-05	11.038
4	558.	107.	5.402D-02	3.169
5	659.	96.	1.457D 01	-2.909
6	759.	104.	2.821D 02	-6.126
7	861.	101.	4.519D 03	-9.138
8	965.	107.	5.803D 04	-11.909
9	1075.	111.	9.121D 05	-14.900
10	1173.	86.	5.872D 06	-16.922
11	1261.	91.	1.900D 07	-18.197
12	1370.	127.	2.047D 07	-18.278
13	1478.	87.	2.311D 07	-18.409
14	1573.	103.	2.678D 07	-18.569
15	1687.	126.	3.791D 07	-18.947
16	1800.	100.	4.956D 07	-19.238
17	1897.	93.	5.875D 07	-19.422
18	1997.	108.	6.258D 07	-19.491
19	2093.	83.	6.637D 07	-19.555
20	2192.	116.	7.046D 07	-19.620
21	2298.	96.	7.643D 07	-19.708
22	2383.	73.	8.010D 07	-19.759
23	2465.	92.	8.255D 07	-19.792
24	2556.	89.	8.316D 07	-19.800
25	2648.	95.	8.286D 07	-19.796
26	2743.	96.	8.158D 07	-19.779
27	2864.	145.	7.694D 07	-19.715
28	2979.	86.	7.316D 07	-19.661
29	3072.	99.	7.053D 07	-19.621
30	3166.	90.	6.813D 07	-19.583
31	3260.	99.	6.610D 07	-19.550
32	3370.	120.	6.417D 07	-19.518
33	3488.	115.	6.259D 07	-19.491
34	3596.	102.	6.153D 07	-19.473
35	3702.	110.	7.954D 07	-19.752
36	3797.	80.	1.038D 08	-20.041
37	3894.	113.	1.379D 08	-20.349
38	3995.	90.	1.374D 08	-20.345
39	4111.	142.	1.351D 08	-20.327

EMERGENT SPECTRUM (LAMBDA IN ANGSTROMS, FLUX IN ERG/CM**2/S/A)

BAND	MID LAMBDA	BAND WIDTH	AVG.F LAMBDA	AVG.M LAMBDA
40	4245.	126.	1.357D 08	-20.331
41	4365.	114.	1.102D 08	-20.105
42	4475.	106.	1.168D 08	-20.168
43	4589.	122.	1.082D 08	-20.086
44	4705.	109.	1.014D 08	-20.015
45	4822.	127.	8.263D 07	-19.793
46	4945.	118.	8.745D 07	-19.854
47	5053.	98.	8.337D 07	-19.803
48	5147.	90.	7.632D 07	-19.707
49	5248.	112.	7.204D 07	-19.644
50	5361.	113.	6.751D 07	-19.573
51	5486.	138.	6.388D 07	-19.513
52	5627.	144.	5.997D 07	-19.445
53	5753.	108.	5.671D 07	-19.384
54	5858.	101.	5.184D 07	-19.287
55	5959.	102.	5.101D 07	-19.269
56	6056.	92.	4.815D 07	-19.207
57	6154.	103.	4.465D 07	-19.125
58	6258.	107.	4.267D 07	-19.075
59	6376.	129.	4.053D 07	-19.019
60	6482.	82.	3.793D 07	-18.947
61	6593.	140.	3.217D 07	-18.769
62	6713.	100.	3.477D 07	-18.853
63	6813.	100.	3.324D 07	-18.804
64	6913.	101.	3.173D 07	-18.754
65	7018.	108.	2.992D 07	-18.690
66	7141.	138.	2.828D 07	-18.629
67	7270.	119.	2.685D 07	-18.572
68	7383.	108.	2.554D 07	-18.518
69	7513.	151.	2.390D 07	-18.446
70	7669.	162.	2.267D 07	-18.389
71	7820.	140.	2.060D 07	-18.285
72	7968.	155.	1.958D 07	-18.230
73	8125.	161.	1.851D 07	-18.169
74	8290.	169.	2.110D 07	-18.311
75	11482.	6213.	8.461D 06	-17.319
76	18691.	8206.	1.422D 06	-15.382
77	27809.	10029.	3.084D 05	-13.723
78	49235.	32823.	4.432D 04	-11.616

9700 CONTINUUM MODEL

TEFF = 9700. LOG G = 4.26 PI F = 5.019D 11

BALMER JUMP = .532 PASCHEN SLOPE = 5.368D-04 MAG/A

PERCENT OF THE FLUX IN THE DIFFERENT HYDROGEN CONTINUA:

LYMAN	BALMER	PASCHEN	THE OTHERS
0.00	39.96	47.75	12.29

TAU	TEMP DEG.K	H ERG/CM**2/SEC/STERADIAN	J	P TOTAL --- DYNE/CM**2 ----	P GAS
1.0D-08	7467.	4.008D 10	6.734D 10	7.838D 00	1.059D-03
1.0D-07	7467.	4.008D 10	6.734D 10	7.848D 00	1.088D-02
1.0D-06	7467.	4.008D 10	6.734D 10	7.946D 00	1.091D-01
1.0D-05	7467.	4.008D 10	6.734D 10	8.928D 00	1.091D 00
1.0D-04	7467.	4.008D 10	6.737D 10	1.875D 01	1.091D 01
2.5D-04	7468.	4.008D 10	6.746D 10	3.865D 01	3.081D 01
5.0D-04	7469.	4.007D 10	6.762D 10	7.253D 01	6.468D 01
7.5D-04	7471.	4.007D 10	6.778D 10	1.057D 02	9.780D 01
1.0D-03	7472.	4.007D 10	6.793D 10	1.377D 02	1.299D 02
2.5D-03	7498.	4.005D 10	6.883D 10	3.124D 02	3.044D 02
5.0D-03	7564.	4.002D 10	7.017D 10	5.472D 02	5.389D 02
7.5D-03	7630.	3.999D 10	7.142D 10	7.360D 02	7.274D 02
1.0D-02	7678.	3.995D 10	7.260D 10	8.976D 02	8.889D 02
2.5D-02	7827.	3.977D 10	7.872D 10	1.629D 03	1.620D 03
5.0D-02	7967.	3.971D 10	8.724D 10	2.495D 03	2.484D 03
7.5D-02	8160.	3.990D 10	9.527D 10	3.115D 03	3.104D 03
1.0D-01	8405.	4.013D 10	1.035D 11	3.552D 03	3.540D 03
2.5D-01	9377.	3.996D 10	1.496D 11	4.640D 03	4.620D 03
5.0D-01	10345.	3.991D 10	2.165D 11	5.242D 03	5.213D 03
7.5D-01	11014.	4.006D 10	2.753D 11	5.531D 03	5.494D 03
1.0D 00	11523.	4.002D 10	3.277D 11	5.753D 03	5.708D 03
2.5D 00	13270.	3.988D 10	5.686D 11	6.861D 03	6.783D 03
5.0D 00	14713.	3.988D 10	8.522D 11	8.725D 03	8.607D 03
7.5D 00	15601.	3.993D 10	1.074D 12	1.057D 04	1.042D 04
1.0D 01	16262.	3.997D 10	1.266D 12	1.235D 04	1.217D 04
2.5D 01	18606.	3.998D 10	2.168D 12	2.155D 04	2.125D 04
5.0D 01	20731.	3.998D 10	3.344D 12	3.404D 04	3.357D 04
7.5D 01	22180.	3.998D 10	4.368D 12	4.505D 04	4.444D 04
1.0D 02	23289.	3.991D 10	5.308D 12	5.519D 04	5.445D 04

TAU	PE	DENSITY	MU	K ZERO	DEPTH
	DYNE/CM**2	GM/CM**3	A.M.U.	CM**2/GM	CM
1.0D-08	2.469D-04	1.837D-15	0.74961	2.475D-01	-5.27D 07
1.0D-07	2.358D-03	1.928D-14	0.74993	2.474D-01	-5.26D 07
1.0D-06	2.347D-02	1.937D-13	0.75311	2.465D-01	-5.22D 07
1.0D-05	2.346D-01	1.938D-12	0.78489	2.372D-01	-4.74D 07
1.0D-04	2.346D 00	1.938D-11	1.10270	1.443D-01	0.0
2.5D-04	4.460D 00	5.961D-11	1.20071	1.341D-01	3.02D 07
5.0D-04	6.848D 00	1.308D-10	1.25470	1.354D-01	5.04D 07
7.5D-04	8.659D 00	2.016D-10	1.27990	1.395D-01	6.16D 07
1.0D-03	1.014D 01	2.706D-10	1.29464	1.440D-01	6.90D 07
2.5D-03	1.645D 01	6.496D-10	1.32890	1.694D-01	9.12D 07
5.0D-03	2.490D 01	1.148D-09	1.33990	2.183D-01	1.06D 08
7.5D-03	3.211D 01	1.539D-09	1.34282	2.621D-01	1.13D 08
1.0D-02	3.821D 01	1.871D-09	1.34445	2.982D-01	1.19D 08
2.5D-02	6.442D 01	3.357D-09	1.34901	4.422D-01	1.34D 08
5.0D-02	9.760D 01	5.059D-09	1.34979	6.167D-01	1.46D 08
7.5D-02	1.424D 02	6.127D-09	1.34093	8.766D-01	1.52D 08
1.0D-01	2.069D 02	6.695D-09	1.32352	1.289D 00	1.56D 08
2.5D-01	6.374D 02	7.176D-09	1.21187	4.748D 00	1.64D 08
5.0D-01	1.333D 03	6.336D-09	1.04572	1.250D 01	1.68D 08
7.5D-01	1.841D 03	5.608D-09	0.93479	1.908D 01	1.71D 08
1.0D 00	2.178D 03	5.177D-09	0.86920	2.297D 01	1.73D 08
2.5D 00	3.052D 03	4.748D-09	0.77298	2.554D 01	1.86D 08
5.0D 00	3.977D 03	5.312D-09	0.75574	2.474D 01	2.06D 08
7.5D 00	4.861D 03	6.018D-09	0.74978	2.541D 01	2.23D 08
1.0D 01	5.719D 03	6.699D-09	0.74496	2.653D 01	2.38D 08
2.5D 01	1.031D 04	9.919D-09	0.72343	3.323D 01	2.99D 08
5.0D 01	1.659D 04	1.381D-08	0.71065	3.978D 01	3.56D 08
7.5D 01	2.209D 04	1.702D-08	0.70669	4.388D 01	3.95D 08
1.0D 02	2.712D 04	1.982D-08	0.70517	4.687D 01	4.25D 08

EMERGENT SPECTRUM (LAMBDA IN ANGSTROMS, FLUX IN ERG/CM**2/S/A)

BAND	MID LAMBDA	BAND WIDTH	AVG.F LAMBDA	AVG.M LAMBDA
1	196.	131.	1.047D-09	22.450
2	332.	141.	1.047D-09	22.450
3	453.	102.	1.898D-05	11.804
4	558.	107.	2.874D-02	3.854
5	659.	96.	1.324D 01	-2.805
6	759.	104.	2.345D 03	-8.425
7	861.	101.	1.656D 05	-13.048
8	965.	107.	4.286D 06	-16.580
9	1075.	111.	2.208D 07	-18.360
10	1173.	86.	6.421D 07	-19.519
11	1261.	91.	1.205D 08	-20.202
12	1370.	127.	1.080D 08	-20.084
13	1478.	87.	9.781D 07	-19.976
14	1573.	103.	9.015D 07	-19.887
15	1687.	126.	8.236D 07	-19.789
16	1800.	100.	7.601D 07	-19.702
17	1897.	93.	7.147D 07	-19.635
18	1997.	108.	6.759D 07	-19.575
19	2093.	83.	6.443D 07	-19.523
20	2192.	116.	6.163D 07	-19.474
21	2298.	96.	5.925D 07	-19.432
22	2383.	73.	5.755D 07	-19.400
23	2465.	92.	5.604D 07	-19.371
24	2556.	89.	5.461D 07	-19.343
25	2648.	95.	5.327D 07	-19.316
26	2743.	96.	5.198D 07	-19.290
27	2864.	145.	5.060D 07	-19.260
28	2979.	86.	4.932D 07	-19.232
29	3072.	99.	4.831D 07	-19.210
30	3166.	90.	4.732D 07	-19.188
31	3260.	99.	4.634D 07	-19.165
32	3370.	120.	4.522D 07	-19.138
33	3488.	115.	4.406D 07	-19.110
34	3596.	102.	4.301D 07	-19.084
35	3702.	110.	1.482D 08	-20.427
36	3797.	80.	1.384D 08	-20.352
37	3894.	113.	1.292D 08	-20.279
38	3995.	90.	1.205D 08	-20.202
39	4111.	142.	1.114D 08	-20.117

EMERGENT SPECTRUM (LAMBDA IN ANGSTROMS, FLUX IN ERG/CM**2/S/A)

BAND	MID LAMBDA	BAND WIDTH	AVG.F LAMBDA	AVG.M LAMBDA
40	4245.	126.	1.020D 08	-20.021
41	4365.	114.	9.441D 07	-19.938
42	4475.	106.	8.812D 07	-19.863
43	4589.	122.	8.217D 07	-19.787
44	4705.	109.	7.666D 07	-19.711
45	4822.	127.	7.153D 07	-19.636
46	4945.	118.	6.666D 07	-19.560
47	5053.	98.	6.272D 07	-19.494
48	5147.	90.	5.953D 07	-19.437
49	5248.	112.	5.634D 07	-19.377
50	5361.	113.	5.304D 07	-19.312
51	5486.	138.	4.966D 07	-19.240
52	5627.	144.	4.618D 07	-19.161
53	5753.	108.	4.333D 07	-19.092
54	5858.	101.	4.113D 07	-19.035
55	5959.	102.	3.913D 07	-18.981
56	6056.	92.	3.734D 07	-18.930
57	6154.	103.	3.564D 07	-18.880
58	6258.	107.	3.392D 07	-18.826
59	6376.	129.	3.212D 07	-18.767
60	6482.	82.	3.059D 07	-18.714
61	6593.	140.	2.910D 07	-18.660
62	6713.	100.	2.759D 07	-18.602
63	6813.	100.	2.641D 07	-18.554
64	6913.	101.	2.528D 07	-18.507
65	7016.	108.	2.418D 07	-18.459
66	7141.	138.	2.295D 07	-18.402
67	7270.	119.	2.175D 07	-18.344
68	7383.	108.	2.076D 07	-18.293
69	7513.	151.	1.970D 07	-18.236
70	7669.	162.	1.850D 07	-18.168
71	7820.	140.	1.743D 07	-18.103
72	7968.	155.	1.646D 07	-18.041
73	8125.	161.	1.550D 07	-17.976
74	8290.	169.	1.765D 07	-18.117
75	11482.	6213.	7.140D 06	-17.134
76	18691.	8206.	1.271D 06	-15.260
77	27809.	10029.	2.794D 05	-13.615
78	49235.	32823.	4.065D 04	-11.523

11160 CONTINUUM MODEL

TEFF = 11160.   LOG G = 4.26   PI F = 8.794D 11

BALMER JUMP = .473   PASCHEN SLOPE = 5.742D-04 MAG/A

PERCENT OF THE FLUX IN THE DIFFERENT HYDROGEN CONTINUA:

LYMAN	BALMER	PASCHEN	THE OTHERS
0.00	53.00	38.50	8.51

TAU	TEMP DEG.K	H ERG/CM**2/SEC/STERADIAN	J	P TOTAL --- DYNE/CM**2 ----	P GAS
1.00-08	7664.	6.992D 10	1.160D 11	8.700D 00	8.582D-04
1.0D-07	7664.	6.992D 10	1.160D 11	8.708D 00	8.676D-03
1.0D-06	7664.	6.992D 10	1.160D 11	8.786D 00	8.685D-02
1.0D-05	7664.	6.992D 10	1.160D 11	9.568D 00	8.686D-01
1.0D-04	7665.	6.992D 10	1.160D 11	1.739D 01	8.686D 00
2.5D-04	7699.	6.993D 10	1.161D 11	3.177D 01	2.291D 01
5.0D-04	7956.	6.994D 10	1.164D 11	5.148D 01	4.138D 01
7.5D-04	8031.	6.995D 10	1.167D 11	6.619D 01	5.570D 01
1.0D-03	8056.	6.996D 10	1.169D 11	7.944D 01	6.882D 01
2.5D-03	8141.	7.000D 10	1.186D 11	1.482D 02	1.371D 02
5.0D-03	8257.	7.005D 10	1.212D 11	2.384D 02	2.266D 02
7.5D-03	8353.	7.009D 10	1.236D 11	3.110D 02	2.987D 02
1.0D-02	8435.	7.012D 10	1.260D 11	3.722D 02	3.594D 02
2.5D-02	8790.	7.022D 10	1.387D 11	6.225D 02	6.075D 02
5.0D-02	9177.	7.028D 10	1.569D 11	8.622D 02	8.443D 02
7.5D-02	9472.	7.032D 10	1.730D 11	1.015D 03	9.948D 02
1.0D-01	9723.	7.034D 10	1.879D 11	1.130D 03	1.107D 03
2.5D-01	10723.	7.011D 10	2.624D 11	1.548D 03	1.514D 03
5.0D-01	11693.	6.986D 10	3.596D 11	2.014D 03	1.967D 03
7.5D-01	12328.	6.979D 10	4.392D 11	2.419D 03	2.361D 03
1.0D 00	12824.	6.981D 10	5.097D 11	2.804D 03	2.735D 03
2.5D 00	14595.	6.998D 10	8.361D 11	4.863D 03	4.749D 03
5.0D 00	16111.	6.996D 10	1.227D 12	7.737D 03	7.567D 03
7.5D 00	17071.	6.993D 10	1.542D 12	1.019D 04	9.975D 03
1.0D 01	17798.	6.990D 10	1.818D 12	1.239D 04	1.213D 04
2.5D 01	20431.	7.000D 10	3.154D 12	2.313D 04	2.269D 04
5.0D 01	22848.	6.989D 10	4.935D 12	3.767D 04	3.698D 04
7.5D 01	24520.	6.994D 10	6.524D 12	5.055D 04	4.964D 04
1.0D 02	25816.	6.977D 10	8.014D 12	6.243D 04	6.131D 04

TAU	PE	DENSITY	MU	K ZERO	DEPTH
	DYNE/CM**2	GM/CM**3	A.M.U.	CM**2/GM	CM
1.0D-08	2.551D-04	1.329D-15	0.74917	2.478D-01	-6.57D 07
1.0D-07	2.449D-03	1.372D-14	0.74941	2.477D-01	-6.56D 07
1.0D-06	2.439D-02	1.376D-13	0.75176	2.473D-01	-6.50D 07
1.0D-05	2.438D-01	1.377D-12	0.77527	2.425D-01	-5.91D 07
1.0D-04	2.438D 00	1.377D-11	1.01034	1.946D-01	0.0
2.5D-04	4.883D 00	3.955D-11	1.10562	1.969D-01	3.16D 07
5.0D-04	9.307D 00	6.806D-11	1.08893	2.933D-01	5.06D 07
7.5D-04	1.212D 01	9.165D-11	1.09884	3.345D-01	6.07D 07
1.0D-03	1.424D 01	1.144D-10	1.11374	3.551D-01	6.77D 07
2.5D-03	2.396D 01	2.348D-10	1.15936	4.418D-01	9.01D 07
5.0D-03	3.673D 01	3.884D-10	1.17709	5.688D-01	1.06D 08
7.5D-03	4.789D 01	5.070D-10	1.17965	6.871D-01	1.15D 08
1.0D-02	5.818D 01	6.030D-10	1.17764	8.002D-01	1.21D 08
2.5D-02	1.119D 02	9.521D-10	1.14657	1.438D 00	1.39D 08
5.0D-02	1.885D 02	1.207D-09	1.09175	2.461D 00	1.51D 08
7.5D-02	2.576D 02	1.314D-09	1.04222	3.484D 00	1.57D 08
1.0D-01	3.208D 02	1.366D-09	0.99915	4.470D 00	1.62D 08
2.5D-01	5.903D 02	1.455D-09	0.85821	8.437D 00	1.78D 08
5.0D-01	8.588D 02	1.601D-09	0.79150	1.072D 01	1.95D 08
7.5D-01	1.062D 03	1.779D-09	0.77344	1.152D 01	2.08D 08
1.0D 00	1.246D 03	1.960D-09	0.76523	1.206D 01	2.20D 08
2.5D 00	2.207D 03	2.937D-09	0.75200	1.430D 01	2.66D 08
5.0D 00	3.572D 03	4.185D-09	0.74193	1.728D 01	3.11D 08
7.5D 00	4.771D 03	5.144D-09	0.73308	1.967D 01	3.40D 08
1.0D 01	5.864D 03	5.944D-09	0.72606	2.162D 01	3.62D 08
2.5D 01	1.123D 04	9.460D-09	0.70953	2.830D 01	4.39D 08
5.0D 01	1.843D 04	1.369D-08	0.70492	3.365D 01	5.08D 08
7.5D 01	2.478D 04	1.713D-08	0.70374	3.706D 01	5.55D 08
1.0D 02	3.062D 04	2.008D-08	0.70328	3.953D 01	5.90D 08

EMERGENT SPECTRUM (LAMBDA IN ANGSTROMS, FLUX IN ERG/CM**2/S/A)

BAND	MID LAMBDA	BAND WIDTH	AVG.F LAMBDA	AVG.M LAMBDA
1	196.	131.	4.146D-09	20.956
2	332.	141.	4.146D-09	20.956
3	453.	102.	5.406D-05	10.668
4	558.	107.	6.713D-02	2.933
5	659.	96.	2.752D 01	-3.599
6	759.	104.	5.018D 03	-9.251
7	861.	101.	3.663D 05	-13.910
8	965.	107.	9.823D 06	-17.481
9	1075.	111.	5.360D 07	-19.323
10	1173.	86.	1.616D 08	-20.521
11	1261.	91.	3.093D 08	-21.226
12	1370.	127.	2.755D 08	-21.100
13	1478.	87.	2.473D 08	-20.983
14	1573.	103.	2.257D 08	-20.884
15	1687.	126.	2.033D 08	-20.770
16	1800.	100.	1.846D 08	-20.666
17	1897.	93.	1.709D 08	-20.582
18	1997.	108.	1.585D 08	-20.500
19	2093.	83.	1.483D 08	-20.428
20	2192.	116.	1.390D 08	-20.358
21	2298.	96.	1.306D 08	-20.290
22	2383.	73.	1.246D 08	-20.238
23	2465.	92.	1.191D 08	-20.190
24	2556.	89.	1.137D 08	-20.139
25	2648.	95.	1.087D 08	-20.090
26	2743.	96.	1.039D 08	-20.041
27	2864.	145.	9.867D 07	-19.985
28	2979.	86.	9.398D 07	-19.933
29	3072.	99.	9.042D 07	-19.891
30	3166.	90.	8.694D 07	-19.848
31	3260.	99.	8.365D 07	-19.806
32	3370.	120.	8.004D 07	-19.758
33	3488.	115.	7.641D 07	-19.708
34	3596.	102.	7.326D 07	-19.662
35	3702.	110.	2.200D 08	-20.856
36	3797.	80.	2.046D 08	-20.777
37	3894.	113.	1.904D 08	-20.699
38	3995.	90.	1.767D 08	-20.618
39	4111.	142.	1.626D 08	-20.528

EMERGENT SPECTRUM (LAMBDA IN ANGSTROMS, FLUX IN ERG/CM**2/S/A)

BAND	MID LAMBDA	BAND WIDTH	AVG.F LAMBDA	AVG.M LAMBDA
40	4245.	126.	1.480D 08	-20.426
41	4365.	114.	1.363D 08	-20.336
42	4475.	106.	1.266D 08	-20.256
43	4589.	122.	1.175D 08	-20.175
44	4705.	109.	1.091D 08	-20.094
45	4822.	127.	1.013D 08	-20.014
46	4945.	118.	9.389D 07	-19.931
47	5053.	98.	8.794D 07	-19.860
48	5147.	90.	8.314D 07	-19.800
49	5248.	112.	7.837D 07	-19.735
50	5361.	113.	7.346D 07	-19.665
51	5486.	138.	6.843D 07	-19.588
52	5627.	144.	6.331D 07	-19.504
53	5753.	108.	5.912D 07	-19.429
54	5858.	101.	5.590D 07	-19.369
55	5959.	102.	5.300D 07	-19.311
56	6056.	92.	5.040D 07	-19.256
57	6154.	103.	4.795D 07	-19.202
58	6258.	107.	4.548D 07	-19.144
59	6376.	129.	4.289D 07	-19.081
60	6482.	82.	4.072D 07	-19.025
61	6593.	140.	3.860D 07	-18.967
62	6713.	100.	3.646D 07	-18.905
63	6813.	100.	3.479D 07	-18.854
64	6913.	101.	3.321D 07	-18.803
65	7018.	108.	3.167D 07	-18.751
66	7141.	138.	2.996D 07	-18.691
67	7270.	119.	2.829D 07	-18.629
68	7383.	108.	2.692D 07	-18.575
69	7513.	151.	2.546D 07	-18.515
70	7669.	162.	2.382D 07	-18.442
71	7820.	140.	2.237D 07	-18.374
72	7968.	155.	2.105D 07	-18.308
73	8125.	161.	1.975D 07	-18.239
74	8290.	169.	2.240D 07	-18.375
75	11482.	6213.	8.731D 06	-17.353
76	18691.	8206.	1.466D 06	-15.415
77	27809.	10029.	3.173D 05	-13.754
78	49235.	32823.	4.543D 04	-11.643

SIRIUS GRID MODEL

TEFF = 10250. LOG G = 4.20 PI F = 6.258D 11

BALMER JUMP = .465 PASCHEN SLOPE = 5.772D-04 MAG/A

PERCENT OF THE FLUX IN THE DIFFERENT HYDROGEN CONTINUA:

LYMAN	BALMER	PASCHEN	THE OTHERS
0.00	37.64	50.08	12.28

TAU	TEMP DEG.K	H ERG/CM**2/SEC/STERADIAN	J	P TOTAL --- DYNE/CM**2 ----	P GAS
1.0D-08	7624.	5.000D 10	8.663D 10	8.519D 00	7.661D-04
1.0D-07	7624.	5.000D 10	8.663D 10	8.526D 00	7.760D-03
1.0D-06	7624.	5.000D 10	8.664D 10	8.596D 00	7.770D-02
1.0D-05	7624.	5.000D 10	8.679D 10	9.295D 00	7.771D-01
1.0D-04	7624.	4.999D 10	8.823D 10	1.629D 01	7.771D 00
2.5D-04	7628.	4.978D 10	8.889D 10	2.951D 01	2.097D 01
5.0D-04	7639.	4.977D 10	8.968D 10	5.189D 01	4.331D 01
7.5D-04	7899.	4.986D 10	9.088D 10	7.242D 01	6.259D 01
1.0D-03	8080.	4.987D 10	9.182D 10	8.513D 01	7.438D 01
2.5D-03	8285.	4.984D 10	9.492D 10	1.378D 02	1.259D 02
5.0D-03	8485.	4.985D 10	9.898D 10	2.001D 02	1.870D 02
7.5D-03	8587.	4.981D 10	1.023D 11	2.483D 02	2.346D 02
1.0D-02	8653.	4.978D 10	1.053D 11	2.899D 02	2.758D 02
2.5D-02	8950.	4.981D 10	1.205D 11	4.748D 02	4.587D 02
5.0D-02	9348.	4.998D 10	1.418D 11	6.651D 02	6.458D 02
7.5D-02	9662.	5.003D 10	1.606D 11	7.904D 02	7.684D 02
1.0D-01	9917.	4.997D 10	1.778D 11	8.880D 02	8.636D 02
2.5D-01	10954.	4.985D 10	2.648D 11	1.280D 03	1.244D 03
5.0D-01	12037.	4.972D 10	3.833D 11	1.763D 03	1.710D 03
7.5D-01	12728.	4.963D 10	4.799D 11	2.192D 03	2.126D 03
1.0D 00	13275.	4.978D 10	5.669D 11	2.599D 03	2.521D 03
2.5D 00	15225.	4.987D 10	9.757D 11	4.739D 03	4.603D 03
5.0D 00	16924.	4.980D 10	1.485D 12	7.645D 03	7.437D 03
7.5D 00	18012.	4.962D 10	1.904D 12	1.010D 04	9.835D 03
1.0D 01	18825.	4.980D 10	2.270D 12	1.231D 04	1.199D 04
2.5D 01	21551.	4.966D 10	3.901D 12	2.314D 04	2.260D 04
5.0D 01	23983.	4.986D 10	5.988D 12	3.757D 04	3.673D 04
7.5D 01	25706.	4.996D 10	7.881D 12	5.018D 04	4.908D 04
1.0D 02	27074.	4.970D 10	9.694D 12	6.171D 04	6.036D 04

TAU	PE	DENSITY	MU	K ZERO	DEPTH
	DYNE/CM**2	GM/CM**3	A.M.U.	CM**2/GM	CM
1.0D-08	2.268D-04	1.194D-15	0.74922	2.478D-01	-7.43D 07
1.0D-07	2.184D-03	1.235D-14	0.74946	2.477D-01	-7.42D 07
1.0D-06	2.176D-02	1.239D-13	0.75182	2.472D-01	-7.36D 07
1.0D-05	2.175D-01	1.240D-12	0.77542	2.416D-01	-6.69D 07
1.0D-04	2.175D 00	1.240D-11	1.01150	1.865D-01	0.0
2.5D-04	4.265D 00	3.700D-11	1.11820	1.769D-01	3.67D 07
5.0D-04	6.758D 00	8.082D-11	1.18403	1.796D-01	6.14D 07
7.5D-04	1.153D 01	1.091D-10	1.14797	2.820D-01	7.37D 07
1.0D-03	1.538D 01	1.233D-10	1.11509	3.726D-01	8.03D 07
2.5D-03	2.614D 01	2.035D-10	1.11333	5.348D-01	1.01D 08
5.0D-03	4.043D 01	2.917D-10	1.10123	7.523D-01	1.16D 08
7.5D-03	5.114D 01	3.608D-10	1.09862	8.987D-01	1.26D 08
1.0D-02	6.010D 01	4.209D-10	1.09876	1.012D 00	1.32D 08
2.5D-02	1.064D 02	6.647D-10	1.07949	1.628D 00	1.54D 08
5.0D-02	1.761D 02	8.486D-10	1.02236	2.695D 00	1.69D 08
7.5D-02	2.376D 02	9.277D-10	0.97169	3.708D 00	1.78D 08
1.0D-01	2.910D 02	9.751D-10	0.93273	4.583D 00	1.84D 08
2.5D-01	5.177D 02	1.119D-09	0.82098	7.598D 00	2.07D 08
5.0D-01	7.678D 02	1.322D-09	0.77408	9.108D 00	2.31D 08
7.5D-01	9.713D 02	1.531D-09	0.76328	9.737D 00	2.50D 08
1.0D 00	1.161D 03	1.728D-09	0.75820	1.021D 01	2.65D 08
2.5D 00	2.158D 03	2.709D-09	0.74660	1.240D 01	3.25D 08
5.0D 00	3.567D 03	3.859D-09	0.73138	1.523D 01	3.80D 08
7.5D 00	4.789D 03	4.727D-09	0.72094	1.730D 01	4.16D 08
1.0D 01	5.890D 03	5.468D-09	0.71489	1.886D 01	4.43D 08
2.5D 01	1.125D 04	8.886D-09	0.70582	2.444D 01	5.39D 08
5.0D 01	1.833D 04	1.294D-08	0.70373	2.920D 01	6.24D 08
7.5D 01	2.452D 04	1.614D-08	0.70312	3.210D 01	6.81D 08
1.0D 02	3.016D 04	1.884D-08	0.70285	3.407D 01	7.24D 08

EMERGENT SPECTRUM (LAMBDA IN ANGSTROMS, FLUX IN ERG/CM**2/S/A)

BAND	MID LAMBDA	BAND WIDTH	AVG.F LAMBDA	AVG.M LAMBDA
1	196.	131.	3.162D-09	21.250
2	332.	141.	3.162D-09	21.250
3	453.	102.	7.273D-05	10.346
4	558.	107.	9.003D-02	2.614
5	659.	96.	2.382D 01	-3.443
6	759.	104.	6.686D 02	-7.063
7	861.	101.	1.299D 04	-10.284
8	965.	107.	1.673D 05	-13.059
9	1075.	111.	1.364D 06	-15.337
10	1173.	86.	6.351D 06	-17.007
11	1261.	91.	1.906D 07	-18.200
12	1370.	127.	4.005D 07	-19.006
13	1478.	87.	7.138D 07	-19.634
14	1573.	103.	1.052D 08	-20.056
15	1687.	126.	1.349D 08	-20.325
16	1800.	100.	1.563D 08	-20.485
17	1897.	93.	1.641D 08	-20.538
18	1997.	108.	1.531D 08	-20.462
19	2093.	83.	1.392D 08	-20.359
20	2192.	116.	1.225D 08	-20.221
21	2298.	96.	9.433D 07	-19.937
22	2383.	73.	8.127D 07	-19.775
23	2465.	92.	7.397D 07	-19.673
24	2556.	89.	7.487D 07	-19.686
25	2648.	95.	7.631D 07	-19.706
26	2743.	96.	7.840D 07	-19.736
27	2864.	145.	8.570D 07	-19.832
28	2979.	86.	8.994D 07	-19.885
29	3072.	99.	9.108D 07	-19.899
30	3166.	90.	8.742D 07	-19.854
31	3260.	99.	8.420D 07	-19.813
32	3370.	120.	8.097D 07	-19.771
33	3488.	115.	7.807D 07	-19.731
34	3596.	102.	7.585D 07	-19.700
35	3702.	110.	9.802D 07	-19.978
36	3797.	80.	1.226D 08	-20.221
37	3894.	113.	1.576D 08	-20.494
38	3995.	90.	1.556D 08	-20.480
39	4111.	142.	1.518D 08	-20.453

EMERGENT SPECTRUM (LAMBDA IN ANGSTROMS, FLUX IN ERG/CM**2/S/A)

BAND	MID LAMBDA	BAND WIDTH'	AVG.F LAMBDA	AVG.M LAMBDA
40	4245.	126.	1.503D 08	-20.442
41	4365.	114.	1.239D 08	-20.232
42	4475.	106.	1.291D 08	-20.277
43	4589.	122.	1.194D 08	-20.193
44	4705.	109.	1.125D 08	-20.128
45	4822.	127.	9.276D 07	-19.918
46	4945.	118.	9.772D 07	-19.975
47	5053.	98.	9.277D 07	-19.919
48	5147.	90.	8.414D 07	-19.812
49	5248.	112.	7.941D 07	-19.750
50	5361.	113.	7.441D 07	-19.679
51	5486.	138.	7.099D 07	-19.628
52	5627.	144.	6.657D 07	-19.558
53	5753.	108.	6.252D 07	-19.490
54	5858.	101.	5.740D 07	-19.397
55	5959.	102.	5.608D 07	-19.372
56	6056.	92.	5.304D 07	-19.311
57	6154.	103.	4.927D 07	-19.231
58	6258.	107.	4.704D 07	-19.181
59	6376.	129.	4.484D 07	-19.129
60	6482.	82.	4.192D 07	-19.056
61	6593.	140.	3.575D 07	-18.883
62	6713.	100.	3.821D 07	-18.956
63	6813.	100.	3.648D 07	-18.905
64	6913.	101.	3.481D 07	-18.854
65	7018.	108.	3.286D 07	-18.792
66	7141.	138.	3.107D 07	-18.731
67	7270.	119.	2.944D 07	-18.672
68	7383.	108.	2.803D 07	-18.619
69	7513.	151.	2.625D 07	-18.548
70	7669.	162.	2.484D 07	-18.488
71	7820.	140.	2.249D 07	-18.380
72	7968.	155.	2.144D 07	-18.328
73	8125.	161.	2.031D 07	-18.269
74	8290.	169.	2.272D 07	-18.391
75	11482.	6213.	9.044D 06	-17.391
76	18691.	8206.	1.503D 06	-15.442
77	27809.	10029.	3.243D 05	-13.777
78	49235.	32823.	4.641D 04	-11.666

SIRIUS GRID MODEL

TEFF = 10000. LOG G = 3.80 PI F = 5.669D 11

BALMER JUMP = .487 PASCHEN SLOPE = 5.743D-04 MAG/A

PERCENT OF THE FLUX IN THE DIFFERENT HYDROGEN CONTINUA:

LYMAN	BALMER	PASCHEN	THE OTHERS
0.00	34.41	52.53	13.06

TAU	TEMP DEG.K	H ERG/CM**2/SEC/STERADIAN	J	P TOTAL --- DYNE/CM**2	P GAS ----
1.0D-08	7629.	4.540D 10	7.886D 10	8.540D 00	2.823D-04
1.0D-07	7629.	4.540D 10	7.886D 10	8.542D 00	2.841D-03
1.0D-06	7629.	4.540D 10	7.888D 10	8.568D 00	2.842D-02
1.0D-05	7629.	4.540D 10	7.901D 10	8.824D 00	2.843D-01
1.0D-04	7629.	4.539D 10	8.037D 10	1.138D 01	2.843D 00
2.5D-04	7633.	4.514D 10	8.091D 10	1.624D 01	7.679D 00
5.0D-04	7635.	4.507D 10	8.146D 10	2.484D 01	1.627D 01
7.5D-04	7637.	4.504D 10	8.195D 10	3.363D 01	2.506D 01
1.0D-03	7639.	4.504D 10	8.242D 10	4.246D 01	3.387D 01
2.5D-03	8090.	4.522D 10	8.603D 10	8.380D 01	7.299D 01
5.0D-03	8273.	4.519D 10	8.976D 10	1.200D 02	1.082D 02
7.5D-03	8403.	4.517D 10	9.295D 10	1.480D 02	1.355D 02
1.0D-02	8485.	4.513D 10	9.576D 10	1.715D 02	1.584D 02
2.5D-02	8761.	4.502D 10	1.095D 11	2.757D 02	2.608D 02
5.0D-02	9126.	4.513D 10	1.287D 11	3.865D 02	3.690D 02
7.5D-02	9432.	4.525D 10	1.459D 11	4.609D 02	4.410D 02
1.0D-01	9690.	4.527D 10	1.617D 11	5.190D 02	4.967D 02
2.5D-01	10713.	4.504D 10	2.418D 11	7.544D 02	7.211D 02
5.0D-01	11807.	4.515D 10	3.539D 11	1.052D 03	1.003D 03
7.5D-01	12500.	4.502D 10	4.456D 11	1.320D 03	1.258D 03
1.0D 00	13047.	4.513D 10	5.281D 11	1.573D 03	1.500D 03
2.5D 00	14991.	4.514D 10	9.168D 11	2.903D 03	2.776D 03
5.0D 00	16693.	4.513D 10	1.406D 12	4.693D 03	4.502D 03
7.5D 00	17791.	4.511D 10	1.812D 12	6.212D 03	5.959D 03
1.0D 01	18610.	4.500D 10	2.168D 12	7.573D 03	7.270D 03
2.5D 01	21311.	4.500D 10	3.730D 12	1.424D 04	1.372D 04
5.0D 01	23635.	4.531D 10	5.647D 12	2.296D 04	2.217D 04
7.5D 01	25249.	4.516D 10	7.335D 12	3.045D 04	2.942D 04
1.0D 02	26524.	4.497D 10	8.930D 12	3.716D 04	3.591D 04

TAU	PF DYNE/CM**2	DENSITY GM/CM**3	MU A.M.U.	K ZERO CM**2/GM	DEPTH CM
1.0D-08	1.037D-04	3.954D-16	0.74827	2.484D-01	-2.17D 08
1.0D-07	1.017D-03	4.037D-15	0.74841	2.484D-01	-2.17D 08
1.0D-06	1.015D-02	4.046D-14	0.74981	2.480D-01	-2.15D 08
1.0D-05	1.015D-01	4.047D-13	0.76376	2.442D-01	-1.96D 08
1.0D-04	1.015D 00	4.047D-12	0.90327	2.062D-01	0.0
2.5D-04	2.169D 00	1.219D-11	1.00681	1.888D-01	1.03D 08
5.0D-04	3.636D 00	2.795D-11	1.08832	1.806D-01	1.74D 08
7.5D-04	4.821D 00	4.476D-11	1.13340	1.787D-01	2.13D 08
1.0D-03	5.228D 00	6.201D-11	1.16196	1.790D-01	2.39D 08
2.5D-03	1.531D 01	1.204D-10	1.11041	3.762D-01	3.06D 08
5.0D-03	2.346D 01	1.729D-10	1.10045	5.136D-01	3.44D 08
7.5D-03	3.051D 01	2.109D-10	1.08876	6.350D-01	3.67D 08
1.0D-02	3.628D 01	2.431D-10	1.08340	7.271D-01	3.83D 08
2.5D-02	6.314D 01	3.810D-10	1.06509	1.136D 00	4.36D 08
5.0D-02	1.033D 02	4.918D-10	1.01232	1.830D 00	4.75D 08
7.5D-02	1.397D 02	5.394D-10	0.96121	2.513D 00	4.97D 08
1.0D-01	1.717D 02	5.663D-10	0.92040	3.113D 00	5.13D 08
2.5D-01	3.047D 02	6.562D-10	0.81202	5.044D 00	5.71D 08
5.0D-01	4.538D 02	7.858D-10	0.76938	5.920D 00	6.34D 08
7.5D-01	5.774D 02	9.186D-10	0.76030	6.296D 00	6.81D 08
1.0D 00	6.930D 02	1.044D-09	0.75609	6.588D 00	7.21D 08
2.5D 00	1.304D 03	1.655D-09	0.74494	8.009D 00	8.74D 08
5.0D 00	2.169D 03	2.359D-09	0.72837	9.844D 00	1.01D 09
7.5D 00	2.915D 03	2.887D-09	0.71784	1.113D 01	1.10D 09
1.0D 01	3.585D 03	3.342D-09	0.71230	1.207D 01	1.17D 09
2.5D 01	6.835D 03	5.447D-09	0.70490	1.549D 01	1.42D 09
5.0D 01	1.107D 04	7.919D-09	0.70335	1.852D 01	1.64D 09
7.5D 01	1.470D 04	9.846D-09	0.70289	2.038D 01	1.79D 09
1.0D 02	1.795D 04	1.144D-08	0.70268	2.161D 01	1.90D 09

EMERGENT SPECTRUM (LAMBDA IN ANGSTROMS, FLUX IN ERG/CM**2/S/A)

BAND	MID LAMBDA	BAND WIDTH	AVG.F LAMBDA	AVG.M LAMBDA
1	196.	131.	3.265D-09	21.215
2	332.	141.	3.265D-09	21.215
3	453.	102.	7.667D-05	10.268
4	558.	107.	9.413D-02	2.566
5	659.	96.	2.415D 01	-3.457
6	759.	104.	6.316D 02	-7.001
7	861.	101.	1.136D 04	-10.138
8	965.	107.	1.346D 05	-12.822
9	1075.	111.	9.408D 05	-14.934
10	1173.	86.	4.029D 06	-16.513
11	1261.	91.	1.173D 07	-17.673
12	1370.	127.	2.717D 07	-18.585
13	1478.	87.	5.232D 07	-19.297
14	1573.	103.	8.134D 07	-19.776
15	1687.	126.	1.080D 08	-20.084
16	1800.	100.	1.282D 08	-20.270
17	1897.	93.	1.363D 08	-20.336
18	1997.	108.	1.267D 08	-20.257
19	2093.	83.	1.148D 08	-20.150
20	2192.	116.	1.006D 08	-20.006
21	2298.	96.	7.644D 07	-19.708
22	2383.	73.	6.555D 07	-19.541
23	2465.	92.	5.968D 07	-19.440
24	2556.	89.	6.111D 07	-19.465
25	2648.	95.	6.304D 07	-19.499
26	2743.	96.	6.559D 07	-19.542
27	2864.	145.	7.315D 07	-19.661
28	2979.	86.	7.796D 07	-19.730
29	3072.	99.	7.971D 07	-19.754
30	3166.	90.	7.681D 07	-19.714
31	3260.	99.	7.431D 07	-19.678
32	3370.	120.	7.187D 07	-19.641
33	3488.	115.	6.975D 07	-19.609
34	3596.	102.	6.822D 07	-19.585
35	3702.	110.	8.894D 07	-19.873
36	3797.	80.	1.201D 08	-20.199
37	3894.	113.	1.535D 08	-20.465
38	3995.	90.	1.503D 08	-20.442
39	4111.	142.	1.460D 08	-20.411

EMERGENT SPECTRUM (LAMBDA IN ANGSTROMS, FLUX IN ERG/CM**2/S/A)

BAND	MID LAMBDA	BAND WIDTH'	AVG.F LAMBDA	AVG.M LAMBDA
40	4245.	126.	1.421D 08	-20.381
41	4365.	114.	1.193D 08	-20.192
42	4475.	106.	1.219D 08	-20.215
43	4589.	122.	1.129D 08	-20.132
44	4705.	109.	1.061D 08	-20.064
45	4822.	127.	8.967D 07	-19.882
46	4945.	118.	9.276D 07	-19.918
47	5053.	98.	8.756D 07	-19.856
48	5147.	90.	7.967D 07	-19.753
49	5248.	112.	7.515D 07	-19.690
50	5361.	113.	7.043D 07	-19.619
51	5486.	138.	6.721D 07	-19.569
52	5627.	144.	6.298D 07	-19.498
53	5753.	108.	5.929D 07	-19.432
54	5858.	101.	5.439D 07	-19.339
55	5959.	102.	5.322D 07	-19.315
56	6056.	92.	5.035D 07	-19.255
57	6154.	103.	4.671D 07	-19.173
58	6258.	107.	4.463D 07	-19.124
59	6376.	129.	4.254D 07	-19.072
60	6482.	82.	3.992D 07	-19.003
61	6593.	140.	3.435D 07	-18.840
62	6713.	100.	3.636D 07	-18.901
63	6813.	100.	3.471D 07	-18.851
64	6913.	101.	3.312D 07	-18.800
65	7018.	108.	3.124D 07	-18.737
66	7141.	138.	2.959D 07	-18.678
67	7270.	119.	2.802D 07	-18.619
68	7383.	108.	2.670D 07	-18.566
69	7513.	151.	2.499D 07	-18.495
70	7669.	162.	2.368D 07	-18.436
71	7820.	140.	2.147D 07	-18.330
72	7968.	155.	2.043D 07	-18.276
73	8125.	161.	1.938D 07	-18.219
74	8290.	169.	2.183D 07	-18.348
75	11482.	6213.	8.722D 06	-17.352
76	18691.	8206.	1.459D 06	-15.410
77	27809.	10029.	3.159D 05	-13.749
78	49235.	32823.	4.530D 04	-11.640

SIRIUS GRID MODEL

TEFF = 10000. LOG G = 4.00 PI F = 5.669D 11

BALMER JUMP = .484 PASCHEN SLOPE = 5.735D-04 MAG/A

PERCENT OF THE FLUX IN THE DIFFERENT HYDROGEN CONTINUA:

LYMAN	BALMER	PASCHEN	THE OTHERS
0.00	34.62	52.30	13.08

TAU	TEMP DEG.K	H ERG/CM**2/SEC/STERADIAN	J	P TOTAL --- DYNE/CM**2 ----	P GAS
1.0D-08	7640.	4.540D 10	7.390D 10	8.592D 00	4.595D-04
1.0D-07	7640.	4.540D 10	7.390D 10	8.597D 00	4.635D-03
1.0D-06	7640.	4.540D 10	7.391D 10	8.638D 00	4.639D-02
1.0D-05	7640.	4.540D 10	7.905D 10	9.056D 00	4.639D-01
1.0D-04	7641.	4.539D 10	8.046D 10	1.323D 01	4.639D 00
2.5D-04	7644.	4.514D 10	8.103D 10	2.113D 01	1.252D 01
5.0D-04	7647.	4.507D 10	8.161D 10	3.483D 01	2.621D 01
7.5D-04	7649.	4.505D 10	8.213D 10	4.860D 01	3.997D 01
1.0D-03	7651.	4.505D 10	8.263D 10	6.223D 01	5.359D 01
2.5D-03	8143.	4.523D 10	8.641D 10	1.199D 02	1.088D 02
5.0D-03	8324.	4.517D 10	9.012D 10	1.697D 02	1.576D 02
7.5D-03	8425.	4.512D 10	9.319D 10	2.083D 02	1.961D 02
1.0D-02	8491.	4.507D 10	9.591D 10	2.425D 02	2.294D 02
2.5D-02	8753.	4.502D 10	1.096D 11	3.942D 02	3.794D 02
5.0D-02	9148.	4.521D 10	1.292D 11	5.514D 02	5.337D 02
7.5D-02	9444.	4.525D 10	1.463D 11	6.527D 02	6.326D 02
1.0D-01	9691.	4.526D 10	1.620D 11	7.308D 02	7.085D 02
2.5D-01	10735.	4.511D 10	2.430D 11	1.033D 03	9.991D 02
5.0D-01	11799.	4.505D 10	3.536D 11	1.396D 03	1.347D 03
7.5D-01	12502.	4.512D 10	4.458D 11	1.722D 03	1.660D 03
1.0D 00	13045.	4.511D 10	5.279D 11	2.033D 03	1.960D 03
2.5D 00	14980.	4.516D 10	9.143D 11	3.682D 03	3.555D 03
5.0D 00	16666.	4.512D 10	1.397D 12	5.939D 03	5.744D 03
7.5D 00	17752.	4.509D 10	1.796D 12	7.848D 03	7.597D 03
1.0D 01	18563.	4.500D 10	2.147D 12	9.563D 03	9.263D 03
2.5D 01	21260.	4.498D 10	3.694D 12	1.798D 04	1.746D 04
5.0D 01	23609.	4.524D 10	5.623D 12	2.910D 04	2.831D 04
7.5D 01	25250.	4.521D 10	7.337D 12	3.874D 04	3.771D 04
1.0D 02	26550.	4.507D 10	8.965D 12	4.748D 04	4.623D 04

TAU	PE	DENSITY	MU	K ZERO	DEPTH
	DYNE/CM**2	GM/CM**3	A.M.U.	CM**2/GM	CM
1.0D-08	1.550D-04	6.732D-16	0.74878	2.481D-01	-1.29D 08
1.0D-07	1.509D-03	6.910D-15	0.74896	2.480D-01	-1.29D 08
1.0D-06	1.505D-02	6.928D-14	0.75076	2.476D-01	-1.28D 08
1.0D-05	1.504D-01	6.930D-13	0.76880	2.432D-01	-1.16D 08
1.0D-04	1.504D 00	6.930D-12	0.94924	1.991D-01	0.0
2.5D-04	3.085D 00	2.084D-11	1.05757	1.853D-01	6.19D 07
5.0D-04	5.005D 00	4.685D-11	1.13434	1.814D-01	1.04D 08
7.5D-04	6.522D 00	7.387D-11	1.17464	1.822D-01	1.27D 08
1.0D-03	7.798D 00	1.011D-10	1.19944	1.847D-01	1.43D 08
2.5D-03	2.080D 01	1.826D-10	1.13664	4.283D-01	1.81D 08
5.0D-03	3.131D 01	2.561D-10	1.12580	5.874D-01	2.03D 08
7.5D-03	3.951D 01	3.138D-10	1.12185	7.017D-01	2.17D 08
1.0D-02	4.636D 01	3.640D-10	1.12097	7.903D-01	2.27D 08
2.5D-02	8.038D 01	5.769D-10	1.10761	1.233D 00	2.59D 08
5.0D-02	1.356D 02	7.350D-10	1.04842	2.096D 00	2.82D 08
7.5D-02	1.837D 02	8.026D-10	0.99807	2.913D 00	2.95D 08
1.0D-01	2.265D 02	8.400D-10	0.95701	3.656D 00	3.04D 08
2.5D-01	4.107D 02	9.256D-10	0.82833	6.393D 00	3.37D 08
5.0D-01	6.032D 02	1.065D-09	0.77586	7.677D 00	3.73D 08
7.5D-01	7.581D 02	1.218D-09	0.76362	8.118D 00	4.00D 08
1.0D 00	9.021D 02	1.368D-09	0.75830	8.459D 00	4.23D 08
2.5D 00	1.666D 03	2.127D-09	0.74668	1.013D 01	5.16D 08
5.0D 00	2.753D 03	3.028D-09	0.73173	1.238D 01	6.02D 08
7.5D 00	3.700D 03	3.705D-09	0.72096	1.403D 01	6.58D 08
1.0D 01	4.551D 03	4.284D-09	0.71474	1.527D 01	7.01D 08
2.5D 01	8.692D 03	6.959D-09	0.70565	1.973D 01	8.53D 08
5.0D 01	1.413D 04	1.013D-08	0.70365	2.362D 01	9.87D 08
7.5D 01	1.884D 04	1.262D-08	0.70307	2.602D 01	1.08D 09
1.0D 02	2.310D 04	1.471D-08	0.70281	2.765D 01	1.15D 09

C.P

EMERGENT SPECTRUM (LAMBDA IN ANGSTROMS, FLUX IN ERG/CM**2/S/A)

BAND	MID LAMBDA	BAND WIDTH'	AVG.F LAMBDA	AVG.M LAMBDA
1	196.	131.	3.539D-09	21.128
2	332.	141.	3.539D-09	21.128
3	453.	102.	8.249D-05	10.209
4	558.	107.	1.001D-01	2.499
5	659.	96.	2.526D 01	-3.506
6	759.	104.	6.295D 02	-6.998
7	861.	101.	1.103D 04	-10.106
8	965.	107.	1.302D 05	-12.786
9	1075.	111.	9.761D 05	-14.974
10	1173.	86.	4.339D 06	-16.593
11	1261.	91.	1.279D 07	-17.767
12	1370.	127.	2.805D 07	-18.620
13	1478.	87.	5.202D 07	-19.290
14	1573.	103.	7.927D 07	-19.748
15	1687.	126.	1.063D 08	-20.066
16	1800.	100.	1.273D 08	-20.262
17	1897.	93.	1.362D 08	-20.336
18	1997.	108.	1.276D 08	-20.264
19	2093.	83.	1.163D 08	-20.164
20	2192.	116.	1.023D 08	-20.025
21	2298.	96.	7.803D 07	-19.731
22	2383.	73.	6.702D 07	-19.565
23	2465.	92.	6.104D 07	-19.464
24	2556.	89.	6.237D 07	-19.487
25	2648.	95.	6.419D 07	-19.519
26	2743.	96.	6.662D 07	-19.559
27	2864.	145.	7.399D 07	-19.673
28	2979.	86.	7.861D 07	-19.739
29	3072.	99.	8.024D 07	-19.761
30	3166.	90.	7.730D 07	-19.720
31	3260.	99.	7.476D 07	-19.684
32	3370.	120.	7.227D 07	-19.647
33	3488.	115.	7.012D 07	-19.615
34	3596.	102.	6.855D 07	-19.590
35	3702.	110.	8.901D 07	-19.874
36	3797.	80.	1.165D 08	-20.166
37	3894.	113.	1.504D 08	-20.443
38	3995.	90.	1.482D 08	-20.427
39	4111.	142.	1.444D 08	-20.399

EMERGENT SPECTRUM (LAMBDA IN ANGSTROMS, FLUX IN ERG/CM**2/S/A)

BAND	MID LAMBDA	BAND WIDTH	AVG.F LAMBDA	AVG.M LAMBDA
40	4245.	126.	1.420D 08	-20.381
41	4365.	114.	1.180D 08	-20.179
42	4475.	106.	1.219D 08	-20.215
43	4589.	122.	1.129D 08	-20.132
44	4705.	109.	1.061D 08	-20.064
45	4822.	127.	3.861D 07	-19.869
46	4945.	118.	9.246D 07	-19.915
47	5053.	98.	3.757D 07	-19.856
48	5147.	90.	7.972D 07	-19.754
49	5248.	112.	7.521D 07	-19.691
50	5361.	113.	7.050D 07	-19.620
51	5486.	138.	6.716D 07	-19.568
52	5627.	144.	6.301D 07	-19.499
53	5753.	108.	5.934D 07	-19.433
54	5855.	101.	5.439D 07	-19.339
55	5959.	102.	5.329D 07	-19.317
56	6056.	92.	5.040D 07	-19.256
57	6154.	103.	4.677D 07	-19.175
58	6258.	107.	4.469D 07	-19.126
59	6376.	129.	4.258D 07	-19.073
60	6482.	82.	3.990D 07	-19.003
61	6593.	140.	3.418D 07	-18.835
62	6713.	100.	3.640D 07	-18.903
63	6813.	100.	3.476D 07	-18.853
64	6913.	101.	3.318D 07	-18.802
65	7018.	108.	3.130D 07	-18.739
66	7141.	138.	2.963D 07	-18.679
67	7270.	119.	2.808D 07	-18.621
68	7383.	108.	2.674D 07	-18.568
69	7513.	151.	2.503D 07	-18.496
70	7669.	162.	2.372D 07	-18.438
71	7820.	140.	2.151D 07	-18.332
72	7968.	155.	2.047D 07	-18.278
73	8125.	161.	1.940D 07	-18.220
74	8290.	169.	2.185D 07	-18.348
75	11482.	6213.	3.734D 06	-17.353
76	18691.	8206.	1.461D 06	-15.412
77	27809.	10029.	3.163D 05	-13.750
78	43235.	32823.	4.536D 04	-11.642

SIRIUS GRID MODEL

TEFF = 10000. LOG G = 4.20 PI F = 5.669D 11

BALMER JUMP = .480 PASCHEN SLOPE = 5.722D-04 MAG/A

PERCENT OF THE FLUX IN THE DIFFERENT HYDROGEN CONTINUA:

LYMAN	BALMER	PASCHEN	THE OTHERS
0.00	34.82	52.08	13.10

TAU	TEMP DEG.K	H ERG/CM**2/SEC/STERADIAN	J	P TOTAL --- DYNE/CM**2 ----	P GAS
1.0D-08	7639.	4.538D 10	7.390D 10	8.585D 00	7.562D-04
1.0D-07	7639.	4.538D 10	7.390D 10	8.592D 00	7.652D-03
1.0D-06	7639.	4.538D 10	7.391D 10	8.661D 00	7.661D-02
1.0D-05	7639.	4.538D 10	7.906D 10	9.351D 00	7.661D-01
1.0D-04	7639.	4.537D 10	8.050D 10	1.625D 01	7.662D 00
2.5D-04	7643.	4.513D 10	8.109D 10	2.918D 01	2.058D 01
5.0D-04	7645.	4.506D 10	8.171D 10	5.111D 01	4.250D 01
7.5D-04	7648.	4.505D 10	8.227D 10	7.274D 01	6.411D 01
1.0D-03	7651.	4.507D 10	8.282D 10	9.385D 01	8.521D 01
2.5D-03	8200.	4.519D 10	8.666D 10	1.681D 02	1.567D 02
5.0D-03	8334.	4.509D 10	9.016D 10	2.383D 02	2.261D 02
7.5D-03	8411.	4.504D 10	9.312D 10	2.961D 02	2.835D 02
1.0D-02	8470.	4.501D 10	9.531D 10	3.468D 02	3.338D 02
2.5D-02	8750.	4.508D 10	1.097D 11	5.725D 02	5.577D 02
5.0D-02	9159.	4.531D 10	1.295D 11	7.957D 02	7.780D 02
7.5D-02	9457.	4.535D 10	1.467D 11	9.362D 02	9.160D 02
1.0D-01	9709.	4.535D 10	1.626D 11	1.042D 03	1.020D 03
2.5D-01	10730.	4.500D 10	2.429D 11	1.433D 03	1.399D 03
5.0D-01	11799.	4.514D 10	3.536D 11	1.878D 03	1.829D 03
7.5D-01	12497.	4.509D 10	4.453D 11	2.273D 03	2.211D 03
1.0D 00	13038.	4.508D 10	5.270D 11	2.651D 03	2.578D 03
2.5D 00	14963.	4.513D 10	9.114D 11	4.688D 03	4.561D 03
5.0D 00	16640.	4.511D 10	1.388D 12	7.515D 03	7.321D 03
7.5D 00	17717.	4.512D 10	1.782D 12	9.920D 03	9.671D 03
1.0D 01	18522.	4.504D 10	2.127D 12	1.208D 04	1.178D 04
2.5D 01	21216.	4.494D 10	3.664D 12	2.268D 04	2.216D 04
5.0D 01	23602.	4.524D 10	5.617D 12	3.677D 04	3.599D 04
7.5D 01	25271.	4.513D 10	7.361D 12	4.909D 04	4.806D 04
1.0D 02	26592.	4.494D 10	9.022D 12	6.033D 04	5.907D 04

TAU	PE	DENSITY	MU	K ZERO	DEPTH
	DYNE/CM**2	GM/CM**3	A.M.U.	CM**2/GM	CM
1.0D-08	2.273D-04	1.169D-15	0.74917	2.478D-01	-7.53D 07
1.0D-07	2.140D-03	1.207D-14	0.74940	2.477D-01	-7.53D 07
1.0D-06	2.161D-02	1.211D-13	0.75170	2.472D-01	-7.46D 07
1.0D-05	2.181D-01	1.212D-12	0.77471	2.420D-01	-6.78D 07
1.0D-04	2.150D 00	1.212D-11	1.00485	1.903D-01	0.0
2.5D-04	4.279D 00	3.603D-11	1.11179	1.809D-01	3.68D 07
5.0D-04	6.730D 00	7.903D-11	1.18047	1.815D-01	6.17D 07
7.5D-04	8.632D 00	1.225D-10	1.21489	1.853D-01	7.56D 07
1.0D-03	1.022D 01	1.655D-10	1.23550	1.900D-01	8.48D 07
2.5D-03	2.764D 01	2.658D-10	1.15716	4.921D-01	1.06D 08
5.0D-03	3.961D 01	3.780D-10	1.15872	6.351D-01	1.19D 08
7.5D-03	4.911D 01	4.706D-10	1.16148	7.355D-01	1.28D 08
1.0D-02	5.751D 01	5.509D-10	1.16284	8.279D-01	1.34D 08
2.5D-02	1.024D 02	8.788D-10	1.14738	1.340D 00	1.54D 08
5.0D-02	1.763D 02	1.110D-09	1.08709	2.361D 00	1.68D 08
7.5D-02	2.410D 02	1.205D-09	1.03643	3.346D 00	1.75D 08
1.0D-01	2.999D 02	1.252D-09	0.99298	4.287D 00	1.81D 08
2.5D-01	5.521D 02	1.333D-09	0.85151	6.028D 00	1.99D 08
5.0D-01	8.082D 02	1.462D-09	0.78424	9.984D 00	2.19D 08
7.5D-01	1.003D 03	1.632D-09	0.76814	1.055D 01	2.34D 08
1.0D 00	1.181D 03	1.807D-09	0.76123	1.094D 01	2.48D 08
2.5D 00	2.131D 03	2.738D-09	0.74877	1.286D 01	3.04D 08
5.0D 00	3.492D 03	3.883D-09	0.73500	1.557D 01	3.57D 08
7.5D 00	4.687D 03	4.748D-09	0.72428	1.765D 01	3.92D 08
1.0D 01	5.767D 03	5.482D-09	0.71750	1.926D 01	4.18D 08
2.5D 01	1.102D 04	8.862D-09	0.70657	2.503D 01	5.12D 08
5.0D 01	1.796D 04	1.288D-08	0.70400	2.993D 01	5.95D 08
7.5D 01	2.400D 04	1.608D-08	0.70328	3.298D 01	6.51D 08
1.0D 02	2.951D 04	1.878D-08	0.70296	3.507D 01	6.93D 08

EMERGENT SPECTRUM (LAMBDA IN ANGSTROMS, FLUX IN ERG/CM**2/S/A)

BAND	MID LAMBDA	BAND WIDTH	AVG.F LAMBDA	AVG.M LAMBDA
1	196.	131.	3.502D-09	21.139
2	332.	141.	3.502D-09	21.139
3	453.	102.	8.219D-05	10.213
4	558.	107.	9.987D-02	2.501
5	659.	96.	2.515D 01	-3.501
6	759.	104.	6.111D 02	-6.965
7	861.	101.	1.059D 04	-10.062
8	965.	107.	1.257D 05	-12.748
9	1075.	111.	1.002D 06	-15.002
10	1173.	86.	4.601D 06	-16.657
11	1261.	91.	1.372D 07	-17.843
12	1370.	127.	2.865D 07	-18.643
13	1478.	87.	5.139D 07	-19.277
14	1573.	103.	7.699D 07	-19.716
15	1687.	126.	1.044D 08	-20.047
16	1800.	100.	1.263D 08	-20.253
17	1897.	93.	1.362D 08	-20.335
18	1997.	108.	1.285D 08	-20.272
19	2093.	83.	1.177D 08	-20.177
20	2192.	116.	1.041D 08	-20.043
21	2293.	96.	7.960D 07	-19.752
22	2383.	73.	6.846D 07	-19.589
23	2465.	92.	6.238D 07	-19.488
24	2556.	89.	6.367D 07	-19.510
25	2648.	95.	6.542D 07	-19.539
26	2743.	96.	6.777D 07	-19.578
27	2864.	145.	7.493D 07	-19.687
28	2979.	86.	7.936D 07	-19.749
29	3072.	99.	8.085D 07	-19.769
30	3166.	90.	7.786D 07	-19.728
31	3260.	99.	7.527D 07	-19.692
32	3370.	120.	7.272D 07	-19.654
33	3488.	115.	7.051D 07	-19.621
34	3596.	102.	6.889D 07	-19.595
35	3702.	110.	8.940D 07	-19.878
36	3797.	80.	1.135D 08	-20.137
37	3894.	113.	1.472D 08	-20.419
38	3995.	90.	1.458D 08	-20.409
39	4111.	142.	1.425D 08	-20.385

EMERGENT SPECTRUM (LAMBDA IN ANGSTROMS, FLUX IN ERG/CM**2/S/A)

BAND	MID LAMBDA	BAND WIDTH	AVG.F LAMBDA	AVG.M LAMBDA
40	4245.	126.	1.417D 08	-20.379
41	4365.	114.	1.164D 08	-20.165
42	4475.	106.	1.218D 08	-20.214
43	4569.	122.	1.129D 08	-20.132
44	4705.	109.	1.060D 08	-20.064
45	4822.	127.	8.745D 07	-19.854
46	4945.	118.	9.207D 07	-19.910
47	5053.	98.	8.754D 07	-19.856
48	5147.	90.	7.974D 07	-19.754
49	5243.	112.	7.526D 07	-19.691
50	5361.	113.	7.055D 07	-19.621
51	5486.	138.	6.710D 07	-19.567
52	5627.	144.	6.302D 07	-19.499
53	5753.	108.	5.938D 07	-19.434
54	5858.	101.	5.439D 07	-19.339
55	5959.	102.	5.335D 07	-19.318
56	6056.	92.	5.044D 07	-19.257
57	6154.	103.	4.683D 07	-19.176
58	6258.	107.	4.475D 07	-19.127
59	6376.	129.	4.261D 07	-19.074
60	6482.	82.	3.989D 07	-19.002
61	6593.	140.	3.401D 07	-18.829
62	6713.	100.	3.645D 07	-18.904
63	6813.	100.	3.482D 07	-18.855
64	6913.	101.	3.324D 07	-18.804
65	7018.	108.	3.137D 07	-18.741
66	7141.	138.	2.967D 07	-18.681
67	7270.	119.	2.814D 07	-18.623
68	7383.	108.	2.679D 07	-18.570
69	7513.	151.	2.508D 07	-18.498
70	7669.	162.	2.377D 07	-18.440
71	7820.	140.	2.156D 07	-18.334
72	7968.	155.	2.052D 07	-18.281
73	8125.	161.	1.943D 07	-18.221
74	8290.	169.	2.185D 07	-18.348
75	11482.	6213.	8.746D 06	-17.355
76	18691.	8206.	1.464D 06	-15.414
77	27809.	10029.	3.167D 05	-13.752
78	49235.	32823.	4.538D 04	-11.642

SIRIUS GRID MODEL

TEFF = 10000. LOG G = 4.40 PI F = 5.669D 11

BALMER JUMP = .474 PASCHEN SLOPE = 5.705D-04 MAG/A

PERCENT OF THE FLUX IN THE DIFFERENT HYDROGEN CONTINUA:

LYMAN	BALMER	PASCHEN	THE OTHERS
0.00	35.09	51.79	13.12

TAU	TEMP DEG.K	H	J	P TOTAL	P GAS
		ERG/CM**2/SEC/STERADIAN		--- DYNE/CM**2 ----	
1.0D-08	7636.	4.541D 10	7.900D 10	8.573D 00	1.246D-03
1.0D-07	7636.	4.541D 10	7.900D 10	8.585D 00	1.265D-02
1.0D-06	7636.	4.541D 10	7.902D 10	8.699D 00	1.267D-01
1.0D-05	7636.	4.541D 10	7.916D 10	9.840D 00	1.267D 00
1.0D-04	7636.	4.539D 10	8.063D 10	2.125D 01	1.267D 01
2.5D-04	7640.	4.516D 10	8.125D 10	4.221D 01	3.362D 01
5.0D-04	7642.	4.510D 10	8.139D 10	7.681D 01	6.821D 01
7.5D-04	7645.	4.510D 10	8.247D 10	1.103D 02	1.017D 02
1.0D-03	7669.	4.514D 10	8.309D 10	1.422D 02	1.335D 02
2.5D-03	8214.	4.520D 10	8.686D 10	2.422D 02	2.307D 02
5.0D-03	8324.	4.512D 10	9.028D 10	3.460D 02	3.339D 02
7.5D-03	8398.	4.510D 10	9.323D 10	4.325D 02	4.200D 02
1.0D-02	8458.	4.509D 10	9.593D 10	5.082D 02	4.953D 02
2.5D-02	8776.	4.527D 10	1.102D 11	8.366D 02	8.216D 02
5.0D-02	9196.	4.536D 10	1.302D 11	1.145D 03	1.126D 03
7.5D-02	9481.	4.527D 10	1.472D 11	1.338D 03	1.317D 03
1.0D-01	9720.	4.518D 10	1.628D 11	1.484D 03	1.461D 03
2.5D-01	10714.	4.495D 10	2.420D 11	2.005D 03	1.971D 03
5.0D-01	11797.	4.521D 10	3.533D 11	2.556D 03	2.507D 03
7.5D-01	12492.	4.510D 10	4.448D 11	3.033D 03	2.972D 03
1.0D 00	13035.	4.513D 10	5.265D 11	3.491D 03	3.418D 03
2.5D 00	14955.	4.511D 10	9.083D 11	5.994D 03	5.868D 03
5.0D 00	16617.	4.513D 10	1.330D 12	9.527D 03	9.334D 03
7.5D 00	17635.	4.512D 10	1.769D 12	1.255D 04	1.231D 04
1.0D 01	18465.	4.507D 10	2.110D 12	1.527D 04	1.498D 04
2.5D 01	21188.	4.515D 10	3.645D 12	2.860D 04	2.810D 04
5.0D 01	23608.	4.507D 10	5.623D 12	4.643D 04	4.534D 04
7.5D 01	25309.	4.513D 10	7.406D 12	6.209D 04	6.105D 04
1.0D 02	26659.	4.501D 10	9.113D 12	7.645D 04	7.518D 04

TAU	PE	DENSITY	MU	K ZERO	DEPTH
	DYNE/CM**2	GM/CM**3	A.M.U.	CM**2/GM	CM
1.0D-08	3.274D-04	2.032D-15	0.74943	2.476D-01	-4.38D 07
1.0D-07	3.109D-03	2.111D-14	0.74971	2.476D-01	-4.38D 07
1.0D-06	3.092D-02	2.119D-13	0.75252	2.470D-01	-4.34D 07
1.0D-05	3.090D-01	2.119D-12	0.78067	2.412D-01	-3.94D 07
1.0D-04	3.090D 00	2.119D-11	1.06211	1.830D-01	0.0
2.5D-04	5.807D 00	6.150D-11	1.16140	1.791D-01	2.18D 07
5.0D-04	8.875D 00	1.311D-10	1.22049	1.842D-01	3.66D 07
7.5D-04	1.122D 01	1.999D-10	1.24918	1.909D-01	4.48D 07
1.0D-03	1.352D 01	2.642D-10	1.26218	2.048D-01	5.02D 07
2.5D-03	3.545D 01	4.016D-10	1.18906	5.345D-01	6.19D 07
5.0D-03	4.965D 01	5.766D-10	1.19590	6.716D-01	7.04D 07
7.5D-03	6.142D 01	7.210D-10	1.19935	7.804D-01	7.57D 07
1.0D-02	7.207D 01	8.450D-10	1.20046	8.787D-01	7.95D 07
2.5D-02	1.331D 02	1.325D-09	1.17778	1.511D 00	9.15D 07
5.0D-02	2.306D 02	1.645D-09	1.11773	2.711D 00	9.97D 07
7.5D-02	3.138D 02	1.788D-09	1.07130	3.830D 00	1.04D 08
1.0D-01	3.904D 02	1.861D-09	1.03075	4.920D 00	1.07D 08
2.5D-01	7.363D 02	1.947D-09	0.88122	9.877D 00	1.18D 08
5.0D-01	1.068D 03	2.032D-09	0.79542	1.298D 01	1.29D 08
7.5D-01	1.335D 03	2.212D-09	0.77422	1.377D 01	1.37D 08
1.0D 00	1.558D 03	2.409D-09	0.76502	1.422D 01	1.45D 08
2.5D 00	2.733D 03	3.535D-09	0.75069	1.639D 01	1.78D 08
5.0D 00	4.432D 03	4.979D-09	0.73811	1.961D 01	2.11D 08
7.5D 00	5.934D 03	6.081D-09	0.72770	2.220D 01	2.32D 08
1.0D 01	7.299D 03	7.012D-09	0.72053	2.427D 01	2.49D 08
2.5D 01	1.395D 04	1.127D-08	0.70766	3.164D 01	3.07D 08
5.0D 01	2.276D 04	1.635D-08	0.70442	3.780D 01	3.59D 08
7.5D 01	3.048D 04	2.040D-08	0.70352	4.160D 01	3.94D 08
1.0D 02	3.755D 04	2.384D-08	0.70313	4.421D 01	4.20D 08

EMERGENT SPECTRUM (LAMBDA IN ANGSTROMS, FLUX IN ERG/CM**2/S/A)

BAND	MID LAMBDA	BAND WIDTH'	AVG.F LAMBDA	AVG.M LAMBDA
1	196.	131.	3.436D-09	21.160
2	332.	141.	3.436D-09	21.160
3	453.	102.	8.129D-05	10.225
4	553.	107.	9.905D-02	2.510
5	659.	96.	2.492D 01	-3.491
6	759.	104.	5.929D 02	-6.933
7	861.	101.	1.019D 04	-10.020
8	965.	107.	1.215D 05	-12.712
9	1075.	111.	1.019D 06	-15.020
10	1173.	86.	4.806D 06	-16.705
11	1261.	91.	1.447D 07	-17.901
12	1370.	127.	2.906D 07	-18.658
13	1478.	87.	5.080D 07	-19.265
14	1573.	103.	7.511D 07	-19.689
15	1687.	126.	1.029D 08	-20.031
16	1800.	100.	1.256D 08	-20.248
17	1897.	93.	1.364D 08	-20.337
18	1997.	108.	1.296D 08	-20.281
19	2093.	83.	1.194D 08	-20.192
20	2192.	116.	1.060D 08	-20.063
21	2298.	96.	8.128D 07	-19.775
22	2383.	73.	7.001D 07	-19.613
23	2465.	92.	6.383D 07	-19.512
24	2556.	89.	6.506D 07	-19.533
25	2648.	95.	6.677D 07	-19.562
26	2743.	96.	6.907D 07	-19.598
27	2864.	145.	7.615D 07	-19.704
28	2979.	86.	8.047D 07	-19.764
29	3072.	99.	8.190D 07	-19.783
30	3166.	90.	7.886D 07	-19.742
31	3260.	99.	7.622D 07	-19.705
32	3370.	120.	7.362D 07	-19.668
33	3488.	115.	7.134D 07	-19.633
34	3596.	102.	6.967D 07	-19.608
35	3702.	110.	9.022D 07	-19.888
36	3797.	80.	1.106D 08	-20.110
37	3894.	113.	1.436D 08	-20.393
38	3995.	90.	1.433D 08	-20.390
39	4111.	142.	1.404D 08	-20.369

EMERGENT SPECTRUM (LAMBDA IN ANGSTROMS, FLUX IN ERG/CM**2/S/A)

BAND	MID LAMBDA	BAND WIDTH'	AVG.F LAMBDA	AVG.M LAMBDA
40	4245.	126.	1.413D 08	-20.376
41	4365.	114.	1.147D 08	-20.149
42	4475.	106.	1.217D 08	-20.213
43	4589.	122.	1.128D 08	-20.131
44	4705.	109.	1.060D 08	-20.063
45	4822.	127.	3.622D 07	-19.839
46	4945.	118.	9.164D 07	-19.905
47	5053.	98.	8.751D 07	-19.855
48	5147.	90.	7.974D 07	-19.754
49	5248.	112.	7.529D 07	-19.692
50	5361.	113.	7.059D 07	-19.622
51	5486.	138.	6.705D 07	-19.566
52	5627.	144.	6.303D 07	-19.499
53	5753.	108.	5.943D 07	-19.435
54	5858.	101.	5.441D 07	-19.339
55	5959.	102.	5.343D 07	-19.319
56	6056.	92.	5.050D 07	-19.258
57	6154.	103.	4.690D 07	-19.178
58	6258.	107.	4.483D 07	-19.129
59	6376.	129.	4.266D 07	-19.075
60	6482.	82.	3.988D 07	-19.002
61	6593.	140.	3.384D 07	-18.824
62	6713.	100.	3.651D 07	-18.906
63	6813.	100.	3.490D 07	-18.857
64	6913.	101.	3.332D 07	-18.807
65	7018.	108.	3.146D 07	-18.744
66	7141.	138.	2.974D 07	-18.683
67	7270.	119.	2.823D 07	-18.627
68	7383.	108.	2.686D 07	-18.573
69	7513.	151.	2.516D 07	-18.502
70	7669.	162.	2.384D 07	-18.443
71	7820.	140.	2.163D 07	-18.338
72	7968.	155.	2.060D 07	-18.284
73	8125.	161.	1.948D 07	-18.224
74	8290.	169.	2.185D 07	-18.348
75	11482.	6213.	3.762D 06	-17.356
76	18691.	8206.	1.469D 06	-15.417
77	27809.	10029.	3.177D 05	-13.755
78	49235.	32823.	4.547D 04	-11.644

SIRIUS GRID MODEL

TEFF = 9750. LOG G = 3.80 PI F = 5.123D 11

BALMER JUMP = .506 PASCHEN SLOPE = 5.696D-04 MAG/A

PERCENT OF THE FLUX IN THE DIFFERENT HYDROGEN CONTINUA:

LYMAN	BALMER	PASCHEN	THE OTHERS
0.00	31.46	54.58	13.96

TAU	TEMP DEG.K	H ERG/CM**2/SEC/STERADIAN	J	P TOTAL --- DYNE/CM**2 ----	P GAS
1.0D-08	7508.	4.105D 10	7.153D 10	8.013D 00	3.047D-04
1.0D-07	7508.	4.105D 10	7.153D 10	8.016D 00	3.085D-03
1.0D-06	7508.	4.105D 10	7.155D 10	8.043D 00	3.089D-02
1.0D-05	7508.	4.105D 10	7.167D 10	8.322D 00	3.089D-01
1.0D-04	7509.	4.105D 10	7.293D 10	1.110D 01	3.089D 00
2.5D-04	7512.	4.081D 10	7.344D 10	1.678D 01	8.756D 00
5.0D-04	7514.	4.073D 10	7.394D 10	2.719D 01	1.915D 01
7.5D-04	7515.	4.069D 10	7.438D 10	3.794D 01	2.990D 01
1.0D-03	7517.	4.068D 10	7.479D 10	4.878D 01	4.073D 01
2.5D-03	7940.	4.086D 10	7.808D 10	1.036D 02	9.359D 01
5.0D-03	8111.	4.077D 10	8.148D 10	1.461D 02	1.352D 02
7.5D-03	8210.	4.074D 10	8.430D 10	1.805D 02	1.690D 02
1.0D-02	8287.	4.071D 10	8.686D 10	2.098D 02	1.979D 02
2.5D-02	8580.	4.062D 10	9.954D 10	3.358D 02	3.222D 02
5.0D-02	8923.	4.068D 10	1.169D 11	4.658D 02	4.498D 02
7.5D-02	9209.	4.082D 10	1.325D 11	5.505D 02	5.324D 02
1.0D-01	9464.	4.095D 10	1.471D 11	6.143D 02	5.940D 02
2.5D-01	10501.	4.068D 10	2.217D 11	8.467D 02	8.160D 02
5.0D-01	11562.	4.085D 10	3.254D 11	1.118D 03	1.073D 03
7.5D-01	12268.	4.084D 10	4.126D 11	1.364D 03	1.306D 03
1.0D 00	12807.	4.075D 10	4.898D 11	1.599D 03	1.531D 03
2.5D 00	14729.	4.079D 10	8.544D 11	2.865D 03	2.746D 03
5.0D 00	16405.	4.080D 10	1.311D 12	4.613D 03	4.430D 03
7.5D 00	17484.	4.080D 10	1.690D 12	6.094D 03	5.858D 03
1.0D 01	18295.	4.075D 10	2.025D 12	7.424D 03	7.141D 03
2.5D 01	20976.	4.074D 10	3.501D 12	1.394D 04	1.345D 04
5.0D 01	23255.	4.077D 10	5.291D 12	2.248D 04	2.174D 04
7.5D 01	24820.	4.081D 10	6.850D 12	2.980D 04	2.885D 04
1.0D 02	26056.	4.074D 10	8.316D 12	3.638D 04	3.522D 04

TAU	PE DYNE/CM**2	DENSITY GM/CM**3	MU A.M.U.	K ZERO CM**2/GM	DEPTH CM
1.0D-08	1.026D-04	4.546D-16	0.74900	2.479D-01	-1.98D 08
1.0D-07	1.004D-03	4.681D-15	0.74918	2.479D-01	-1.98D 08
1.0D-06	1.002D-02	4.695D-14	0.75098	2.473D-01	-1.96D 08
1.0D-05	1.001D-01	4.696D-13	0.76901	2.413D-01	-1.79D 08
1.0D-04	1.001D 00	4.696D-12	0.94930	1.813D-01	0.0
2.5D-04	2.122D 00	1.492D-11	1.06313	1.583D-01	1.01D 08
5.0D-04	3.527D 00	3.512D-11	1.14357	1.482D-01	1.69D 08
7.5D-04	4.651D 00	5.675D-11	1.18525	1.457D-01	2.07D 08
1.0D-03	5.597D 00	7.895D-11	1.21073	1.456D-01	2.33D 08
2.5D-03	1.534D 01	1.665D-10	1.17525	3.104D-01	2.99D 08
5.0D-03	2.303D 01	2.335D-10	1.16563	4.216D-01	3.33D 08
7.5D-03	2.926D 01	2.875D-10	1.16181	5.054D-01	3.54D 08
1.0D-02	3.487D 01	3.322D-10	1.15753	5.808D-01	3.69D 08
2.5D-02	6.238D 01	5.113D-10	1.13318	9.549D-01	4.16D 08
5.0D-02	1.029D 02	6.565D-10	1.08406	1.572D 00	4.50D 08
7.5D-02	1.412D 02	7.172D-10	1.03343	2.231D 00	4.69D 08
1.0D-01	1.773D 02	7.436D-10	0.98693	2.891D 00	4.83D 08
2.5D-01	3.287D 02	7.837D-10	0.83992	5.408D 00	5.29D 08
5.0D-01	4.787D 02	8.685D-10	0.77831	6.540D 00	5.79D 08
7.5D-01	5.958D 02	9.773D-10	0.76434	6.840D 00	6.19D 08
1.0D 00	7.044D 02	1.089D-09	0.75860	7.071D 00	6.53D 08
2.5D 00	1.286D 03	1.672D-09	0.74726	8.297D 00	7.95D 08
5.0D 00	2.122D 03	2.374D-09	0.73221	1.006D 01	9.31D 08
7.5D 00	2.852D 03	2.901D-09	0.72116	1.138D 01	1.02D 09
1.0D 01	3.509D 03	3.350D-09	0.71469	1.236D 01	1.09D 09
2.5D 01	6.696D 03	5.431D-09	0.70548	1.588D 01	1.33D 09
5.0D 01	1.085D 04	7.894D-09	0.70357	1.902D 01	1.54D 09
7.5D 01	1.441D 04	9.822D-09	0.70302	2.097D 01	1.68D 09
1.0D 02	1.760D 04	1.142D-08	0.70277	2.228D 01	1.79D 09

EMERGENT SPECTRUM (LAMBDA IN ANGSTROMS, FLUX IN ERG/CM**2/S/A)

BAND	MID LAMBDA	BAND WIDTH'	AVG.F LAMBDA	AVG.M LAMBDA
1	196.	131.	1.408D-09	22.129
2	332.	141.	1.408D-09	22.129
3	453.	102.	4.039D-05	10.984
4	558.	107.	5.600D-02	3.129
5	659.	96.	1.547D 01	-2.974
6	759.	104.	3.901D 02	-6.478
7	861.	101.	6.914D 03	-9.599
8	965.	107.	8.261D 04	-12.293
9	1075.	111.	6.243D 05	-14.488
10	1173.	86.	2.808D 05	-16.121
11	1261.	91.	8.404D 06	-17.311
12	1370.	127.	1.888D 07	-18.190
13	1478.	87.	3.604D 07	-18.892
14	1573.	103.	5.660D 07	-19.382
15	1687.	126.	8.077D 07	-19.768
16	1800.	100.	1.012D 08	-20.013
17	1897.	93.	1.112D 08	-20.115
18	1997.	108.	1.047D 08	-20.050
19	2093.	83.	9.566D 07	-19.952
20	2192.	116.	8.408D 07	-19.812
21	2298.	96.	6.308D 07	-19.500
22	2383.	73.	5.385D 07	-19.328
23	2465.	92.	4.904D 07	-19.226
24	2556.	89.	5.086D 07	-19.266
25	2648.	95.	5.307D 07	-19.312
26	2743.	96.	5.581D 07	-19.367
27	2864.	145.	6.293D 07	-19.497
28	2979.	86.	6.767D 07	-19.576
29	3072.	99.	6.962D 07	-19.607
30	3166.	90.	6.736D 07	-19.571
31	3260.	99.	6.545D 07	-19.540
32	3370.	120.	6.365D 07	-19.509
33	3488.	115.	6.217D 07	-19.484
34	3596.	102.	6.120D 07	-19.467
35	3702.	110.	7.955D 07	-19.752
36	3797.	80.	1.101D 08	-20.104
37	3894.	113.	1.425D 08	-20.385
38	3995.	90.	1.401D 08	-20.366
39	4111.	142.	1.367D 08	-20.339

EMERGENT SPECTRUM (LAMBDA IN ANGSTROMS, FLUX IN ERG/CM**2/S/A)

BAND	MID LAMBDA	BAND WIDTH'	AVG.F LAMBDA	AVG.M LAMBDA
40	4245.	126.	1.336D 08	-20.314
41	4365.	114.	1.118D 08	-20.121
42	4475.	106.	1.147D 08	-20.149
43	4589.	122.	1.064D 08	-20.067
44	4705.	109.	9.972D 07	-19.997
45	4822.	127.	8.422D 07	-19.813
46	4945.	118.	8.707D 07	-19.850
47	5053.	98.	8.228D 07	-19.788
48	5147.	90.	7.524D 07	-19.691
49	5248.	112.	7.099D 07	-19.628
50	5361.	113.	6.656D 07	-19.558
51	5486.	138.	6.330D 07	-19.503
52	5627.	144.	5.938D 07	-19.434
53	5753.	108.	5.612D 07	-19.373
54	5858.	101.	5.136D 07	-19.277
55	5959.	102.	5.047D 07	-19.257
56	6056.	92.	4.773D 07	-19.197
57	6154.	103.	4.423D 07	-19.114
58	6258.	107.	4.231D 07	-19.066
59	6376.	129.	4.027D 07	-19.012
60	6482.	82.	3.784D 07	-18.945
61	6593.	140.	3.257D 07	-18.782
62	6713.	100.	3.456D 07	-18.846
63	6813.	100.	3.302D 07	-18.797
64	6913.	101.	3.152D 07	-18.747
65	7018.	108.	2.972D 07	-18.683
66	7141.	138.	2.816D 07	-18.624
67	7270.	119.	2.669D 07	-18.566
68	7383.	108.	2.543D 07	-18.513
69	7513.	151.	2.379D 07	-18.441
70	7669.	162.	2.258D 07	-18.384
71	7820.	140.	2.050D 07	-18.280
72	7968.	155.	1.949D 07	-18.225
73	8125.	161.	1.848D 07	-18.167
74	8290.	169.	2.096D 07	-18.303
75	11482.	6213.	8.418D 06	-17.313
76	18691.	8206.	1.419D 05	-15.383
77	27809.	10029.	3.081D 05	-13.722
78	49235.	32823.	4.425D 04	-11.615

SIRIUS GRID MODEL

TEFF = 9750. LOG G = 4.00 PI F = 5.123D 11

BALMER JUMP = .501 PASCHEN SLOPE = 5.680D-04 MAG/A

PERCENT OF THE FLUX IN THE DIFFERENT HYDROGEN CONTINUA:

LYMAN	BALMER	PASCHEN	THE OTHERS
0.00	31.68	54.33	13.99

TAU	TEMP DEG.K	H	J	P TOTAL	P GAS
		ERG/CM**2/SEC/STERADIAN		--- DYNE/CM**2 ----	
1.0D-08	7526.	4.107D 10	7.159D 10	8.090D 00	5.028D-04
1.0D-07	7526.	4.107D 10	7.159D 10	8.095D 00	5.109D-03
1.0D-06	7526.	4.107D 10	7.160D 10	8.141D 00	5.117D-02
1.0D-05	7526.	4.107D 10	7.173D 10	8.602D 00	5.118D-01
1.0D-04	7527.	4.106D 10	7.305D 10	1.321D 01	5.118D 00
2.5D-04	7529.	4.082D 10	7.357D 10	2.253D 01	1.442D 01
5.0D-04	7531.	4.074D 10	7.410D 10	3.906D 01	3.095D 01
7.5D-04	7533.	4.070D 10	7.455D 10	5.576D 01	4.765D 01
1.0D-03	7534.	4.069D 10	7.497D 10	7.232D 01	6.419D 01
2.5D-03	7937.	4.088D 10	7.322D 10	1.534D 02	1.434D 02
5.0D-03	8078.	4.082D 10	8.157D 10	2.186D 02	2.078D 02
7.5D-03	8192.	4.084D 10	8.451D 10	2.715D 02	2.601D 02
1.0D-02	8288.	4.084D 10	8.718D 10	3.151D 02	3.032D 02
2.5D-02	8618.	4.074D 10	1.001D 11	4.926D 02	4.787D 02
5.0D-02	8928.	4.071D 10	1.173D 11	6.748D 02	6.538D 02
7.5D-02	9233.	4.092D 10	1.332D 11	7.941D 02	7.757D 02
1.0D-01	9501.	4.100D 10	1.430D 11	8.805D 02	8.599D 02
2.5D-01	10489.	4.064D 10	2.215D 11	1.184D 03	1.153D 03
5.0D-01	11564.	4.078D 10	3.255D 11	1.517D 03	1.472D 03
7.5D-01	12258.	4.073D 10	4.118D 11	1.812D 03	1.755D 03
1.0D 00	12802.	4.080D 10	4.832D 11	2.096D 03	2.028D 03
2.5D 00	14718.	4.075D 10	8.519D 11	3.654D 03	3.535D 03
5.0D 00	16380.	4.078D 10	1.303D 12	5.842D 03	5.660D 03
7.5D 00	17446.	4.074D 10	1.676D 12	7.708D 03	7.474D 03
1.0D 01	18247.	4.069D 10	2.004D 12	9.385D 03	9.105D 03
2.5D 01	20920.	4.067D 10	3.464D 12	1.760D 04	1.712D 04
5.0D 01	23227.	4.079D 10	5.267D 12	2.847D 04	2.774D 04
7.5D 01	24817.	4.071D 10	6.846D 12	3.789D 04	3.694D 04
1.0D 02	26072.	4.065D 10	8.336D 12	4.643D 04	4.526D 04

TAU	PE DYNE/CM**2	DENSITY GM/CM**3	MU A.M.U.	K ZERO CM**2/GM	DEPTH CM
1.0D-08	1.529D-04	7.852D-16	0.74925	2.477D-01	-1.17D 08
1.0D-07	1.485D-03	8.132D-15	0.74948	2.477D-01	-1.16D 08
1.0D-06	1.480D-02	8.160D-14	0.75172	2.470D-01	-1.15D 08
1.0D-05	1.480D-01	8.163D-13	0.77415	2.402D-01	-1.05D 08
1.0D-04	1.480D 00	8.163D-12	0.99843	1.726D-01	0.0
2.5D-04	3.007D 00	2.561D-11	1.11089	1.548D-01	6.04D 07
5.0D-04	4.836D 00	5.857D-11	1.18321	1.497D-01	1.01D 08
7.5D-04	6.265D 00	9.279D-11	1.21923	1.501D-01	1.24D 08
1.0D-03	7.454D 00	1.272D-10	1.24087	1.520D-01	1.39D 08
2.5D-03	1.972D 01	2.632D-10	1.21218	3.252D-01	1.79D 08
5.0D-03	2.876D 01	3.744D-10	1.21061	4.274D-01	1.99D 08
7.5D-03	3.725D 01	4.595D-10	1.20401	5.284D-01	2.12D 08
1.0D-02	4.522D 01	5.257D-10	1.19572	6.271D-01	2.21D 08
2.5D-02	8.263D 01	7.762D-10	1.16272	1.091D 00	2.48D 08
5.0D-02	1.323D 02	9.960D-10	1.12326	1.738D 00	2.68D 08
7.5D-02	1.859D 02	1.079D-09	1.06963	2.562D 00	2.79D 08
1.0D-01	2.366D 02	1.108D-09	1.01970	3.406D 00	2.87D 08
2.5D-01	4.422D 02	1.145D-09	0.86719	6.725D 00	3.13D 08
5.0D-01	6.467D 02	1.205D-09	0.78760	8.536D 00	3.40D 08
7.5D-01	7.941D 02	1.322D-09	0.76935	8.945D 00	3.63D 08
1.0D 00	9.291D 02	1.449D-09	0.76164	9.190D 00	3.83D 08
2.5D 00	1.651D 03	2.159D-09	0.74906	1.056D 01	4.67D 08
5.0D 00	2.698D 03	3.051D-09	0.73545	1.258D 01	5.50D 08
7.5D 00	3.621D 03	3.727D-09	0.72453	1.434D 01	6.04D 08
1.0D 01	4.456D 03	4.300D-09	0.71753	1.563D 01	6.46D 08
2.5D 01	8.513D 03	6.941D-09	0.70640	2.022D 01	7.95D 08
5.0D 01	1.384D 04	1.009D-08	0.70392	2.423D 01	9.26D 08
7.5D 01	1.845D 04	1.258D-08	0.70323	2.676D 01	1.01D 09
1.0D 02	2.262D 04	1.467D-08	0.70293	2.849D 01	1.08D 09

EMERGENT SPECTRUM (LAMBDA IN ANGSTROMS, FLUX IN ERG/CM**2/S/A)

BAND	MID LAMBDA	BAND WIDTH	AVG.F LAMBDA	AVG.M LAMBDA
1	196.	131.	1.600D-09	21.989
2	332.	141.	1.600D-09	21.989
3	453.	102.	4.502D-05	10.867
4	558.	107.	6.125D-02	3.032
5	659.	96.	1.658D 01	-3.049
6	759.	104.	4.015D 02	-6.509
7	861.	101.	6.943D 03	-9.604
8	965.	107.	3.231D 04	-12.289
9	1075.	111.	6.514D 05	-14.535
10	1173.	86.	2.996D 06	-16.191
11	1261.	91.	9.002D 06	-17.386
12	1370.	127.	1.919D 07	-18.208
13	1478.	87.	3.538D 07	-18.872
14	1573.	103.	5.461D 07	-19.343
15	1687.	126.	7.916D 07	-19.746
16	1800.	100.	1.005D 08	-20.005
17	1897.	93.	1.114D 08	-20.117
18	1997.	108.	1.057D 08	-20.060
19	2093.	83.	9.706D 07	-19.968
20	2192.	116.	8.565D 07	-19.832
21	2298.	96.	6.439D 07	-19.522
22	2383.	73.	5.501D 07	-19.351
23	2465.	92.	5.010D 07	-19.250
24	2556.	89.	5.186D 07	-19.287
25	2648.	95.	5.403D 07	-19.332
26	2743.	96.	5.673D 07	-19.384
27	2864.	145.	6.383D 07	-19.513
28	2979.	86.	6.853D 07	-19.590
29	3072.	99.	7.044D 07	-19.620
30	3166.	90.	6.812D 07	-19.583
31	3260.	99.	6.616D 07	-19.551
32	3370.	120.	6.431D 07	-19.521
33	3488.	115.	6.279D 07	-19.495
34	3596.	102.	6.179D 07	-19.477
35	3702.	110.	7.976D 07	-19.754
36	3797.	80.	1.069D 08	-20.073
37	3894.	113.	1.396D 08	-20.362
38	3995.	90.	1.380D 08	-20.349
39	4111.	142.	1.350D 08	-20.326

EMERGENT SPECTRUM (LAMBDA IN ANGSTROMS, FLUX IN ERG/CM**2/S/A)

BAND	MID LAMBDA	BAND WIDTH*	AVG.F LAMBDA	AVG.M LAMBDA
40	4245.	126.	1.334D 08	-20.313
41	4365.	114.	1.104D 08	-20.108
42	4475.	106.	1.147D 08	-20.149
43	4589.	122.	1.064D 08	-20.067
44	4705.	109.	9.971D 07	-19.997
45	4822.	127.	8.319D 07	-19.800
46	4945.	118.	8.675D 07	-19.846
47	5053.	98.	8.228D 07	-19.788
48	5147.	90.	7.531D 07	-19.692
49	5248.	112.	7.107D 07	-19.629
50	5361.	113.	6.664D 07	-19.559
51	5486.	138.	6.327D 07	-19.503
52	5627.	144.	5.941D 07	-19.435
53	5753.	108.	5.620D 07	-19.374
54	5858.	101.	5.138D 07	-19.277
55	5959.	102.	5.057D 07	-19.260
56	6056.	92.	4.781D 07	-19.199
57	6154.	103.	4.431D 07	-19.116
58	6258.	107.	4.240D 07	-19.068
59	6376.	129.	4.033D 07	-19.014
60	6482.	82.	3.787D 07	-18.946
61	6593.	140.	3.244D 07	-18.778
62	6713.	100.	3.464D 07	-18.849
63	6813.	100.	3.311D 07	-18.800
64	6913.	101.	3.162D 07	-18.750
65	7018.	108.	2.982D 07	-18.686
66	7141.	138.	2.823D 07	-18.627
67	7270.	119.	2.679D 07	-18.570
68	7383.	108.	2.551D 07	-18.517
69	7513.	151.	2.386D 07	-18.444
70	7669.	162.	2.266D 07	-18.388
71	7820.	140.	2.058D 07	-18.283
72	7968.	155.	1.956D 07	-18.228
73	8125.	161.	1.853D 07	-18.169
74	8290.	169.	2.096D 07	-18.304
75	11482.	6213.	3.436D 06	-17.315
76	18691.	8206.	1.423D 06	-15.383
77	27809.	10029.	3.089D 05	-13.725
78	49235.	32823.	4.430D 04	-11.616

SIRIUS GRID MODEL

TEFF = 9750. LOG G = 4.20 PI F = 5.123D 11

BALMER JUMP = .496 PASCHEN SLOPE = 5.666D-04 MAG/A

PERCENT OF THE FLUX IN THE DIFFERENT HYDROGEN CONTINUA:

LYMAN	BALMER	PASCHEN	THE OTHERS
0.00	31.89	54.09	14.02

TAU	TEMP DEG.K	H ERG/CM**2/SEC/STERADIAN	J	P TOTAL --- DYNE/CM**2	P GAS ----
1.0D-08	7522.	4.104D 10	7.154D 10	8.074D 00	8.474D-04
1.0D-07	7522.	4.104D 10	7.154D 10	8.082D 00	8.653D-03
1.0D-06	7522.	4.104D 10	7.155D 10	8.160D 00	8.671D-02
1.0D-05	7522.	4.103D 10	7.159D 10	8.940D 00	8.673D-01
1.0D-04	7523.	4.102D 10	7.304D 10	1.675D 01	8.673D 00
2.5D-04	7525.	4.079D 10	7.358D 10	3.230D 01	2.422D 01
5.0D-04	7527.	4.071D 10	7.413D 10	5.900D 01	5.090D 01
7.5D-04	7529.	4.068D 10	7.460D 10	8.534D 01	7.724D 01
1.0D-03	7531.	4.067D 10	7.504D 10	1.110D 02	1.029D 02
2.5D-03	7946.	4.083D 10	7.830D 10	2.240D 02	2.139D 02
5.0D-03	8103.	4.081D 10	8.170D 10	3.207D 02	3.099D 02
7.5D-03	8230.	4.080D 10	8.464D 10	3.949D 02	3.833D 02
1.0D-02	8314.	4.076D 10	8.721D 10	4.560D 02	4.440D 02
2.5D-02	8583.	4.066D 10	9.965D 10	7.192D 02	7.055D 02
5.0D-02	8924.	4.089D 10	1.172D 11	9.943D 02	9.783D 02
7.5D-02	9260.	4.109D 10	1.336D 11	1.161D 03	1.143D 03
1.0D-01	9515.	4.104D 10	1.483D 11	1.280D 03	1.259D 03
2.5D-01	10494.	4.077D 10	2.217D 11	1.685D 03	1.654D 03
5.0D-01	11558.	4.070D 10	3.252D 11	2.094D 03	2.049D 03
7.5D-01	12255.	4.071D 10	4.114D 11	2.448D 03	2.391D 03
1.0D 00	12795.	4.072D 10	4.833D 11	2.789D 03	2.721D 03
2.5D 00	14709.	4.083D 10	8.498D 11	4.691D 03	4.572D 03
5.0D 00	16356.	4.077D 10	1.236D 12	7.413D 03	7.237D 03
7.5D 00	17414.	4.075D 10	1.663D 12	9.764D 03	9.531D 03
1.0D 01	18207.	4.064D 10	1.936D 12	1.187D 04	1.160D 04
2.5D 01	20884.	4.067D 10	3.440D 12	2.223D 04	2.175D 04
5.0D 01	23213.	4.079D 10	5.255D 12	3.599D 04	3.525D 04
7.5D 01	24839.	4.091D 10	6.871D 12	4.800D 04	4.704D 04
1.0D 02	26118.	4.065D 10	8.395D 12	5.896D 04	5.779D 04

TAU	PE DYNE/CM**2	DENSITY GM/CM**3	MU A.M.U.	K ZERC CM**2/GM	DEPTH CM
1.0D-08	2.233D-04	1.401D-15	0.74948	2.476D-01	-6.67D 07
1.0D-07	2.145D-03	1.461D-14	0.74976	2.475D-01	-6.67D 07
1.0D-06	2.136D-02	1.467D-13	0.75254	2.467D-01	-6.61D 07
1.0D-05	2.135D-01	1.468D-12	0.78038	2.389D-01	-6.01D 07
1.0D-04	2.135D 00	1.468D-11	1.05881	1.609D-01	0.0
2.5D-04	4.145D 00	4.505D-11	1.16351	1.491D-01	3.58D 07
5.0D-04	6.455D 00	9.974D-11	1.22502	1.489D-01	5.99D 07
7.5D-04	8.225D 00	1.548D-10	1.25456	1.522D-01	7.33D 07
1.0D-03	9.682D 00	2.091D-10	1.27203	1.561D-01	8.21D 07
2.5D-03	2.510D 01	4.013D-10	1.24030	3.482D-01	1.05D 08
5.0D-03	3.734D 01	5.679D-10	1.23581	4.746D-01	1.17D 08
7.5D-03	4.875D 01	6.865D-10	1.22647	5.996D-01	1.25D 08
1.0D-02	5.818D 01	7.836D-10	1.22098	6.936D-01	1.30D 08
2.5D-02	1.008D 02	1.190D-09	1.20438	1.125D 00	1.47D 08
5.0D-02	1.690D 02	1.532D-09	1.16272	1.900D 00	1.60D 08
7.5D-02	2.450D 02	1.637D-09	1.10493	2.936D 00	1.66D 08
1.0D-01	3.110D 02	1.682D-09	1.05889	3.904D 00	1.70D 08
2.5D-01	5.933D 02	1.700D-09	0.89786	8.298D 00	1.85D 08
5.0D-01	8.817D 02	1.707D-09	0.80059	1.118D 01	2.00D 08
7.5D-01	1.071D 03	1.818D-09	0.77604	1.178D 01	2.12D 08
1.0D 00	1.238D 03	1.956D-09	0.76576	1.207D 01	2.23D 08
2.5D 00	2.129D 03	2.801D-09	0.75086	1.351D 01	2.73D 08
5.0D 00	3.434D 03	3.923D-09	0.73851	1.600D 01	3.23D 08
7.5D 00	4.594D 03	4.784D-09	0.72797	1.807D 01	3.57D 08
1.0D 01	5.650D 03	5.513D-09	0.72063	1.972D 01	3.83D 08
2.5D 01	1.080D 04	8.845D-09	0.70749	2.564D 01	4.74D 08
5.0D 01	1.758D 04	1.284D-08	0.70435	3.073D 01	5.56D 08
7.5D 01	2.349D 04	1.602D-08	0.70347	3.389D 01	6.10D 08
1.0D 02	2.887D 04	1.871D-08	0.70310	3.609D 01	6.51D 08

EMERGENT SPECTRUM (LAMBDA IN ANGSTROMS, FLUX IN ERG/CM**2/S/A)

BAND	MID LAMBDA	BAND WIDTH	AVG.F LAMBDA	AVG.M LAMBDA
1	196.	131.	1.558D-09	22.018
2	332.	141.	1.558D-09	22.018
3	453.	102.	4.420D-05	10.886
4	558.	107.	6.038D-02	3.048
5	659.	96.	1.636D 01	-3.034
6	759.	104.	3.902D 02	-6.478
7	861.	101.	6.714D 03	-9.567
8	965.	107.	8.005D 04	-12.258
9	1075.	111.	6.633D 05	-14.554
10	1173.	86.	3.122D 06	-16.236
11	1261.	91.	9.443D 06	-17.438
12	1370.	127.	1.925D 07	-18.211
13	1478.	87.	3.446D 07	-18.843
14	1573.	103.	5.248D 07	-19.300
15	1687.	126.	7.742D 07	-19.722
16	1800.	100.	9.970D 07	-19.997
17	1897.	93.	1.116D 08	-20.119
18	1997.	108.	1.067D 08	-20.070
19	2093.	83.	9.850D 07	-19.984
20	2192.	116.	8.725D 07	-19.852
21	2298.	96.	6.565D 07	-19.543
22	2383.	73.	5.610D 07	-19.372
23	2465.	92.	5.108D 07	-19.271
24	2556.	89.	5.283D 07	-19.307
25	2648.	95.	5.497D 07	-19.350
26	2743.	96.	5.763D 07	-19.402
27	2864.	145.	6.463D 07	-19.526
28	2979.	86.	6.922D 07	-19.601
29	3072.	99.	7.103D 07	-19.629
30	3166.	90.	6.865D 07	-19.592
31	3260.	99.	6.664D 07	-19.559
32	3370.	120.	6.473D 07	-19.528
33	3485.	115.	6.316D 07	-19.501
34	3596.	102.	6.211D 07	-19.483
35	3702.	110.	7.999D 07	-19.758
36	3797.	80.	1.038D 08	-20.041
37	3894.	113.	1.362D 08	-20.336
38	3995.	90.	1.355D 08	-20.330
39	4111.	142.	1.331D 08	-20.310

EMERGENT SPECTRUM (LAMBDA IN ANGSTROMS, FLUX IN ERG/CM**2/S/A)

BAND	MID LAMBDA	BAND WIDTH	AVG.F LAMBDA	AVG.M LAMBDA
40	4245.	126.	1.331D 08	-20.310
41	4365.	114.	1.088D 08	-20.091
42	4475.	106.	1.146D 08	-20.148
43	4589.	122.	1.063D 08	-20.067
44	4705.	109.	9.964D 07	-19.996
45	4822.	127.	8.201D 07	-19.785
46	4945.	118.	8.633D 07	-19.840
47	5053.	98.	8.223D 07	-19.788
48	5147.	90.	7.533D 07	-19.692
49	5248.	112.	7.111D 07	-19.630
50	5361.	113.	6.669D 07	-19.560
51	5486.	138.	6.322D 07	-19.502
52	5627.	144.	5.941D 07	-19.435
53	5753.	108.	5.624D 07	-19.375
54	5858.	101.	5.140D 07	-19.277
55	5959.	102.	5.064D 07	-19.261
56	6056.	92.	4.786D 07	-19.200
57	6154.	103.	4.438D 07	-19.118
58	6258.	107.	4.246D 07	-19.070
59	6376.	129.	4.036D 07	-19.015
60	6482.	82.	3.784D 07	-18.945
61	6593.	140.	3.225D 07	-18.771
62	6713.	100.	3.469D 07	-18.851
63	6813.	100.	3.317D 07	-18.802
64	6913.	101.	3.169D 07	-18.752
65	7018.	108.	2.989D 07	-18.689
66	7141.	138.	2.828D 07	-18.629
67	7270.	119.	2.685D 07	-18.573
68	7383.	108.	2.556D 07	-18.519
69	7513.	151.	2.391D 07	-18.447
70	7669.	162.	2.271D 07	-18.390
71	7820.	140.	2.062D 07	-18.286
72	7968.	155.	1.961D 07	-18.231
73	8125.	161.	1.855D 07	-18.171
74	8290.	169.	2.096D 07	-18.303
75	11482.	6213.	3.449D 06	-17.317
76	18691.	8206.	1.426D 06	-15.385
77	27809.	10029.	3.093D 05	-13.726
78	49235.	32823.	4.433D 04	-11.617

SIRIUS GRID MODEL

TEFF = 9750. LOG G = 4.40 PI F = 5.123D 11

BALMER JUMP = .488 PASCHEN SLOPE = 5.645D-04 MAG/A

PERCENT OF THE FLUX IN THE DIFFERENT HYDROGEN CONTINUA:

LYMAN	BALMER	PASCHEN	THE OTHERS
0.00	32.24	53.73	14.03

TAU	TEMP DEG.K	H ERG/CM**2/SEC/STERADIAN	J	P TOTAL --- DYNE/CM**2 ----	P GAS
1.0D-08	7517.	4.109D 10	7.168D 10	8.054D 00	1.429D-03
1.0D-07	7517.	4.108D 10	7.168D 10	8.067D 00	1.466D-02
1.0D-06	7517.	4.108D 10	7.170D 10	8.199D 00	1.470D-01
1.0D-05	7517.	4.108D 10	7.184D 10	9.523D 00	1.470D 00
1.0D-04	7518.	4.106D 10	7.321D 10	2.276D 01	1.471D 01
2.5D-04	7520.	4.083D 10	7.378D 10	4.829D 01	4.022D 01
5.0D-04	7522.	4.076D 10	7.435D 10	9.054D 01	8.246D 01
7.5D-04	7524.	4.074D 10	7.483D 10	1.313D 02	1.232D 02
1.0D-03	7526.	4.075D 10	7.528D 10	1.705D 02	1.624D 02
2.5D-03	7988.	4.087D 10	7.865D 10	3.219D 02	3.116D 02
5.0D-03	8131.	4.084D 10	8.194D 10	4.594D 02	4.484D 02
7.5D-03	8237.	4.082D 10	8.476D 10	5.660D 02	5.544D 02
1.0D-02	8306.	4.080D 10	8.725D 10	6.562D 02	6.442D 02
2.5D-02	8581.	4.081D 10	9.982D 10	1.050D 03	1.036D 03
5.0D-02	9003.	4.096D 10	1.181D 11	1.429D 03	1.413D 03
7.5D-02	9284.	4.078D 10	1.336D 11	1.655D 03	1.636D 03
1.0D-01	9492.	4.059D 10	1.474D 11	1.823D 03	1.803D 03
2.5D-01	10484.	4.085D 10	2.208D 11	2.392D 03	2.362D 03
5.0D-01	11552.	4.078D 10	3.246D 11	2.908D 03	2.863D 03
7.5D-01	12252.	4.078D 10	4.111D 11	3.334D 03	3.277D 03
1.0D 00	12792.	4.075D 10	4.879D 11	3.743D 03	3.676D 03
2.5D 00	14697.	4.078D 10	8.472D 11	6.055D 03	5.937D 03
5.0D 00	16336.	4.078D 10	1.289D 12	9.441D 03	9.261D 03
7.5D 00	17385.	4.079D 10	1.652D 12	1.238D 04	1.215D 04
1.0D 01	18175.	4.076D 10	1.972D 12	1.504D 04	1.476D 04
2.5D 01	20850.	4.078D 10	3.418D 12	2.806D 04	2.758D 04
5.0D 01	23220.	4.077D 10	5.261D 12	4.545D 04	4.471D 04
7.5D 01	24873.	4.076D 10	6.908D 12	6.071D 04	5.974D 04
1.0D 02	26179.	4.069D 10	8.475D 12	7.470D 04	7.351D 04

TAU	PE	DENSITY	MU	K ZERO	DEPTH
	DYNE/CM**2	GM/CM**3	A.M.U.	CM**2/GM	CM
1.0D-08	3.201D-04	2.492D-15	0.74963	2.475D-01	-3.81D 07
1.0D-07	3.028D-03	2.614D-14	0.74996	2.474D-01	-3.81D 07
1.0D-06	3.011D-02	2.626D-13	0.75327	2.465D-01	-3.78D 07
1.0D-05	3.009D-01	2.627D-12	0.78635	2.379D-01	-3.43D 07
1.0D-04	3.009D 00	2.627D-11	1.11720	1.517D-01	0.0
2.5D-04	5.585D 00	7.730D-11	1.20905	1.465D-01	2.12D 07
5.0D-04	8.445D 00	1.662D-10	1.25968	1.511D-01	3.54D 07
7.5D-04	1.060D 01	2.529D-10	1.28349	1.570D-01	4.33D 07
1.0D-03	1.236D 01	3.368D-10	1.29743	1.629D-01	4.86D 07
2.5D-03	3.264D 01	5.898D-10	1.25777	3.950D-01	6.13D 07
5.0D-03	4.757D 01	8.324D-10	1.25598	5.289D-01	6.89D 07
7.5D-03	6.063D 01	1.012D-09	1.25137	6.482D-01	7.35D 07
1.0D-02	7.139D 01	1.165D-09	1.24931	7.409D-01	7.68D 07
2.5D-02	1.260D 02	1.791D-09	1.23426	1.217D 00	8.74D 07
5.0D-02	2.264D 02	2.225D-09	1.18017	2.276D 00	9.48D 07
7.5D-02	3.133D 02	2.406D-09	1.13664	3.297D 00	9.86D 07
1.0D-01	3.890D 02	2.515D-09	1.10268	4.232D 00	1.01D 08
2.5D-01	7.930D 02	2.528D-09	0.93433	9.930D 00	1.10D 08
5.0D-01	1.198D 03	2.436D-09	0.81738	1.448D 01	1.18D 08
7.5D-01	1.447D 03	2.522D-09	0.78489	1.549D 01	1.25D 08
1.0D 00	1.659D 03	2.662D-09	0.77118	1.587D 01	1.31D 08
2.5D 00	2.756D 03	3.650D-09	0.75282	1.738D 01	1.60D 08
5.0D 00	4.375D 03	5.047D-09	0.74139	2.024D 01	1.90D 08
7.5D 00	5.828D 03	6.140D-09	0.73143	2.276D 01	2.11D 08
1.0D 01	7.159D 03	7.063D-09	0.72390	2.485D 01	2.27D 08
2.5D 01	1.367D 04	1.126D-08	0.70881	3.243D 01	2.84D 08
5.0D 01	2.228D 04	1.629D-08	0.70484	3.879D 01	3.34D 08
7.5D 01	2.982D 04	2.032D-08	0.70375	4.275D 01	3.68D 08
1.0D 02	3.671D 04	2.375D-08	0.70330	4.549D 01	3.94D 08

EMERGENT SPECTRUM (LAMBDA IN ANGSTROMS, FLUX IN ERG/CM**2/S/A)

BAND	MID LAMBDA	BAND WIDTH	AVG.F LAMBDA	AVG.M LAMBDA
1	196.	131.	1.507D-09	22.055
2	332.	141.	1.507D-09	22.055
3	453.	102.	4.314D-05	10.913
4	558.	107.	5.922D-02	3.069
5	659.	96.	1.608D 01	-3.015
6	759.	104.	3.789D 02	-6.446
7	861.	101.	6.495D 03	-9.531
8	965.	107.	7.783D 04	-12.228
9	1075.	111.	6.689D 05	-14.563
10	1173.	86.	3.212D 06	-16.267
11	1261.	91.	9.780D 06	-17.476
12	1370.	127.	1.937D 07	-18.218
13	1478.	87.	3.403D 07	-18.830
14	1573.	103.	5.136D 07	-19.277
15	1687.	126.	7.659D 07	-19.710
16	1800.	100.	9.954D 07	-19.995
17	1897.	93.	1.122D 08	-20.125
18	1997.	108.	1.079D 08	-20.083
19	2093.	83.	1.002D 08	-20.002
20	2192.	116.	9.908D 07	-19.874
21	2298.	96.	6.728D 07	-19.570
22	2383.	73.	5.759D 07	-19.401
23	2465.	92.	5.248D 07	-19.300
24	2556.	89.	5.423D 07	-19.336
25	2648.	95.	5.635D 07	-19.377
26	2743.	96.	5.899D 07	-19.427
27	2864.	145.	6.592D 07	-19.548
28	2979.	86.	7.044D 07	-19.620
29	3072.	99.	7.219D 07	-19.646
30	3166.	90.	6.978D 07	-19.609
31	3260.	99.	6.773D 07	-19.577
32	3370.	120.	6.577D 07	-19.545
33	3488.	115.	6.413D 07	-19.518
34	3596.	102.	6.302D 07	-19.499
35	3702.	110.	8.075D 07	-19.768
36	3797.	80.	1.010D 08	-20.011
37	3894.	113.	1.326D 08	-20.306
38	3995.	90.	1.329D 08	-20.309
39	4111.	142.	1.308D 08	-20.292

EMERGENT SPECTRUM (LAMBDA IN ANGSTROMS, FLUX IN ERG/CM**2/S/A)

BAND	MID LAMBDA	BAND WIDTH	AVG.F LAMBDA	AVG.M LAMBDA
40	4245.	126.	1.326D 08	-20.306
41	4365.	114.	1.070D 08	-20.074
42	4475.	106.	1.144D 08	-20.146
43	4589.	122.	1.062D 08	-20.065
44	4705.	109.	9.952D 07	-19.995
45	4822.	127.	8.076D 07	-19.768
46	4945.	118.	8.587D 07	-19.835
47	5053.	98.	8.218D 07	-19.787
48	5147.	90.	7.530D 07	-19.692
49	5248.	112.	7.111D 07	-19.630
50	5361.	113.	6.671D 07	-19.560
51	5486.	138.	6.319D 07	-19.502
52	5627.	144.	5.942D 07	-19.435
53	5753.	108.	5.627D 07	-19.376
54	5858.	101.	5.142D 07	-19.278
55	5959.	102.	5.070D 07	-19.263
56	6056.	92.	4.790D 07	-19.201
57	6154.	103.	4.445D 07	-19.120
58	6258.	107.	4.253D 07	-19.072
59	6376.	129.	4.040D 07	-19.016
60	6482.	82.	3.782D 07	-18.944
61	6593.	140.	3.208D 07	-18.765
62	6713.	100.	3.474D 07	-18.852
63	6813.	100.	3.324D 07	-18.804
64	6913.	101.	3.176D 07	-18.755
65	7018.	108.	2.998D 07	-18.692
66	7141.	138.	2.833D 07	-18.631
67	7270.	119.	2.693D 07	-18.576
68	7383.	108.	2.563D 07	-18.522
69	7513.	151.	2.398D 07	-18.450
70	7669.	162.	2.277D 07	-18.394
71	7820.	140.	2.069D 07	-18.289
72	7968.	155.	1.968D 07	-18.235
73	8125.	161.	1.861D 07	-18.174
74	8290.	169.	2.095D 07	-18.303
75	11482.	6213.	8.461D 06	-17.319
76	18691.	8206.	1.431D 06	-15.389
77	27809.	10029.	3.104D 05	-13.730
78	49235.	32823.	4.447D 04	-11.620

SIRIUS GRID MODEL

TEFF = 9500. LOG G = 1.00 PI F = 4.618D 11

BALMER JUMP = .520 PASCHEN SLOPE = 5.621D-04 MAG/A

PERCENT OF THE FLUX IN THE DIFFERENT HYDROGEN CONTINUA:

LYMAN	BALMER	PASCHEN	THE OTHERS
0.00	28.74	56.30	14.96

TAU	TEMP DEG.K	H	J	P TOTAL	P GAS
		ERG/CM**2/SEC/STERADIAN		--- DYNE/CM**2	----
1.0D-08	7512.	3.706D 10	6.476D 10	8.029D 00	5.093D-04
1.0D-07	7512.	3.706D 10	6.476D 10	8.034D 00	5.181D-03
1.0D-06	7512.	3.706D 10	6.477D 10	8.081D 00	5.190D-02
1.0D-05	7512.	3.706D 10	6.490D 10	8.548D 00	5.191D-01
1.0D-04	7512.	3.705D 10	6.520D 10	1.322D 01	5.191D 00
2.5D-04	7515.	3.680D 10	6.570D 10	2.275D 01	1.471D 01
5.0D-04	7517.	3.670D 10	6.717D 10	3.971D 01	3.166D 01
7.5D-04	7518.	3.664D 10	6.756D 10	5.685D 01	4.380D 01
1.0D-03	7518.	3.660D 10	6.791D 10	7.384D 01	6.579D 01
2.5D-03	7542.	3.659D 10	6.977D 10	1.701D 02	1.620D 02
5.0D-03	7875.	3.670D 10	7.326D 10	2.761D 02	2.664D 02
7.5D-03	8003.	3.666D 10	7.591D 10	3.440D 02	3.336D 02
1.0D-02	8076.	3.663D 10	7.320D 10	4.006D 02	3.899D 02
2.5D-02	8342.	3.661D 10	8.350D 10	6.445D 02	6.323D 02
5.0D-02	8730.	3.691D 10	1.059D 11	8.854D 02	8.707D 02
7.5D-02	9048.	3.697D 10	1.207D 11	1.023D 03	1.006D 03
1.0D-01	9279.	3.687D 10	1.338D 11	1.122D 03	1.103D 03
2.5D-01	10262.	3.676D 10	2.018D 11	1.445D 03	1.417D 03
5.0D-01	11305.	3.672D 10	2.973D 11	1.749D 03	1.708D 03
7.5D-01	12012.	3.682D 10	3.751D 11	2.008D 03	1.955D 03
1.0D 00	12552.	3.678D 10	4.518D 11	2.259D 03	2.196D 03
2.5D 00	14454.	3.674D 10	7.322D 11	3.690D 03	3.579D 03
5.0D 00	16092.	3.677D 10	1.214D 12	5.784D 03	5.615D 03
7.5D 00	17141.	3.679D 10	1.561D 12	7.598D 03	7.380D 03
1.0D 01	17932.	3.678D 10	1.369D 12	9.233D 03	8.972D 03
2.5D 01	20589.	3.678D 10	3.250D 12	1.726D 04	1.680D 04
5.0D 01	22844.	3.669D 10	4.028D 12	2.787D 04	2.718D 04
7.5D 01	24389.	3.667D 10	6.336D 12	3.706D 04	3.617D 04
1.0D 02	25603.	3.662D 10	7.752D 12	4.539D 04	4.431D 04

TAU	PE	DENSITY	MU	K ZERO	DEPTH
	DYNE/CM**2	GM/CM**3	A.M.U.	CM**2/GM	CM
1.0D-08	1.526D-04	8.020D-16	0.74930	2.477D-01	-1.15D 08
1.0D-07	1.482D-03	8.316D-15	0.74953	2.476D-01	-1.15D 08
1.0D-06	1.477D-02	8.345D-14	0.75183	2.469D-01	-1.14D 08
1.0D-05	1.477D-01	8.348D-13	0.77484	2.399D-01	-1.03D 08
1.0D-04	1.477D 00	8.349D-12	1.00495	1.692D-01	0.0
2.5D-04	2.996D 00	2.633D-11	1.11762	1.511D-01	6.02D 07
5.0D-04	4.812D 00	6.033D-11	1.18923	1.459D-01	1.01D 08
7.5D-04	6.228D 00	9.565D-11	1.22469	1.462D-01	1.23D 08
1.0D-03	7.401D 00	1.312D-10	1.24597	1.479D-01	1.38D 08
2.5D-03	1.266D 01	3.344D-10	1.29499	1.678D-01	1.82D 08
5.0D-03	2.616D 01	5.148D-10	1.26721	3.225D-01	2.07D 08
7.5D-03	3.460D 01	6.310D-10	1.25933	4.101D-01	2.19D 08
1.0D-02	4.119D 01	7.292D-10	1.25657	4.729D-01	2.27D 08
2.5D-02	7.353D 01	1.131D-09	1.24175	7.791D-01	2.53D 08
5.0D-02	1.320D 02	1.429D-09	1.19246	1.441D 00	2.72D 08
7.5D-02	1.914D 02	1.521D-09	1.13867	2.233D 00	2.81D 08
1.0D-01	2.424D 02	1.566D-09	1.09714	2.962D 00	2.87D 08
2.5D-01	4.892D 02	1.528D-09	0.92101	6.935D 00	3.07D 08
5.0D-01	7.248D 02	1.469D-09	0.80889	9.759D 00	3.27D 08
7.5D-01	8.715D 02	1.523D-09	0.77892	1.024D 01	3.43D 08
1.0D 00	9.974D 02	1.612D-09	0.76698	1.038D 01	3.59D 08
2.5D 00	1.666D 03	2.233D-09	0.75117	1.123D 01	4.32D 08
5.0D 00	2.662D 03	3.097D-09	0.73907	1.309D 01	5.09D 08
7.5D 00	3.555D 03	3.766D-09	0.72841	1.472D 01	5.61D 08
1.0D 01	4.370D 03	4.331D-09	0.72079	1.603D 01	6.01D 08
2.5D 01	8.344D 03	6.930D-09	0.70732	2.074D 01	7.46D 08
5.0D 01	1.356D 04	1.006D-08	0.70427	2.489D 01	8.74D 08
7.5D 01	1.806D 04	1.254D-08	0.70343	2.752D 01	9.60D 08
1.0D 02	2.213D 04	1.463D-08	0.70307	2.935D 01	1.02D 09

EMERGENT SPECTRUM (LAMBDA IN ANGSTROMS, FLUX IN ERG/CM**2/S/A)

BAND	MID LAMBDA	BAND WIDTH	AVG.F LAMBDA	AVG.M LAMBDA
1	196.	131.	1.448D-09	22.098
2	332.	141.	1.448D-09	22.098
3	453.	102.	4.295D-05	10.917
4	558.	107.	5.915D-02	3.070
5	659.	96.	1.572D 01	-2.991
6	759.	104.	3.480D 02	-6.354
7	861.	101.	5.564D 03	-9.364
8	965.	107.	6.179D 04	-11.977
9	1075.	111.	4.662D 05	-14.171
10	1173.	86.	2.070D 06	-15.790
11	1261.	91.	6.063D 06	-16.957
12	1370.	127.	1.239D 07	-17.732
13	1478.	87.	2.255D 07	-18.383
14	1573.	103.	3.529D 07	-18.869
15	1687.	126.	5.662D 07	-19.382
16	1800.	100.	7.749D 07	-19.723
17	1897.	93.	8.983D 07	-19.884
18	1997.	108.	8.640D 07	-19.841
19	2093.	83.	7.999D 07	-19.758
20	2192.	116.	7.085D 07	-19.626
21	2298.	96.	5.261D 07	-19.303
22	2383.	73.	4.477D 07	-19.127
23	2465.	92.	4.082D 07	-19.027
24	2556.	89.	4.294D 07	-19.082
25	2648.	95.	4.535D 07	-19.142
26	2743.	96.	4.817D 07	-19.207
27	2864.	145.	5.457D 07	-19.342
28	2979.	86.	5.895D 07	-19.426
29	3072.	99.	6.088D 07	-19.461
30	3166.	90.	5.909D 07	-19.429
31	3260.	99.	5.765D 07	-19.402
32	3370.	120.	5.637D 07	-19.378
33	3488.	115.	5.547D 07	-19.360
34	3596.	102.	5.502D 07	-19.351
35	3702.	110.	7.014D 07	-19.615
36	3797.	80.	9.696D 07	-19.966
37	3894.	113.	1.286D 08	-20.273
38	3995.	90.	1.276D 08	-20.265
39	4111.	142.	1.255D 08	-20.246

the spectral points where the transfer equation is solved are expressed as wavelengths in Table C.3, but the quadrature weights are set up for integrations over frequency. Each four wavelength points constitute one interval, or edge. A Lobatto-Gauss quadrature method was used for all frequency integrations. This automatically provides flux discontinuity values at edge heads, and is accurate to 0.1% or better. Within each interval the weights are symmetric, so the first and last weights are equal and the second and third are equal.

4. Blanketing Opacities

Table C.4-1 presents the values of the artificial edge opacity at each frequency point for all temperatures and electron pressures in the grid. The table gives the log of the opacity, which is to be interpolated in T and Log P_e. This interpolation scheme worked best in the test described in Chapter V, section 1. Figures III.3-1 and III.3-2 show that a linear dependence on T and Log P_e is quite reasonable.

Table C.4-2 lists the corresponding values for the statistical UV blanketing opacity which was used in Chapter V, section 3. From 2940 Å to the red, the opacity is the same as in Table C.4-1, and so these are not listed.

TABLE C.2
NORMALIZED ABUNDANCE FRACTIONS (BY NUMBER)
AND LINES CONTRIBUTED TO BLEND

ATOM	NAME	ABUNDANCE	# LINES	ATOM	NAME	ABUNDANCE	# LINES
1	H	8.73D-01	94	46	PD	1.55D-11	80
2	HE	1.26D-01	0	47	AG	4.37D-12	15
3	LI	8.73D-10	7	48	CD	2.76D-11	24
4	BE	2.19D-10	11	49	IN	6.93D-12	22
5	B	5.51D-10	4	50	SN	3.10D-11	59
6	C	2.64D-04	433	51	SB	3.47D-11	51
7	N	7.96D-05	750	52	TE	8.73D-11	11
8	O	5.90D-04	831	53	I	2.19D-11	0
9	F	2.19D-07	0	54	XE	8.73D-11	0
10	NE	2.40D-04	0	55	CS	1.10D-11	19
11	NA	1.45D-06	12	56	BA	1.12D-10	95
12	MG	2.52D-05	25	57	LA	2.19D-11	540
13	AL	1.66D-06	14	58	CE	3.47D-11	1322
14	SI	2.58D-05	15	59	PR	5.51D-12	232
15	P	2.96D-07	9	60	ND	2.76D-11	349
16	S	1.45D-05	0	61	PM	1.10D-12	0
17	CL	2.19D-07	0	62	SM	8.73D-12	981
18	AR	3.64D-06	0	63	EU	4.37D-12	444
19	K	6.62D-08	8	64	GD	1.10D-11	1073
20	CA	1.45D-06	79	65	TB	2.19D-12	3
21	SC	7.09D-10	415	66	DY	1.38D-11	86
22	TI	5.77D-08	1157	67	HO	2.76D-12	3
23	V	5.26D-09	1572	68	ER	6.93D-12	78
24	CR	2.09D-07	1408	69	TM	1.10D-12	215
25	MN	1.10D-07	654	70	YB	1.10D-11	332
26	FE	6.93D-06	1330	71	LU	1.74D-12	154
27	CO	4.58D-08	670	72	HF	3.47D-12	737
28	NI	7.43D-07	274	73	TA	1.74D-12	1061
29	CU	3.90D-08	54	74	W	1.10D-11	1137
30	ZN	1.66D-08	18	75	RE	3.47D-12	851
31	GA	2.46D-10	15	76	OS	1.74D-11	944
32	GE	1.32D-09	43	77	IR	1.38D-11	505
33	AS	1.74D-10	25	78	PT	3.47D-11	161
34	SE	1.38D-09	5	79	AU	4.37D-12	26
35	BR	3.47D-10	0	80	HG	6.93D-12	19
36	KR	1.38D-09	0	81	TL	2.76D-12	18
37	RB	1.95D-10	13	82	PB	3.47D-11	39
38	SR	4.91D-10	76	83	BI	4.37D-12	29
39	Y	2.19D-10	368	84	PO	8.93D-13	0
40	ZR	2.19D-10	1011	85	AT	8.93D-13	0
41	NB	4.37D-11	1351	86	RN	8.93D-13	0
42	MO	7.26D-11	1439	87	FR	8.93D-13	0
43	TC	1.10D-12	0	88	RA	8.93D-13	0
44	RU	2.89D-11	961	89	AC	8.93D-13	0
45	RH	5.26D-12	457	90	TH	1.74D-12	1096

TABLE C.3

LAMBDA 1	LAMBDA 2	LAMBDA 3	LAMBDA 4	WEIGHTS 1&4	WEIGHTS 2&3
130.68	151.63	204.75	261.34	9.5587D 14	4.7794D 15
261.36	289.34	349.97	402.03	3.3446D 14	1.6723D 15
402.05	425.91	471.15	504.26	1.2595D 14	6.2975D 14
504.28	529.82	577.11	610.81	8.6404D 13	4.3202D 14
610.83	634.69	677.51	706.99	5.5629D 13	2.7814D 14
707.01	732.99	779.33	811.02	4.5317D 13	2.2658D 14
811.04	836.58	861.50	911.75	3.4026D 13	1.7013D 14
911.77	939.12	987.01	1019.13	2.8864D 13	1.4432D 14
1019.15	1047.52	1096.93	1129.87	2.4021D 13	1.2011D 14
1129.89	1152.36	1190.68	1215.66	1.5600D 13	7.8000D 13
1215.68	1239.60	1280.37	1306.94	1.4350D 13	7.1749D 13
1306.96	1339.76	1396.48	1433.99	1.6933D 13	8.4666D 13
1434.01	1457.06	1495.96	1521.06	9.9703D 12	4.9852D 13
1521.08	1548.18	1594.13	1623.92	1.0401D 13	5.2006D 13
1623.94	1656.92	1713.23	1749.98	1.1080D 13	5.5401D 13
1750.00	1776.54	1821.23	1849.99	7.7159D 12	3.8580D 13
1850.01	1874.85	1916.49	1943.16	6.4735D 12	3.2368D 13
1943.18	1971.95	2020.34	2051.46	6.7860D 12	3.3930D 13
2051.48	2073.76	2110.85	2134.45	4.7338D 12	2.3669D 13
2134.47	2165.20	2216.83	2249.99	6.0093D 12	3.0047D 13
2250.01	2275.74	2318.65	2345.99	4.5427D 12	2.2713D 13
2346.01	2365.74	2398.37	2418.99	3.2128D 12	1.6064D 13
2419.01	2443.85	2485.14	2511.37	3.7982D 12	1.8991D 13
2511.39	2535.39	2575.21	2600.45	3.4069D 12	1.7035D 13
2600.47	2625.93	2668.19	2694.99	3.3694D 12	1.6847D 13
2695.01	2720.95	2764.00	2791.30	3.1978D 12	1.5989D 13
2791.32	2829.86	2894.53	2935.99	4.4102D 12	2.2051D 13
2936.01	2959.28	2997.73	3021.99	2.4210D 12	1.2105D 13
3022.01	3048.73	3092.99	3120.99	2.6218D 12	1.3109D 13
3121.01	3145.32	3185.46	3210.78	2.2380D 12	1.1190D 13
3210.80	3237.62	3281.97	3309.99	2.3317D 12	1.1658D 13
3310.01	3342.32	3395.97	3429.99	2.6401D 12	1.3201D 13
3430.01	3461.04	3512.45	3544.99	2.3624D 12	1.1812D 13
3545.01	3572.64	3618.26	3647.04	1.9716D 12	9.8582D 12
3647.06	3676.77	3725.87	3756.88	2.0023D 12	1.0012D 13
3756.90	3778.78	3814.74	3837.30	1.3933D 12	6.9664D 12
3837.32	3867.81	3918.19	3949.99	1.8571D 12	9.2853D 12
3950.01	3974.53	4014.86	4040.19	1.4117D 12	7.0586D 12
4040.21	4078.43	4141.82	4181.99	2.0964D 12	1.0482D 13

TABLE C.3

LAMBDA 1	LAMBDA 2	LAMBDA 3	LAMBDA 4	WEIGHTS 1&4	WEIGHTS 2&3
4182.01	4216.15	4272.59	4308.23	1.7502D 12	8.7509D 12
4308.25	4339.10	4389.96	4421.99	1.4915D 12	7.4577D 12
4422.01	4450.80	4498.19	4527.99	1.3223D 12	6.6116D 12
4528.01	4561.08	4615.62	4649.99	1.4473D 12	7.2367D 12
4650.01	4679.63	4728.36	4758.99	1.2303D 12	6.1516D 12
4759.01	4793.43	4850.19	4885.95	1.3639D 12	6.8193D 12
4885.97	4918.03	4970.80	5003.99	1.2059D 12	6.0297D 12
5004.01	5030.71	5074.53	5101.99	9.5878D 11	4.7939D 12
5102.01	5126.68	5167.11	5192.41	8.5251D 11	4.2625D 12
5192.43	5222.79	5272.68	5303.99	1.0120D 12	5.0599D 12
5304.01	5334.89	5385.62	5417.46	9.8638D 11	4.9319D 12
5417.48	5454.80	5516.29	5554.99	1.1415D 12	5.7077D 12
5555.01	5593.94	5658.11	5698.51	1.1325D 12	5.6626D 12
5698.53	5728.10	5776.60	5806.99	8.1883D 11	4.0942D 12
5807.01	5834.57	5879.73	5907.99	7.3533D 11	3.6767D 12
5908.01	5935.85	5981.45	6009.99	7.1753D 11	3.5877D 12
6010.01	6035.15	6076.29	6101.99	6.2659D 11	3.1330D 12
6102.01	6130.13	6176.18	6204.99	6.7948D 11	3.3974D 12
6205.01	6234.12	6281.80	6311.64	6.8020D 11	3.4010D 12
6311.66	6346.88	6404.72	6440.99	7.9477D 11	3.9739D 12
6441.01	6463.58	6500.44	6523.43	4.9005D 11	2.4503D 12
6523.45	6561.43	6623.83	6662.99	8.0203D 11	4.0102D 12
6663.01	6690.35	6735.06	6762.99	5.5430D 11	2.7715D 12
6763.01	6790.35	6835.06	6862.99	5.3815D 11	2.6907D 12
6863.01	6890.53	6935.54	6963.65	5.2609D 11	2.6304D 12
6963.67	6993.28	7041.72	7071.99	5.4950D 11	2.7475D 12
7072.01	7109.62	7171.32	7209.99	6.7605D 11	3.3802D 12
7210.01	7242.51	7295.71	7328.99	5.6251D 11	2.8126D 12
7329.01	7358.59	7406.96	7437.18	4.9578D 11	2.4789D 12
7437.20	7478.27	7545.70	7587.99	6.6754D 11	3.3377D 12
7588.01	7632.10	7704.53	7749.99	6.8813D 11	3.4407D 12
7750.01	7788.20	7850.80	7889.99	5.7191D 11	2.8595D 12
7890.01	7932.25	8001.55	8044.99	6.0998D 11	3.0499D 12
8045.01	8088.83	8160.76	8205.86	6.0872D 11	3.0436D 12
8205.88	8251.94	8327.56	8374.99	6.1475D 11	3.0737D 12
8375.01	9492.43	12105.90	14588.20	1.2705D 13	6.3524D 13
14588.22	16200.16	19727.09	22794.08	6.1651D 12	3.0825D 13
22794.09	24896.70	29264.53	32823.47	3.3489D 12	1.6745D 13
32823.49	38086.98	51431.62	65646.96	3.8056D 12	1.9028D 13

TABLE C.4-1
LOG OF THE BLANKETING OPACITY

T	6000.	8000.	11000.	17500.	50000.
		LAMBDA 1:	130.68 ANGSTROMS		
PE					
3.	-1.479D 01	-9.770D 00	-6.763D 00	-4.278D 00	-1.285D 01
30.	-1.553D 01	-1.031D 01	-6.793D 00	-5.303D 00	-1.170D 01
300.	-1.622D 01	-1.093D 01	-7.082D 00	-6.495D 00	-1.075D 01
10000.	-1.798D 01	-1.201D 01	-7.825D 00	-5.044D 00	-1.006D 01
		LAMBDA 2:	151.63 ANGSTROMS		
PE					
3.	-1.368D 01	-8.497D 00	-5.397D 00	-2.862D 00	-1.142D 01
30.	-1.442D 01	-9.037D 00	-5.427D 00	-3.887D 00	-1.027D 01
300.	-1.511D 01	-9.656D 00	-5.716D 00	-5.079D 00	-9.325D 00
10000.	-1.687D 01	-1.074D 01	-6.459D 00	-3.628D 00	-8.626D 00
		LAMBDA 3:	204.75 ANGSTROMS		
PE					
3.	-1.221D 01	-7.028D 00	-3.860D 00	-1.276D 00	-8.261D 00
30.	-1.295D 01	-7.568D 00	-3.890D 00	-2.301D 00	-7.110D 00
300.	-1.364D 01	-8.187D 00	-4.179D 00	-3.493D 00	-6.165D 00
10000.	-1.540D 01	-9.267D 00	-4.922D 00	-2.042D 00	-5.466D 00
		LAMBDA 4:	261.34 ANGSTROMS		
PE					
3.	-8.387D 00	-3.531D 00	-5.811D-01	2.076D 00	3.739D 00
30.	-9.128D 00	-4.071D 00	-6.105D-01	1.051D 00	4.890D 00
300.	-9.813D 00	-4.690D 00	-9.004D-01	-1.406D-01	5.835D 00
10000.	-1.157D 01	-5.770D 00	-1.643D 00	1.310D 00	6.534D 00
		LAMBDA 5:	261.36 ANGSTROMS		
PE					
3.	-5.037D 00	-3.303D 00	-2.126D 00	3.016D-01	-1.372D 01
30.	-5.184D 00	-3.543D 00	-3.126D 00	4.052D-02	-1.257D 01
300.	-5.113D 00	-3.862D 00	-4.130D 00	-1.514D-01	-1.162D 01
10000.	-5.287D 00	-4.456D 00	-2.871D 00	-1.292D 00	-1.092D 01
		LAMBDA 6:	289.34 ANGSTROMS		
PE					
3.	-3.926D 00	-2.030D 00	-7.604D-01	1.718D 00	-1.229D 01
30.	-4.073D 00	-2.270D 00	-1.750D 00	1.457D 00	-1.114D 01
300.	-4.002D 00	-2.589D 00	-2.764D 00	1.265D 00	-1.019D 01
10000.	-4.176D 00	-3.183D 00	-1.505D 00	1.236D-01	-9.493D 00
		LAMBDA 7:	349.97 ANGSTROMS		
PE					
3.	-2.455D 00	-5.606D-01	7.766D-01	3.304D 00	-9.127D 00
30.	-2.602D 00	-8.009D-01	-2.227D-01	3.043D 00	-7.976D 00
300.	-2.531D 00	-1.120D 00	-1.227D 00	2.851D 00	-7.031D 00
10000.	-2.705D 00	-1.714D 00	3.159D-02	1.710D 00	-6.333D 00

TABLE C.4-1
LOG OF THE BLANKETING OPACITY

T	6000.	8000.	11000.	17500.	50000.
		LAMBDA 8:	402.03 ANGSTROMS		
PE					
3.	1.369D 00	2.936D 00	4.056D 00	6.656D 00	2.873D 00
30.	1.222D 00	2.696D 00	3.056D 00	6.395D 00	4.024D 00
300.	1.293D 00	2.377D 00	2.052D 00	6.203D 00	4.969D 00
10000.	1.119D 00	1.783D 00	3.311D 00	5.062D 00	5.657D 00
		LAMBDA 9:	402.05 ANGSTROMS		
PE					
3.	-2.227D 00	6.642D-01	8.703D-01	1.773D-01	-1.576D 01
30.	-3.227D 00	2.539D-03	8.649D-01	4.841D-01	-1.476D 01
300.	-4.251D 00	-9.430D-01	8.156D-01	5.309D-01	-1.376D 01
10000.	-5.287D 00	-2.515D 00	1.313D-01	5.332D-01	-1.233D 01
		LAMBDA 10:	425.91 ANGSTROMS		
PE					
3.	-1.116D 00	1.937D 00	2.236D 00	1.593D 00	-1.433D 01
30.	-2.116D 00	1.276D 00	2.231D 00	1.900D 00	-1.333D 01
300.	-3.140D 00	3.300D-01	2.182D 00	1.947D 00	-1.233D 01
10000.	-4.176D 00	-1.242D 00	1.497D 00	1.949D 00	-1.090D 01
		LAMBDA 11:	471.15 ANGSTROMS		
PE					
3.	3.554D-01	3.406D 00	3.773D 00	3.179D 00	-1.117D 01
30.	-6.449D-01	2.745D 00	3.758D 00	3.486D 00	-1.017D 01
300.	-1.669D 00	1.799D 00	3.719D 00	3.533D 00	-9.174D 00
10000.	-2.705D 00	2.267D-01	3.034D 00	3.535D 00	-7.737D 00
		LAMBDA 12:	504.26 ANGSTROMS		
PE					
3.	4.179D 00	6.903D 00	7.052D 00	6.531D 00	8.296D-01
30.	3.179D 00	6.242D 00	7.047D 00	6.838D 00	1.829D 00
300.	2.155D 00	5.296D 00	6.998D 00	6.885D 00	2.826D 00
10000.	1.119D 00	3.724D 00	6.313D 00	6.887D 00	4.263D 00
		LAMBDA 13:	504.28 ANGSTROMS		
PE					
3.	-2.543D 00	3.433D-01	5.448D-01	2.353D-01	-1.256D 01
30.	-3.544D 00	-3.184D-01	5.394D-01	1.523D-01	-1.141D 01
300.	-4.576D 00	-1.264D 00	4.901D-01	1.991D-01	-1.046D 01
10000.	-5.287D 00	-2.854D 00	-1.943D-01	2.014D-01	-9.763D 00
		LAMBDA 14:	529.82 ANGSTROMS		
PE					
3.	-1.432D 00	1.615D 00	1.911D 00	1.651D 00	-1.113D 01
30.	-2.433D 00	9.546D-01	1.905D 00	1.568D 00	-9.977D 00
300.	-3.465D 00	9.057D-03	1.856D 00	1.615D 00	-9.031D 00
10000.	-4.176D 00	-1.581D 00	1.172D 00	1.617D 00	-8.333D 00

TABLE C.4-1
LOG OF THE BLANKETING OPACITY

LAMBDA 15: 577.11 ANGSTROMS

PE \ T	6000.	8000.	11000.	17500.	50000.
3.	3.892D-02	3.085D 00	3.448D 00	3.237D 00	-7.968D 00
30.	-9.617D-01	2.424D 00	3.442D 00	3.154D 00	-6.817D 00
300.	-1.994D 00	1.478D 00	3.393D 00	3.201D 00	-5.871D 00
10000.	-2.705D 00	-1.118D-01	2.709D 00	3.203D 00	-5.173D 00

LAMBDA 16: 610.81 ANGSTROMS

PE \ T	6000.	8000.	11000.	17500.	50000.
3.	3.863D 00	6.582D 00	6.727D 00	6.589D 00	4.032D 00
30.	2.862D 00	5.921D 00	6.721D 00	6.506D 00	5.183D 00
300.	1.830D 00	4.975D 00	6.672D 00	6.553D 00	6.129D 00
10000.	1.119D 00	3.385D 00	5.988D 00	6.555D 00	6.827D 00

LAMBDA 17: 610.83 ANGSTROMS

PE \ T	6000.	8000.	11000.	17500.	50000.
3.	-4.017D-01	6.309D-01	6.375D-01	3.633D-01	-1.351D 01
30.	-1.353D 00	5.732D-01	6.382D-01	-1.046D-01	-1.236D 01
300.	-2.396D 00	2.239D-01	6.344D-01	-4.228D-02	-1.141D 01
10000.	-5.287D 00	-1.203D 00	5.245D-01	3.396D-01	-1.071D 01

LAMBDA 18: 634.69 ANGSTROMS

PE \ T	6000.	8000.	11000.	17500.	50000.
3.	7.093D-01	1.904D 00	2.003D 00	1.779D 00	-1.208D 01
30.	-2.421D-01	1.846D 00	2.004D 00	1.311D 00	-1.093D 01
300.	-1.285D 00	1.497D 00	2.000D 00	1.374D 00	-9.982D 00
10000.	-4.176D 00	6.979D-02	1.890D 00	1.756D 00	-9.284D 00

LAMBDA 19: 677.51 ANGSTROMS

PE \ T	6000.	8000.	11000.	17500.	50000.
3.	2.180D 00	3.373D 00	3.540D 00	3.365D 00	-8.918D 00
30.	1.229D 00	3.315D 00	3.541D 00	2.897D 00	-7.768D 00
300.	1.859D-01	2.966D 00	3.537D 00	2.960D 00	-6.822D 00
10000.	-2.705D 00	1.539D 00	3.427D 00	3.342D 00	-6.124D 00

LAMBDA 20: 706.99 ANGSTROMS

PE \ T	6000.	8000.	11000.	17500.	50000.
3.	6.004D 00	6.870D 00	6.819D 00	6.717D 00	3.082D 00
30.	5.053D 00	6.812D 00	6.820D 00	6.249D 00	4.232D 00
300.	4.010D 00	6.463D 00	6.816D 00	6.312D 00	5.178D 00
10000.	1.119D 00	5.036D 00	6.706D 00	6.694D 00	5.876D 00

LAMBDA 21: 707.01 ANGSTROMS

PE \ T	6000.	8000.	11000.	17500.	50000.
3.	-4.473D 00	-8.855D-01	-1.120D-01	-2.408D-01	-1.280D 01
30.	-5.474D 00	-1.548D 00	-1.174D-01	6.602D-02	-1.155D 01
300.	-4.355D 00	-2.494D 00	-1.668D-01	1.128D-01	-1.070D 01
10000.	-2.319D 00	-3.794D 00	-8.511D-01	1.151D-01	-1.000D 01

TABLE C.4-1
LOG OF THE BLANKETING OPACITY

T	6000.	8000.	11000.	17500.	50000.
		LAMBDA 22:	732.99 ANGSTROMS		
PE					
3.	-3.362D 00	3.864D-01	1.254D 00	1.175D 00	-1.137D 01
30.	-4.363D 00	-2.753D-01	1.249D 00	1.482D 00	-1.022D 01
300.	-3.244D 00	-1.221D 00	1.199D 00	1.529D 00	-9.271D 00
10000.	-1.208D 00	-2.521D 00	5.149D-01	1.531D 00	-8.572D 00
		LAMBDA 23:	779.33 ANGSTROMS		
PE					
3.	-1.891D 00	1.855D 00	2.791D 00	2.761D 00	-8.207D 00
30.	-2.892D 00	1.194D 00	2.786D 00	3.068D 00	-7.056D 00
300.	-1.773D 00	2.481D-01	2.736D 00	3.115D 00	-6.111D 00
10000.	2.632D-01	-1.052D 00	2.052D 00	3.117D 00	-5.412D 00
		LAMBDA 24:	811.02 ANGSTROMS		
PE					
3.	1.933D 00	5.352D 00	6.070D 00	6.113D 00	3.793D 00
30.	9.325D-01	4.691D 00	6.055D 00	6.420D 00	4.944D 00
300.	2.051D 00	3.745D 00	6.015D 00	6.467D 00	5.889D 00
10000.	4.087D 00	2.445D 00	5.331D 00	6.469D 00	6.588D 00
		LAMBDA 25:	811.04 ANGSTROMS		
PE					
3.	1.889D-01	1.090D 00	1.294D 00	5.979D-01	-1.816D 01
30.	1.859D-01	9.797D-01	1.288D 00	9.047D-01	-1.601D 01
300.	7.774D-02	6.303D-01	1.239D 00	9.515D-01	-1.407D 01
10000.	-1.687D 00	7.293D-02	9.325D-01	9.537D-01	-1.185D 01
		LAMBDA 26:	836.58 ANGSTROMS		
PE					
3.	1.300D 00	2.363D 00	2.660D 00	2.014D 00	-1.673D 01
30.	1.297D 00	2.253D 00	2.654D 00	2.321D 00	-1.458D 01
300.	1.139D 00	1.903D 00	2.605D 00	2.367D 00	-1.264D 01
10000.	-5.765D-01	1.346D 00	2.299D 00	2.370D 00	-1.042D 01
		LAMBDA 27:	881.50 ANGSTROMS		
PE					
3.	2.771D 00	3.832D 00	4.197D 00	3.600D 00	-1.357D 01
30.	2.768D 00	3.722D 00	4.191D 00	3.907D 00	-1.142D 01
300.	2.660D 00	3.372D 00	4.142D 00	3.953D 00	-9.477D 00
10000.	8.945D-01	2.815D 00	3.836D 00	3.956D 00	-7.256D 00
		LAMBDA 28:	911.75 ANGSTROMS		
PE					
3.	6.595D 00	7.329D 00	7.476D 00	6.952D 00	-1.573D 00
30.	6.592D 00	7.219D 00	7.470D 00	7.259D 00	5.773D-01
300.	6.484D 00	6.869D 00	7.421D 00	7.305D 00	2.523D 00
10000.	4.719D 00	6.312D 00	7.115D 00	7.308D 00	4.744D 00

TABLE C.4-1
LOG OF THE BLANKETING OPACITY

T	6000.	8000.	11000.	17500.	50000.
			LAMBDA 29: 911.77 ANGSTROMS		
PE					
3.	6.080D-01	1.351D-01	1.817D-01	9.608D-01	-1.500D 01
30.	6.542D-01	4.735D-01	1.781D-01	9.357D-01	-1.332D 01
300.	5.415D-01	5.562D-01	1.461D-01	7.438D-01	-1.213D 01
10000.	-1.247D 00	5.117D-01	4.353D-01	-1.154D-01	-1.098D 01
			LAMBDA 30: 939.12 ANGSTROMS		
PE					
3.	1.719D 00	1.408D 00	1.548D 00	2.377D 00	-1.357D 01
30.	1.765D 00	1.746D 00	1.544D 00	2.352D 00	-1.189D 01
300.	1.652D 00	1.829D 00	1.512D 00	2.160D 00	-1.070D 01
10000.	-1.362D-01	1.785D 00	1.801D 00	1.301D 00	-9.551D 00
			LAMBDA 31: 987.01 ANGSTROMS		
PE					
3.	3.190D 00	2.877D 00	3.085D 00	3.963D 00	-1.041D 01
30.	3.236D 00	3.215D 00	3.081D 00	3.938D 00	-8.729D 00
300.	3.123D 00	3.298D 00	3.049D 00	3.746D 00	-7.542D 00
10000.	1.335D 00	3.254D 00	3.338D 00	2.887D 00	-6.391D 00
			LAMBDA 32: 1019.13 ANGSTROMS		
PE					
3.	7.014D 00	6.374D 00	6.354D 00	7.315D 00	1.594D 00
30.	7.060D 00	6.712D 00	6.360D 00	7.290D 00	3.271D 00
300.	6.947D 00	6.795D 00	6.328D 00	7.098D 00	4.458D 00
10000.	5.159D 00	6.751D 00	6.617D 00	6.239D 00	5.609D 00
			LAMBDA 33: 1019.15 ANGSTROMS		
PE					
3.	-3.006D-01	1.915D-01	1.953D-01	-1.371D 00	-2.564D 01
30.	-3.042D-01	1.338D-01	1.961D-01	-5.597D-01	-2.493D 01
300.	-4.294D-01	-1.927D-01	1.922D-01	-2.153D-01	-2.174D 01
10000.	-2.250D 00	-4.497D-01	8.224D-02	-1.061D-01	-1.755D 01
			LAMBDA 34: 1047.52 ANGSTROMS		
PE					
3.	8.104D-01	1.465D 00	1.561D 00	4.474D-02	-2.421D 01
30.	8.068D-01	1.407D 00	1.562D 00	8.563D-01	-2.350D 01
300.	6.816D-01	1.080D 00	1.558D 00	1.201D 00	-2.031D 01
10000.	-1.139D 00	8.233D-01	1.448D 00	1.310D 00	-1.612D 01
			LAMBDA 35: 1096.93 ANGSTROMS		
PE					
3.	2.281D 00	2.934D 00	3.098D 00	1.631D 00	-2.105D 01
30.	2.278D 00	2.876D 00	3.099D 00	2.442D 00	-2.034D 01
300.	2.153D 00	2.549D 00	3.095D 00	2.787D 00	-1.715D 01
10000.	3.317D-01	2.292D 00	2.985D 00	2.896D 00	-1.296D 01

TABLE C.4-1
LOG OF THE BLANKETING OPACITY

T	6000.	8000.	11000.	17500.	50000.

LAMBDA 36: 1129.87 ANGSTROMS

PE					
3.	6.105D 00	6.431D 00	6.377D 00	4.983D 00	-9.054D 00
30.	6.102D 00	6.373D 00	6.378D 00	5.794D 00	-8.342D 00
300.	5.977D 00	6.046D 00	6.374D 00	6.139D 00	-5.155D 00
10000.	4.156D 00	5.789D 00	6.264D 00	6.248D 00	-9.583D-01

LAMBDA 37: 1129.89 ANGSTROMS

PE					
3.	3.901D-01	2.807D-02	-2.642D 00	-1.890D-01	-2.027D 01
30.	3.863D-01	4.114D-01	-1.646D 00	-2.141D-01	-1.827D 01
300.	2.584D-01	4.779D-01	-6.779D-01	-4.060D-01	-1.627D 01
10000.	-1.448D 00	2.180D-01	3.028D-01	-1.547D 00	-1.331D 01

LAMBDA 38: 1152.36 ANGSTROMS

PE					
3.	1.501D 00	1.301D 00	-1.276D 00	1.227D 00	-1.884D 01
30.	1.497D 00	1.684D 00	-2.798D-01	1.202D 00	-1.684D 01
300.	1.369D 00	1.751D 00	6.881D-01	1.010D 00	-1.484D 01
10000.	-3.373D-01	1.491D 00	1.659D 00	-1.309D-01	-1.188D 01

LAMBDA 39: 1190.68 ANGSTROMS

PE					
3.	2.972D 00	2.770D 00	2.607D-01	2.813D 00	-1.568D 01
30.	2.968D 00	3.153D 00	1.257D 00	2.788D 00	-1.368D 01
300.	2.840D 00	3.220D 00	2.225D 00	2.596D 00	-1.168D 01
10000.	1.134D 00	2.960D 00	3.206D 00	1.455D 00	-8.719D 00

LAMBDA 40: 1215.66 ANGSTROMS

PE					
3.	6.796D 00	6.267D 00	3.540D 00	6.165D 00	-3.675D 00
30.	6.792D 00	6.650D 00	4.536D 00	6.140D 00	-1.676D 00
300.	6.664D 00	6.717D 00	5.504D 00	5.948D 00	3.214D-01
10000.	4.958D 00	6.457D 00	6.485D 00	4.807D 00	3.281D 00

LAMBDA 41: 1215.68 ANGSTROMS

PE					
3.	3.018D-01	1.732D-02	-2.466D 00	-3.031D 00	-2.195D 01
30.	2.971D-01	3.557D-01	-1.472D 00	-3.056D 00	-1.995D 01
300.	1.421D-01	4.098D-01	-5.209D-01	-3.248D 00	-1.795D 01
10000.	-1.731D 00	9.748D-02	3.171D-01	-2.108D 00	-1.499D 01

LAMBDA 42: 1239.60 ANGSTROMS

PE					
3.	1.413D 00	1.290D 00	-1.100D 00	-1.615D 00	-2.052D 01
30.	1.408D 00	1.629D 00	-1.056D-01	-1.640D 00	-1.852D 01
300.	1.253D 00	1.683D 00	8.451D-01	-1.832D 00	-1.652D 01
10000.	-6.204D-01	1.370D 00	1.683D 00	-6.924D-01	-1.356D 01

TABLE C.4-1
LOG OF THE BLANKETING OPACITY

T	6000.	8000.	11000.	17500.	50000.
			LAMBDA 43: 1280.37 ANGSTROMS		
PE					
3.	2.884D 00	2.759D 00	4.358D-01	-2.860D-02	-1.736D 01
30.	2.879D 00	3.098D 00	1.431D 00	-5.363D-02	-1.536D 01
300.	2.724D 00	3.152D 00	2.382D 00	-2.455D-01	-1.336D 01
10000.	8.506D-01	2.839D 00	3.220D 00	8.936D-01	-1.040D 01
			LAMBDA 44: 1306.94 ANGSTROMS		
PE					
3.	6.708D 00	6.256D 00	3.716D 00	3.323D 00	-5.361D 00
30.	6.703D 00	6.595D 00	4.710D 00	3.298D 00	-3.361D 00
300.	6.548D 00	6.649D 00	5.661D 00	3.106D 00	-1.364D 00
10000.	4.675D 00	6.336D 00	6.499D 00	4.246D 00	1.596D 00
			LAMBDA 45: 1306.96 ANGSTROMS		
PE					
3.	-8.331D-02	9.416D-01	9.456D-01	-1.518D 00	-2.860D 01
30.	-3.925D-02	8.839D-01	9.474D-01	-5.432D-01	-2.551D 01
300.	-1.985D-01	5.345D-01	9.435D-01	2.649D-01	-2.252D 01
10000.	-1.961D 00	-2.673D-01	8.335D-01	6.468D-01	-1.803D 01
			LAMBDA 46: 1339.76 ANGSTROMS		
PE					
3.	1.027D 00	2.215D 00	2.313D 00	-1.022D-01	-2.717D 01
30.	1.072D 00	2.157D 00	2.313D 00	8.728D-01	-2.408D 01
300.	9.125D-01	1.807D 00	2.310D 00	1.681D 00	-2.109D 01
10000.	-8.505D-01	1.006D 00	2.199D 00	2.063D 00	-1.660D 01
			LAMBDA 47: 1396.48 ANGSTROMS		
PE					
3.	2.498D 00	3.684D 00	3.850D 00	1.484D 00	-2.401D 01
30.	2.543D 00	3.626D 00	3.850D 00	2.459D 00	-2.092D 01
300.	2.383D 00	3.276D 00	3.847D 00	3.267D 00	-1.793D 01
10000.	6.205D-01	2.475D 00	3.736D 00	3.649D 00	-1.344D 01
			LAMBDA 48: 1433.99 ANGSTROMS		
PE					
3.	6.322D 00	7.181D 00	7.129D 00	4.836D 00	-1.201D 01
30.	6.367D 00	7.123D 00	7.129D 00	5.811D 00	-8.924D 00
300.	6.207D 00	6.773D 00	7.126D 00	6.619D 00	-5.927D 00
10000.	4.445D 00	5.972D 00	7.015D 00	7.001D 00	-1.444D 00
			LAMBDA 49: 1434.01 ANGSTROMS		
PE					
3.	-9.634D-01	-1.472D 00	-3.735D 00	-7.821D 00	-2.860D 01
30.	-9.200D-01	-1.089D 00	-2.739D 00	-6.010D 00	-2.563D 01
300.	-1.109D 00	-7.526D-01	-1.771D 00	-4.665D 00	-2.280D 01
10000.	-3.206D 00	-9.351D-01	-7.904D-01	-3.084D 00	-1.910D 01

TABLE C.4-1
LOG OF THE BLANKETING OPACITY

T	6000.	8000.	11000.	17500.	50000.
			LAMBDA 50: 1457.06 ANGSTROMS		
PE					
3.	1.476D-01	-1.995D-01	-2.359D 00	-6.405D 00	-2.717D 01
30.	1.910D-01	1.838D-01	-1.373D 00	-4.594D 00	-2.420D 01
300.	2.038D-03	5.204D-01	-4.048D-01	-3.249D 00	-2.137D 01
10000.	-2.095D 00	3.379D-01	5.756D-01	-1.668D 00	-1.757D 01
			LAMBDA 51: 1495.96 ANGSTROMS		
PE					
3.	1.619D 00	1.270D 00	-8.322D-01	-4.819D 00	-2.401D 01
30.	1.662D 00	1.653D 00	1.643D-01	-3.008D 00	-2.104D 01
300.	1.473D 00	1.989D 00	1.132D 00	-1.663D 00	-1.821D 01
10000.	-6.241D-01	1.807D 00	2.113D 00	-8.240D-02	-1.451D 01
			LAMBDA 52: 1521.06 ANGSTROMS		
PE					
3.	5.443D 00	4.767D 00	2.447D 00	-1.467D 00	-1.201D 01
30.	5.486D 00	5.150D 00	3.443D 00	3.444D-01	-9.037D 00
300.	5.297D 00	5.486D 00	4.411D 00	1.689D 00	-6.211D 00
10000.	3.200D 00	5.304D 00	5.392D 00	3.270D 00	-2.513D 00
			LAMBDA 53: 1521.08 ANGSTROMS		
PE					
3.	3.636D-01	-1.283D 00	-3.559D 00	-2.793D 00	-1.399D 01
30.	4.073D-01	-3.406D-01	-2.558D 00	-3.818D 00	-1.299D 01
300.	2.235D-01	3.098D-01	-1.562D 00	-4.662D 00	-1.199D 01
10000.	-1.612D 00	1.372D-01	-1.498D-01	-2.758D 00	-1.055D 01
			LAMBDA 54: 1548.18 ANGSTROMS		
PE					
3.	1.475D 00	-9.857D-03	-2.193D 00	-1.377D 00	-1.256D 01
30.	1.518D 00	9.324D-01	-1.192D 00	-2.402D 00	-1.156D 01
300.	1.335D 00	1.583D 00	-1.962D-01	-3.246D 00	-1.056D 01
10000.	-5.012D-01	1.410D 00	1.216D 00	-1.342D 00	-9.122D 00
			LAMBDA 55: 1594.13 ANGSTROMS		
PE					
3.	2.946D 00	1.459D 00	-6.561D-01	2.086D-01	-9.395D 00
30.	2.989D 00	2.401D 00	3.446D-01	-8.164D-01	-8.396D 00
300.	2.806D 00	3.052D 00	1.341D 00	-1.660D 00	-7.399D 00
10000.	9.698D-01	2.879D 00	2.753D 00	2.444D-01	-5.962D 00
			LAMBDA 56: 1623.92 ANGSTROMS		
PE					
3.	6.770D 00	4.956D 00	2.623D 00	3.561D 00	2.605D 00
30.	6.813D 00	5.898D 00	3.624D 00	2.536D 00	3.604D 00
300.	6.630D 00	6.549D 00	4.620D 00	1.692D 00	4.601D 00
10000.	4.794D 00	6.376D 00	6.032D 00	3.596D 00	6.038D 00

TABLE C.4-1
LOG OF THE BLANKETING OPACITY

T	6000.	8000.	11000.	17500.	50000.
LAMBDA 57: 1623.94 ANGSTROMS					
PE					
3.	6.562D-01	-9.899D-01	-3.266D 00	-5.516D 00	-1.575D 01
30.	6.995D-01	-4.764D-02	-2.265D 00	-5.705D 00	-1.407D 01
300.	5.073D-01	6.027D-01	-1.269D 00	-4.369D 00	-1.288D 01
10000.	-1.316D 00	4.174D-01	1.434D-01	-2.464D 00	-1.173D 01
LAMBDA 58: 1656.92 ANGSTROMS					
PE					
3.	1.767D 00	2.831D-01	-1.900D 00	-4.100D 00	-1.432D 01
30.	1.810D 00	1.225D 00	-8.991D-01	-4.289D 00	-1.264D 01
300.	1.618D 00	1.876D 00	9.710D-02	-2.953D 00	-1.145D 01
10000.	-2.053D-01	1.690D 00	1.509D 00	-1.048D 00	-1.030D 01
LAMBDA 59: 1713.23 ANGSTROMS					
PE					
3.	3.238D 00	1.752D 00	-3.628D-01	-2.514D 00	-1.116D 01
30.	3.281D 00	2.694D 00	6.379D-01	-2.703D 00	-9.482D 00
300.	3.089D 00	3.345D 00	1.634D 00	-1.367D 00	-8.295D 00
10000.	1.266D 00	3.159D 00	3.046D 00	5.382D-01	-7.144D 00
LAMBDA 60: 1749.98 ANGSTROMS					
PE					
3.	7.062D 00	5.249D 00	2.916D 00	8.379D-01	8.411D-01
30.	7.105D 00	6.191D 00	3.917D 00	6.495D-01	2.518D 00
300.	6.913D 00	6.842D 00	4.913D 00	1.985D 00	3.705D 00
10000.	5.090D 00	6.656D 00	6.325D 00	3.890D 00	4.856D 00
LAMBDA 61: 1750.00 ANGSTROMS					
PE					
3.	-2.668D 00	-3.752D 00	-5.568D 00	-5.038D 00	-2.221D 01
30.	-2.618D 00	-2.810D 00	-4.557D 00	-5.227D 00	-1.953D 01
300.	-2.613D 00	-2.159D 00	-3.571D 00	-5.882D 00	-1.735D 01
10000.	-2.612D 00	-1.956D 00	-2.158D 00	-4.310D 00	-1.467D 01
LAMBDA 62: 1776.54 ANGSTROMS					
PE					
3.	-1.557D 00	-2.479D 00	-4.202D 00	-3.622D 00	-2.078D 01
30.	-1.507D 00	-1.537D 00	-3.201D 00	-3.811D 00	-1.810D 01
300.	-1.502D 00	-8.859D-01	-2.205D 00	-4.466D 00	-1.592D 01
10000.	-1.501D 00	-6.826D-01	-7.916D-01	-2.894D 00	-1.324D 01
LAMBDA 63: 1821.23 ANGSTROMS					
PE					
3.	-8.637D-02	-1.010D 00	-2.665D 00	-2.036D 00	-1.762D 01
30.	-3.634D-02	-6.773D-02	-1.664D 00	-2.225D 00	-1.494D 01
300.	-3.100D-02	5.831D-01	-6.678D-01	-2.880D 00	-1.276D 01
10000.	-3.042D-02	7.864D-01	7.454D-01	-1.308D 00	-1.008D 01

TABLE C.4-1
LOG OF THE BLANKETING OPACITY

T	6000.	8000.	11000.	17500.	50000.
		LAMBDA 64: 1849.99 ANGSTROMS			
PE					
3.	3.738D 00	2.437D 00	6.143D-01	1.316D 00	-5.622D 00
30.	3.788D 00	3.429D 00	1.615D 00	1.127D 00	-2.945D 00
300.	3.793D 00	4.080D 00	2.611D 00	4.717D-01	-7.575D-01
10000.	3.794D 00	4.283D 00	4.024D 00	2.044D 00	1.916D 00
		LAMBDA 65: 1850.01 ANGSTROMS			
PE					
3.	-9.012D-01	-2.233D 00	-4.343D 00	-7.707D 00	-2.284D 01
30.	-8.511D-01	-1.341D 00	-3.342D 00	-6.896D 00	-2.016D 01
300.	-8.458D-01	-6.902D-01	-2.346D 00	-5.232D 00	-1.797D 01
10000.	-8.452D-01	-4.868D-01	-9.331D-01	-3.327D 00	-1.530D 01
		LAMBDA 66: 1874.85 ANGSTROMS			
PE					
3.	2.098D-01	-1.010D 00	-2.977D 00	-6.291D 00	-2.141D 01
30.	2.599D-01	-6.798D-02	-1.976D 00	-5.480D 00	-1.873D 01
300.	2.652D-01	5.828D-01	-9.802D-01	-3.816D 00	-1.654D 01
10000.	2.658D-01	7.862D-01	4.329D-01	-1.911D 00	-1.387D 01
		LAMBDA 67: 1916.49 ANGSTROMS			
PE					
3.	1.681D 00	4.587D-01	-1.440D 00	-4.705D 00	-1.825D 01
30.	1.731D 00	1.401D 00	-4.394D-01	-3.894D 00	-1.557D 01
300.	1.736D 00	2.052D 00	5.558D-01	-2.230D 00	-1.338D 01
10000.	1.737D 00	2.255D 00	1.970D 00	-3.254D-01	-1.071D 01
		LAMBDA 68: 1943.16 ANGSTROMS			
PE					
3.	5.505D 00	3.956D 00	1.839D 00	-1.353D 00	-6.247D 00
30.	5.555D 00	4.898D 00	2.840D 00	-5.416D-01	-3.570D 00
300.	5.560D 00	5.549D 00	3.836D 00	1.122D 00	-1.383D 00
10000.	5.561D 00	5.752D 00	5.249D 00	3.027D 00	1.291D 00
		LAMBDA 69: 1943.18 ANGSTROMS			
PE					
3.	-2.704D 00	-2.531D 00	-3.467D 00	-7.321D 00	-2.843D 01
30.	-2.888D 00	-2.531D 00	-2.761D 00	-6.211D 00	-2.566D 01
300.	-3.537D 00	-2.543D 00	-2.533D 00	-5.200D 00	-2.292D 01
10000.	-3.061D 00	-2.848D 00	-2.504D 00	-3.719D 00	-1.938D 01
		LAMBDA 70: 1971.95 ANGSTROMS			
PE					
3.	-1.593D 00	-1.258D 00	-2.101D 00	-5.905D 00	-2.700D 01
30.	-1.777D 00	-1.258D 00	-1.395D 00	-4.795D 00	-2.423D 01
300.	-2.426D 00	-1.270D 00	-1.157D 00	-3.784D 00	-2.149D 01
10000.	-1.950D 00	-1.575D 00	-1.138D 00	-2.303D 00	-1.795D 01

TABLE C.4-1
LOG OF THE BLANKETING OPACITY

T	6000.	8000.	11000.	17500.	50000.
	LAMBDA 71: 2020.34 ANGSTROMS				
PE					
3.	-1.218D-01	2.111D-01	-5.643D-01	-4.319D 00	-2.384D 01
30.	-3.062D-01	2.111D-01	1.422D-01	-3.209D 00	-2.107D 01
300.	-9.555D-01	1.987D-01	3.703D-01	-2.198D 00	-1.833D 01
10000.	-4.786D-01	-1.057D-01	3.939D-01	-7.175D-01	-1.479D 01
	LAMBDA 72: 2051.46 ANGSTROMS				
PE					
3.	3.702D 00	3.708D 00	2.715D 00	-9.673D-01	-1.184D 01
30.	3.518D 00	3.708D 00	3.421D 00	1.428D-01	-9.067D 00
300.	2.869D 00	3.696D 00	3.649D 00	1.154D 00	-6.326D 00
10000.	3.345D 00	3.391D 00	3.678D 00	2.635D 00	-2.792D 00
	LAMBDA 73: 2051.48 ANGSTROMS				
PE					
3.	-2.246D 00	-2.064D 00	-2.988D 00	-6.822D 00	-2.354D 01
30.	-2.251D 00	-2.064D 00	-2.281D 00	-5.712D 00	-2.086D 01
300.	-1.641D 00	-2.076D 00	-2.053D 00	-4.700D 00	-1.867D 01
10000.	-1.467D 00	-1.605D 00	-2.025D 00	-3.220D 00	-1.600D 01
	LAMBDA 74: 2073.76 ANGSTROMS				
PE					
3.	-1.135D 00	-7.907D-01	-1.622D 00	-5.406D 00	-2.211D 01
30.	-1.140D 00	-7.907D-01	-9.154D-01	-4.296D 00	-1.943D 01
300.	-5.305D-01	-8.031D-01	-6.873D-01	-3.284D 00	-1.724D 01
10000.	-3.560D-01	-3.317D-01	-6.587D-01	-1.804D 00	-1.457D 01
	LAMBDA 75: 2110.85 ANGSTROMS				
PE					
3.	3.357D-01	6.783D-01	-8.485D-02	-3.820D 00	-1.895D 01
30.	3.314D-01	6.783D-01	6.216D-01	-2.710D 00	-1.627D 01
300.	9.405D-01	6.659D-01	8.497D-01	-1.698D 00	-1.408D 01
10000.	1.115D 00	1.137D 00	8.783D-01	-2.179D-01	-1.141D 01
	LAMBDA 76: 2134.45 ANGSTROMS				
PE					
3.	4.160D 00	4.175D 00	3.194D 00	-4.677D-01	-6.948D 00
30.	4.155D 00	4.175D 00	3.901D 00	6.423D-01	-4.271D 00
300.	4.765D 00	4.163D 00	4.129D 00	1.654D 00	-2.084D 00
10000.	4.939D 00	4.634D 00	4.157D 00	3.134D 00	5.895D-01
	LAMBDA 77: 2134.47 ANGSTROMS				
PE					
3.	-3.398D 00	-3.221D 00	-4.334D 00	-6.627D 00	-2.383D 01
30.	-2.467D 00	-3.210D 00	-3.676D 00	-5.652D 00	-2.115D 01
300.	-1.858D 00	-3.212D 00	-3.289D 00	-4.844D 00	-1.896D 01
10000.	-1.549D 00	-1.980D 00	-3.100D 00	-4.462D 00	-1.629D 01

TABLE C.4-1
LOG OF THE BLANKETING OPACITY

T	6000.	8000.	11000.	17500.	50000.
	LAMBDA 78: 2165.20 ANGSTROMS				
PE					
3.	-2.287D 00	-1.948D 00	-2.968D 00	-5.211D 00	-2.240D 01
30.	-1.356D 00	-1.937D 00	-2.310D 00	-4.236D 00	-1.972D 01
300.	-7.465D-01	-1.939D 00	-1.923D 00	-3.428D 00	-1.753D 01
10000.	-4.376D-01	-7.070D-01	-1.734D 00	-3.046D 00	-1.486D 01
	LAMBDA 79: 2216.83 ANGSTROMS				
PE					
3.	-8.161D-01	-4.793D-01	-1.431D 00	-3.625D 00	-1.924D 01
30.	1.154D-01	-4.678D-01	-7.733D-01	-2.650D 00	-1.656D 01
300.	7.245D-01	-4.703D-01	-3.858D-01	-1.842D 00	-1.437D 01
10000.	1.033D 00	7.620D-01	-1.974D-01	-1.460D 00	-1.170D 01
	LAMBDA 80: 2249.99 ANGSTROMS				
PE					
3.	3.008D 00	3.018D 00	1.848D 00	-2.734D-01	-7.236D 00
30.	3.939D 00	3.029D 00	2.506D 00	7.015D-01	-4.559D 00
300.	4.548D 00	3.027D 00	2.893D 00	1.510D 00	-2.372D 00
10000.	4.857D 00	4.259D 00	3.082D 00	1.892D 00	3.017D-01
	LAMBDA 81: 2250.01 ANGSTROMS				
PE					
3.	-1.271D 00	-1.219D 00	-2.947D 00	-2.052D 00	-2.097D 01
30.	-1.290D 00	-1.208D 00	-2.035D 00	-2.077D 00	-1.897D 01
300.	-1.435D 00	-1.219D 00	-1.470D 00	-2.269D 00	-1.697D 01
10000.	-2.150D 00	-1.332D 00	-1.324D 00	-3.094D 00	-1.401D 01
	LAMBDA 82: 2275.74 ANGSTROMS				
PE					
3.	-1.601D-01	5.409D-02	-1.581D 00	-6.361D-01	-1.954D 01
30.	-1.794D-01	6.489D-02	-6.689D-01	-6.611D-01	-1.754D 01
300.	-3.238D-01	5.367D-02	-1.035D-01	-8.530D-01	-1.554D 01
10000.	-1.039D 00	-5.902D-02	4.153D-02	-1.678D 00	-1.258D 01
	LAMBDA 83: 2318.65 ANGSTROMS				
PE					
3.	1.311D 00	1.523D 00	-4.416D-02	9.499D-01	-1.638D 01
30.	1.292D 00	1.534D 00	8.681D-01	9.249D-01	-1.438D 01
300.	1.147D 00	1.523D 00	1.433D 00	7.330D-01	-1.238D 01
10000.	4.317D-01	1.410D 00	1.579D 00	-9.236D-02	-9.423D 00
	LAMBDA 84: 2345.99 ANGSTROMS				
PE					
3.	5.135D 00	5.020D 00	3.235D 00	4.302D 00	-4.380D 00
30.	5.116D 00	5.031D 00	4.147D 00	4.277D 00	-2.380D 00
300.	4.971D 00	5.020D 00	4.712D 00	4.085D 00	-3.830D-01
10000.	4.256D 00	4.907D 00	4.858D 00	3.260D 00	2.577D 00

TABLE C.4-1
LOG OF THE BLANKETING OPACITY

T	6000.	8000.	11000.	17500.	50000.
	LAMBDA 85: 2346.01 ANGSTROMS				
PE					
3.	-1.048D 00	-1.184D 00	-2.913D 00	-7.006D 00	-2.701D 01
30.	-9.804D-01	-1.096D 00	-1.987D 00	-5.528D 00	-2.301D 01
300.	-9.379D-01	-1.044D 00	-1.362D 00	-4.375D 00	-1.904D 01
10000.	-1.463D 00	-9.406D-01	-1.086D 00	-2.755D 00	-1.345D 01
	LAMBDA 86: 2365.74 ANGSTROMS				
PE					
3.	5.132D-01	4.953D-01	-1.217D 00	-5.139D 00	-2.512D 01
30.	5.786D-01	5.182D-01	-3.010D-01	-3.673D 00	-2.114D 01
300.	4.659D-01	5.447D-01	3.351D-01	-2.596D 00	-1.722D 01
10000.	-4.046D-01	5.095D-01	5.415D-01	-1.071D 00	-1.163D 01
	LAMBDA 87: 2398.37 ANGSTROMS				
PE					
3.	1.856D 00	1.854D 00	2.144D-01	-3.715D 00	-2.355D 01
30.	1.881D 00	1.859D 00	1.143D 00	-2.276D 00	-1.950D 01
300.	1.802D 00	1.864D 00	1.712D 00	-1.180D 00	-1.566D 01
10000.	9.484D-01	1.857D 00	1.865D 00	3.285D-01	-1.023D 01
	LAMBDA 88: 2418.99 ANGSTROMS				
PE					
3.	5.575D 00	5.471D 00	3.699D 00	-4.332D-01	-1.880D 01
30.	5.555D 00	5.482D 00	4.612D 00	1.102D 00	-1.606D 01
300.	5.411D 00	5.470D 00	5.177D 00	2.229D 00	-1.216D 01
10000.	4.568D 00	5.358D 00	5.322D 00	3.725D 00	-7.014D 00
	LAMBDA 89: 2419.01 ANGSTROMS				
PE					
3.	-1.592D 00	-1.891D 00	-3.634D 00	-7.792D 00	-2.745D 01
30.	-1.037D 00	-1.664D 00	-2.608D 00	-6.227D 00	-2.345D 01
300.	-7.333D-01	-1.363D 00	-1.816D 00	-4.945D 00	-1.947D 01
10000.	-1.199D 00	-6.277D-01	-1.237D 00	-3.132D 00	-1.375D 01
	LAMBDA 90: 2443.85 ANGSTROMS				
PE					
3.	-4.308D-01	-3.407D-01	-1.840D 00	-5.628D 00	-2.503D 01
30.	-2.556D-01	-2.158D-01	-8.756D-01	-4.100D 00	-2.103D 01
300.	-1.193D-01	-1.531D-02	-2.045D-01	-2.814D 00	-1.723D 01
10000.	-1.399D-01	1.270D-01	2.092D-01	-1.173D 00	-1.154D 01
	LAMBDA 91: 2485.14 ANGSTROMS				
PE					
3.	6.382D-01	8.534D-01	-4.741D-01	-4.086D 00	-2.354D 01
30.	9.314D-01	9.261D-01	4.482D-01	-2.566D 00	-1.961D 01
300.	1.291D 00	1.051D 00	1.025D 00	-1.438D 00	-1.569D 01
10000.	1.372D 00	1.346D 00	1.294D 00	6.532D-02	-1.026D 01

TABLE C.4-1
LOG OF THE BLANKETING OPACITY

T	6000.	8000.	11000.	17500.	50000.
		LAMBDA 92: 2511.37 ANGSTROMS			
PE					
3.	5.031D 00	4.211D 00	3.018D 00	9.275D-01	-1.551D 00
30.	5.175D 00	4.728D 00	3.903D 00	1.903D 00	-4.002D-01
300.	5.784D 00	5.379D 00	4.380D 00	2.711D 00	5.456D-01
10000.	5.959D 00	5.582D 00	5.329D 00	3.356D 00	1.245D 00
		LAMBDA 93: 2511.39 ANGSTROMS			
PE					
3.	-2.883D-01	-1.367D-01	-1.524D 00	-5.200D 00	-2.477D 01
30.	-1.982D-01	-4.943D-02	-5.993D-01	-3.654D 00	-2.078D 01
300.	-1.937D-01	5.426D-02	6.878D-03	-2.514D 00	-1.682D 01
10000.	-6.253D-01	1.172D-01	2.940D-01	-9.914D-01	-1.133D 01
		LAMBDA 94: 2535.39 ANGSTROMS			
PE					
3.	8.385D-01	1.009D 00	-4.522D-01	-4.248D 00	-2.397D 01
30.	1.015D 00	1.054D 00	4.695D-01	-2.730D 00	-1.998D 01
300.	1.008D 00	1.103D 00	1.068D 00	-1.603D 00	-1.603D 01
10000.	3.900D-01	1.221D 00	1.317D 00	-1.035D-01	-1.056D 01
		LAMBDA 95: 2575.21 ANGSTROMS			
PE					
3.	2.307D 00	2.485D 00	1.073D 00	-2.674D 00	-2.238D 01
30.	2.355D 00	2.515D 00	1.986D 00	-1.158D 00	-1.839D 01
300.	2.368D 00	2.549D 00	2.563D 00	-4.181D-02	-1.445D 01
10000.	1.975D 00	2.580D 00	2.730D 00	1.447D 00	-8.974D 00
		LAMBDA 96: 2600.45 ANGSTROMS			
PE					
3.	5.788D 00	5.686D 00	3.916D 00	7.078D-01	-1.076D 00
30.	5.769D 00	5.696D 00	4.828D 00	1.684D 00	-7.609D-02
300.	6.073D 00	5.685D 00	5.393D 00	2.493D 00	9.210D-01
10000.	6.248D 00	5.788D 00	5.538D 00	3.937D 00	2.358D 00
		LAMBDA 97: 2600.47 ANGSTROMS			
PE					
3.	-1.645D 00	-1.405D 00	-3.103D 00	-6.696D 00	-2.589D 01
30.	-1.449D 00	-1.259D 00	-2.106D 00	-5.045D 00	-2.190D 01
300.	-1.198D 00	-1.168D 00	-1.305D 00	-3.816D 00	-1.805D 01
10000.	-1.346D 00	-9.178D-01	-7.817D-01	-2.240D 00	-1.257D 01
		LAMBDA 98: 2625.93 ANGSTROMS			
PE					
3.	-4.184D-01	-5.645D-02	-1.814D 00	-5.559D 00	-2.471D 01
30.	-3.621D-01	6.404D-03	-8.420D-01	-3.901D 00	-2.073D 01
300.	-2.741D-01	1.567D-02	-5.913D-02	-2.666D 00	-1.704D 01
10000.	-4.575D-01	5.144D-02	3.837D-01	-1.112D 00	-1.151D 01

TABLE C.4-1
LOG OF THE BLANKETING OPACITY

T	6000.	8000.	11000.	17500.	50000.
			LAMBDA 99: 2668.19 ANGSTROMS		
PE					
3.	1.572D 00	1.727D 00	1.879D-01	-3.590D 00	-2.245D 01
30.	1.585D 00	1.776D 00	1.120D 00	-2.006D 00	-1.871D 01
300.	1.521D 00	1.778D 00	1.713D 00	-8.695D-01	-1.477D 01
10000.	8.335D-01	1.770D 00	1.945D 00	6.464D-01	-9.300D 00
			LAMBDA 100: 2694.99 ANGSTROMS		
PE					
3.	5.622D 00	5.522D 00	3.751D 00	-3.889D-01	-5.207D 00
30.	5.603D 00	5.533D 00	4.664D 00	1.146D 00	-3.056D 00
300.	5.458D 00	5.522D 00	5.229D 00	2.273D 00	-1.110D 00
10000.	4.912D 00	5.409D 00	5.374D 00	3.770D 00	1.111D 00
			LAMBDA 101: 2695.01 ANGSTROMS		
PE					
3.	-1.274D 00	-1.031D 00	-2.629D 00	-6.150D 00	-2.516D 01
30.	-9.332D-01	-9.330D-01	-1.632D 00	-4.510D 00	-2.117D 01
300.	-5.821D-01	-7.698D-01	-8.604D-01	-3.269D 00	-1.721D 01
10000.	-5.818D-01	-3.401D-01	-3.204D-01	-1.651D 00	-1.171D 01
			LAMBDA 102: 2720.95 ANGSTROMS		
PE					
3.	7.081D-02	2.895D-01	-1.285D 00	-4.833D 00	-2.407D 01
30.	2.382D-01	3.622D-01	-3.495D-01	-3.351D 00	-2.007D 01
300.	4.454D-01	4.197D-01	3.447D-01	-2.211D 00	-1.611D 01
10000.	2.151D-01	6.737D-01	6.894D-01	-6.686D-01	-1.068D 01
			LAMBDA 103: 2764.00 ANGSTROMS		
PE					
3.	1.868D 00	2.053D 00	5.354D-01	-3.172D 00	-2.202D 01
30.	1.927D 00	2.074D 00	1.456D 00	-1.648D 00	-1.816D 01
300.	1.882D 00	2.104D 00	2.055D 00	-5.141D-01	-1.442D 01
10000.	1.430D 00	2.117D 00	2.272D 00	9.862D-01	-9.105D 00
			LAMBDA 104: 2791.30 ANGSTROMS		
PE					
3.	5.058D 00	5.167D 00	3.574D 00	4.845D-01	-2.059D 00
30.	5.038D 00	5.178D 00	4.486D 00	1.484D 00	-1.060D 00
300.	4.894D 00	5.167D 00	5.051D 00	2.483D 00	-6.251D-02
10000.	5.298D 00	5.054D 00	5.196D 00	3.995D 00	1.374D 00
			LAMBDA 105: 2791.32 ANGSTROMS		
PE					
3.	-1.884D 00	-1.750D 00	-3.611D 00	-7.439D 00	-2.663D 01
30.	-1.582D 00	-1.541D 00	-2.595D 00	-5.670D 00	-2.253D 01
300.	-1.219D 00	-1.386D 00	-1.688D 00	-4.325D 00	-1.868D 01
10000.	-1.081D 00	-9.391D-01	-9.857D-01	-2.672D 00	-1.304D 01

TABLE C.4-1
LOG OF THE BLANKETING OPACITY

T	6000.	8000.	11000.	17500.	50000.
LAMBDA 106: 2829.86 ANGSTROMS					
PE					
3.	-8.634D-01	-6.697D-01	-2.456D 00	-6.261D 00	-2.571D 01
30.	-7.089D-01	-4.974D-01	-1.475D 00	-4.532D 00	-2.172D 01
300.	-4.420D-01	-3.656D-01	-6.219D-01	-3.239D 00	-1.781D 01
10000.	-4.995D-01	-1.389D-01	2.313D-02	-1.643D 00	-1.225D 01
LAMBDA 107: 2894.53 ANGSTROMS					
PE					
3.	6.223D-01	8.755D-01	-9.757D-01	-4.582D 00	-2.372D 01
30.	7.992D-01	9.951D-01	2.363D-03	-2.952D 00	-1.973D 01
300.	1.013D 00	1.083D 00	8.538D-01	-1.707D 00	-1.579D 01
10000.	8.981D-01	1.339D 00	1.454D 00	-1.399D-01	-1.036D 01
LAMBDA 108: 2935.99 ANGSTROMS					
PE					
3.	6.919D 00	6.791D 00	4.536D 00	1.405D 00	-6.980D 00
30.	6.911D 00	6.872D 00	5.516D 00	2.405D 00	-4.556D 00
300.	6.832D 00	6.878D 00	6.356D 00	3.404D 00	-2.497D 00
10000.	7.183D 00	6.832D 00	6.800D 00	4.916D 00	3.603D-01
LAMBDA 109: 2936.01 ANGSTROMS					
PE					
3.	-2.076D 00	-2.202D 00	-4.195D 00	-7.871D 00	-2.736D 01
30.	-1.676D 00	-1.872D 00	-3.159D 00	-6.061D 00	-2.336D 01
300.	-1.290D 00	-1.618D 00	-2.188D 00	-4.730D 00	-1.938D 01
10000.	-1.156D 00	-9.921D-01	-1.313D 00	-3.059D 00	-1.361D 01
LAMBDA 110: 2959.28 ANGSTROMS					
PE					
3.	-1.219D 00	-1.163D 00	-3.111D 00	-6.698D 00	-2.616D 01
30.	-8.527D-01	-9.516D-01	-2.059D 00	-4.960D 00	-2.218D 01
300.	-3.895D-01	-7.579D-01	-1.113D 00	-3.669D 00	-1.824D 01
10000.	-3.575D-01	-2.080D-01	-4.346D-01	-2.077D 00	-1.259D 01
LAMBDA 111: 2997.73 ANGSTROMS					
PE					
3.	1.839D-01	2.220D-01	-1.526D 00	-4.944D 00	-2.429D 01
30.	3.867D-01	4.357D-01	-5.603D-01	-3.426D 00	-2.029D 01
300.	7.516D-01	6.074D-01	2.351D-01	-2.211D 00	-1.634D 01
10000.	9.751D-01	9.246D-01	9.491D-01	-7.317D-01	-1.065D 01
LAMBDA 112: 3021.99 ANGSTROMS					
PE					
3.	4.194D 00	4.438D 00	2.948D 00	2.483D-02	-4.375D 00
30.	4.174D 00	4.449D 00	3.850D 00	9.998D-01	-2.224D 00
300.	4.605D 00	4.438D 00	4.425D 00	1.968D 00	-2.784D-01
10000.	5.097D 00	4.325D 00	4.611D 00	3.480D 00	1.943D 00

TABLE C.4-1
LOG OF THE BLANKETING OPACITY

T	6000.	8000.	11000.	17500.	50000.

LAMBDA 113: 3022.01 ANGSTROMS

PE					
3.	-1.908D 00	-1.997D 00	-4.050D 00	-8.066D 00	-2.625D 01
30.	-1.650D 00	-1.677D 00	-3.033D 00	-6.239D 00	-2.228D 01
300.	-1.419D 00	-1.507D 00	-2.095D 00	-4.789D 00	-1.848D 01
10000.	-1.401D 00	-1.159D 00	-1.252D 00	-3.105D 00	-1.333D 01

LAMBDA 114: 3048.73 ANGSTROMS

PE					
3.	-1.326D 00	-1.445D 00	-3.486D 00	-7.319D 00	-2.566D 01
30.	-1.095D 00	-1.126D 00	-2.440D 00	-5.546D 00	-2.169D 01
300.	-6.818D-01	-9.712D-01	-1.507D 00	-4.185D 00	-1.791D 01
10000.	-5.960D-01	-5.304D-01	-7.233D-01	-2.505D 00	-1.264D 01

LAMBDA 115: 3092.99 ANGSTROMS

PE					
3.	-7.060D-02	-1.195D-01	-2.097D 00	-5.667D 00	-2.387D 01
30.	1.626D-01	1.875D-01	-1.099D 00	-3.959D 00	-1.993D 01
300.	5.244D-01	3.552D-01	-1.357D-01	-2.720D 00	-1.612D 01
10000.	8.216D-01	7.386D-01	7.003D-01	-1.097D 00	-1.073D 01

LAMBDA 116: 3120.99 ANGSTROMS

PE					
3.	3.711D 00	3.593D 00	1.564D 00	-5.263D-01	6.199D-02
30.	3.709D 00	3.669D 00	2.552D 00	-2.194D-01	1.213D 00
300.	4.279D 00	3.690D 00	3.449D 00	5.862D-01	2.158D 00
10000.	5.071D 00	4.073D 00	4.038D 00	2.156D 00	2.856D 00

LAMBDA 117: 3121.01 ANGSTROMS

PE					
3.	-2.001D 00	-2.049D 00	-4.006D 00	-8.050D 00	-2.703D 01
30.	-1.902D 00	-1.711D 00	-3.001D 00	-6.218D 00	-2.305D 01
300.	-1.747D 00	-1.541D 00	-2.081D 00	-4.775D 00	-1.917D 01
10000.	-1.700D 00	-1.343D 00	-1.277D 00	-3.092D 00	-1.357D 01

LAMBDA 118: 3145.32 ANGSTROMS

PE					
3.	-1.250D 00	-1.221D 00	-3.239D 00	-6.992D 00	-2.579D 01
30.	-1.105D 00	-9.383D-01	-2.232D 00	-5.303D 00	-2.181D 01
300.	-8.615D-01	-7.825D-01	-1.319D 00	-4.007D 00	-1.796D 01
10000.	-9.684D-01	-5.317D-01	-4.920D-01	-2.353D 00	-1.261D 01

LAMBDA 119: 3185.46 ANGSTROMS

PE					
3.	1.991D-02	1.663D-01	-1.726D 00	-5.360D 00	-2.275D 01
30.	1.388D-01	3.774D-01	-7.418D-01	-3.707D 00	-1.877D 01
300.	3.142D-01	4.876D-01	1.516D-01	-2.441D 00	-1.491D 01
10000.	3.499D-01	7.030D-01	8.154D-01	-8.550D-01	-9.726D 00

TABLE C.4-1
LOG OF THE BLANKETING OPACITY

T	6000.	8000.	11000.	17500.	50000.
LAMBDA 120: 3210.78 ANGSTROMS					
PE					
3.	3.392D 00	3.646D 00	1.619D 00	3.676D-01	-1.378D 00
30.	3.403D 00	3.721D 00	2.607D 00	6.744D-01	-2.273D-01
300.	3.903D 00	3.886D 00	3.504D 00	8.333D-01	7.185D-01
10000.	4.219D 00	3.938D 00	4.093D 00	2.351D 00	1.738D 00
LAMBDA 121: 3210.80 ANGSTROMS					
PE					
3.	-2.106D 00	-2.389D 00	-4.492D 00	-8.542D 00	-2.756D 01
30.	-1.734D 00	-1.976D 00	-3.442D 00	-6.674D 00	-2.357D 01
300.	-1.405D 00	-1.691D 00	-2.442D 00	-5.201D 00	-1.965D 01
10000.	-1.391D 00	-1.147D 00	-1.452D 00	-3.472D 00	-1.406D 01
LAMBDA 122: 3237.62 ANGSTROMS					
PE					
3.	-1.205D 00	-1.427D 00	-3.602D 00	-7.682D 00	-2.584D 01
30.	-8.996D-01	-1.040D 00	-2.585D 00	-5.853D 00	-2.189D 01
300.	-5.448D-01	-8.402D-01	-1.604D 00	-4.406D 00	-1.815D 01
10000.	-3.442D-01	-3.215D-01	-6.443D-01	-2.664D 00	-1.304D 01
LAMBDA 123: 3281.97 ANGSTROMS					
PE					
3.	2.500D-01	6.388D-02	-1.964D 00	-5.342D 00	-2.373D 01
30.	4.904D-01	4.160D-01	-9.457D-01	-3.769D 00	-1.975D 01
300.	8.278D-01	6.017D-01	2.718D-02	-2.552D 00	-1.599D 01
10000.	1.016D 00	1.048D 00	8.004D-01	-9.545D-01	-1.078D 01
LAMBDA 124: 3309.99 ANGSTROMS					
PE					
3.	4.531D 00	4.777D 00	3.292D 00	1.222D-01	-2.624D 00
30.	4.512D 00	4.788D 00	4.204D 00	9.707D-01	-1.473D 00
300.	4.367D 00	4.777D 00	4.770D 00	2.097D 00	1.653D-01
10000.	4.051D 00	4.664D 00	4.915D 00	3.594D 00	2.386D 00
LAMBDA 125: 3310.01 ANGSTROMS					
PE					
3.	-2.055D 00	-2.209D 00	-4.319D 00	-8.387D 00	-2.755D 01
30.	-1.708D 00	-1.898D 00	-3.276D 00	-6.587D 00	-2.356D 01
300.	-1.347D 00	-1.636D 00	-2.299D 00	-5.191D 00	-1.958D 01
10000.	-1.300D 00	-1.095D 00	-1.386D 00	-3.479D 00	-1.396D 01
LAMBDA 126: 3342.32 ANGSTROMS					
PE					
3.	-1.255D 00	-1.324D 00	-3.458D 00	-7.356D 00	-2.593D 01
30.	-1.018D 00	-1.027D 00	-2.429D 00	-5.631D 00	-2.195D 01
300.	-6.957D-01	-8.705D-01	-1.473D 00	-4.256D 00	-1.814D 01
10000.	-5.877D-01	-4.938D-01	-6.190D-01	-2.638D 00	-1.290D 01

TABLE C.4-1
LOG OF THE BLANKETING OPACITY

T	6000.	8000.	11000.	17500.	50000.
	LAMBDA 127: 3395.97 ANGSTROMS				
PE					
3.	-7.872D-02	-1.360D-01	-2.152D 00	-5.499D 00	-1.476D 01
30.	1.419D-01	1.321D-01	-1.148D 00	-3.977D 00	-1.158D 01
300.	4.499D-01	3.014D-01	-2.316D-01	-2.864D 00	-8.590D 00
10000.	6.195D-01	6.751D-01	5.454D-01	-1.300D 00	-4.698D 00
	LAMBDA 128: 3429.99 ANGSTROMS				
PE					
3.	3.818D 00	3.593D 00	1.570D 00	3.441D-01	-8.974D-02
30.	3.816D 00	3.707D 00	2.558D 00	6.508D-01	1.061D 00
300.	4.165D 00	3.798D 00	3.455D 00	7.293D-01	2.007D 00
10000.	4.482D 00	3.897D 00	4.044D 00	2.167D 00	2.705D 00
	LAMBDA 129: 3430.01 ANGSTROMS				
PE					
3.	-2.234D 00	-2.859D 00	-5.144D 00	-9.471D 00	-2.828D 01
30.	-1.839D 00	-2.310D 00	-4.001D 00	-7.656D 00	-2.429D 01
300.	-1.493D 00	-1.889D 00	-2.918D 00	-6.043D 00	-2.030D 01
10000.	-1.318D 00	-1.240D 00	-1.731D 00	-3.989D 00	-1.474D 01
	LAMBDA 130: 3461.04 ANGSTROMS				
PE					
3.	-1.602D 00	-1.725D 00	-3.877D 00	-7.799D 00	-2.665D 01
30.	-1.215D 00	-1.444D 00	-2.738D 00	-6.087D 00	-2.267D 01
300.	-7.700D-01	-1.200D 00	-1.777D 00	-4.697D 00	-1.876D 01
10000.	-5.437D-01	-6.255D-01	-9.856D-01	-2.913D 00	-1.341D 01
	LAMBDA 131: 3512.45 ANGSTROMS				
PE					
3.	-3.240D-01	-5.093D-01	-2.484D 00	-6.124D 00	-2.322D 01
30.	-1.126D-02	-2.055D-01	-1.465D 00	-4.524D 00	-1.927D 01
300.	4.271D-01	3.039D-02	-5.450D-01	-3.206D 00	-1.546D 01
10000.	6.418D-01	5.703D-01	2.648D-01	-1.582D 00	-1.032D 01
	LAMBDA 132: 3544.99 ANGSTROMS				
PE					
3.	3.385D 00	3.682D 00	1.906D 00	-5.931D-02	-1.703D 00
30.	3.647D 00	3.737D 00	2.790D 00	4.264D-01	-2.582D-02
300.	4.503D 00	3.742D 00	3.605D 00	8.773D-01	1.161D 00
10000.	4.994D 00	3.992D 00	4.007D 00	2.425D 00	2.312D 00
	LAMBDA 133: 3545.01 ANGSTROMS				
PE					
3.	-2.534D 00	-3.747D 00	-6.446D 00	-1.195D 01	-3.229D 01
30.	-1.856D 00	-2.944D 00	-4.960D 00	-9.606D 00	-2.801D 01
300.	-1.181D 00	-2.220D 00	-3.624D 00	-7.534D 00	-2.355D 01
10000.	-7.173D-01	-1.124D 00	-2.116D 00	-4.906D 00	-1.707D 01

TABLE C.4-1
LOG OF THE BLANKETING OPACITY

T	6000.	8000.	11000.	17500.	50000.
	LAMBDA 134: 3572.64 ANGSTROMS				
PE					
3.	-1.788D 00	-2.883D 00	-5.480D 00	-1.023D 01	-2.914D 01
30.	-1.154D 00	-2.104D 00	-4.130D 00	-8.254D 00	-2.514D 01
300.	-4.579D-01	-1.461D 00	-2.838D 00	-6.446D 00	-2.108D 01
10000.	1.705D-02	-4.182D-01	-1.353D 00	-4.083D 00	-1.497D 01
	LAMBDA 135: 3618.26 ANGSTROMS				
PE					
3.	-5.505D-01	-1.378D 00	-3.675D 00	-7.811D 00	-2.538D 01
30.	1.088D-01	-8.012D-01	-2.449D 00	-6.056D 00	-2.141D 01
300.	8.313D-01	-2.286D-01	-1.328D 00	-4.531D 00	-1.760D 01
10000.	1.292D 00	8.831D-01	-8.200D-02	-2.528D 00	-1.237D 01
	LAMBDA 136: 3647.04 ANGSTROMS				
PE					
3.	2.781D 00	3.189D 00	1.882D 00	-1.084D 00	-1.043D 00
30.	3.762D 00	3.265D 00	2.757D 00	-1.091D-01	1.072D-01
300.	4.618D 00	3.281D 00	3.244D 00	7.694D-01	1.053D 00
10000.	5.109D 00	4.295D 00	3.671D 00	2.284D 00	1.751D 00
	LAMBDA 137: 3647.06 ANGSTROMS				
PE					
3.	-2.580D 00	-3.498D 00	-6.102D 00	-1.079D 01	-3.076D 01
30.	-1.972D 00	-2.803D 00	-4.671D 00	-8.773D 00	-2.657D 01
300.	-1.408D 00	-2.160D 00	-3.393D 00	-7.071D 00	-2.254D 01
10000.	-1.043D 00	-1.181D 00	-2.037D 00	-4.627D 00	-1.634D 01
	LAMBDA 138: 3676.77 ANGSTROMS				
PE					
3.	-1.946D 00	-2.664D 00	-5.136D 00	-9.362D 00	-2.800D 01
30.	-1.300D 00	-2.015D 00	-3.863D 00	-7.536D 00	-2.400D 01
300.	-5.906D-01	-1.506D 00	-2.682D 00	-5.974D 00	-2.001D 01
10000.	-9.829D-02	-4.849D-01	-1.307D 00	-3.847D 00	-1.440D 01
	LAMBDA 139: 3725.87 ANGSTROMS				
PE					
3.	-6.801D-01	-1.109D 00	-3.284D 00	-6.395D 00	-2.330D 01
30.	-1.319D-01	-6.983D-01	-2.043D 00	-5.120D 00	-1.929D 01
300.	5.517D-01	-3.322D-01	-1.031D 00	-3.884D 00	-1.536D 01
10000.	1.050D 00	6.263D-01	-1.044D-02	-1.996D 00	-1.024D 01
	LAMBDA 140: 3756.88 ANGSTROMS				
PE					
3.	3.262D 00	2.873D 00	8.752D-01	9.522D-01	-6.571D-01
30.	3.771D 00	3.265D 00	1.863D 00	1.259D 00	4.934D-01
300.	4.627D 00	3.488D 00	2.761D 00	1.306D 00	1.439D 00
10000.	5.118D 00	4.303D 00	3.658D 00	1.940D 00	2.137D 00

TABLE C.4-1
LOG OF THE BLANKETING OPACITY

T	6000.	8000.	11000.	17500.	50000.
		LAMBDA 141: 3756.90 ANGSTROMS			
PE					
3.	-3.062D 00	-4.136D 00	-6.939D 00	-1.263D 01	-3.352D 01
30.	-2.447D 00	-3.381D 00	-5.357D 00	-1.019D 01	-2.888D 01
300.	-1.983D 00	-2.681D 00	-4.003D 00	-8.050D 00	-2.419D 01
10000.	-1.677D 00	-1.708D 00	-2.546D 00	-5.285D 00	-1.747D 01
		LAMBDA 142: 3778.78 ANGSTROMS			
PE					
3.	-2.107D 00	-3.290D 00	-5.950D 00	-1.068D 01	-3.000D 01
30.	-1.472D 00	-2.535D 00	-4.537D 00	-8.550D 00	-2.599D 01
300.	-8.298D-01	-1.730D 00	-3.197D 00	-6.779D 00	-2.191D 01
10000.	-3.231D-01	-6.958D-01	-1.615D 00	-4.445D 00	-1.598D 01
		LAMBDA 143: 3814.74 ANGSTROMS			
PE					
3.	-6.149D-01	-1.456D 00	-4.041D 00	-8.497D 00	-2.442D 01
30.	9.618D-02	-8.083D-01	-2.578D 00	-6.487D 00	-2.045D 01
300.	9.228D-01	-2.067D-01	-1.375D 00	-4.895D 00	-1.673D 01
10000.	1.497D 00	9.700D-01	4.696D-03	-2.583D 00	-1.132D 01
		LAMBDA 144: 3837.30 ANGSTROMS			
PE					
3.	3.267D 00	2.875D 00	1.911D 00	-3.095D-01	-2.044D 00
30.	3.992D 00	3.269D 00	2.796D 00	-2.724D-03	-8.939D-01
300.	4.914D 00	3.619D 00	3.273D 00	8.035D-01	2.493D-01
10000.	5.599D 00	5.096D 00	3.878D 00	2.318D 00	2.470D 00
		LAMBDA 145: 3837.32 ANGSTROMS			
PE					
3.	-3.749D 00	-4.747D 00	-7.558D 00	-1.348D 01	-3.394D 01
30.	-3.150D 00	-3.989D 00	-5.917D 00	-1.104D 01	-2.972D 01
300.	-2.493D 00	-3.362D 00	-4.631D 00	-8.910D 00	-2.539D 01
10000.	-1.970D 00	-2.301D 00	-3.195D 00	-6.034D 00	-1.890D 01
		LAMBDA 146: 3867.81 ANGSTROMS			
PE					
3.	-2.922D 00	-3.958D 00	-6.717D 00	-1.212D 01	-3.260D 01
30.	-2.255D 00	-3.212D 00	-5.188D 00	-9.726D 00	-2.834D 01
300.	-1.583D 00	-2.486D 00	-3.876D 00	-7.773D 00	-2.394D 01
10000.	-1.078D 00	-1.364D 00	-2.277D 00	-5.135D 00	-1.753D 01
		LAMBDA 147: 3918.19 ANGSTROMS			
PE					
3.	-1.088D 00	-2.015D 00	-4.449D 00	-7.616D 00	-2.231D 01
30.	-6.834D-01	-1.316D 00	-3.144D 00	-6.510D 00	-1.835D 01
300.	-8.208D-02	-8.205D-01	-1.919D 00	-5.161D 00	-1.447D 01
10000.	5.118D-01	1.266D-02	-6.905D-01	-2.907D 00	-9.852D 00

TABLE C.4-1
LOG OF THE BLANKETING OPACITY

T	6000.	8000.	11000.	17500.	50000.
	LAMBDA 148: 3949.99 ANGSTROMS				
PE					
3.	5.116D 00	3.780D 00	1.385D 00	4.434D-01	-2.340D 00
30.	5.127D 00	4.593D 00	2.382D 00	1.318D 00	-1.190D 00
300.	5.122D 00	4.942D 00	3.367D 00	2.127D 00	-2.438D-01
10000.	5.744D 00	5.247D 00	4.558D 00	2.508D 00	8.490D-01
	LAMBDA 149: 3950.01 ANGSTROMS				
PE					
3.	-3.459D 00	-4.541D 00	-7.451D 00	-1.329D 01	-3.440D 01
30.	-2.704D 00	-3.680D 00	-5.791D 00	-1.080D 01	-2.999D 01
300.	-1.956D 00	-2.873D 00	-4.322D 00	-8.615D 00	-2.542D 01
10000.	-1.327D 00	-1.700D 00	-2.612D 00	-5.607D 00	-1.856D 01
	LAMBDA 150: 3974.53 ANGSTROMS				
PE					
3.	-2.870D 00	-3.785D 00	-6.526D 00	-1.194D 01	-3.271D 01
30.	-2.160D 00	-3.025D 00	-5.037D 00	-9.392D 00	-2.834D 01
300.	-1.386D 00	-2.370D 00	-3.647D 00	-7.492D 00	-2.383D 01
10000.	-6.744D-01	-1.168D 00	-2.039D 00	-4.820D 00	-1.708D 01
	LAMBDA 151: 4014.86 ANGSTROMS				
PE					
3.	-1.307D 00	-2.097D 00	-4.328D 00	-7.604D 00	-2.594D 01
30.	-7.456D-01	-1.470D 00	-3.140D 00	-6.125D 00	-2.197D 01
300.	-1.483D-01	-8.547D-01	-1.879D 00	-4.793D 00	-1.802D 01
10000.	5.031D-01	5.966D-02	-5.751D-01	-2.915D 00	-1.243D 01
	LAMBDA 152: 4040.19 ANGSTROMS				
PE					
3.	4.833D 00	3.497D 00	1.101D 00	9.882D-01	-1.479D 00
30.	4.844D 00	4.310D 00	2.099D 00	1.295D 00	-3.283D-01
300.	4.839D 00	4.659D 00	3.083D 00	1.477D 00	6.175D-01
10000.	4.786D 00	4.711D 00	4.285D 00	2.028D 00	1.798D 00
	LAMBDA 153: 4040.21 ANGSTROMS				
PE					
3.	-3.949D 00	-5.097D 00	-7.741D 00	-1.329D 01	-3.408D 01
30.	-3.280D 00	-4.251D 00	-6.217D 00	-1.086D 01	-2.979D 01
300.	-2.576D 00	-3.492D 00	-4.878D 00	-8.740D 00	-2.529D 01
10000.	-1.887D 00	-2.320D 00	-3.289D 00	-5.809D 00	-1.855D 01
	LAMBDA 154: 4078.43 ANGSTROMS				
PE					
3.	-3.183D 00	-4.215D 00	-6.881D 00	-1.112D 01	-3.158D 01
30.	-2.480D 00	-3.425D 00	-5.381D 00	-9.052D 00	-2.744D 01
300.	-1.770D 00	-2.706D 00	-4.036D 00	-7.275D 00	-2.319D 01
10000.	-1.203D 00	-1.505D 00	-2.488D 00	-4.751D 00	-1.674D 01

TABLE C.4-1
LOG OF THE BLANKETING OPACITY

T	6000.	8000.	11000.	17500.	50000.

LAMBDA 155: 4141.82 ANGSTROMS

PE					
3.	-1.595D 00	-2.518D 00	-4.933D 00	-4.226D 00	-1.451D 01
30.	-1.014D 00	-1.805D 00	-3.690D 00	-3.788D 00	-1.132D 01
300.	-3.902D-01	-1.162D 00	-2.445D 00	-3.521D 00	-8.344D 00
10000.	1.069D-01	-2.637D-01	-1.017D 00	-2.872D 00	-4.588D 00

LAMBDA 156: 4181.99 ANGSTROMS

PE					
3.	2.381D 00	1.787D 00	9.801D-01	1.182D 00	-2.086D 00
30.	3.361D 00	2.193D 00	1.865D 00	1.489D 00	-4.094D-01
300.	4.217D 00	2.615D 00	2.342D 00	1.536D 00	7.778D-01
10000.	4.709D 00	4.026D 00	2.573D 00	1.542D 00	1.929D 00

LAMBDA 157: 4182.01 ANGSTROMS

PE					
3.	-3.818D 00	-5.107D 00	-7.864D 00	-1.344D 01	-3.468D 01
30.	-3.035D 00	-4.125D 00	-6.245D 00	-1.095D 01	-3.007D 01
300.	-2.284D 00	-3.286D 00	-4.832D 00	-8.764D 00	-2.540D 01
10000.	-1.650D 00	-2.051D 00	-3.052D 00	-5.751D 00	-1.866D 01

LAMBDA 158: 4216.15 ANGSTROMS

PE					
3.	-3.001D 00	-4.271D 00	-7.026D 00	-1.240D 01	-3.308D 01
30.	-2.209D 00	-3.387D 00	-5.394D 00	-9.855D 00	-2.872D 01
300.	-1.423D 00	-2.524D 00	-3.977D 00	-7.691D 00	-2.411D 01
10000.	-8.414D-01	-1.226D 00	-2.316D 00	-4.879D 00	-1.739D 01

LAMBDA 159: 4272.59 ANGSTROMS

PE					
3.	-1.570D 00	-2.628D 00	-5.029D 00	-4.655D 00	-1.516D 01
30.	-9.361D-01	-1.746D 00	-3.695D 00	-4.079D 00	-1.203D 01
300.	-2.855D-01	-1.099D 00	-2.411D 00	-3.859D 00	-9.059D 00
10000.	3.703D-01	-1.000D-01	-8.674D-01	-3.026D 00	-5.233D 00

LAMBDA 160: 4308.23 ANGSTROMS

PE					
3.	2.225D 00	2.078D 00	7.303D-01	1.128D 00	-6.788D 00
30.	2.966D 00	2.317D 00	1.643D 00	2.103D 00	-4.111D 00
300.	3.789D 00	2.453D 00	2.208D 00	2.911D 00	-1.924D 00
10000.	4.994D 00	3.615D 00	2.446D 00	3.293D 00	7.500D-01

LAMBDA 161: 4308.25 ANGSTROMS

PE					
3.	-4.653D 00	-5.890D 00	-8.721D 00	-1.472D 01	-3.564D 01
30.	-3.992D 00	-4.938D 00	-7.065D 00	-1.230D 01	-3.101D 01
300.	-3.304D 00	-4.168D 00	-5.641D 00	-1.007D 01	-2.655D 01
10000.	-2.738D 00	-3.037D 00	-3.955D 00	-6.986D 00	-2.003D 01

TABLE C.4-1
LOG OF THE BLANKETING OPACITY

LAMBDA 162: 4339.10 ANGSTROMS

T / PE	6000.	8000.	11000.	17500.	50000.
3.	-3.679D 00	-4.726D 00	-7.394D 00	-1.314D 01	-3.361D 01
30.	-3.068D 00	-3.925D 00	-5.873D 00	-1.077D 01	-2.921D 01
300.	-2.422D 00	-3.249D 00	-4.611D 00	-8.661D 00	-2.490D 01
10000.	-1.795D 00	-2.170D 00	-3.053D 00	-5.788D 00	-1.834D 01

LAMBDA 163: 4389.96 ANGSTROMS

T / PE	6000.	8000.	11000.	17500.	50000.
3.	-1.915D 00	-3.018D 00	-5.342D 00	-6.033D 00	-2.222D 01
30.	-1.360D 00	-2.229D 00	-4.164D 00	-4.789D 00	-1.825D 01
300.	-7.769D-01	-1.627D 00	-2.970D 00	-4.201D 00	-1.451D 01
10000.	-2.634D-01	-6.552D-01	-1.547D 00	-3.140D 00	-9.598D 00

LAMBDA 164: 4421.99 ANGSTROMS

T / PE	6000.	8000.	11000.	17500.	50000.
3.	2.301D 00	1.937D 00	3.571D-01	1.393D 00	-6.666D 00
30.	3.112D 00	2.400D 00	1.269D 00	1.700D 00	-4.554D 00
300.	3.967D 00	2.492D 00	1.835D 00	1.747D 00	-2.367D 00
10000.	4.459D 00	3.771D 00	2.515D 00	1.749D 00	3.069D-01

LAMBDA 165: 4422.01 ANGSTROMS

T / PE	6000.	8000.	11000.	17500.	50000.
3.	-4.773D 00	-6.143D 00	-9.417D 00	-1.487D 01	-3.612D 01
30.	-3.965D 00	-5.002D 00	-7.493D 00	-1.224D 01	-3.124D 01
300.	-3.144D 00	-4.108D 00	-5.721D 00	-9.928D 00	-2.655D 01
10000.	-2.311D 00	-2.785D 00	-3.759D 00	-6.878D 00	-1.975D 01

LAMBDA 166: 4450.80 ANGSTROMS

T / PE	6000.	8000.	11000.	17500.	50000.
3.	-3.861D 00	-5.052D 00	-7.897D 00	-1.343D 01	-3.387D 01
30.	-3.110D 00	-4.098D 00	-6.213D 00	-1.093D 01	-2.944D 01
300.	-2.288D 00	-3.258D 00	-4.772D 00	-8.789D 00	-2.494D 01
10000.	-1.527D 00	-2.048D 00	-3.003D 00	-5.928D 00	-1.831D 01

LAMBDA 167: 4498.19 ANGSTROMS

T / PE	6000.	8000.	11000.	17500.	50000.
3.	-2.078D 00	-3.292D 00	-5.770D 00	-6.783D 00	-1.622D 01
30.	-1.408D 00	-2.389D 00	-4.389D 00	-6.711D 00	-1.254D 01
300.	-6.989D-01	-1.602D 00	-3.068D 00	-5.415D 00	-9.352D 00
10000.	6.900D-03	-4.699D-01	-1.391D 00	-3.501D 00	-5.390D 00

LAMBDA 168: 4527.99 ANGSTROMS

T / PE	6000.	8000.	11000.	17500.	50000.
3.	2.138D 00	1.862D 00	5.595D-01	-1.348D-02	-1.589D 00
30.	2.136D 00	2.247D 00	1.472D 00	6.380D-01	-5.892D-01
300.	2.902D 00	2.339D 00	2.037D 00	9.824D-01	4.078D-01
10000.	4.273D 00	3.104D 00	2.359D 00	1.040D 00	1.845D 00

TABLE C.4-1
LOG OF THE BLANKETING OPACITY

T	6000.	8000.	11000.	17500.	50000.
			LAMBDA 169: 4528.01 ANGSTROMS		
PE					
3.	-5.401D 00	-6.819D 00	-9.917D 00	-1.534D 01	-3.669D 01
30.	-4.484D 00	-5.689D 00	-8.018D 00	-1.277D 01	-3.171D 01
300.	-3.656D 00	-4.718D 00	-6.279D 00	-1.051D 01	-2.690D 01
10000.	-2.970D 00	-3.354D 00	-4.358D 00	-7.405D 00	-2.010D 01
			LAMBDA 170: 4561.08 ANGSTROMS		
PE					
3.	-4.297D 00	-5.534D 00	-8.267D 00	-1.376D 01	-3.414D 01
30.	-3.488D 00	-4.546D 00	-6.651D 00	-1.135D 01	-2.984D 01
300.	-2.689D 00	-3.665D 00	-5.157D 00	-9.171D 00	-2.532D 01
10000.	-2.081D 00	-2.335D 00	-3.295D 00	-6.229D 00	-1.858D 01
			LAMBDA 171: 4615.62 ANGSTROMS		
PE					
3.	-2.419D 00	-3.128D 00	-5.251D 00	-5.086D 00	-1.618D 01
30.	-1.900D 00	-2.552D 00	-4.042D 00	-4.396D 00	-1.295D 01
300.	-1.251D 00	-1.935D 00	-2.902D 00	-4.038D 00	-9.842D 00
10000.	-6.517D-01	-9.243D-01	-1.620D 00	-3.114D 00	-5.561D 00
			LAMBDA 172: 4649.99 ANGSTROMS		
PE					
3.	2.378D 00	2.215D 00	8.419D-01	1.297D 00	-1.374D 00
30.	2.376D 00	2.509D 00	1.754D 00	1.604D 00	-3.748D-01
300.	2.847D 00	2.601D 00	2.337D 00	1.756D 00	6.222D-01
10000.	3.339D 00	2.793D 00	2.926D 00	1.814D 00	2.059D 00
			LAMBDA 173: 4650.01 ANGSTROMS		
PE					
3.	-5.343D 00	-6.790D 00	-9.789D 00	-1.530D 01	-3.664D 01
30.	-4.498D 00	-5.651D 00	-7.945D 00	-1.275D 01	-3.156D 01
300.	-3.733D 00	-4.678D 00	-6.282D 00	-1.052D 01	-2.682D 01
10000.	-3.072D 00	-3.355D 00	-4.362D 00	-7.401D 00	-2.001D 01
			LAMBDA 174: 4679.63 ANGSTROMS		
PE					
3.	-4.371D 00	-5.680D 00	-8.347D 00	-1.382D 01	-3.486D 01
30.	-3.499D 00	-4.641D 00	-6.611D 00	-1.126D 01	-3.016D 01
300.	-2.722D 00	-3.670D 00	-5.120D 00	-9.138D 00	-2.547D 01
10000.	-1.979D 00	-2.320D 00	-3.318D 00	-6.106D 00	-1.868D 01
			LAMBDA 175: 4728.36 ANGSTROMS		
PE					
3.	-2.875D 00	-4.066D 00	-6.536D 00	-1.094D 01	-3.032D 01
30.	-2.098D 00	-3.110D 00	-5.057D 00	-8.678D 00	-2.596D 01
300.	-1.371D 00	-2.272D 00	-3.630D 00	-6.680D 00	-2.170D 01
10000.	-6.940D-01	-9.418D-01	-1.917D 00	-4.052D 00	-1.512D 01

TABLE C.4-1
LOG OF THE BLANKETING OPACITY

T	6000.	8000.	11000.	17500.	50000.
	LAMBDA 176: 4758.99 ANGSTROMS				
PE					
3.	1.269D 00	1.103D 00	-1.918D-01	1.690D 00	-1.770D 00
30.	1.987D 00	1.132D 00	7.205D-01	1.997D 00	-6.199D-01
300.	2.909D 00	1.948D 00	1.286D 00	2.044D 00	3.259D-01
10000.	3.593D 00	3.424D 00	2.477D 00	2.046D 00	1.024D 00
	LAMBDA 177: 4759.01 ANGSTROMS				
PE					
3.	-5.679D 00	-7.178D 00	-1.033D 01	-1.579D 01	-3.718D 01
30.	-4.734D 00	-6.028D 00	-8.386D 00	-1.319D 01	-3.221D 01
300.	-3.924D 00	-4.983D 00	-6.633D 00	-1.094D 01	-2.737D 01
10000.	-3.355D 00	-3.580D 00	-4.686D 00	-7.790D 00	-2.049D 01
	LAMBDA 178: 4793.43 ANGSTROMS				
PE					
3.	-4.715D 00	-6.071D 00	-9.013D 00	-1.428D 01	-3.577D 01
30.	-3.744D 00	-5.000D 00	-7.075D 00	-1.182D 01	-3.083D 01
300.	-2.927D 00	-3.988D 00	-5.448D 00	-9.683D 00	-2.600D 01
10000.	-2.251D 00	-2.565D 00	-3.620D 00	-6.629D 00	-1.918D 01
	LAMBDA 179: 4850.19 ANGSTROMS				
PE					
3.	-3.108D 00	-4.478D 00	-7.178D 00	-1.230D 01	-3.332D 01
30.	-2.324D 00	-3.446D 00	-5.339D 00	-9.971D 00	-2.840D 01
300.	-1.564D 00	-2.517D 00	-3.919D 00	-7.863D 00	-2.358D 01
10000.	-9.545D-01	-1.208D 00	-2.212D 00	-4.916D 00	-1.694D 01
	LAMBDA 180: 4885.95 ANGSTROMS				
PE					
3.	1.782D 00	1.622D 00	-5.987D-01	-2.272D-01	-1.028D 00
30.	1.796D 00	2.086D 00	3.984D-01	5.844D-01	1.227D-01
300.	2.652D 00	2.178D 00	1.369D 00	9.288D-01	1.068D 00
10000.	3.143D 00	2.744D 00	2.368D 00	9.868D-01	1.767D 00
	LAMBDA 181: 4885.97 ANGSTROMS				
PE					
3.	-6.447D 00	-8.347D 00	-1.195D 01	-1.768D 01	-3.758D 01
30.	-5.452D 00	-6.890D 00	-9.939D 00	-1.483D 01	-3.262D 01
300.	-4.566D 00	-5.760D 00	-7.992D 00	-1.228D 01	-2.791D 01
10000.	-3.564D 00	-4.301D 00	-5.529D 00	-9.031D 00	-2.142D 01
	LAMBDA 182: 4918.03 ANGSTROMS				
PE					
3.	-4.905D 00	-6.602D 00	-9.396D 00	-1.515D 01	-3.591D 01
30.	-3.974D 00	-5.290D 00	-7.785D 00	-1.254D 01	-3.094D 01
300.	-3.097D 00	-4.262D 00	-6.223D 00	-1.008D 01	-2.616D 01
10000.	-2.219D 00	-2.799D 00	-3.996D 00	-6.976D 00	-1.942D 01

TABLE C.4-1
LOG OF THE BLANKETING OPACITY

T	6000.	8000.	11000.	17500.	50000.
		LAMBDA 183: 4970.80 ANGSTROMS			
PE					
3.	-3.281D 00	-4.715D 00	-7.221D 00	-1.194D 01	-3.296D 01
30.	-2.393D 00	-3.659D 00	-5.564D 00	-9.607D 00	-2.810D 01
300.	-1.559D 00	-2.673D 00	-4.105D 00	-7.616D 00	-2.351D 01
10000.	-8.753D-01	-1.280D 00	-2.396D 00	-4.632D 00	-1.698D 01
		LAMBDA 184: 5003.99 ANGSTROMS			
PE					
3.	1.106D 00	-3.857D-01	-2.083D 00	6.419D-01	-9.200D 00
30.	2.087D 00	6.251D-01	-1.082D 00	9.486D-01	-6.522D 00
300.	2.942D 00	1.614D 00	8.932D-02	1.134D 00	-4.335D 00
10000.	3.434D 00	3.024D 00	1.757D 00	1.192D 00	-6.520D-01
		LAMBDA 185: 5004.01 ANGSTROMS			
PE					
3.	-6.628D 00	-8.394D 00	-1.172D 01	-1.784D 01	-3.740D 01
30.	-5.727D 00	-7.033D 00	-9.780D 00	-1.494D 01	-3.245D 01
300.	-4.895D 00	-5.961D 00	-8.024D 00	-1.238D 01	-2.777D 01
10000.	-3.960D 00	-4.606D 00	-5.732D 00	-9.094D 00	-2.139D 01
		LAMBDA 186: 5030.71 ANGSTROMS			
PE					
3.	-4.903D 00	-6.470D 00	-9.457D 00	-1.524D 01	-3.540D 01
30.	-4.023D 00	-5.253D 00	-7.543D 00	-1.255D 01	-3.053D 01
300.	-3.197D 00	-4.221D 00	-5.799D 00	-1.014D 01	-2.579D 01
10000.	-2.402D 00	-2.881D 00	-3.935D 00	-6.875D 00	-1.928D 01
		LAMBDA 187: 5074.53 ANGSTROMS			
PE					
3.	-3.316D 00	-4.529D 00	-6.814D 00	-1.165D 01	-3.234D 01
30.	-2.482D 00	-3.555D 00	-5.250D 00	-9.495D 00	-2.746D 01
300.	-1.708D 00	-2.663D 00	-3.922D 00	-7.560D 00	-2.279D 01
10000.	-1.055D 00	-1.343D 00	-2.338D 00	-4.723D 00	-1.632D 01
		LAMBDA 188: 5101.99 ANGSTROMS			
PE					
3.	7.863D-01	1.272D-01	-1.659D 00	5.041D-01	-2.222D 00
30.	1.407D 00	8.086D-01	-7.821D-01	1.316D 00	-1.223D 00
300.	2.263D 00	1.162D 00	2.141D-01	1.660D 00	-2.258D-01
10000.	3.011D 00	2.558D 00	1.632D 00	1.718D 00	1.211D 00
		LAMBDA 189: 5102.01 ANGSTROMS			
PE					
3.	-5.564D 00	-6.833D 00	-9.585D 00	-1.493D 01	-3.651D 01
30.	-4.695D 00	-5.753D 00	-7.754D 00	-1.245D 01	-3.162D 01
300.	-3.886D 00	-4.791D 00	-6.123D 00	-1.028D 01	-2.690D 01
10000.	-3.269D 00	-3.402D 00	-4.358D 00	-7.208D 00	-1.993D 01

TABLE C.4-1
LOG OF THE BLANKETING OPACITY

T	6000.	8000.	11000.	17500.	50000.
			LAMBDA 190: 5126.68 ANGSTROMS		
PE					
3.	-4.376D 00	-5.577D 00	-8.127D 00	-1.339D 01	-3.501D 01
30.	-3.442D 00	-4.569D 00	-6.351D 00	-1.099D 01	-3.007D 01
300.	-2.650D 00	-3.566D 00	-4.852D 00	-8.876D 00	-2.523D 01
10000.	-2.147D 00	-2.198D 00	-3.137D 00	-5.839D 00	-1.844D 01
			LAMBDA 191: 5167.11 ANGSTROMS		
PE					
3.	-2.180D 00	-3.237D 00	-5.666D 00	-8.888D 00	-2.115D 01
30.	-1.349D 00	-2.339D 00	-4.294D 00	-6.856D 00	-1.773D 01
300.	-5.374D-01	-1.561D 00	-2.915D 00	-5.257D 00	-1.462D 01
10000.	1.027D-01	-2.016D-01	-1.237D 00	-3.476D 00	-1.015D 01
			LAMBDA 192: 5192.41 ANGSTROMS		
PE					
3.	2.904D 00	1.949D 00	-3.547D-01	-2.953D-04	-1.102D 01
30.	3.895D 00	2.510D 00	6.424D-01	8.513D-01	-7.858D 00
300.	4.817D 00	3.517D 00	1.803D 00	1.659D 00	-4.922D 00
10000.	5.501D 00	4.993D 00	3.759D 00	2.041D 00	-1.178D 00
			LAMBDA 193: 5192.43 ANGSTROMS		
PE					
3.	-5.864D 00	-7.032D 00	-9.906D 00	-1.560D 01	-3.712D 01
30.	-4.913D 00	-5.989D 00	-8.013D 00	-1.293D 01	-3.216D 01
300.	-4.073D 00	-5.000D 00	-6.415D 00	-1.063D 01	-2.733D 01
10000.	-3.366D 00	-3.595D 00	-4.534D 00	-7.514D 00	-2.052D 01
			LAMBDA 194: 5222.79 ANGSTROMS		
PE					
3.	-4.449D 00	-5.796D 00	-8.819D 00	-1.418D 01	-3.565D 01
30.	-3.555D 00	-4.709D 00	-6.992D 00	-1.168D 01	-3.070D 01
300.	-2.770D 00	-3.734D 00	-5.249D 00	-9.462D 00	-2.587D 01
10000.	-2.078D 00	-2.364D 00	-3.391D 00	-6.402D 00	-1.903D 01
			LAMBDA 195: 5272.68 ANGSTROMS		
PE					
3.	-2.920D 00	-4.197D 00	-7.008D 00	-1.227D 01	-3.256D 01
30.	-2.095D 00	-3.172D 00	-5.299D 00	-9.729D 00	-2.762D 01
300.	-1.293D 00	-2.276D 00	-3.794D 00	-7.656D 00	-2.287D 01
10000.	-5.098D-01	-1.028D 00	-1.988D 00	-4.834D 00	-1.618D 01
			LAMBDA 196: 5303.99 ANGSTROMS		
PE					
3.	2.205D 00	1.941D 00	-3.654D-01	-3.021D-01	-2.571D 00
30.	2.203D 00	2.404D 00	6.317D-01	4.707D-03	-8.944D-01
300.	2.893D 00	2.495D 00	1.602D 00	5.153D-02	2.928D-01
10000.	3.827D 00	2.959D 00	2.601D 00	5.427D-01	1.444D 00

TABLE C.4-1
LOG OF THE BLANKETING OPACITY

T	6000.	8000.	11000.	17500.	50000.
	LAMBDA 197: 5304.01 ANGSTROMS				
PE					
3.	-5.674D 00	-6.944D 00	-9.847D 00	-1.503D 01	-3.664D 01
30.	-4.721D 00	-5.848D 00	-7.903D 00	-1.254D 01	-3.156D 01
300.	-3.920D 00	-4.823D 00	-6.227D 00	-1.038D 01	-2.676D 01
10000.	-3.392D 00	-3.417D 00	-4.364D 00	-7.288D 00	-1.978D 01
	LAMBDA 198: 5334.89 ANGSTROMS				
PE					
3.	-4.277D 00	-5.442D 00	-8.249D 00	-1.354D 01	-3.528D 01
30.	-3.478D 00	-4.431D 00	-6.360D 00	-1.105D 01	-3.034D 01
300.	-2.706D 00	-3.515D 00	-4.837D 00	-8.909D 00	-2.547D 01
10000.	-2.269D 00	-2.300D 00	-3.217D 00	-5.892D 00	-1.847D 01
	LAMBDA 199: 5385.62 ANGSTROMS				
PE					
3.	-2.979D 00	-4.046D 00	-6.692D 00	-1.163D 01	-3.302D 01
30.	-2.235D 00	-3.070D 00	-4.977D 00	-9.288D 00	-2.810D 01
300.	-1.449D 00	-2.280D 00	-3.475D 00	-7.328D 00	-2.326D 01
10000.	-9.042D-01	-1.053D 00	-1.856D 00	-4.503D 00	-1.632D 01
	LAMBDA 200: 5417.46 ANGSTROMS				
PE					
3.	2.168D 00	1.908D 00	-3.955D-01	-2.126D 00	-1.848D 00
30.	2.166D 00	2.372D 00	6.016D-01	-9.439D-01	-6.974D-01
300.	2.812D 00	2.463D 00	1.572D 00	1.029D-01	2.484D-01
10000.	3.348D 00	2.849D 00	2.571D 00	1.628D 00	9.455D-01
	LAMBDA 201: 5417.48 ANGSTROMS				
PE					
3.	-7.646D 00	-9.743D 00	-1.242D 01	-1.786D 01	-3.992D 01
30.	-6.639D 00	-8.275D 00	-1.056D 01	-1.537D 01	-3.494D 01
300.	-5.748D 00	-6.898D 00	-8.869D 00	-1.299D 01	-2.995D 01
10000.	-5.057D 00	-5.290D 00	-6.707D 00	-9.682D 00	-2.256D 01
	LAMBDA 202: 5454.80 ANGSTROMS				
PE					
3.	-5.925D 00	-7.518D 00	-1.046D 01	-1.577D 01	-3.676D 01
30.	-5.013D 00	-6.308D 00	-8.563D 00	-1.327D 01	-3.180D 01
300.	-4.220D 00	-5.186D 00	-6.897D 00	-1.104D 01	-2.700D 01
10000.	-3.520D 00	-3.829D 00	-4.839D 00	-7.873D 00	-2.029D 01
	LAMBDA 203: 5516.29 ANGSTROMS				
PE					
3.	-3.940D 00	-5.165D 00	-7.865D 00	-1.312D 01	-3.402D 01
30.	-3.097D 00	-4.147D 00	-6.071D 00	-1.061D 01	-2.914D 01
300.	-2.320D 00	-3.228D 00	-4.598D 00	-8.429D 00	-2.440D 01
10000.	-1.686D 00	-1.937D 00	-2.897D 00	-5.492D 00	-1.770D 01

TABLE C.4-1
LOG OF THE BLANKETING OPACITY

T	6000.	8000.	11000.	17500.	50000.
	LAMBDA 204: 5554.99 ANGSTROMS				
PE					
3.	1.059D 00	4.626D-02	-1.209D 00	-3.681D-01	-5.297D 00
30.	2.050D 00	1.004D 00	-2.143D-01	4.435D-01	-3.147D 00
300.	2.972D 00	2.010D 00	7.364D-01	7.878D-01	-1.201D 00
10000.	3.656D 00	3.487D 00	2.540D 00	1.147D 00	1.020D 00
	LAMBDA 205: 5555.01 ANGSTROMS				
PE					
3.	-8.410D 00	-1.019D 01	-1.319D 01	-1.985D 01	-4.304D 01
30.	-7.576D 00	-8.845D 00	-1.126D 01	-1.695D 01	-3.804D 01
300.	-6.910D 00	-7.624D 00	-9.546D 00	-1.424D 01	-3.304D 01
10000.	-6.230D 00	-6.434D 00	-7.406D 00	-1.064D 01	-2.555D 01
	LAMBDA 206: 5593.94 ANGSTROMS				
PE					
3.	-5.548D 00	-7.192D 00	-1.044D 01	-1.595D 01	-3.648D 01
30.	-4.583D 00	-5.871D 00	-8.476D 00	-1.325D 01	-3.157D 01
300.	-3.777D 00	-4.787D 00	-6.642D 00	-1.086D 01	-2.676D 01
10000.	-3.126D 00	-3.435D 00	-4.445D 00	-7.654D 00	-2.003D 01
	LAMBDA 207: 5658.11 ANGSTROMS				
PE					
3.	-3.595D 00	-4.805D 00	-7.198D 00	-1.208D 01	-3.188D 01
30.	-2.828D 00	-3.813D 00	-5.748D 00	-9.665D 00	-2.695D 01
300.	-1.996D 00	-2.990D 00	-4.399D 00	-7.739D 00	-2.219D 01
10000.	-1.049D 00	-1.659D 00	-2.678D 00	-5.256D 00	-1.552D 01
	LAMBDA 208: 5698.51 ANGSTROMS				
PE					
3.	7.000D-01	2.428D-02	-9.807D-01	8.279D-01	-4.608D 00
30.	1.681D 00	7.057D-01	-9.799D-01	1.640D 00	-2.457D 00
300.	2.539D 00	1.317D 00	1.971D-02	1.984D 00	-5.117D-01
10000.	3.910D 00	2.872D 00	1.550D 00	2.042D 00	1.709D 00
	LAMBDA 209: 5698.53 ANGSTROMS				
PE					
3.	-1.030D 01	-1.170D 01	-1.454D 01	-2.099D 01	-4.409D 01
30.	-9.333D 00	-1.049D 01	-1.256D 01	-1.799D 01	-3.909D 01
300.	-8.400D 00	-9.327D 00	-1.085D 01	-1.519D 01	-3.409D 01
10000.	-7.207D 00	-7.839D 00	-8.852D 00	-1.172D 01	-2.651D 01
	LAMBDA 210: 5728.10 ANGSTROMS				
PE					
3.	-6.224D 00	-7.738D 00	-1.118D 01	-1.704D 01	-3.772D 01
30.	-5.250D 00	-6.507D 00	-9.192D 00	-1.416D 01	-3.274D 01
300.	-4.295D 00	-5.454D 00	-7.306D 00	-1.163D 01	-2.785D 01
10000.	-3.409D 00	-3.962D 00	-4.992D 00	-8.294D 00	-2.105D 01

TABLE C.4-1
LOG OF THE BLANKETING OPACITY

T	6000.	8000.	11000.	17500.	50000.
			LAMBDA 211: 5776.60 ANGSTROMS		
PE					
3.	-4.371D 00	-5.709D 00	-8.772D 00	-1.405D 01	-3.483D 01
30.	-3.422D 00	-4.547D 00	-6.846D 00	-1.146D 01	-2.998D 01
300.	-2.539D 00	-3.500D 00	-5.125D 00	-9.231D 00	-2.530D 01
10000.	-1.661D 00	-2.086D 00	-3.053D 00	-6.143D 00	-1.865D 01
			LAMBDA 212: 5806.99 ANGSTROMS		
PE					
3.	-1.698D-01	-1.134D 00	-2.065D 00	-2.631D-01	-3.773D-01
30.	8.108D-01	-1.913D-01	-1.102D 00	5.485D-01	6.223D-01
300.	1.666D 00	6.307D-01	-1.058D-01	8.928D-01	1.619D 00
10000.	2.305D 00	2.041D 00	1.307D 00	9.508D-01	3.056D 00
			LAMBDA 213: 5807.01 ANGSTROMS		
PE					
3.	-7.496D 01	-7.496D 01	-7.496D 01	-7.496D 01	-7.496D 01
30.	-7.496D 01	-7.495D 01	-7.496D 01	-7.496D 01	-7.495D 01
300.	-7.496D 01	-7.496D 01	-7.496D 01	-7.496D 01	-7.496D 01
10000.	-7.496D 01	-7.496D 01	-7.496D 01	-7.496D 01	-7.496D 01
			LAMBDA 214: 5834.57 ANGSTROMS		
PE					
3.	-9.883D 00	-1.112D 01	-1.397D 01	-2.056D 01	-4.490D 01
30.	-8.923D 00	-1.006D 01	-1.197D 01	-1.759D 01	-3.990D 01
300.	-8.081D 00	-9.035D 00	-1.030D 01	-1.471D 01	-3.490D 01
10000.	-7.432D 00	-7.550D 00	-8.549D 00	-1.118D 01	-2.729D 01
			LAMBDA 215: 5879.73 ANGSTROMS		
PE					
3.	-5.057D 00	-6.949D 00	-1.007D 01	-1.590D 01	-3.695D 01
30.	-4.174D 00	-5.621D 00	-8.158D 00	-1.304D 01	-3.224D 01
300.	-3.433D 00	-4.475D 0C	-6.495D 00	-1.069D 01	-2.756D 01
10000.	-2.686D 00	-3.055D 00	-4.272D 00	-7.487D 00	-2.098D 01
			LAMBDA 216: 5907.99 ANGSTROMS		
PE					
3.	1.752D 00	3.233D-01	-6.228D-01	1.159D-01	-8.521D-01
30.	2.752D 00	1.323D 00	9.402D-02	1.091D 00	1.476D-01
300.	3.748D 00	2.322D 00	1.053D 00	1.899D 00	1.145D 00
10000.	5.186D 00	3.837D 00	2.559D 00	2.281D 00	2.581D 00
			LAMBDA 217: 5908.01 ANGSTROMS		
PE					
3.	-7.496D 01	-7.496D 01	-7.496D 01	-7.496D 01	-7.496D 01
30.	-7.496D 01	-7.495D 01	-7.496D 01	-7.496D 01	-7.496D 01
300.	-7.496D 01	-7.496D 01	-7.496D 01	-7.496D 01	-7.496D 01
10000.	-7.496D 01	-7.496D 01	-7.496D 01	-7.496D 01	-7.496D 01

TABLE C.4-1
LOG OF THE BLANKETING OPACITY

T	6000.	8000.	11000.	17500.	50000.
			LAMBDA 218: 5935.85 ANGSTROMS		
PE					
3.	-9.527D 00	-1.073D 01	-1.385D 01	-2.048D 01	-4.415D 01
30.	-8.472D 00	-9.942D 00	-1.139D 01	-1.747D 01	-3.915D 01
300.	-7.663D 00	-8.709D 00	-1.004D 01	-1.464D 01	-3.415D 01
10000.	-6.699D 00	-7.147D 00	-7.957D 00	-1.109D 01	-2.656D 01
			LAMBDA 219: 5981.45 ANGSTROMS		
PE					
3.	-5.442D 00	-7.140D 00	-9.832D 00	-1.539D 01	-3.611D 01
30.	-4.555D 00	-5.879D 00	-7.930D 00	-1.283D 01	-3.119D 01
300.	-3.673D 00	-4.780D 00	-6.476D 00	-1.051D 01	-2.649D 01
10000.	-2.849D 00	-3.362D 00	-4.484D 00	-7.351D 00	-1.978D 01
			LAMBDA 220: 6009.99 ANGSTROMS		
PE					
3.	-9.321D-01	-1.307D 00	-2.151D 00	1.062D-01	-1.294D 01
30.	6.608D-02	-8.817D-01	-2.155D 00	9.178D-01	-9.262D 00
300.	1.042D 00	-2.550D-01	-1.474D 00	1.262D 00	-6.075D 00
10000.	2.092D 00	1.263D 00	-3.722D-02	1.320D 00	-1.878D 00
			LAMBDA 221: 6010.01 ANGSTROMS		
PE					
3.	-7.496D 01	-7.496D 01	-7.496D 01	-7.496D 01	-7.496D 01
30.	-7.496D 01	-7.496D 01	-7.496D 01	-7.496D 01	-7.496D 01
300.	-7.496D 01	-7.496D 01	-7.496D 01	-7.496D 01	-7.496D 01
10000.	-7.496D 01	-7.496D 01	-7.496D 01	-7.496D 01	-7.496D 01
			LAMBDA 222: 6035.15 ANGSTROMS		
PE					
3.	-9.359D 00	-1.122D 01	-1.368D 01	-2.077D 01	-4.530D 01
30.	-8.392D 00	-9.815D 00	-1.185D 01	-1.774D 01	-4.030D 01
300.	-7.635D 00	-8.580D 00	-1.033D 01	-1.477D 01	-3.530D 01
10000.	-6.562D 00	-7.087D 00	-8.157D 00	-1.106D 01	-2.768D 01
			LAMBDA 223: 6076.29 ANGSTROMS		
PE					
3.	-5.319D 00	-6.769D 00	-9.659D 00	-1.491D 01	-3.650D 01
30.	-4.415D 00	-5.621D 00	-7.760D 00	-1.238D 01	-3.156D 01
300.	-3.530D 00	-4.596D 00	-6.162D 00	-1.022D 01	-2.669D 01
10000.	-2.697D 00	-3.159D 00	-4.216D 00	-7.144D 00	-1.977D 01
			LAMBDA 224: 6101.99 ANGSTROMS		
PE					
3.	-2.209D-03	-8.670D-01	-1.521D 00	-3.002D 00	-1.410D 01
30.	9.785D-01	-3.326D-01	-5.258D-01	-1.695D 00	-1.207D 01
300.	1.834D 00	6.562D-01	4.239D-01	-6.487D-01	-1.009D 01
10000.	2.326D 00	2.066D 00	1.263D 00	8.765D-01	-7.261D 00

TABLE C.4-1
LOG OF THE BLANKETING OPACITY

T	6000.	8000.	11000.	17500.	50000.
	LAMBDA 225: 6102.01 ANGSTROMS				
PE					
3.	-7.496D 01	-7.496D 01	-7.496D 01	-7.496D 01	-7.496D 01
30.	-7.496D 01	-7.496D 01	-7.496D 01	-7.496D 01	-7.496D 01
300.	-7.496D 01	-7.496D 01	-7.496D 01	-7.496D 01	-7.496D 01
10000.	-7.496D 01	-7.496D 01	-7.496D 01	-7.496D 01	-7.496D 01
	LAMBDA 226: 6130.13 ANGSTROMS				
PE					
3.	-7.496D 01	-7.496D 01	-7.496D 01	-7.496D 01	-7.496D 01
30.	-7.496D 01	-7.496D 01	-7.496D 01	-7.496D 01	-7.496D 01
300.	-7.496D 01	-7.496D 01	-7.496D 01	-7.496D 01	-7.496D 01
10000.	-7.496D 01	-7.496D 01	-7.496D 01	-7.496D 01	-7.496D 01
	LAMBDA 227: 6176.18 ANGSTROMS				
PE					
3.	-4.979D 00	-6.432D 00	-8.839D 00	-1.375D 01	-3.474D 01
30.	-4.029D 00	-5.166D 00	-7.188D 00	-1.151D 01	-2.995D 01
300.	-3.383D 00	-4.186D 00	-5.671D 00	-9.384D 00	-2.530D 01
10000.	-2.720D 00	-3.024D 00	-3.852D 00	-6.379D 00	-1.866D 01
	LAMBDA 228: 6204.99 ANGSTROMS				
PE					
3.	7.340D-01	7.104D-01	1.351D-02	-6.028D-01	-1.092D 01
30.	1.745D 00	1.049D 00	1.008D 00	2.088D-01	-8.885D 00
300.	2.740D 00	1.364D 00	1.959D 00	8.441D-01	-6.405D 00
10000.	4.112D 00	2.939D 00	2.797D 00	2.369D 00	-2.209D 00
	LAMBDA 229: 6205.01 ANGSTROMS				
PE					
3.	-7.496D 01	-7.496D 01	-7.496D 01	-7.496D 01	-7.496D 01
30.	-7.496D 01	-7.496D 01	-7.496D 01	-7.496D 01	-7.496D 01
300.	-7.496D 01	-7.496D 01	-7.496D 01	-7.496D 01	-7.496D 01
10000.	-7.496D 01	-7.496D 01	-7.496D 01	-7.496D 01	-7.496D 01
	LAMBDA 230: 6234.12 ANGSTROMS				
PE					
3.	-8.924D 00	-1.028D 01	-1.339D 01	-2.050D 01	-4.463D 01
30.	-8.111D 00	-9.145D 00	-1.142D 01	-1.750D 01	-3.963D 01
300.	-7.689D 00	-8.074D 00	-9.696D 00	-1.456D 01	-3.463D 01
10000.	-7.417D 00	-6.962D 00	-7.647D 00	-1.082D 01	-2.703D 01
	LAMBDA 231: 6281.80 ANGSTROMS				
PE					
3.	-4.581D 00	-5.959D 00	-9.056D 00	-1.458D 01	-3.522D 01
30.	-4.024D 00	-4.650D 00	-7.170D 00	-1.200D 01	-3.049D 01
300.	-3.489D 00	-3.897D 00	-5.519D 00	-9.640D 00	-2.594D 01
10000.	-2.814D 00	-3.134D 00	-3.785D 00	-6.598D 00	-1.926D 01

TABLE C.4-1
LOG OF THE BLANKETING OPACITY

T	6000.	8000.	11000.	17500.	50000.
	LAMBDA 232: 6311.64 ANGSTROMS				
PE					
3.	6.615D-01	1.713D-01	-2.160D-01	-9.970D-01	-1.380D 01
30.	1.183D 00	7.153D-01	7.785D-01	6.296D-02	-1.012D 01
300.	2.039D 00	9.228D-01	1.729D 00	9.652D-01	-6.937D 00
10000.	2.535D 00	2.064D 00	2.558D 00	2.448D 00	-2.739D 00
	LAMBDA 233: 6311.66 ANGSTROMS				
PE					
3.	-7.496D 01	-7.496D 01	-7.496D 01	-7.496D 01	-7.496D 01
30.	-7.496D 01	-7.496D 01	-7.496D 01	-7.496D 01	-7.496D 01
300.	-7.496D 01	-7.496D 01	-7.496D 01	-7.496D 01	-7.496D 01
10000.	-7.496D 01	-7.496D 01	-7.496D 01	-7.496D 01	-7.496D 01
	LAMBDA 234: 6346.88 ANGSTROMS				
PE					
3.	-1.017D 01	-1.313D 01	-1.706D 01	-2.527D 01	-4.889D 01
30.	-9.176D 00	-1.115D 01	-1.460D 01	-2.165D 01	-4.389D 01
300.	-8.333D 00	-9.589D 00	-1.251D 01	-1.849D 01	-3.889D 01
10000.	-7.659D 00	-7.810D 00	-9.505D 00	-1.404D 01	-3.127D 01
	LAMBDA 235: 6404.72 ANGSTROMS				
PE					
3.	-5.361D 00	-6.777D 00	-9.315D 00	-1.408D 01	-3.588D 01
30.	-4.436D 00	-5.542D 00	-7.476D 00	-1.177D 01	-3.097D 01
300.	-3.869D 00	-4.501D 00	-5.935D 00	-9.704D 00	-2.606D 01
10000.	-3.347D 00	-3.390D 00	-4.045D 00	-6.660D 00	-1.910D 01
	LAMBDA 236: 6440.99 ANGSTROMS				
PE					
3.	6.455D-01	1.650D-02	-2.251D 00	-8.936D-01	-2.312D 00
30.	1.511D 00	6.979D-01	-1.252D 00	-8.197D-02	-6.349D-01
300.	2.507D 00	1.263D 00	-2.674D-01	2.623D-01	5.522D-01
10000.	3.878D 00	2.839D 00	1.453D 00	3.204D-01	1.703D 00
	LAMBDA 237: 6441.01 ANGSTROMS				
PE					
3.	-7.496D 01	-7.495D 01	-7.496D 01	-7.496D 01	-7.496D 01
30.	-7.496D 01	-7.496D 01	-7.496D 01	-7.496D 01	-7.496D 01
300.	-7.496D 01	-7.496D 01	-7.496D 01	-7.496D 01	-7.496D 01
10000.	-7.496D 01	-7.495D 01	-7.496D 01	-7.496D 01	-7.496D 01
	LAMBDA 238: 6463.58 ANGSTROMS				
PE					
3.	-9.288D 00	-1.158D 01	-1.470D 01	-2.008D 01	-4.439D 01
30.	-8.327D 00	-9.833D 00	-1.270D 01	-1.707D 01	-3.939D 01
300.	-7.624D 00	-8.467D 00	-1.075D 01	-1.443D 01	-3.439D 01
10000.	-7.000D 00	-7.009D 00	-8.119D 00	-1.110D 01	-2.678D 01

TABLE C.4-1
LOG OF THE BLANKETING OPACITY

T	6000.	8000.	11000.	17500.	50000.
			LAMBDA 239: 6500.44 ANGSTROMS		
PE					
3.	-4.636D 00	-6.789D 00	-9.901D 00	-1.377D 01	-3.289D 01
30.	-3.648D 00	-5.167D 00	-7.950D 00	-1.171D 01	-2.790D 01
300.	-2.810D 00	-3.865D 00	-6.103D 00	-9.663D 00	-2.303D 01
10000.	-2.107D 00	-2.490D 00	-3.622D 00	-6.784D 00	-1.637D 01
			LAMBDA 240: 6523.43 ANGSTROMS		
PE					
3.	5.045D-01	7.951D-02	-6.184D-01	9.962D-02	-6.545D 00
30.	1.515D 00	4.211D-01	3.763D-01	9.112D-01	-3.868D 00
300.	2.511D 00	1.257D 00	1.327D 00	1.256D 00	-1.681D 00
10000.	3.882D 00	2.842D 00	2.157D 00	1.737D 00	9.926D-01
			LAMBDA 241: 6523.45 ANGSTROMS		
PE					
3.	-7.496D 01	-7.496D 01	-7.496D 01	-7.496D 01	-7.496D 01
30.	-7.496D 01	-7.495D 01	-7.496D 01	-7.496D 01	-7.496D 01
300.	-7.496D 01	-7.496D 01	-7.496D 01	-7.496D 01	-7.496D 01
10000.	-7.496D 01	-7.496D 01	-7.496D 01	-7.496D 01	-7.496D 01
			LAMBDA 242: 6561.43 ANGSTROMS		
PE					
3.	-7.496D 01	-7.496D 01	-7.496D 01	-7.496D 01	-7.496D 01
30.	-7.496D 01	-7.495D 01	-7.496D 01	-7.496D 01	-7.496D 01
300.	-7.496D 01	-7.496D 01	-7.496D 01	-7.496D 01	-7.496D 01
10000.	-7.496D 01	-7.496D 01	-7.496D 01	-7.496D 01	-7.496D 01
			LAMBDA 243: 6623.83 ANGSTROMS		
PE					
3.	-6.946D 00	-8.147D 00	-1.093D 01	-1.662D 01	-3.815D 01
30.	-6.171D 00	-7.014D 00	-9.171D 00	-1.422D 01	-3.322D 01
300.	-5.263D 00	-5.885D 00	-7.409D 00	-1.180D 01	-2.826D 01
10000.	-4.251D 00	-4.690D 00	-5.354D 00	-8.422D 00	-2.114D 01
			LAMBDA 244: 6662.99 ANGSTROMS		
PE					
3.	7.921D-01	1.329D-01	1.279D 00	1.444D 00	-2.665D 00
30.	8.551D-01	8.143D-01	1.280D 00	2.419D 00	-1.666D 00
300.	1.711D 00	1.022D 00	1.276D 00	3.227D 00	-6.685D-01
10000.	2.202D 00	1.772D 00	1.502D 00	3.609D 00	7.682D-01
			LAMBDA 245: 6663.01 ANGSTROMS		
PE					
3.	-7.496D 01	-7.496D 01	-7.496D 01	-7.496D 01	-7.496D 01
30.	-7.496D 01	-7.495D 01	-7.496D 01	-7.496D 01	-7.496D 01
300.	-7.496D 01	-7.496D 01	-7.496D 01	-7.496D 01	-7.496D 01
10000.	-7.496D 01	-7.496D 01	-7.496D 01	-7.496D 01	-7.496D 01

TABLE C.4-1
LOG OF THE BLANKETING OPACITY

T	6000.	8000.	11000.	17500.	50000.
		LAMBDA 246: 6690.35 ANGSTROMS			
PE					
3.	-1.086D 01	-1.389D 01	-1.504D 01	-2.149D 01	-4.569D 01
30.	-9.798D 00	-1.193D 01	-1.455D 01	-1.837D 01	-4.059D 01
300.	-8.973D 00	-1.016D 01	-1.311D 01	-1.540D 01	-3.569D 01
10000.	-8.045D 00	-8.381D 00	-1.013D 01	-1.135D 01	-2.808D 01
		LAMBDA 247: 6735.06 ANGSTROMS			
PE					
3.	-6.473D 00	-7.939D 00	-1.074D 01	-1.604D 01	-3.823D 01
30.	-5.561D 00	-6.784D 00	-8.956D 00	-1.336D 01	-3.329D 01
300.	-4.676D 00	-5.601D 00	-7.351D 00	-1.108D 01	-2.834D 01
10000.	-3.909D 00	-4.168D 00	-5.444D 00	-7.963D 00	-2.148D 01
		LAMBDA 248: 6762.99 ANGSTROMS			
PE					
3.	1.614D-01	-1.310D 00	-2.966D 00	4.918D-01	-6.195D 00
30.	1.139D 00	-3.296D-01	-2.426D 00	7.986D-01	-4.195D 00
300.	1.995D 00	6.416D-01	-8.965D-01	8.454D-01	-2.198D 00
10000.	2.695D 00	2.049D 00	7.619D-01	8.477D-01	7.615D-01
		LAMBDA 249: 6763.01 ANGSTROMS			
PE					
3.	-7.496D 01	-7.496D 01	-7.496D 01	-7.496D 01	-7.496D 01
30.	-7.496D 01	-7.496D 01	-7.496D 01	-7.496D 01	-7.496D 01
300.	-7.496D 01	-7.496D 01	-7.496D 01	-7.496D 01	-7.496D 01
10000.	-7.496D 01	-7.496D 01	-7.496D 01	-7.496D 01	-7.496D 01
		LAMBDA 250: 6790.35 ANGSTROMS			
PE					
3.	-1.077D 01	-1.251D 01	-1.559D 01	-2.366D 01	-4.697D 01
30.	-9.722D 00	-1.129D 01	-1.370D 01	-2.009D 01	-4.197D 01
300.	-8.732D 00	-9.885D 00	-1.168D 01	-1.696D 01	-3.697D 01
10000.	-7.539D 00	-8.229D 00	-9.582D 00	-1.248D 01	-2.936D 01
		LAMBDA 251: 6835.06 ANGSTROMS			
PE					
3.	-7.451D 00	-8.636D 00	-1.094D 01	-1.725D 01	-3.979D 01
30.	-6.568D 00	-7.513D 00	-9.109D 00	-1.437D 01	-3.498D 01
300.	-5.846D 00	-6.546D 00	-7.620D 00	-1.185D 01	-3.010D 01
10000.	-5.060D 00	-5.297D 00	-5.842D 00	-8.544D 00	-2.254D 01
		LAMBDA 252: 6862.99 ANGSTROMS			
PE					
3.	-3.258D-01	-1.638D 00	-1.132D 00	9.692D-02	-7.597D 00
30.	6.416D-01	-6.343D-01	-1.131D 00	1.072D 00	-5.597D 00
300.	1.405D 00	3.620D-01	-8.031D-01	1.880D 00	-3.600D 00
10000.	1.721D 00	1.758D 00	8.220D-01	2.262D 00	-6.406D-01

TABLE C.4-1
LOG OF THE BLANKETING OPACITY

T	6000.	8000.	11000.	17500.	50000.
	LAMBDA 253: 6863.01 ANGSTROMS				
PE					
3.	-7.496D 01	-7.496D 01	-7.496D 01	-7.496D 01	-7.496D 01
30.	-7.496D 01	-7.496D 01	-7.496D 01	-7.496D 01	-7.496D 01
300.	-7.496D 01	-7.496D 01	-7.496D 01	-7.496D 01	-7.496D 01
10000.	-7.496D 01	-7.495D 01	-7.496D 01	-7.496D 01	-7.496D 01
	LAMBDA 254: 6890.53 ANGSTROMS				
PE					
3.	-7.496D 01	-7.496D 01	-7.496D 01	-7.496D 01	-7.496D 01
30.	-7.496D 01	-7.496D 01	-7.496D 01	-7.496D 01	-7.496D 01
300.	-7.496D 01	-7.496D 01	-7.496D 01	-7.496D 01	-7.496D 01
10000.	-7.496D 01	-7.496D 01	-7.496D 01	-7.496D 01	-7.496D 01
	LAMBDA 255: 6935.54 ANGSTROMS				
PE					
3.	-6.360D 00	-7.998D 00	-1.070D 01	-1.685D 01	-3.758D 01
30.	-5.458D 00	-6.615D 00	-8.756D 00	-1.396D 01	-3.259D 01
300.	-4.565D 00	-5.531D 00	-7.147D 00	-1.130D 01	-2.772D 01
10000.	-3.680D 00	-4.062D 00	-5.202D 00	-7.908D 00	-2.101D 01
	LAMBDA 256: 6963.65 ANGSTROMS				
PE					
3.	-5.267D-01	-1.288D 00	-1.984D 00	8.324D-02	-6.960D 00
30.	4.538D-01	-9.050D-01	-9.872D-01	3.900D-01	-4.960D 00
300.	1.309D 00	-7.681D-02	-1.923D-02	4.368D-01	-2.963D 00
10000.	1.801D 00	1.308D 00	9.619D-01	4.478D-01	-3.685D-03
	LAMBDA 257: 6963.67 ANGSTROMS				
PE					
3.	-7.496D 01	-7.496D 01	-7.496D 01	-7.496D 01	-7.496D 01
30.	-7.496D 01	-7.496D 01	-7.496D 01	-7.496D 01	-7.496D 01
300.	-7.496D 01	-7.496D 01	-7.496D 01	-7.496D 01	-7.496D 01
10000.	-7.496D 01	-7.496D 01	-7.496D 01	-7.496D 01	-7.496D 01
	LAMBDA 258: 6993.28 ANGSTROMS				
PE					
3.	-7.496D 01	-7.496D 01	-7.496D 01	-7.496D 01	-7.496D 01
30.	-7.496D 01	-7.496D 01	-7.496D 01	-7.496D 01	-7.496D 01
300.	-7.496D 01	-7.496D 01	-7.496D 01	-7.496D 01	-7.496D 01
10000.	-7.496D 01	-7.496D 01	-7.496D 01	-7.496D 01	-7.496D 01
	LAMBDA 259: 7041.72 ANGSTROMS				
PE					
3.	-6.076D 00	-7.502D 00	-1.045D 01	-1.570D 01	-3.705D 01
30.	-5.120D 00	-6.305D 00	-8.557D 00	-1.312D 01	-3.216D 01
300.	-4.253D 00	-5.254D 00	-6.840D 00	-1.090D 01	-2.740D 01
10000.	-3.458D 00	-3.816D 00	-4.853D 00	-7.795D 00	-2.069D 01

TABLE C.4-1
LOG OF THE BLANKETING OPACITY

T	6000.	8000.	11000.	17500.	50000.
	LAMBDA 260: 7071.99 ANGSTROMS				
PE					
3.	-6.454D-01	1.653D-01	-4.890D-01	-1.373D 00	-1.400D 01
30.	3.353D-01	5.037D-01	5.056D-01	-5.611D-01	-1.032D 01
300.	1.191D 00	5.582D-01	1.456D 00	3.838D-01	-7.132D 00
10000.	1.683D 00	1.201D 00	2.295D 00	1.909D 00	-2.935D 00
	LAMBDA 261: 7072.01 ANGSTROMS				
PE					
3.	-7.496D 01	-7.496D 01	-7.496D 01	-7.496D 01	-7.496D 01
30.	-7.496D 01	-7.496D 01	-7.496D 01	-7.496D 01	-7.496D 01
300.	-7.496D 01	-7.496D 01	-7.496D 01	-7.496D 01	-7.496D 01
10000.	-7.496D 01	-7.496D 01	-7.496D 01	-7.496D 01	-7.496D 01
	LAMBDA 262: 7109.62 ANGSTROMS				
PE					
3.	-7.496D 01	-5.556D 01	-3.282D 01	-2.600D 01	-4.943D 01
30.	-7.496D 01	-5.828D 01	-3.483D 01	-2.243D 01	-4.443D 01
300.	-7.496D 01	-6.121D 01	-3.686D 01	-1.929D 01	-3.943D 01
10000.	-7.496D 01	-6.578D 01	-4.045D 01	-1.714D 01	-3.182D 01
	LAMBDA 263: 7171.32 ANGSTROMS				
PE					
3.	-4.611D 00	-5.890D 00	-8.598D 00	-1.366D 01	-3.534D 01
30.	-3.666D 00	-4.779D 00	-6.701D 00	-1.133D 01	-3.044D 01
300.	-2.867D 00	-3.781D 00	-5.150D 00	-9.225D 00	-2.551D 01
10000.	-2.463D 00	-2.415D 00	-3.365D 00	-6.206D 00	-1.860D 01
	LAMBDA 264: 7209.99 ANGSTROMS				
PE					
3.	3.568D-01	-2.197D-01	-5.747D-01	-1.759D 00	-1.847D 00
30.	1.337D 00	1.481D-01	4.199D-01	-4.521D-01	-1.699D-01
300.	2.193D 00	1.137D 00	1.371D 00	5.947D-01	1.017D 00
10000.	3.353D 00	2.547D 00	2.209D 00	2.120D 00	2.168D 00
	LAMBDA 265: 7210.01 ANGSTROMS				
PE					
3.	-7.496D 01	-7.496D 01	-7.496D 01	-7.496D 01	-7.496D 01
30.	-7.496D 01	-7.495D 01	-7.496D 01	-7.496D 01	-7.496D 01
300.	-7.496D 01	-7.496D 01	-7.496D 01	-7.496D 01	-7.496D 01
10000.	-7.496D 01	-7.496D 01	-7.496D 01	-7.496D 01	-7.496D 01
	LAMBDA 266: 7242.51 ANGSTROMS				
PE					
3.	-1.056D 01	-1.280D 01	-1.635D 01	-2.418D 01	-4.709D 01
30.	-9.618D 00	-1.089D 01	-1.397D 01	-2.061D 01	-4.209D 01
300.	-8.700D 00	-9.690D 00	-1.190D 01	-1.747D 01	-3.709D 01
10000.	-7.474D 00	-8.079D 00	-9.286D 00	-1.297D 01	-2.948D 01

TABLE C.4-1
LOG OF THE BLANKETING OPACITY

T	6000.	8000.	11000.	17500.	50000.
		LAMBDA 267: 7295.71 ANGSTROMS			
PE					
3.	-6.016D 00	-7.023D 00	-1.000D 01	-1.519D 01	-3.649D 01
30.	-5.029D 00	-5.976D 00	-8.065D 00	-1.249D 01	-3.153D 01
300.	-4.115D 00	-4.971D 00	-6.271D 00	-1.025D 01	-2.673D 01
10000.	-3.307D 00	-3.511D 00	-4.273D 00	-7.193D 00	-1.992D 01
		LAMBDA 268: 7328.99 ANGSTROMS			
PE					
3.	-4.857D-01	-2.130D-01	7.389D-01	1.223D 00	-1.248D 01
30.	5.253D-01	1.253D-01	7.396D-01	2.198D 00	-9.482D 00
300.	1.521D 00	3.607D-01	1.078D 00	3.006D 00	-6.485D 00
10000.	2.892D 00	1.936D 00	1.917D 00	3.388D 00	-2.003D 00
		LAMBDA 269: 7329.01 ANGSTROMS			
PE					
3.	-7.496D 01	-7.496D 01	-7.496D 01	-7.496D 01	-7.496D 01
30.	-7.496D 01	-7.496D 01	-7.496D 01	-7.496D 01	-7.496D 01
300.	-7.496D 01	-7.496D 01	-7.496D 01	-7.496D 01	-7.496D 01
10000.	-7.496D 01	-7.496D 01	-7.496D 01	-7.496D 01	-7.496D 01
		LAMBDA 270: 7358.59 ANGSTROMS			
PE					
3.	-1.181D 01	-1.480D 01	-1.839D 01	-2.626D 01	-4.953D 01
30.	-1.070D 01	-1.283D 01	-1.600D 01	-2.269D 01	-4.453D 01
300.	-9.688D 00	-1.102D 01	-1.393D 01	-1.955D 01	-3.953D 01
10000.	-8.215D 00	-9.118D 00	-1.093D 01	-1.505D 01	-3.192D 01
		LAMBDA 271: 7406.96 ANGSTROMS			
PE					
3.	-4.888D 00	-6.104D 00	-8.768D 00	-1.410D 01	-3.586D 01
30.	-3.902D 00	-5.073D 00	-6.859D 00	-1.153D 01	-3.099D 01
300.	-3.078D 00	-4.053D 00	-5.317D 00	-9.440D 00	-2.603D 01
10000.	-2.505D 00	-2.627D 00	-3.588D 00	-6.398D 00	-1.898D 01
		LAMBDA 272: 7437.18 ANGSTROMS			
PE					
3.	5.102D-02	-3.358D-01	-1.291D 00	-3.855D 00	-2.279D 01
30.	1.018D 00	4.755D-02	-2.950D-01	-2.043D 00	-1.811D 01
300.	1.782D 00	8.756D-01	6.729D-01	-6.988D-01	-1.392D 01
10000.	2.268D 00	2.271D 00	1.654D 00	8.821D-01	-8.205D 00
		LAMBDA 273: 7437.20 ANGSTROMS			
PE					
3.	-1.138D 01	-1.272D 01	-1.415D 01	-2.031D 01	-4.429D 01
30.	-1.037D 01	-1.152D 01	-1.270D 01	-1.734D 01	-3.929D 01
300.	-9.429D 00	-1.041D 01	-1.158D 01	-1.472D 01	-3.429D 01
10000.	-8.630D 00	-8.809D 00	-9.916D 00	-1.167D 01	-2.673D 01

TABLE C.4-1
LOG OF THE BLANKETING OPACITY

T	6000.	8000.	11000.	17500.	50000.
	LAMBDA 274: 7478.27 ANGSTROMS				
PE					
3.	-8.125D 00	-9.221D 00	-1.192D 01	-1.788D 01	-4.191D 01
30.	-7.389D 00	-8.171D 00	-1.007D 01	-1.506D 01	-3.691D 01
300.	-6.756D 00	-7.109D 00	-8.476D 00	-1.255D 01	-3.191D 01
10000.	-6.334D 00	-5.709D 00	-6.610D 00	-9.311D 00	-2.431D 01
	LAMBDA 275: 7545.70 ANGSTROMS				
PE					
3.	-4.200D 00	-5.249D 00	-7.923D 00	-1.315D 01	-3.494D 01
30.	-3.255D 00	-4.281D 00	-6.037D 00	-1.069D 01	-2.997D 01
300.	-2.417D 00	-3.333D 00	-4.493D 00	-8.569D 00	-2.503D 01
10000.	-1.920D 00	-1.952D 00	-2.793D 00	-5.532D 00	-1.813D 01
	LAMBDA 276: 7587.99 ANGSTROMS				
PE					
3.	5.158D-01	4.469D-01	-5.077D-01	-1.673D 00	-1.870D 01
30.	1.497D 00	8.302D-01	4.887D-01	-3.663D-01	-1.455D 01
300.	2.352D 00	1.314D 00	1.457D 00	6.805D-01	-1.060D 01
10000.	2.844D 00	2.724D 00	2.438D 00	2.206D 00	-5.335D 00
	LAMBDA 277: 7588.01 ANGSTROMS				
PE					
3.	-7.496D 01	-7.496D 01	-7.496D 01	-7.496D 01	-7.496D 01
30.	-7.496D 01	-7.496D 01	-7.496D 01	-7.496D 01	-7.496D 01
300.	-7.496D 01	-7.496D 01	-7.496D 01	-7.496D 01	-7.496D 01
10000.	-7.496D 01	-7.496D 01	-7.496D 01	-7.496D 01	-7.496D 01
	LAMBDA 278: 7632.10 ANGSTROMS				
PE					
3.	-1.018D 01	-1.257D 01	-1.537D 01	-2.090D 01	-4.394D 01
30.	-9.180D 00	-1.071D 01	-1.337D 01	-1.770D 01	-3.894D 01
300.	-8.234D 00	-9.194D 00	-1.137D 01	-1.484D 01	-3.394D 01
10000.	-7.085D 00	-7.700D 00	-8.731D 00	-1.154D 01	-2.639D 01
	LAMBDA 279: 7704.53 ANGSTROMS				
PE					
3.	-5.103D 00	-6.464D 00	-9.293D 00	-1.435D 01	-3.607D 01
30.	-4.113D 00	-5.275D 00	-7.380D 00	-1.179D 01	-3.113D 01
300.	-3.347D 00	-4.243D 00	-5.655D 00	-9.564D 00	-2.622D 01
10000.	-2.829D 00	-2.848D 00	-3.754D 00	-6.520D 00	-1.912D 01
	LAMBDA 280: 7749.99 ANGSTROMS				
PE					
3.	8.055D-02	-1.115D 00	-2.301D 00	-5.126D 00	-2.886D 01
30.	1.080D 00	-1.118D-01	-1.301D 00	-3.223D 00	-2.387D 01
300.	2.079D 00	8.844D-01	-2.796D-01	-1.729D 00	-1.893D 01
10000.	3.576D 00	2.344D 00	1.346D 00	-8.990D-02	-1.206D 01

TABLE C.4-1
LOG OF THE BLANKETING OPACITY

T	6000.	8000.	11000.	17500.	50000.
	LAMBDA 281: 7750.01 ANGSTROMS				
PE					
3.	-1.241D 01	-1.534D 01	-1.893D 01	-2.677D 01	-4.977D 01
30.	-1.134D 01	-1.337D 01	-1.658D 01	-2.324D 01	-4.477D 01
300.	-1.033D 01	-1.163D 01	-1.452D 01	-2.013D 01	-3.977D 01
10000.	-9.357D 00	-9.810D 00	-1.154D 01	-1.564D 01	-3.215D 01
	LAMBDA 282: 7788.20 ANGSTROMS				
PE					
3.	-8.725D 00	-1.003D 01	-1.274D 01	-1.934D 01	-4.295D 01
30.	-7.808D 00	-8.803D 00	-1.087D 01	-1.635D 01	-3.795D 01
300.	-7.091D 00	-7.760D 00	-9.220D 00	-1.356D 01	-3.295D 01
10000.	-6.685D 00	-6.398D 00	-7.229D 00	-1.014D 01	-2.535D 01
	LAMBDA 283: 7850.80 ANGSTROMS				
PE					
3.	-4.875D 00	-5.978D 00	-8.554D 00	-1.361D 01	-3.550D 01
30.	-3.904D 00	-4.954D 00	-6.681D 00	-1.118D 01	-3.053D 01
300.	-3.113D 00	-3.980D 00	-5.162D 00	-9.089D 00	-2.560D 01
10000.	-2.619D 00	-2.605D 00	-3.465D 00	-6.098D 00	-1.869D 01
	LAMBDA 284: 7889.99 ANGSTROMS				
PE					
3.	1.005D 00	2.473D 00	1.503D 00	-2.902D-01	-1.825D 01
30.	1.196D 00	2.811D 00	2.497D 00	1.017D 00	-1.410D 01
300.	2.052D 00	2.866D 00	3.448D 00	2.063D 00	-1.016D 01
10000.	2.543D 00	2.872D 00	4.287D 00	3.589D 00	-4.891D 00
	LAMBDA 285: 7890.01 ANGSTROMS				
PE					
3.	-7.496D 01	-7.496D 01	-7.496D 01	-7.496D 01	-7.496D 01
30.	-7.496D 01	-7.495D 01	-7.496D 01	-7.496D 01	-7.496D 01
300.	-7.496D 01	-7.496D 01	-7.496D 01	-7.496D 01	-7.496D 01
10000.	-7.496D 01	-7.495D 01	-7.496D 01	-7.496D 01	-7.496D 01
	LAMBDA 286: 7932.25 ANGSTROMS				
PE					
3.	-8.834D 00	-9.909D 00	-1.199D 01	-1.764D 01	-4.200D 01
30.	-7.855D 00	-8.876D 00	-1.033D 01	-1.480D 01	-3.700D 01
300.	-7.049D 00	-7.871D 00	-8.966D 00	-1.242D 01	-3.200D 01
10000.	-6.181D 00	-6.426D 00	-7.261D 00	-9.408D 00	-2.444D 01
	LAMBDA 287: 8001.55 ANGSTROMS				
PE					
3.	-4.628D 00	-5.559D 00	-8.229D 00	-1.347D 01	-3.529D 01
30.	-3.690D 00	-4.522D 00	-6.332D 00	-1.097D 01	-3.033D 01
300.	-2.878D 00	-3.545D 00	-4.797D 00	-8.844D 00	-2.540D 01
10000.	-2.404D 00	-2.352D 00	-3.071D 00	-5.806D 00	-1.838D 01

TABLE C.4-1
LOG OF THE BLANKETING OPACITY

T	6000.	8000.	11000.	17500.	50000.
LAMBDA 288: 8044.99 ANGSTROMS					
PE					
3.	2.474D-01	1.275D 00	6.207D-01	-8.594D-01	-1.838D 01
30.	1.228D 00	1.613D 00	1.615D 00	4.474D-01	-1.423D 01
300.	2.084D 00	1.667D 00	2.566D 00	1.494D 00	-1.028D 01
10000.	2.575D 00	2.492D 00	3.405D 00	3.019D 00	-5.016D 00
LAMBDA 289: 8045.01 ANGSTROMS					
PE					
3.	-7.496D 01	-7.496D 01	-7.496D 01	-7.496D 01	-7.496D 01
30.	-7.496D 01	-7.496D 01	-7.496D 01	-7.496D 01	-7.496D 01
300.	-7.496D 01	-7.496D 01	-7.496D 01	-7.496D 01	-7.496D 01
10000.	-7.496D 01	-7.496D 01	-7.496D 01	-7.496D 01	-7.496D 01
LAMBDA 290: 8088.83 ANGSTROMS					
PE					
3.	-7.496D 01	-7.496D 01	-7.496D 01	-7.496D 01	-7.496D 01
30.	-7.496D 01	-7.496D 01	-7.496D 01	-7.496D 01	-7.496D 01
300.	-7.496D 01	-7.496D 01	-7.496D 01	-7.496D 01	-7.496D 01
10000.	-7.496D 01	-7.495D 01	-7.496D 01	-7.496D 01	-7.496D 01
LAMBDA 291: 8160.76 ANGSTROMS					
PE					
3.	-4.484D 00	-5.565D 00	-8.113D 00	-1.345D 01	-3.530D 01
30.	-3.511D 00	-4.532D 00	-6.296D 00	-1.088D 01	-3.030D 01
300.	-2.652D 00	-3.548D 00	-4.805D 00	-8.680D 00	-2.536D 01
10000.	-2.107D 00	-2.154D 00	-3.096D 00	-5.774D 00	-1.834D 01
LAMBDA 292: 8205.86 ANGSTROMS					
PE					
3.	1.005D 00	4.607D-02	-8.802D-01	-1.966D 00	-1.172D 01
30.	2.005D 00	1.025D 00	1.196D-01	-9.652D-01	-9.685D 00
300.	3.001D 00	2.024D 00	1.119D 00	3.476D-02	-7.706D 00
10000.	4.439D 00	3.539D 00	2.640D 00	1.557D 00	-4.576D 00
LAMBDA 293: 8205.88 ANGSTROMS					
PE					
3.	-7.496D 01	-7.496D 01	-7.496D 01	-7.496D 01	-7.496D 01
30.	-7.496D 01	-7.496D 01	-7.496D 01	-7.496D 01	-7.496D 01
300.	-7.496D 01	-7.496D 01	-7.496D 01	-7.496D 01	-7.496D 01
10000.	-7.496D 01	-7.496D 01	-7.496D 01	-7.496D 01	-7.496D 01
LAMBDA 294: 8251.94 ANGSTROMS					
PE					
3.	-7.496D 01	-7.496D 01	-7.496D 01	-7.496D 01	-7.496D 01
30.	-7.496D 01	-7.496D 01	-7.496D 01	-7.496D 01	-7.496D 01
300.	-7.496D 01	-7.496D 01	-7.496D 01	-7.496D 01	-7.496D 01
10000.	-7.496D 01	-7.496D 01	-7.496D 01	-7.496D 01	-7.496D 01

TABLE C.4-1
LOG OF THE BLANKETING OPACITY

T	6000.	8000.	11000.	17500.	50000.

LAMBDA 295: 8327.56 ANGSTROMS

PE					
3.	-5.250D 00	-6.562D 00	-9.373D 00	-1.446D 01	-3.568D 01
30.	-4.346D 00	-5.409D 00	-7.435D 00	-1.200D 01	-3.070D 01
300.	-3.510D 00	-4.321D 00	-5.812D 00	-9.806D 00	-2.578D 01
10000.	-2.843D 00	-2.924D 00	-3.849D 00	-6.696D 00	-1.881D 01

LAMBDA 296: 8374.99 ANGSTROMS

PE					
3.	6.589D-01	9.058D-01	4.861D-03	-1.212D 00	-1.792D 01
30.	1.517D 00	1.400D 00	9.995D-01	9.526D-02	-1.439D 01
300.	2.373D 00	2.051D 00	1.950D 00	1.142D 00	-1.045D 01
10000.	2.865D 00	2.776D 00	2.897D 00	2.667D 00	-5.179D 00

LAMBDA 297: 8375.01 ANGSTROMS

PE					
3.	-1.000D 02	-1.000D 02	-1.000D 02	-1.000D 02	-1.000D 02
30.	-1.000D 02	-1.000D 02	-1.000D 02	-1.000D 02	-1.000D 02
300.	-1.000D 02	-1.000D 02	-1.000D 02	-1.000D 02	-1.000D 02
10000.	-1.000D 02	-1.000D 02	-1.000D 02	-1.000D 02	-1.000D 02

LAMBDA 298: 9492.43 ANGSTROMS

PE					
3.	-1.000D 02	-1.000D 02	-1.000D 02	-1.000D 02	-1.000D 02
30.	-1.000D 02	-1.000D 02	-1.000D 02	-1.000D 02	-1.000D 02
300.	-1.000D 02	-1.000D 02	-1.000D 02	-1.000D 02	-1.000D 02
10000.	-1.000D 02	-1.000D 02	-1.000D 02	-1.000D 02	-1.000D 02

LAMBDA 299:12105.90 ANGSTROMS

PE					
3.	-1.000D 02	-1.000D 02	-1.000D 02	-1.000D 02	-1.000D 02
30.	-1.000D 02	-1.000D 02	-1.000D 02	-1.000D 02	-1.000D 02
300.	-1.000D 02	-1.000D 02	-1.000D 02	-1.000D 02	-1.000D 02
10000.	-1.000D 02	-1.000D 02	-1.000D 02	-1.000D 02	-1.000D 02

LAMBDA 300:14588.20 ANGSTROMS

PE					
3.	-1.000D 02	-1.000D 02	-1.000D 02	-1.000D 02	-1.000D 02
30.	-1.000D 02	-1.000D 02	-1.000D 02	-1.000D 02	-1.000D 02
300.	-1.000D 02	-1.000D 02	-1.000D 02	-1.000D 02	-1.000D 02
10000.	-1.000D 02	-1.000D 02	-1.000D 02	-1.000D 02	-1.000D 02

TABLE C.4-2
LOG OF THE STATISTICAL UV BLANKETING OPACITY

LAMBDA 1: 130.68 ANGSTROMS

PE \ T	6000.	8000.	11000.	17500.	50000.
3.	-2.227D 01	-1.858D 01	-1.559D 01	-8.620D 00	-1.793D 01
30.	-2.327D 01	-2.067D 01	-1.685D 01	-1.087D 01	-1.838D 01
300.	-2.420D 01	-2.343D 01	-1.969D 01	-1.391D 01	-1.927D 01
10000.	-2.570D 01	-2.455D 01	-2.444D 01	-2.126D 01	-2.027D 01

LAMBDA 2: 151.63 ANGSTROMS

PE \ T	6000.	8000.	11000.	17500.	50000.
3.	3.774D 00	6.990D 00	7.680D 00	1.182D 01	-6.775D 00
30.	3.127D 00	5.492D 00	7.776D 00	1.075D 01	-3.850D 00
300.	2.808D 00	2.964D 00	6.181D 00	9.027D 00	-2.498D 00
10000.	1.761D 00	2.309D 00	2.303D 00	3.706D 00	-1.509D 00

LAMBDA 3: 204.75 ANGSTROMS

PE \ T	6000.	8000.	11000.	17500.	50000.
3.	5.033D 00	7.679D 00	7.610D 00	-7.179D 00	-5.186D 01
30.	4.650D 00	6.561D 00	8.763D 00	-1.816D 00	-4.595D 01
300.	4.578D 00	4.502D 00	7.398D 00	1.712D 00	-4.019D 01
10000.	4.193D 00	4.358D 00	4.024D 00	2.615D 00	-3.056D 01

LAMBDA 4: 261.34 ANGSTROMS

PE \ T	6000.	8000.	11000.	17500.	50000.
3.	7.923D 00	8.838D 00	6.558D 00	5.321D-01	2.665D 00
30.	7.307D 00	8.250D 00	7.927D 00	6.913D-01	3.193D 00
300.	7.240D 00	7.508D 00	8.336D 00	1.426D 00	3.652D 00
10000.	6.908D 00	6.526D 00	7.423D 00	4.065D 00	3.738D 00

LAMBDA 5: 261.36 ANGSTROMS

PE \ T	6000.	8000.	11000.	17500.	50000.
3.	-2.245D 01	-1.881D 01	-1.580D 01	-8.629D 00	-1.812D 01
30.	-2.342D 01	-2.086D 01	-1.707D 01	-1.087D 01	-1.854D 01
300.	-2.432D 01	-2.359D 01	-1.990D 01	-1.391D 01	-1.940D 01
10000.	-2.579D 01	-2.465D 01	-2.459D 01	-2.133D 01	-2.034D 01

LAMBDA 6: 289.34 ANGSTROMS

PE \ T	6000.	8000.	11000.	17500.	50000.
3.	3.591D 00	6.762D 00	7.475D 00	1.181D 01	-6.971D 00
30.	2.981D 00	5.299D 00	7.554D 00	1.075D 01	-4.010D 00
300.	2.687D 00	2.807D 00	5.972D 00	9.023D 00	-2.626D 00
10000.	1.673D 00	2.213D 00	2.156D 00	3.636D 00	-1.585D 00

LAMBDA 7: 349.97 ANGSTROMS

PE \ T	6000.	8000.	11000.	17500.	50000.
3.	4.851D 00	7.451D 00	7.404D 00	-7.188D 00	-5.205D 01
30.	4.504D 00	6.368D 00	8.541D 00	-1.811D 00	-4.611D 01
300.	4.456D 00	4.345D 00	7.189D 00	1.708D 00	-4.032D 01
10000.	4.104D 00	4.262D 00	3.876D 00	2.544D 00	-3.064D 01

TABLE C.4-2
LOG OF THE STATISTICAL UV BLANKETING OPACITY

T	6000.	8000.	11000.	17500.	50000.
			LAMBDA 8: 402.03 ANGSTROMS		
PE					
3.	7.740D 00	8.610D 00	6.353D 00	5.225D-01	2.469D 00
30.	7.161D 00	8.056D 00	7.705D 00	6.970D-01	3.032D 00
300.	7.119D 00	7.351D 00	8.127D 00	1.422D 00	3.524D 00
10000.	6.819D 00	6.430D 00	7.275D 00	3.994D 00	3.662D 00
			LAMBDA 9: 402.05 ANGSTROMS		
PE					
3.	-2.259D 01	-1.897D 01	-1.595D 01	-8.636D 00	-1.827D 01
30.	-2.352D 01	-2.100D 01	-1.723D 01	-1.086D 01	-1.865D 01
300.	-2.441D 01	-2.370D 01	-2.005D 01	-1.391D 01	-1.950D 01
10000.	-2.585D 01	-2.472D 01	-2.470D 01	-2.138D 01	-2.040D 01
			LAMBDA 10: 425.91 ANGSTROMS		
PE					
3.	3.459D 00	6.597D 00	7.325D 00	1.180D 01	-7.113D 00
30.	2.874D 00	5.158D 00	7.393D 00	1.076D 01	-4.126D 00
300.	2.599D 00	2.693D 00	5.820D 00	9.021D 00	-2.720D 00
10000.	1.608D 00	2.143D 00	2.048D 00	3.585D 00	-1.640D 00
			LAMBDA 11: 471.15 ANGSTROMS		
PE					
3.	4.718D 00	7.285D 00	7.255D 00	-7.195D 00	-5.220D 01
30.	4.398D 00	6.227D 00	8.380D 00	-1.807D 00	-4.623D 01
300.	4.368D 00	4.231D 00	7.038D 00	1.706D 00	-4.041D 01
10000.	4.040D 00	4.192D 00	3.769D 00	2.493D 00	-3.069D 01
			LAMBDA 12: 504.26 ANGSTROMS		
PE					
3.	7.607D 00	8.444D 00	6.203D 00	5.156D-01	2.327D 00
30.	7.055D 00	7.915D 00	7.544D 00	7.012D-01	2.916D 00
300.	7.031D 00	7.237D 00	7.975D 00	1.420D 00	3.430D 00
10000.	6.755D 00	6.360D 00	7.158D 00	3.943D 00	3.607D 00
			LAMBDA 13: 504.28 ANGSTROMS		
PE					
3.	-2.273D 01	-1.915D 01	-1.610D 01	-8.643D 00	-1.841D 01
30.	-2.364D 01	-2.115D 01	-1.740D 01	-1.086D 01	-1.878D 01
300.	-2.450D 01	-2.382D 01	-2.021D 01	-1.392D 01	-1.959D 01
10000.	-2.592D 01	-2.479D 01	-2.481D 01	-2.143D 01	-2.046D 01
			LAMBDA 14: 529.82 ANGSTROMS		
PE					
3.	3.320D 00	6.425D 00	7.170D 00	1.179D 01	-7.261D 00
30.	2.763D 00	5.011D 00	7.225D 00	1.076D 01	-4.248D 00
300.	2.507D 00	2.575D 00	5.662D 00	9.018D 00	-2.817D 00
10000.	1.541D 00	2.070D 00	1.937D 00	3.531D 00	-1.698D 00

TABLE C.4-2
LOG OF THE STATISTICAL UV BLANKETING OPACITY

T	6000.	8000.	11000.	17500.	50000.
		LAMBDA 15:	577.11 ANGSTROMS		
PE					
3.	4.580D 00	7.113D 00	7.100D 00	-7.202D 00	-5.234D 01
30.	4.287D 00	6.081D 00	8.211D 00	-1.802D 00	-4.635D 01
300.	4.277D 00	4.112D 00	6.880D 00	1.703D 00	-4.051D 01
10000.	3.973D 00	4.119D 00	3.657D 00	2.440D 00	-3.075D 01
		LAMBDA 16:	610.81 ANGSTROMS		
PE					
3.	7.469D 00	8.272D 00	6.048D 00	5.083D-01	2.179D 00
30.	6.944D 00	7.769D 00	7.375D 00	7.056D-01	2.795D 00
300.	6.939D 00	7.118D 00	7.817D 00	1.417D 00	3.332D 00
10000.	6.688D 00	6.287D 00	7.056D 00	3.890D 00	3.550D 00
		LAMBDA 17:	610.83 ANGSTROMS		
PE					
3.	-2.173D 01	-1.842D 01	-1.558D 01	-8.916D 00	-1.947D 01
30.	-2.265D 01	-2.029D 01	-1.675D 01	-1.087D 01	-1.956D 01
300.	-2.356D 01	-2.282D 01	-1.944D 01	-1.359D 01	-2.004D 01
10000.	-2.491D 01	-2.379D 01	-2.381D 01	-2.067D 01	-2.048D 01
		LAMBDA 18:	634.69 ANGSTROMS		
PE					
3.	3.239D 00	6.166D 00	6.812D 00	1.083D 01	-8.627D 00
30.	2.666D 00	4.828D 00	6.933D 00	9.998D 00	-5.486D 00
300.	2.350D 00	2.501D 00	5.422D 00	8.501D 00	-3.820D 00
10000.	1.464D 00	1.972D 00	1.854D 00	3.330D 00	-2.389D 00
		LAMBDA 19:	677.51 ANGSTROMS		
PE					
3.	4.475D 00	6.848D 00	6.766D 00	-7.335D 00	-5.140D 01
30.	4.172D 00	5.878D 00	7.893D 00	-1.979D 00	-4.541D 01
300.	4.108D 00	4.002D 00	6.624D 00	1.553D 00	-3.955D 01
10000.	3.821D 00	4.000D 00	3.533D 00	2.340D 00	-2.989D 01
		LAMBDA 20:	706.99 ANGSTROMS		
PE					
3.	7.344D 00	8.116D 00	5.907D 00	5.018D-01	2.045D 00
30.	6.844D 00	7.637D 00	7.224D 00	7.095D-01	2.685D 00
300.	6.856D 00	7.010D 00	7.675D 00	1.415D 00	3.244D 00
10000.	6.628D 00	6.221D 00	6.955D 00	3.842D 00	3.498D 00
		LAMBDA 21:	707.01 ANGSTROMS		
PE					
3.	-2.092D 01	-1.807D 01	-1.570D 01	-9.555D 00	-2.078D 01
30.	-2.189D 01	-1.976D 01	-1.657D 01	-1.139D 01	-2.065D 01
300.	-2.272D 01	-2.207D 01	-1.906D 01	-1.384D 01	-2.083D 01
10000.	-2.386D 01	-2.295D 01	-2.305D 01	-2.040D 01	-2.077D 01

TABLE C.4-2
LOG OF THE STATISTICAL UV BLANKETING OPACITY

T	6000.	8000.	11000.	17500.	50000.
		LAMBDA 22: 732.99 ANGSTROMS			
PE					
3.	3.160D 00	5.653D 00	5.951D 00	9.666D 00	-9.790D 00
30.	2.509D 00	4.485D 00	6.191D 00	8.846D 00	-6.608D 00
300.	2.220D 00	2.353D 00	4.925D 00	7.534D 00	-4.802D 00
10000.	1.513D 00	1.865D 00	1.700D 00	2.759D 00	-3.052D 00
		LAMBDA 23: 779.33 ANGSTROMS			
PE					
3.	4.394D 00	6.406D 00	6.046D 00	-7.575D 00	-5.036D 01
30.	4.006D 00	5.542D 00	7.236D 00	-2.486D 00	-4.446D 01
300.	3.974D 00	3.828D 00	6.163D 00	1.001D 00	-3.868D 01
10000.	3.801D 00	3.871D 00	3.334D 00	1.892D 00	-2.922D 01
		LAMBDA 24: 811.02 ANGSTROMS			
PE					
3.	7.209D 00	7.948D 00	5.755D 00	4.947D-01	1.900D 00
30.	6.736D 00	7.494D 00	7.059D 00	7.138D-01	2.567D 00
300.	6.767D 00	6.894D 00	7.520D 00	1.412D 00	3.149D 00
10000.	6.562D 00	6.150D 00	6.846D 00	3.790D 00	3.442D 00
		LAMBDA 25: 811.04 ANGSTROMS			
PE					
3.	-2.017D 01	-1.753D 01	-1.549D 01	-1.019D 01	-2.200D 01
30.	-2.109D 01	-1.911D 01	-1.628D 01	-1.183D 01	-2.168D 01
300.	-2.186D 01	-2.122D 01	-1.845D 01	-1.403D 01	-2.163D 01
10000.	-2.292D 01	-2.204D 01	-2.218D 01	-1.990D 01	-2.113D 01
		LAMBDA 26: 836.58 ANGSTROMS			
PE					
3.	2.875D 00	5.228D 00	5.307D 00	8.331D 00	-1.110D 01
30.	2.262D 00	4.130D 00	5.642D 00	7.645D 00	-7.883D 00
300.	2.024D 00	2.159D 00	4.526D 00	6.528D 00	-5.961D 00
10000.	1.444D 00	1.713D 00	1.526D 00	2.299D 00	-3.936D 00
		LAMBDA 27: 881.50 ANGSTROMS			
PE					
3.	4.111D 00	6.030D 00	5.532D 00	-7.816D 00	-4.939D 01
30.	3.733D 00	5.198D 00	6.771D 00	-2.956D 00	-4.357D 01
300.	3.749D 00	3.605D 00	5.807D 00	4.533D-01	-3.787D 01
10000.	3.654D 00	3.667D 00	3.143D 00	1.604D 00	-2.856D 01
		LAMBDA 28: 911.75 ANGSTROMS			
PE					
3.	7.079D 00	7.785D 00	5.608D 00	4.878D-01	1.760D 00
30.	6.631D 00	7.356D 00	6.900D 00	7.179D-01	2.452D 00
300.	6.680D 00	6.782D 00	7.371D 00	1.409D 00	3.057D 00
10000.	6.499D 00	6.082D 00	6.740D 00	3.739D 00	3.388D 00

TABLE C.4-2
LOG OF THE STATISTICAL UV BLANKETING OPACITY

T	6000.	8000.	11000.	17500.	50000.
	LAMBDA 29: 911.77 ANGSTROMS				
PE					
3.	-1.932D 01	-1.685D 01	-1.526D 01	-1.089D 01	-2.365D 01
30.	-2.028D 01	-1.835D 01	-1.584D 01	-1.216D 01	-2.303D 01
300.	-2.119D 01	-2.033D 01	-1.778D 01	-1.400D 01	-2.255D 01
10000.	-2.233D 01	-2.132D 01	-2.130D 01	-1.932D 01	-2.158D 01
	LAMBDA 30: 939.12 ANGSTROMS				
PE					
3.	2.768D 00	4.928D 00	4.698D 00	7.096D 00	-1.277D 01
30.	2.111D 00	3.898D 00	5.157D 00	6.684D 00	-9.501D 00
300.	1.748D 00	2.076D 00	4.225D 00	5.811D 00	-7.323D 00
10000.	1.071D 00	1.469D 00	1.434D 00	1.958D 00	-4.977D 00
	LAMBDA 31: 987.01 ANGSTROMS				
PE					
3.	4.013D 00	5.823D 00	5.037D 00	-8.279D 00	-4.847D 01
30.	3.608D 00	5.029D 00	6.359D 00	-3.372D 00	-4.274D 01
300.	3.527D 00	3.531D 00	5.552D 00	8.356D-02	-3.703D 01
10000.	3.330D 00	3.445D 00	3.072D 00	1.392D 00	-2.787D 01
	LAMBDA 32: 1019.13 ANGSTROMS				
PE					
3.	6.939D 00	7.611D 00	5.451D 00	4.805D-01	1.611D 00
30.	6.519D 00	7.208D 00	6.731D 00	7.223D-01	2.330D 00
300.	6.588D 00	6.662D 00	7.211D 00	1.407D 00	2.959D 00
10000.	6.431D 00	6.008D 00	6.627D 00	3.685D 00	3.330D 00
	LAMBDA 33: 1019.15 ANGSTROMS				
PE					
3.	-1.907D 01	-1.671D 01	-1.538D 01	-1.190D 01	-2.483D 01
30.	-1.993D 01	-1.815D 01	-1.575D 01	-1.299D 01	-2.400D 01
300.	-2.065D 01	-2.000D 01	-1.750D 01	-1.465D 01	-2.325D 01
10000.	-2.169D 01	-2.085D 01	-2.081D 01	-1.916D 01	-2.193D 01
	LAMBDA 34: 1047.52 ANGSTROMS				
PE					
3.	1.989D 00	4.042D 00	3.647D 00	5.355D 00	-1.441D 01
30.	1.456D 00	3.035D 00	4.246D 00	5.074D 00	-1.105D 01
300.	1.264D 00	1.384D 00	3.468D 00	4.294D 00	-8.663D 00
10000.	6.502D-01	9.332D-01	8.896D-01	1.137D 00	-5.994D 00
	LAMBDA 35: 1096.93 ANGSTROMS				
PE					
3.	3.368D 00	5.115D 00	4.242D 00	-8.637D 00	-4.828D 01
30.	3.025D 00	4.325D 00	5.629D 00	-4.085D 00	-4.248D 01
300.	3.091D 00	2.928D 00	4.946D 00	-8.257D-01	-3.669D 01
10000.	2.941D 00	2.918D 00	2.597D 00	8.529D-01	-2.766D 01

TABLE C.4-2
LOG OF THE STATISTICAL UV BLANKETING OPACITY

LAMBDA 36: 1129.87 ANGSTROMS

PE \ T	6000.	8000.	11000.	17500.	50000.
3.	6.796D 00	7.432D 00	5.289D 00	4.730D-01	1.457D 00
30.	6.404D 00	7.056D 00	6.556D 00	7.268D-01	2.203D 00
300.	6.492D 00	6.538D 00	7.047D 00	1.404D 00	2.857D 00
10000.	6.362D 00	5.933D 00	6.511D 00	3.630D 00	3.270D 00

LAMBDA 37: 1129.89 ANGSTROMS

PE \ T	6000.	8000.	11000.	17500.	50000.
3.	-1.869D 01	-1.625D 01	-1.515D 01	-1.284D 01	-2.642D 01
30.	-1.937D 01	-1.758D 01	-1.533D 01	-1.360D 01	-2.523D 01
300.	-1.979D 01	-1.941D 01	-1.687D 01	-1.489D 01	-2.413D 01
10000.	-2.058D 01	-2.006D 01	-2.002D 01	-1.863D 01	-2.230D 01

LAMBDA 38: 1152.36 ANGSTROMS

PE \ T	6000.	8000.	11000.	17500.	50000.
3.	1.291D 00	3.381D 00	2.869D 00	3.527D 00	-1.641D 01
30.	9.078D-01	2.388D 00	3.563D 00	3.561D 00	-1.284D 01
300.	9.803D-01	8.531D-01	2.937D 00	3.065D 00	-1.019D 01
10000.	6.113D-01	6.063D-01	5.419D-01	5.869D-01	-7.086D 00

LAMBDA 39: 1190.68 ANGSTROMS

PE \ T	6000.	8000.	11000.	17500.	50000.
3.	2.729D 00	4.576D 00	3.691D 00	-9.051D 00	-4.754D 01
30.	2.507D 00	3.752D 00	5.090D 00	-4.654D 00	-4.173D 01
300.	2.792D 00	2.444D 00	4.531D 00	-1.438D 00	-3.597D 01
10000.	2.854D 00	2.563D 00	2.275D 00	5.257D-01	-2.706D 01

LAMBDA 40: 1215.66 ANGSTROMS

PE \ T	6000.	8000.	11000.	17500.	50000.
3.	6.684D 00	7.293D 00	5.164D 00	4.672D-01	1.337D 00
30.	6.315D 00	6.938D 00	6.421D 00	7.303D-01	2.106D 00
300.	6.419D 00	6.443D 00	6.920D 00	1.402D 00	2.779D 00
10000.	6.308D 00	5.874D 00	6.421D 00	3.587D 00	3.224D 00

LAMBDA 41: 1215.68 ANGSTROMS

PE \ T	6000.	8000.	11000.	17500.	50000.
3.	-1.821D 01	-1.569D 01	-1.484D 01	-1.354D 01	-2.686D 01
30.	-1.886D 01	-1.710D 01	-1.494D 01	-1.401D 01	-2.552D 01
300.	-1.923D 01	-1.880D 01	-1.636D 01	-1.499D 01	-2.442D 01
10000.	-1.991D 01	-1.946D 01	-1.927D 01	-1.807D 01	-2.242D 01

LAMBDA 42: 1239.60 ANGSTROMS

PE \ T	6000.	8000.	11000.	17500.	50000.
3.	9.400D-01	3.133D 00	2.417D 00	2.282D 00	-1.730D 01
30.	6.036D-01	2.137D 00	3.173D 00	2.556D 00	-1.377D 01
300.	7.042D-01	6.216D-01	2.639D 00	2.319D 00	-1.107D 01
10000.	3.898D-01	3.680D-01	4.450D-01	3.976D-01	-7.846D 00

TABLE C.4-2
LOG OF THE STATISTICAL UV BLANKETING OPACITY

T	6000.	8000.	11000.	17500.	50000.
			LAMBDA 43: 1280.37 ANGSTROMS		
PE					
3.	2.450D 00	4.389D 00	3.318D 00	-8.719D 00	-4.415D 01
30.	2.235D 00	3.573D 00	4.718D 00	-4.578D 00	-3.858D 01
300.	2.515D 00	2.268D 00	4.255D 00	-1.526D 00	-3.321D 01
10000.	2.603D 00	2.285D 00	2.206D 00	4.846D-01	-2.485D 01
			LAMBDA 44: 1306.94 ANGSTROMS		
PE					
3.	6.566D 00	7.146D 00	5.031D 00	4.609D-01	1.210D 00
30.	6.220D 00	6.812D 00	6.277D 00	7.340D-01	2.002D 00
300.	6.340D 00	6.341D 00	6.784D 00	1.399D 00	2.695D 00
10000.	6.250D 00	5.812D 00	6.325D 00	3.541D 00	3.175D 00
			LAMBDA 45: 1306.96 ANGSTROMS		
PE					
3.	-1.757D 01	-1.531D 01	-1.480D 01	-1.409D 01	-2.676D 01
30.	-1.817D 01	-1.655D 01	-1.477D 01	-1.445D 01	-2.557D 01
300.	-1.844D 01	-1.808D 01	-1.596D 01	-1.534D 01	-2.434D 01
10000.	-1.916D 01	-1.868D 01	-1.845D 01	-1.796D 01	-2.240D 01
			LAMBDA 46: 1339.76 ANGSTROMS		
PE					
3.	7.355D-01	2.644D 00	1.648D 00	9.827D-01	-1.778D 01
30.	4.250D-01	1.796D 00	2.524D 00	1.366D 00	-1.445D 01
300.	5.797D-01	4.686D-01	2.191D 00	1.200D 00	-1.178D 01
10000.	1.858D-01	2.572D-01	3.589D-01	-3.120D-01	-8.577D 00
			LAMBDA 47: 1396.48 ANGSTROMS		
PE					
3.	2.281D 00	3.940D 00	2.633D 00	-8.335D 00	-4.028D 01
30.	2.068D 00	3.306D 00	4.061D 00	-4.599D 00	-3.536D 01
300.	2.370D 00	2.157D 00	3.797D 00	-1.988D 00	-3.040D 01
10000.	2.373D 00	2.149D 00	2.137D 00	-1.354D-01	-2.285D 01
			LAMBDA 48: 1433.99 ANGSTROMS		
PE					
3.	6.401D 00	6.940D 00	4.845D 00	4.523D-01	1.034D 00
30.	6.088D 00	6.637D 00	6.076D 00	7.392D-01	1.857D 00
300.	6.231D 00	6.199D 00	6.596D 00	1.396D 00	2.579D 00
10000.	6.171D 00	5.725D 00	6.192D 00	3.478D 00	3.106D 00
			LAMBDA 49: 1434.01 ANGSTROMS		
PE					
3.	-1.663D 01	-1.459D 01	-1.421D 01	-1.481D 01	-2.662D 01
30.	-1.718D 01	-1.568D 01	-1.405D 01	-1.499D 01	-2.543D 01
300.	-1.734D 01	-1.703D 01	-1.507D 01	-1.549D 01	-2.424D 01
10000.	-1.791D 01	-1.749D 01	-1.728D 01	-1.729D 01	-2.213D 01

TABLE C.4-2
LOG OF THE STATISTICAL UV BLANKETING OPACITY

T	6000.	8000.	11000.	17500.	50000.
	LAMBDA 50: 1457.06 ANGSTROMS				
PE					
3.	4.512D-01	2.234D 00	1.218D 00	-7.569D-01	-1.842D 01
30.	1.558D-01	1.459D 00	2.165D 00	-1.976D-01	-1.516D 01
300.	3.531D-01	2.729D-01	1.913D 00	3.697D-03	-1.256D 01
10000.	6.414D-02	1.492D-01	2.620D-01	-7.453D-01	-9.141D 00
	LAMBDA 51: 1495.96 ANGSTROMS				
PE					
3.	2.053D 00	3.540D 00	2.307D 00	-8.078D 00	-3.737D 01
30.	1.814D 00	2.975D 00	3.674D 00	-4.687D 00	-3.276D 01
300.	2.095D 00	1.970D 00	3.492D 00	-2.238D 00	-2.813D 01
10000.	2.141D 00	1.971D 00	2.000D 00	-2.877D-01	-2.102D 01
	LAMBDA 52: 1521.06 ANGSTROMS				
PE					
3.	6.288D 00	6.799D 00	4.718D 00	4.464D-01	9.125D-01
30.	5.997D 00	6.518D 00	5.939D 00	7.428D-01	1.758D 00
300.	6.156D 00	6.102D 00	6.466D 00	1.394D 00	2.499D 00
10000.	6.116D 00	5.665D 00	6.101D 00	3.434D 00	3.059D 00
	LAMBDA 53: 1521.08 ANGSTROMS				
PE					
3.	-1.557D 01	-1.394D 01	-1.404D 01	-1.497D 01	-2.751D 01
30.	-1.603D 01	-1.479D 01	-1.373D 01	-1.494D 01	-2.601D 01
300.	-1.626D 01	-1.593D 01	-1.445D 01	-1.516D 01	-2.460D 01
10000.	-1.686D 01	-1.638D 01	-1.619D 01	-1.657D 01	-2.229D 01
	LAMBDA 54: 1548.18 ANGSTROMS				
PE					
3.	6.911D-01	2.117D 00	7.736D-01	-1.552D 00	-1.946D 01
30.	4.516D-01	1.535D 00	1.801D 00	-8.339D-01	-1.611D 01
300.	5.520D-01	5.104D-01	1.742D 00	-4.040D-01	-1.341D 01
10000.	2.036D-01	3.582D-01	4.552D-01	-8.227D-01	-9.879D 00
	LAMBDA 55: 1594.13 ANGSTROMS				
PE					
3.	2.285D 00	3.409D 00	1.886D 00	-7.751D 00	-3.530D 01
30.	2.127D 00	3.019D 00	3.282D 00	-4.650D 00	-3.079D 01
300.	2.293D 00	2.199D 00	3.276D 00	-2.199D 00	-2.638D 01
10000.	2.232D 00	2.193D 00	2.185D 00	-2.405D-01	-1.962D 01
	LAMBDA 56: 1623.92 ANGSTROMS				
PE					
3.	6.155D 00	6.633D 00	4.568D 00	4.394D-01	7.695D-01
30.	5.890D 00	6.376D 00	5.776D 00	7.470D-01	1.641D 00
300.	6.067D 00	5.987D 00	6.314D 00	1.391D 00	2.405D 00
10000.	6.051D 00	5.595D 00	5.993D 00	3.383D 00	3.004D 00

TABLE C.4-2
LOG OF THE STATISTICAL UV BLANKETING OPACITY

T	6000.	8000.	11000.	17500.	50000.
	LAMBDA 57: 1623.94 ANGSTROMS				
PE					
3.	-1.468D 01	-1.351D 01	-1.405D 01	-1.542D 01	-2.836D 01
30.	-1.504D 01	-1.410D 01	-1.358D 01	-1.521D 01	-2.654D 01
300.	-1.530D 01	-1.504D 01	-1.402D 01	-1.524D 01	-2.491D 01
10000.	-1.593D 01	-1.540D 01	-1.537D 01	-1.619D 01	-2.241D 01
	LAMBDA 58: 1656.92 ANGSTROMS				
PE					
3.	6.924D-01	1.683D 00	2.979D-02	-2.717D 00	-2.052D 01
30.	5.195D-01	1.326D 00	1.138D 00	-1.917D 00	-1.711D 01
300.	5.630D-01	5.057D-01	1.277D 00	-1.308D 00	-1.433D 01
10000.	1.323D-01	4.073D-01	3.510D-01	-1.315D 00	-1.069D 01
	LAMBDA 59: 1713.23 ANGSTROMS				
PE					
3.	2.351D 00	3.145D 00	1.357D 00	-7.229D 00	-3.220D 01
30.	2.219D 00	2.909D 00	2.779D 00	-4.434D 00	-2.788D 01
300.	2.322D 00	2.228D 00	2.917D 00	-2.268D 00	-2.374D 01
10000.	2.168D 00	2.247D 00	2.109D 00	-3.905D-01	-1.748D 01
	LAMBDA 60: 1749.98 ANGSTROMS				
PE					
3.	5.991D 00	6.429D 00	4.383D 00	4.308D-01	5.941D-01
30.	5.759D 00	6.203D 00	5.577D 00	7.522D-01	1.497D 00
300.	5.959D 00	5.847D 00	6.127D 00	1.388D 00	2.290D 00
10000.	5.972D 00	5.509D 00	5.860D 00	3.319D 00	2.936D 00
	LAMBDA 61: 1750.00 ANGSTROMS				
PE					
3.	-1.370D 01	-1.285D 01	-1.361D 01	-1.588D 01	-2.931D 01
30.	-1.391D 01	-1.320D 01	-1.296D 01	-1.546D 01	-2.705D 01
300.	-1.412D 01	-1.404D 01	-1.318D 01	-1.526D 01	-2.509D 01
10000.	-1.472D 01	-1.431D 01	-1.441D 01	-1.573D 01	-2.219D 01
	LAMBDA 62: 1776.54 ANGSTROMS				
PE					
3.	4.976D-01	1.197D 00	-4.980D-01	-4.260D 00	-2.209D 01
30.	4.511D-01	1.045D 00	7.049D-01	-3.234D 00	-1.843D 01
300.	5.256D-01	3.146D-01	9.704D-01	-2.409D 00	-1.541D 01
10000.	1.370D-01	2.778D-01	1.088D-01	-1.970D 00	-1.142D 01
	LAMBDA 63: 1821.23 ANGSTROMS				
PE					
3.	2.141D 00	2.675D 00	8.870D-01	-8.570D 00	-3.391D 01
30.	2.125D 00	2.623D 00	2.339D 00	-5.600D 00	-2.937D 01
300.	2.252D 00	1.998D 00	2.600D 00	-3.200D 00	-2.504D 01
10000.	2.114D 00	2.106D 00	1.834D 00	-8.876D-01	-1.837D 01

TABLE C.4-2
LOG OF THE STATISTICAL UV BLANKETING OPACITY

LAMBDA 64: 1849.99 ANGSTROMS

PE \ T	6000.	8000.	11000.	17500.	50000.
3.	5.861D 00	6.267D 00	4.237D 00	4.240D-01	4.551D-01
30.	5.655D 00	6.065D 00	5.419D 00	7.563D-01	1.383D 00
300.	5.873D 00	5.735D 00	5.978D 00	1.385D 00	2.198D 00
10000.	5.909D 00	5.440D 00	5.755D 00	3.269D 00	2.882D 00

LAMBDA 65: 1850.01 ANGSTROMS

PE \ T	6000.	8000.	11000.	17500.	50000.
3.	-1.318D 01	-1.251D 01	-1.337D 01	-1.605D 01	-3.127D 01
30.	-1.316D 01	-1.278D 01	-1.259D 01	-1.543D 01	-2.847D 01
300.	-1.331D 01	-1.346D 01	-1.267D 01	-1.495D 01	-2.606D 01
10000.	-1.374D 01	-1.352D 01	-1.382D 01	-1.499D 01	-2.251D 01

LAMBDA 66: 1874.85 ANGSTROMS

PE \ T	6000.	8000.	11000.	17500.	50000.
3.	8.316D-02	6.449D-01	-1.022D 00	-5.081D 00	-2.447D 01
30.	2.531D-01	5.520D-01	2.658D-01	-3.935D 00	-2.036D 01
300.	3.542D-01	-4.296D-02	5.845D-01	-2.908D 00	-1.697D 01
10000.	1.665D-01	1.061D-01	-2.256D-01	-2.090D 00	-1.241D 01

LAMBDA 67: 1916.49 ANGSTROMS

PE \ T	6000.	8000.	11000.	17500.	50000.
3.	1.763D 00	2.138D 00	3.903D-01	-9.746D 00	-3.751D 01
30.	1.946D 00	2.122D 00	1.915D 00	-6.543D 00	-3.240D 01
300.	2.104D 00	1.640D 00	2.214D 00	-3.763D 00	-2.754D 01
10000.	2.118D 00	1.949D 00	1.476D 00	-9.385D-01	-2.010D 01

LAMBDA 68: 1943.16 ANGSTROMS

PE \ T	6000.	8000.	11000.	17500.	50000.
3.	5.740D 00	6.116D 00	4.101D 00	4.177D-01	3.255D-01
30.	5.558D 00	5.937D 00	5.272D 00	7.601D-01	1.277D 00
300.	5.792D 00	5.631D 00	5.840D 00	1.383D 00	2.113D 00
10000.	5.850D 00	5.377D 00	5.658D 00	3.223D 00	2.831D 00

LAMBDA 69: 1943.18 ANGSTROMS

PE \ T	6000.	8000.	11000.	17500.	50000.
3.	-1.257D 01	-1.196D 01	-1.313D 01	-1.647D 01	-3.148D 01
30.	-1.248D 01	-1.215D 01	-1.221D 01	-1.561D 01	-2.857D 01
300.	-1.254D 01	-1.283D 01	-1.218D 01	-1.494D 01	-2.594D 01
10000.	-1.282D 01	-1.278D 01	-1.316D 01	-1.465D 01	-2.237D 01

LAMBDA 70: 1971.95 ANGSTROMS

PE \ T	6000.	8000.	11000.	17500.	50000.
3.	-1.004D-01	4.351D-01	-1.331D 00	-6.001D 00	-2.510D 01
30.	1.381D-01	4.023D-01	-7.687D-03	-4.709D 00	-2.095D 01
300.	3.144D-01	-2.058D-01	3.379D-01	-3.532D 00	-1.738D 01
10000.	2.183D-01	4.235D-02	-3.702D-01	-2.443D 00	-1.284D 01

TABLE C.4-2
LOG OF THE STATISTICAL UV BLANKETING OPACITY

T	6000.	8000.	11000.	17500.	50000.

LAMBDA 71: 2020.34 ANGSTROMS

PE					
3.	1.554D 00	1.987D 00	1.612D-01	-1.070D 01	-3.808D 01
30.	1.796D 00	1.968D 00	1.761D 00	-7.419D 00	-3.298D 01
300.	2.023D 00	1.463D 0C	2.059D 00	-4.472D 00	-2.803D 01
10000.	2.093D 00	1.857D 00	1.338D 00	-1.261D 00	-2.063D 01

LAMBDA 72: 2051.46 ANGSTROMS

PE					
3.	5.600D 00	5.941D 00	3.943D 00	4.103D-01	1.748D-01
30.	5.446D 00	5.788D 00	5.101D 00	7.645D-01	1.154D 00
300.	5.699D 00	5.510D 00	5.679D 00	1.380D 00	2.014D 00
10000.	5.782D 00	5.303D 00	5.544D 00	3.168D 00	2.773D 00

LAMBDA 73: 2051.48 ANGSTROMS

PE					
3.	-1.178D 01	-1.132D 01	-1.261D 01	-1.713D 01	-3.192D 01
30.	-1.174D 01	-1.143D 01	-1.158D 01	-1.610D 01	-2.883D 01
300.	-1.177D 01	-1.201D 01	-1.149D 01	-1.519D 01	-2.602D 01
10000.	-1.184D 01	-1.203D 01	-1.241D 01	-1.447D 01	-2.229D 01

LAMBDA 74: 2073.76 ANGSTROMS

PE					
3.	-1.887D-01	2.204D-01	-1.596D 00	-7.241D 00	-2.601D 01
30.	-1.565D-02	2.465D-01	-1.756D-01	-5.834D 00	-2.174D 01
300.	1.699D-01	-2.729D-01	2.427D-01	-4.476D 00	-1.804D 01
10000.	2.431D-01	-8.740D-02	-4.880D-01	-3.010D 00	-1.336D 01

LAMBDA 75: 2110.85 ANGSTROMS

PE					
3.	1.428D 00	1.836D 00	6.412D-02	-1.169D 01	-3.987D 01
30.	1.599D 00	1.823D 00	1.704D 00	-8.185D 00	-3.453D 01
300.	1.835D 00	1.367D 00	2.017D 00	-5.207D 00	-2.949D 01
10000.	2.035D 00	1.686D 00	1.202D 00	-1.777D 00	-2.180D 01

LAMBDA 76: 2134.45 ANGSTROMS

PE					
3.	5.492D 00	5.806D 00	3.822D 00	4.046D-01	5.942D-02
30.	5.360D 00	5.674D 00	4.970D 00	7.679D-01	1.059D 00
300.	5.628D 00	5.417D 00	5.556D 00	1.378D 00	1.938D 00
10000.	5.730D 00	5.246D 00	5.457D 00	3.127D 00	2.728D 00

LAMBDA 77: 2134.47 ANGSTROMS

PE					
3.	-1.130D 01	-1.078D 01	-1.198D 01	-1.677D 01	-3.027D 01
30.	-1.141D 01	-1.087D 01	-1.090D 01	-1.573D 01	-2.749D 01
300.	-1.149D 01	-1.154D 01	-1.083D 01	-1.484D 01	-2.493D 01
10000.	-1.156D 01	-1.174D 01	-1.187D 01	-1.392D 01	-2.141D 01

TABLE C.4-2
LOG OF THE STATISTICAL UV BLANKETING OPACITY

T	6000.	8000.	11000.	17500.	50000.
			LAMBDA 78: 2165.20 ANGSTROMS		
PE					
3.	-4.922D-01	-3.228D-02	-1.710D 00	-7.503D 00	-2.488D 01
30.	-4.538D-01	8.995D-03	-2.454D-01	-6.117D 00	-2.088D 01
300.	-3.306D-01	-5.784D-01	1.385D-01	-4.812D 00	-1.742D 01
10000.	-2.755D-01	-5.911D-01	-7.400D-01	-3.189D 00	-1.306D 01
			LAMBDA 79: 2216.83 ANGSTROMS		
PE					
3.	1.190D 00	1.591D 00	-1.113D-01	-1.213D 01	-3.801D 01
30.	1.253D 00	1.641D 00	1.538D 00	-8.582D 00	-3.322D 01
300.	1.452D 00	1.110D 00	1.855D 00	-5.564D 00	-2.853D 01
10000.	1.645D 00	1.274D 00	9.824D-01	-2.025D 00	-2.141D 01
			LAMBDA 80: 2249.99 ANGSTROMS		
PE					
3.	5.342D 00	5.619D 00	3.653D 00	3.968D-01	-1.013D-01
30.	5.239D 00	5.515D 00	4.788D 00	7.726D-01	9.277D-01
300.	5.528D 00	5.289D 00	5.385D 00	1.375D 00	1.832D 00
10000.	5.657D 00	5.167D 00	5.336D 00	3.069D 00	2.666D 00
			LAMBDA 81: 2250.01 ANGSTROMS		
PE					
3.	-1.064D 01	-1.021D 01	-1.141D 01	-1.640D 01	-3.056D 01
30.	-1.054D 01	-1.031D 01	-1.024D 01	-1.516D 01	-2.770D 01
300.	-1.050D 01	-1.071D 01	-1.010D 01	-1.406D 01	-2.499D 01
10000.	-1.055D 01	-1.062D 01	-1.088D 01	-1.284D 01	-2.130D 01
			LAMBDA 82: 2275.74 ANGSTROMS		
PE					
3.	-8.651D-01	-5.320D-01	-2.205D 00	-8.003D 00	-2.566D 01
30.	-6.405D-01	-4.938D-01	-6.918D-01	-6.511D 00	-2.158D 01
300.	-4.402D-01	-8.265D-01	-2.330D-01	-5.052D 00	-1.815D 01
10000.	-4.029D-01	-5.891D-01	-8.715D-01	-3.209D 00	-1.370D 01
			LAMBDA 83: 2318.65 ANGSTROMS		
PE					
3.	8.259D-01	1.118D 00	-5.384D-01	-1.190D 01	-3.692D 01
30.	1.067D 00	1.151D 00	1.142D 00	-8.472D 00	-3.222D 01
300.	1.342D 00	8.637D-01	1.485D 00	-5.544D 00	-2.759D 01
10000.	1.526D 00	1.231D 00	8.349D-01	-2.030D 00	-2.076D 01
			LAMBDA 84: 2345.99 ANGSTROMS		
PE					
3.	5.218D 00	5.464D 00	3.513D 00	3.902D-01	-2.348D-01
30.	5.140D 00	5.383D 00	4.637D 00	7.766D-01	8.184D-01
300.	5.446D 00	5.181D 00	5.242D 00	1.373D 00	1.744D 00
10000.	5.597D 00	5.102D 00	5.235D 00	3.021D 00	2.614D 00

TABLE C.4-2
LOG OF THE STATISTICAL UV BLANKETING OPACITY

LAMBDA 85: 2346.01 ANGSTROMS

T / PE	6000.	8000.	11000.	17500.	50000.
3.	-9.924D 00	-9.562D 00	-1.088D 01	-1.584D 01	-3.057D 01
30.	-9.771D 00	-9.534D 00	-9.619D 00	-1.455D 01	-2.755D 01
300.	-9.652D 00	-9.887D 00	-9.361D 00	-1.345D 01	-2.468D 01
10000.	-9.672D 00	-9.716D 00	-9.957D 00	-1.219D 01	-2.074D 01

LAMBDA 86: 2365.74 ANGSTROMS

PE	6000.	8000.	11000.	17500.	50000.
3.	-9.872D-01	-7.090D-01	-2.445D 00	-8.162D 00	-2.605D 01
30.	-7.642D-01	-6.228D-01	-9.010D-01	-6.641D 00	-2.204D 01
300.	-5.080D-01	-8.858D-01	-3.750D-01	-5.209D 00	-1.842D 01
10000.	-4.936D-01	-6.207D-01	-9.009D-01	-3.404D 00	-1.379D 01

LAMBDA 87: 2398.37 ANGSTROMS

PE	6000.	8000.	11000.	17500.	50000.
3.	6.437D-01	9.260D-01	-7.771D-01	-1.131D 01	-3.553D 01
30.	8.981D-01	9.923D-01	8.888D-01	-8.096D 00	-3.093D 01
300.	1.233D 00	7.491D-01	1.316D 00	-5.424D 00	-2.639D 01
10000.	1.408D 00	1.148D 00	7.822D-01	-2.196D 00	-1.968D 01

LAMBDA 88: 2418.99 ANGSTROMS

PE	6000.	8000.	11000.	17500.	50000.
3.	5.123D 00	5.346D 00	3.406D 00	3.853D-01	-3.363D-01
30.	5.064D 00	5.283D 00	4.521D 00	7.795D-01	7.352D-01
300.	5.383D 00	5.100D 00	5.134D 00	1.371D 00	1.677D 00
10000.	5.551D 00	5.052D 00	5.158D 00	2.984D 00	2.575D 00

LAMBDA 89: 2419.01 ANGSTROMS

PE	6000.	8000.	11000.	17500.	50000.
3.	-9.599D 00	-9.485D 00	-1.085D 01	-1.565D 01	-3.208D 01
30.	-9.401D 00	-9.422D 00	-9.548D 00	-1.443D 01	-2.883D 01
300.	-9.256D 00	-9.594D 00	-9.192D 00	-1.327D 01	-2.572D 01
10000.	-9.330D 00	-9.352D 00	-9.726D 00	-1.182D 01	-2.113D 01

LAMBDA 90: 2443.85 ANGSTROMS

PE	6000.	8000.	11000.	17500.	50000.
3.	-1.330D 00	-1.225D 00	-3.155D 00	-8.607D 00	-2.754D 01
30.	-1.081D 00	-1.094D 00	-1.526D 00	-7.132D 00	-2.339D 01
300.	-8.311D-01	-1.265D 00	-8.658D-01	-5.696D 00	-1.966D 01
10000.	-8.564D-01	-9.931D-01	-1.328D 00	-3.756D 00	-1.463D 01

LAMBDA 91: 2485.14 ANGSTROMS

PE	6000.	8000.	11000.	17500.	50000.
3.	3.742D-01	5.217D-01	-1.359D 00	-1.129D 01	-3.570D 01
30.	6.408D-01	6.343D-01	3.315D-01	-8.243D 00	-3.104D 01
300.	9.664D-01	4.378D-01	8.682D-01	-5.634D 00	-2.648D 01
10000.	1.113D 00	8.274D-01	4.236D-01	-2.469D 00	-1.957D 01

TABLE C.4-2
LOG OF THE STATISTICAL UV BLANKETING OPACITY

T	6000.	8000.	11000.	17500.	50000.

LAMBDA 92: 2511.37 ANGSTROMS

PE					
3.	5.003D 00	5.197D 00	3.271D 00	3.790D-01	-4.648D-01
30.	4.968D 00	5.155D 00	4.376D 00	7.833D-01	6.300D-01
300.	5.303D 00	4.997D 00	4.997D 00	1.369D 00	1.593D 00
10000.	5.493D 00	4.989D 00	5.051D 00	2.938D 00	2.525D 00

LAMBDA 93: 2511.39 ANGSTROMS

PE					
3.	-9.198D 00	-9.219D 00	-1.085D 01	-1.610D 01	-3.303D 01
30.	-9.039D 00	-9.074D 00	-9.294D 00	-1.473D 01	-2.985D 01
300.	-8.883D 00	-9.166D 00	-8.817D 00	-1.339D 01	-2.670D 01
10000.	-9.079D 00	-8.931D 00	-9.213D 00	-1.156D 01	-2.183D 01

LAMBDA 94: 2535.39 ANGSTROMS

PE					
3.	-1.594D 00	-1.616D 00	-3.856D 00	-9.476D 00	-2.792D 01
30.	-1.366D 00	-1.402D 00	-2.002D 00	-7.903D 00	-2.397D 01
300.	-1.096D 00	-1.523D 00	-1.240D 00	-6.364D 00	-2.033D 01
10000.	-1.237D 00	-1.241D 00	-1.500D 00	-4.192D 00	-1.527D 01

LAMBDA 95: 2575.21 ANGSTROMS

PE					
3.	1.855D-01	2.435D-01	-1.885D 00	-1.136D 01	-3.404D 01
30.	3.888D-01	4.077D-01	-3.964D-02	-8.404D 00	-2.968D 01
300.	7.406D-01	2.193D-01	5.744D-01	-5.881D 00	-2.538D 01
10000.	8.388D-01	5.984D-01	2.722D-01	-2.766D 00	-1.876D 01

LAMBDA 96: 2600.45 ANGSTROMS

PE					
3.	4.887D 00	5.052D 00	3.141D 00	3.729D-01	-5.887D-01
30.	4.875D 00	5.033D 00	4.235D 00	7.870D-01	5.286D-01
300.	5.227D 00	4.897D 00	4.865D 00	1.366D 00	1.511D 00
10000.	5.437D 00	4.928D 00	4.958D 00	2.894D 00	2.477D 00

LAMBDA 97: 2600.47 ANGSTROMS

PE					
3.	-8.828D 00	-9.006D 00	-1.111D 01	-1.723D 01	-3.697D 01
30.	-8.599D 00	-8.824D 00	-9.427D 00	-1.562D 01	-3.319D 01
300.	-8.361D 00	-8.743D 00	-8.777D 00	-1.391D 01	-2.944D 01
10000.	-8.380D 00	-8.416D 00	-8.827D 00	-1.163D 01	-2.377D 01

LAMBDA 98: 2625.93 ANGSTROMS

PE					
3.	-1.507D 00	-1.703D 00	-4.492D 00	-1.079D 01	-3.122D 01
30.	-1.235D 00	-1.458D 00	-2.553D 00	-9.021D 00	-2.680D 01
300.	-8.916D-01	-1.445D 00	-1.597D 00	-7.205D 00	-2.269D 01
10000.	-9.102D-01	-1.081D 00	-1.471D 00	-4.677D 00	-1.703D 01

TABLE C.4-2
LOG OF THE STATISTICAL UV BLANKETING OPACITY

LAMBDA 99: 2668.19 ANGSTROMS

PE \ T	6000.	8000.	11000.	17500.	50000.
3.	2.060D-01	1.169D-01	-2.478D 00	-1.227D 01	-3.787D 01
30.	4.587D-01	3.061D-01	-5.169D-01	-9.324D 00	-3.287D 01
300.	8.541D-01	2.814D-01	2.726D-01	-6.664D 00	-2.794D 01
10000.	1.028D 00	7.057D-01	2.962D-01	-3.207D 00	-2.059D 01

LAMBDA 100: 2694.99 ANGSTROMS

PE \ T	6000.	8000.	11000.	17500.	50000.
3.	4.765D 00	4.899D 00	3.003D 00	3.665D-01	-7.202D-01
30.	4.777D 00	4.903D 00	4.086D 00	7.908D-01	4.209D-01
300.	5.145D 00	4.792D 00	4.724D 00	1.364D 00	1.425D 00
10000.	5.378D 00	4.863D 00	4.859D 00	2.846D 00	2.426D 00

LAMBDA 101: 2695.01 ANGSTROMS

PE \ T	6000.	8000.	11000.	17500.	50000.
3.	-2.181D 01	-2.166D 01	-2.364D 01	-2.916D 01	-4.519D 01
30.	-2.192D 01	-2.170D 01	-2.219D 01	-2.807D 01	-4.211D 01
300.	-2.186D 01	-2.190D 01	-2.173D 01	-2.681D 01	-3.913D 01
10000.	-2.207D 01	-2.200D 01	-2.206D 01	-2.482D 01	-3.465D 01

LAMBDA 102: 2720.95 ANGSTROMS

PE \ T	6000.	8000.	11000.	17500.	50000.
3.	-2.665D 00	-2.726D 00	-5.852D 00	-1.283D 01	-3.408D 01
30.	-2.545D 00	-2.528D 00	-3.787D 00	-1.100D 01	-2.949D 01
300.	-2.225D 00	-2.593D 00	-2.755D 00	-9.095D 00	-2.522D 01
10000.	-2.314D 00	-2.373D 00	-2.590D 00	-6.202D 00	-1.932D 01

LAMBDA 103: 2764.00 ANGSTROMS

PE \ T	6000.	8000.	11000.	17500.	50000.
3.	-2.914D-01	-3.673D-01	-3.365D 00	-1.300D 01	-3.798D 01
30.	-2.033D-01	-1.745D-01	-1.312D 00	-1.027D 01	-3.298D 01
300.	1.352D-01	-2.544D-01	-4.081D-01	-7.790D 00	-2.811D 01
10000.	2.202D-01	1.675D-02	-2.617D-01	-4.215D 00	-2.101D 01

LAMBDA 104: 2791.30 ANGSTROMS

PE \ T	6000.	8000.	11000.	17500.	50000.
3.	4.640D 00	4.744D 00	2.862D 00	3.599D-01	-8.541D-01
30.	4.677D 00	4.771D 00	3.934D 00	7.948D-01	3.112D-01
300.	5.063D 00	4.685D 00	4.581D 00	1.361D 00	1.337D 00
10000.	5.317D 00	4.797D 00	4.758D 00	2.798D 00	2.374D 00

LAMBDA 105: 2791.32 ANGSTROMS

PE \ T	6000.	8000.	11000.	17500.	50000.
3.	-3.434D 01	-3.407D 01	-3.594D 01	-4.157D 01	-5.102D 01
30.	-3.478D 01	-3.423D 01	-3.450D 01	-4.075D 01	-4.927D 01
300.	-3.489D 01	-3.461D 01	-3.427D 01	-3.963D 01	-4.753D 01
10000.	-3.524D 01	-3.514D 01	-3.485D 01	-3.765D 01	-4.491D 01

TABLE C.4-2
LOG OF THE STATISTICAL UV BLANKETING OPACITY

T	6000.	8000.	11000.	17500.	50000.
		LAMBDA 106: 2829.86 ANGSTROMS			
PE					
3.	-3.321D 00	-3.502D 00	-7.080D 00	-1.536D 01	-3.438D 01
30.	-3.301D 00	-3.264D 00	-4.757D 00	-1.324D 01	-3.024D 01
300.	-3.004D 00	-3.265D 00	-3.518D 00	-1.095D 01	-2.630D 01
10000.	-3.040D 00	-3.138D 00	-3.161D 00	-7.431D 00	-2.081D 01
		LAMBDA 107: 2894.53 ANGSTROMS			
PE					
3.	-3.878D-01	-6.809D-01	-4.053D 00	-1.413D 01	-3.532D 01
30.	-4.346D-01	-3.607D-01	-1.759D 00	-1.141D 01	-3.089D 01
300.	-1.178D-01	-3.959D-01	-7.232D-01	-8.812D 00	-2.657D 01
10000.	-4.943D-02	-2.708D-01	-4.241D-01	-4.880D 00	-2.038D 01
		LAMBDA 108: 2935.99 ANGSTROMS			
PE					
3.	4.452D 00	4.509D 00	2.651D 00	3.501D-01	-1.055D 00
30.	4.526D 00	4.572D 00	3.705D 00	8.007D-01	1.464D-01
300.	4.938D 00	4.523D 00	4.367D 00	1.358D 00	1.204D 00
10000.	5.226D 00	4.698D 00	4.616D 00	2.726D 00	2.296D 00

REFERENCES

Allen, C. W. 1964, Astrophysical Quantities, University of London, Athlone Press.

Aller, L. H. 1963, The Atmospheres of the Sun and Stars, Ronald Press.

Auer, L. H. 1967, Ap. J. Letters, 150, L53.

Auer, L. H. and Mihalas, D. 1969, Ap. J. 156, 157.

Auer, L. H. and Mihalas, D. 1969, Ap. J. 156, 681.

Auer, L. H. and Mihalas, D. 1969, Ap. J. 158, 641.

Auer, L. H. and Mihalas, D. 1970, Ap. J. 160, 233.

Avrett, E. H. and Krook, M. 1963, Ap. J. 137, 874.

Avrett, E. H. and Strom, S. E. 1964, Ann. Astrophysics 27, 781.

Bell, R. A. and Upson, W. L. 1971, Astrophysical Letters 9, 109.

Bless, R. C. 1969, private communication.

Bless, R. C., Fairchild, T., and Code, A. D. 1971, NASA Special Publication (to be published).

Bless, R. C. and Savage, B. D. 1972, Ap. J. 171, 293.

Böhm, K. H. 1954, Zeits. für Astrophysik 34, 182.

Böhm-Vitense, E. 1969, J. Q. S. R. T. 9, 1167.

Breger, M. and Kuhi, L. V. 1970, Ap. J. 160, 1129.

Burgess, D. D. and Grindlay, J. C. 1970, Ap. J. 161, 343.

Carbon, D. and Gingerich, O. 1969, Proc. 3rd Harvard-Smithsonian Conf. St. Atm., M.I.T. Press, 377.

Cayrel, R. 1966, J. Q. S. R. T. 6, 621.

Chandrasekhar, S. 1935, Mon. Not. R. A. S., 96, 21.

Condon, E. U. and Shortley, G. H. 1959, The Theory of Atomic Spectra, Cambridge University Press.

Edmonds, F. M., Schlüter, H., and Wells, D. C. 1967, Memoirs R. A. S. 71, 271.

Evans, D. C. 1971, NASA Publication, X-672-71-492.

Feautrier, P. 1964, C. R. Acad. Sci. Paris 258, 3189.

Fischel, D. 1964, Ap. J. 140, 221.

Fischel, D. 1964, Proc. 1st Harvard-Smithsonian Conf. St. Atm., S. A. O. Special Report No. 167.

Fischel, D. and Sparks, W. 1971, Ap. J. 164, 359.

Fowler, J. W. 1970, Maryland Astronomical Journal 1, No. 3, 42.

Fullerton, W. and Cowley, C. 1970, Ap. J. 162, 327.

Gingerich, O. 1966, J. Q. S. R. T. 6, 609.

Griem, H. 1964, Plasma Spectroscopy, McGraw-Hill, Inc.

Hammond, G. 1969, private communication.

Hanbury Brown, R. and Twiss, R. Q. 1958, Proc. Royal Society of London, A248, 199.

Hanbury Brown, R., Davis, J., and Allen, L. R. 1967, Mon. Not. R. A. S. 137, 375.

Hanbury Brown, R., Davis, J., Allen, L. R., and Rome, J. M. 1967, Mon. Not. R. A. S. 137, 393.

Heitler, W. 1954, Quantum Theory of Radiation, Oxford University Press.

Herzberg, G. 1944, Atomic Spectra and Atomic Structure, Dover Publications, Inc.

Hummer, D. G. 1965, Memoirs R. A. S. 70, Part 1.

Jefferies, J. T. 1968, Spectral Line Formation, Blaisdell Publishing Co.

Karp, A. H. 1972, Ap. J. 173, 649.

Klinglesmith, D. A. and Sobieski, S. 1970, Astronomical Journal 75, No. 2, 175.

Kourganoff, V. 1963, Basic Methods in Transfer Problems, Dover Publications, Inc.

Labs, D. 1951, Zeits. für Astrophysik 29, 199.

Latham, D. 1970, Thesis, S. A. O. Special Report No. 321.

Matsushima, S. 1968, Ap. J. 154, 715.

Meggers, W. F., Corliss, C. H., and Scribner, B. F. 1961, N.B.S. Monograph No. 32, Part II.

Mihalas, D. 1966, J. Q. S. R. T. 6, 581.

Mihalas, D. 1967, Methods in Computational Physics 7, Academic Press.

Mihalas, D. 1970, Stellar Atmospheres, Freeman and Co.

Mihalas, D. and Auer, L. H. 1970, Ap. J. 160, 1161.

Mihalas, D. and Auer, L. H. 1970, Ap. J. 161, 1129.

Mihalas, D. and Luebke, W. R. 1971, Mon. Not. R. A. S. 153, 229.

Mihalas, D. and Morton, D. C. 1965, Ap. J. 142, 253.

Peterson, D. M. 1969, Thesis, S. A. O. Special Report No. 293.

Petrie, R. M. 1965, Pub. Dom. Astrophysical Obs., 12, No. 9.

Peytremann, E. 1971, Bulletin A. A. S. 3, No. 4, Part 1, 455.

Schild, R., Peterson, D. M., and Oke, J. B. 1971, Ap. J. 166, 95.

Shore, B. W. and Menzel, D. H. 1968, Principles of Atomic Spectra, J. Wiley and Sons, Inc.

Slater, J. C. 1960, Quantum Theory of Atomic Structure, McGraw-Hill, Inc.

Stecher, T. P. 1970, Ap. J. 159, 543.

Strom, S. E. and Avrett, E. H. 1964, Ap. J. 140, 1381.

Strom, S. E., Gingerich, O., and Strom, K. M. 1966, Ap. J. 146, 880.

Strom, S. E. and Kurucz, R. L. 1966, J. Q. S. R. T. 6, 591.

Travis, L. D. and Matsushima, S. 1968, Ap. J. 154, 689.

Vardya, M. S. 1966, J. Q. S. R. T. 6, 539.

Warner, B. 1967, Memoirs R. A. S. 70, Part 5.

Weber, S. V., Henry, R. C., and Carruthers, G. R. 1971, Ap. J. 166, 543.

Weisskopf, V. F. and Wigner, E. P. 1930, Zeits. für Astrophysik 63, 54.

Wiese, W. L., Smith, M. W., and Glennon, B. M. 1966, Atomic Transition Probabilities, Vol. 1, N. S. R. D. S. - N. B. S. 4.

Wiese, W. L. and Weiss, A. W. 1968, Phys. Rev. 175, No. 1, 50.

Wildey, R. L., Burbidge, E., Sandage, A., and Burgidge, G. 1962, Ap. J. 135, 94.

Woolley, R. v.d. R. and Stibbs, D. W. N. 1953, The Outer Layers of a Star, Oxford University Press.